UNIVERSITÀ DI PARMA

UNIVERSITA' DEGLI STUDI DI PARMA

DOTTORATO DI RICERCA IN SCIENZE DELLA TERRA

CICLO XXXVIII

Debris-flows in Northern Apennines and climate change: recent events analysis and reconstructions at different temporal scales

Coordinatore:

Chiar.mo Prof. Fabrizio Balsamo

Tutore:

Chiar.mo Prof. Alessandro Chelli

Chiar.mo Prof. Giovanni Leonelli

Dottorando: Dr. Muhammad Ahsan Rashid

Anni Accademici 2022/2023 – 2024/2025

Abstract

This thesis investigates debris flow processes in the Northern Apennines, Italy, through a multidisciplinary, multi-scalar and novel approach that integrates geomorphological mapping, dendrogeomorphology, sedimentological analysis, climatological data, GIS-based geomorphometry, susceptibility and numerical modeling. Debris flows represent one of the most hazardous geomorphic processes in this mountain range. By combining traditional methods with advanced quantitative techniques, this work provides both localized reconstructions of past events and regional-scale insights into debris flow dynamics.

At the local scale, a detailed geomorphological survey supported by a high-resolution digital elevation model (5 m) allowed systematically mapping the existing landforms in the study site: i.e. glacial, cryogenic, and slope-related landforms, and to particularly emphasize debris flow channels. GIS-derived morphometric indices, including slope angle, Topographic Wetness Index (TWI), Terrain Ruggedness Index (TRI), and elevation, that were extracted along channel profiles and analyzed in relation to channel length classes. This analysis revealed anomalous morphometric patterns in debris flow channels, indicating distinctive topographic anomalies compared to non-affected debris flow channels.

Dendrogeomorphological analyses extended the temporal resolution, reconstructing debris flow activity over the past six decades. Growth disturbances in tree rings, combined with soil infiltration studies, precipitation data, and orthophoto interpretation, enabled the identification and classification of major, intermediate, and minor debris flow events. The events of 1972 and 1987 were particularly significant, disturbing up to 54% of trees, causing widespread tree damage and substantial geomorphic change, while intermediate events in 1996, 2003, and 2013 with 20-30% of disturbed trees produced more localized impacts. Minor events were characterized by less than 20% of disturbed trees, indicating limited geomorphic impact and localized disturbance. It is noteworthy that the multidisciplinary analysis revealed that not all high-intensity rainfall events corresponded to debris flows, highlighting the importance of other parameters such as soil temperature and saturation that influence slope stability by affecting infiltration and runoff dynamics.

Sedimentological analysis of debris flow features such as levee and lobe deposits showed sorting patterns and different slope geometries, indicating differential energy dissipation during transport

and deposition. The 1987 debris flow event, identified as the last major event in the study area, was reconstructed using the RAMMS-DF numerical model. Calibration based on field evidence, mapped deposit extents, and channel morphology showed good agreement with simulated runout, demonstrating the potential of physically based models to reproduce debris flow dynamics in steep Apennine catchments.

At the regional scale, a database of approximately 500 documented debris flows was analyzed to evaluate catchments characteristics by using Melton Ruggedness Index (MRI), Hypsometric Integral (HI), average slope, and channel gradient indices together with the hydro-geomorphological Stream Power Index (SPI) to analyze DFs drainage basins in the Northern Apennines. This broader analysis distinguished zones where debris flow susceptibility is high across the Apennine chain.

By integrating local reconstructions with regional analyses, this thesis develops a robust framework for understanding debris flow initiation, propagation, and deposition. The findings provide critical insights into hazard assessment, offering methodological advances that combine geomorphological mapping, tree ring evidence, and modeling. Ultimately, this research contributes to improving predictive capability and informing risk mitigation strategies in mountain environments increasingly threatened by hydroclimatic extremes.

Table of Contents

1. Introduction

1.1 Research background and justification

The Northern Apennines, with their structurally complex and geomorphologically active landscape, offer a valuable setting for studying the dynamics of slope instability and natural hazard processes under the influence of ongoing tectonic forcing (Chelli et al., 2013; Argnani et al., 2003). Moreover, the Apennines climatic fluctuations (Corsini et al., 2017) interact with tectonically elevated landscape and cause slope water pressure, trigger erosive events, and destabilize hillslopes. Among the wide range of geomorphic processes observed in this region, debris flows (DFs) represent one of the most hazardous phenomena. DFs, consisting of rapid downslope movements of water-saturated sediment, pose significant threats to infrastructure, agricultural land, and ecosystems, particularly in steep mountain catchments (Hungr et al., 2014; Tiranti et al., 2018; Giano et al., 2021). A comprehensive understanding of DF dynamics is essential for effective hazard assessment and mitigation strategies.

In the Emilia-Romagna region, DFs and other mass movements have become increasingly prominent due to a combination of lithology, steep topography, and climate variability (Corsini et al., 2017; Ciccarese et al., 2021; Peruccacci et al., 2023; Rashid et al., 2024; Berti et al., 2025). Regional inventories have recorded over 80,000 landslide events associated with May 2023 rainfall, affecting nearly 12% of the regional territory and DFs were the second highest type of landslide, consisting of 15% of the total count and 29% by area (Berti et al., 2025) highlighting their significance in national risk assessments and disaster management strategies (ISPRA, 2021). Within this highly dynamic setting, the Province of Reggio Emilia emerges as one of the most severely impacted areas. The Alpe di Succiso is recognized as a hotspot of slope instability, where litho-structural predisposition, valleys shaped by past glaciation, and intense orographic precipitation converge to produce repeated mass-movement activity.

Field investigations in Alpe di Succiso confirm that DFs are the dominant geomorphic process shaping the landscape, particularly in deep incised mountain channels, with landforms such as lobes and levees (Rashid et al., 2024). These events are characterized by matrix-supported deposits with a fine grained muddy or sandy matrix enclosing clasts that range from gravel to boulder size. The DF deposits often form lobate bodies, coarse angular frontal deposits, and well-developed steep levees

along channel margins, produced by lateral segregation of coarse material during transport (Costa, 1984; Pierson, 1980a). The triggering mechanism is typically linked to short-duration, high-intensity rainfall, which saturates slope materials and mobilizes colluvial deposits (Hungr et al., 2001; Iverson & George, 2014). Although such processes are well documented in alpine contexts, there remains a scarcity of detailed, site-specific studies within the Northern Apennines. The existing contributions (e.g., Ciccarese et al., 2020, 2021) have established rainfall thresholds for DF initiation, but integrated, multidisciplinary reconstructions remain rare.

In the vicinity of Alpe di Succiso area, there has been no prior information about the temporal and spatial pattern of DFs. To build this knowledge, the study first relies on detailed geological and geomorphological mapping as a starting point, documenting the lithologies, source zones, and depositional features that control slope instability. This foundational framework is then expanded through dendrogeomorphology, which makes it possible to reconstruct historical events with annual and seasonal precision by analyzing growth disturbances in trees. Possible rainfall triggers dates are then correlated with dendro-defined window. Additional evidence is drawn from sediment analyses and orthophoto interpretation, which assist in characterizing depositional attributes and trace the extent of historical flows, most notably the catastrophic events of 1972 and 1987. To enhance the understanding of flow dynamics, numerical simulations with RAMMS (Rapid Mass Movements Simulations) are executed, allowing the dynamics of the 1987 DF to be reproduced and compared with field observations. In order to contextualize the local analyses, this research also explores debris-flow occurrences on a regional level throughout the Northern Apennines. A comprehensive dataset comprising over 500 documented DF events was compiled and analyzed to investigate spatial patterns and to compare the studied catchment with other areas in the region affected by DFs. Additionally, a catchment-scale susceptibility analysis was employed to pinpoint regions that exhibit a higher likelihood of DF activity. The study integrates geomorphological mapping, dendrogeomorphology, sedimentological studies, climatic assessments, remote sensing, and numerical modeling. By synthesizing these diverse techniques, the research seeks to enhance the comprehension of DF mechanisms and their influencing factors, as well as to establish a methodological framework applicable to DF studies in mountainous regions.

1.2 Objective of the Thesis

The objective of this thesis is to advance the understanding of DF dynamics, and hazard assessment in the Northern Apennines, with an emphasis on the Alpe di Succiso, a site representative of the region's climatic and geomorphic complexity.

More specifically, the study aims to:

1. Reconstruct past DF activity through a multidisciplinary approach that combines field mapping, sedimentological characterization, and dendrogeomorphology. This includes identifying depositional features, extent of DFs and dating past disturbances using tree-ring evidence.

2. Investigate the climatic drivers of DFs, particularly the role of extreme rainfall events. By analyzing long-term meteorological data (1960–2024), the thesis explores rainfall patterns that may explain DF triggering in high-relief Apennine environments.

3. Simulate DF propagation and impact zones at the local scale using RAMMS-DF, a physically based modeling tool. The model is calibrated using empirical data from the 1987 event and validated against observed geomorphic evidence, orthophoto and dendrochronological records.

4. Conduct a regional-scale analysis using a database of over 500 DF initiation sites. This includes morphometric analysis based on slope, elevation, terrain ruggedness, and topographic wetness index to identify terrain conditions most associated with DF occurrence.

5. Carry out a susceptibility analysis in the Northern Apennines to map DF prone areas, based on morphometric indices including the Melton Ruggedness Index (MRI), Hypsometric Integral (HI), average slope, and channel gradient.

6. Develop a transferable framework for DF hazard assessment. By combining site-specific insights with regional patterns, the thesis provides a reproducible strategy that can support early warning, land-use planning, and climate risk adaptation in other mountainous regions. Through these objectives, the thesis contributes to both the scientific understanding of DFs in understudied regions and the practical tools required for risk mitigation and sustainable landscape management.

1.3 Structure of Thesis

This thesis is organized as a compilation of three scientific articles developed during the doctoral research period, supported by an introductory chapter, a chapter on the general characteristics of DFs, a regional framework chapter, and three concluding chapters. Chapter investigates DF processes from a different scale and methodological perspective, with particular emphasis on the Alpe di Succiso area of the Northern Apennines.

Chapter 2 introduces the general characteristics of DFs, discussing their landforms, depositional facies, and dynamics. Chapter 3 provides an overview of the regional geography, geology, geomorphology, and tectonic framework of the Northern Apennines, emphasizing the relevant aspects, in general, for slope stability and, in particular, for DFs occurrence.

The first article (Chapter 4) presents detailed geomorphological map and morphometric analysis of DFs channels at Alpe di Succiso. It establishes the local geomorphic setting and highlights the characteristic features of DF deposits in this high-altitude Apennine environment.

The second article (Chapter 5) demonstrates the spatial and temporal resolution of DFs by using multi-disciplinary approach such as geomorphology, dendrogeomorphology, climate, orthophoto, geopedological and soil hydraulic properties. Using a GIS-based approach, more than 500 debris-flow sites across the Northern Apennines were analyzed. Morphometric and topographic variables were extracted to identify catchments most susceptible to DFs, and the results were used to produce a regional-scale susceptibility map.

The third article (Chapter 6) provides an in-depth reconstruction of the 1987 debris-flow event at Alpe di Succiso, one of the most severe recorded in the area. The study integrates dendrogeomorphology, sedimentological analysis, channel analysis, rock mass characterization and numerical modeling with RAMMS-DF to reconstruct the event's magnitude, and runout behavior. Calibrated model parameters allowed accurate estimates of deposition height, while tree-ring data provided valuable chronological control.

Chapter 7 offers an overall discussion and conclusion that integrates the results of the three articles, highlighting key patterns in DF dynamics and their implications for hazard management and concludes the thesis by summarizing the main scientific contributions. Overall, the thesis advances both theoretical understanding and practical approaches to DF hazard assessment.

2. Overview of Debris Flows

2.1 Classification of Debris Flows

Debris flows (DFs) represent extremely rapid (velocities are capable of exceeding 10 m/s) (Figure 2.1), gravity-induced mass movements characterized by a composite of water, sediments, and organic materials, exhibiting properties of a non-Newtonian, visco-plastic fluid (Iverson, 1997; Jakob & Hungr, 2005). These phenomena typically occur due to intense or prolonged precipitation, snowmelt, or abrupt slope failure, which mobilizes unconsolidated materials from hillslopes or channel beds. In contrast to shallow landslides or floods, DFs demonstrate both fluid-like dynamics and granular interactions, facilitating the transportation of substantial boulders and debris across considerable distances. The flow characteristics of DFs are depending upon sediment concentration, grain-size distribution, water content, and slope gradient, with velocities capable of exceeding 10 m/s and impact pressures sufficient to damage on infrastructure and alter valley morphology (Costa, 1984; Takahashi, 2014).

DFs produce distinctive geomorphic features that help differentiate them from other mass movements and fluvial processes. These landforms can be broadly classified into initiation, transport, and depositional zones. One of the most frequently referenced classifications of landslides was formulated by Varnes (1978) and Cruden and Varnes (1996), which categorized the DFs based on two attributes (i) the type of movement (Hungr et al., 2014) (ii) and velocity (Cruden and Varnes, 1996). Specifically, DFs are defined by the flow (i.e., fluid-like behavior) of predominantly coarse soil (comprising more than 20% gravel and coarser materials).

Landslide classifications have developed over a century. Varnes (1978) developed the first contemporary framework, categorizing landslides by material type and movement. Later, Pierson and Costa (1987) refined flow-type landslides using velocity and sediment concentration. Hutchinson (1988) introduced a geomorphological-geotechnical approach and Dikau et al. (1996) further systematized landslide methods while ensuring compatibility with previous schemes. Hungr (2001) reorganized flow-type landslides based on morphological criteria, then in 2014, he amended the Varnes system (Hunger et al., 2014) to update material classifications and align nomenclature with geotechnical standards. The redesigned methodology detected 32 distinct landslide types, making it one of the most comprehensive systems now in use.

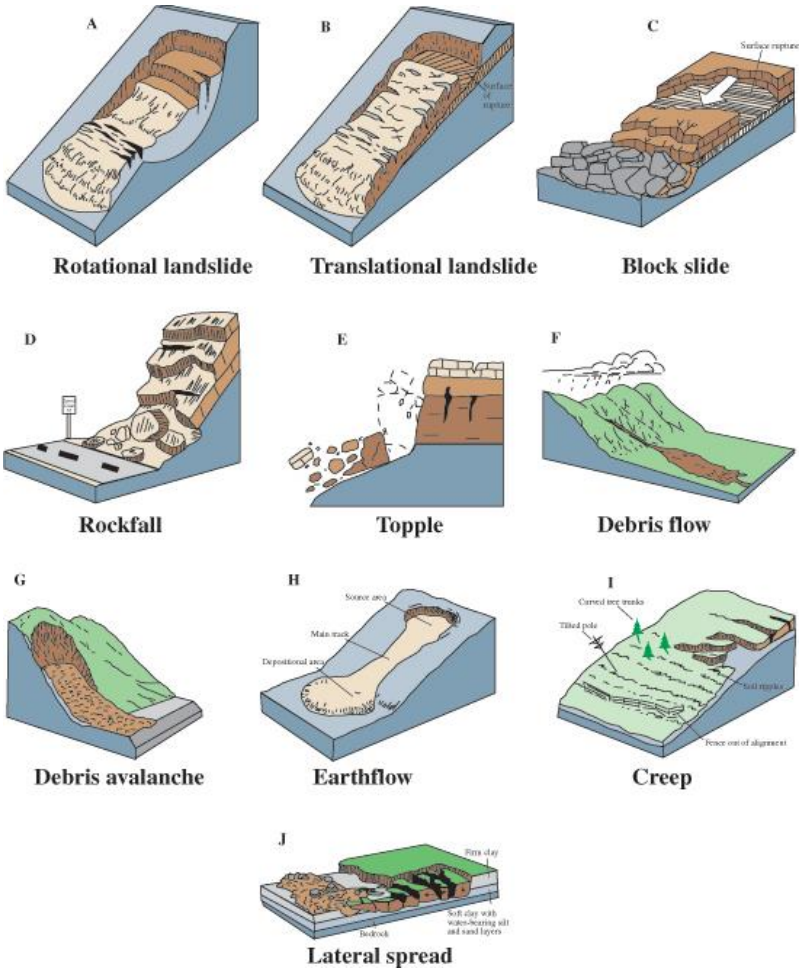

Figure 2.1. Types of landslide movement, independent of material. Complex landslides include two or more movement types, occurring either simultaneously or sequentially during failure. Modified after USGS (2004) and Cruden & Varnes (1996); adapted from Novellino et al. (2024).

2.2 Triggering Mechanism

DFs are typically triggered by either natural processes or human activities. On the natural side, three broad mechanisms dominate and often interact: (i) hydrometeorological forcing (intense or prolonged rainfall, rain-on-snow, rapid snowmelt, or sudden water releases), (ii) seismic shaking, which fractures and loosens hillslope materials and can evolve them for later storms, and (iii) volcanic activity, where eruptive melting of snow/ice or crater-lake outbursts mobilize loose tephra into lahars. Human triggers include slope cuts for roads and building pads, quarrying, deforestation and post-fire effects, drainage concentration from culverts and irrigation, and water-related issues such as reservoir drawdown or pipeline leaks that saturate colluvium (Takahashi, 2007).

The effectiveness of any trigger varies widely with slope gradient and curvature, landform position, soil thickness and texture, lithology and structural fabric, vegetation cover, and the presence of infrastructure or channel obstructions downslope. In many mountain regions including the Northern Apennines precipitation driven DFs are the most frequent, particularly during high-intensity convective storms that exceed local intensity duration thresholds (e.g., Corsini et al., 2019; Ciccarese et al., 2020; Berti et al., 2025).

2.3 Morphological, Sedimentological, and Dynamic Characteristics of DFs

DFs generally initiate in steep depressions, swales, or headwater gullies where colluvial and weathered materials tend to aggregate. Slopes exceeding 20–45° exhibit heightened vulnerability to failure, particularly in instances where the superficial materials are loose, fine-grained, or unconsolidated (Jakob et al., 2005; Rashid et al., 2024). Failures predominantly occur at the origins of first-order catchments; however, preliminary failures may also arise on convex ridge slopes, where instability can propagate rapidly downslope (Smith & Hart, 1982). The initiation scars frequently possess a concave morphology (Figure 2.2a), revealing compact subsoils or bedrock, and function as the source regions for mobilized debris.

Upon mobilization, the flows typically can utilize pre-existing channel systems, eroding and enlarging these channels as they progress downslope. Channels subjected to recurrent flows tend to exhibit U-shaped cross-sectional profiles (Figure 2.2b), which reflect the erosional capacity of the slurry (Johnson, 1970). Transport zones are further characterized by scour, undercutting, and the formation of lateral levees comprised of coarse clasts that segregate towards the channel margins. Pierson (1980b) documented instances in New Zealand where debris flows eroded several meters of channel bedrock within a span of less than 24 hours, highlighting their role as remarkably efficient geomorphic agents.

DFs typically start deposition on gentler slopes such as alluvial/debris fans or valley floors, where the gradient diminishes and flow competence decreases. Deposition during DF events commonly produces lobate landforms, where coarse boulders accumulate at the flow front and finer sediments settle behind (Bardou, 2002). This pattern reflects the process of grain-size segregation that occurs as the flow moves downslope. Larger clasts and coarse particles are pushed toward the surge front

and along the margins (Figure 2.3), forming lateral levees under the influence of frictional interactions and flow dynamics (Figure 2.4). In contrast, the slowing and the flow front generates depositional lobes, where finer-grained materials infill behind the coarser deposits. Together, these processes give rise to steep levees bordering the channel and gently sloping lobes at the toe, features that align closely with the field observations from the present study. These lobes frequently display the impression of large clasts “floating” in a muddy matrix, a diagnostic feature of DF diamicts (Costa, 1984; Beaty, 1974).

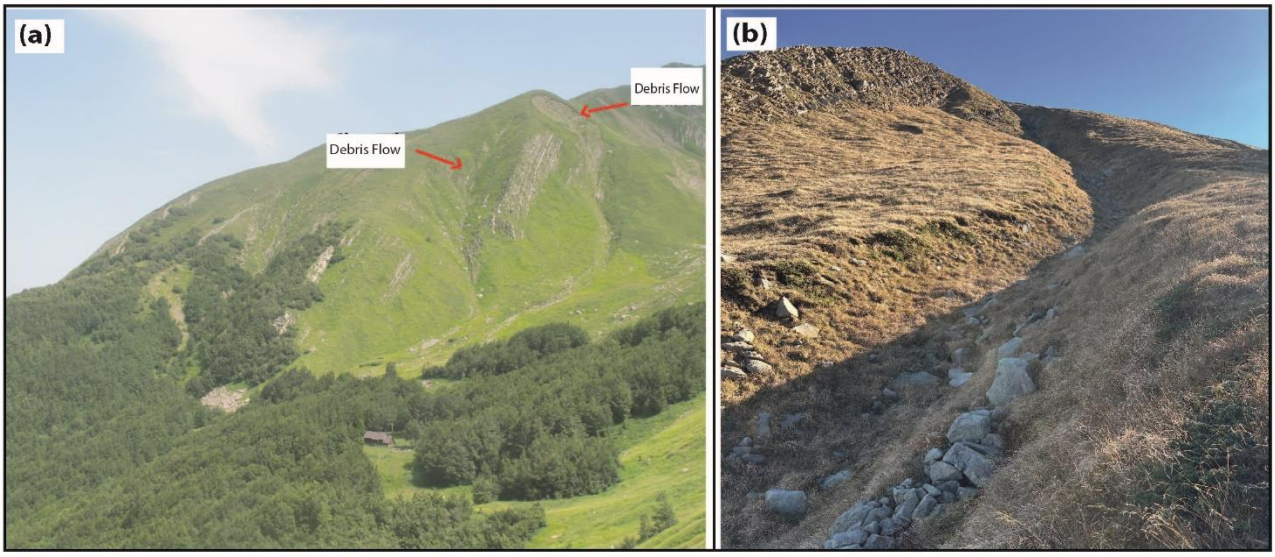

Figure 2.2. Concave morphology of debris-flow scars at the Fossa Lattara site, showing Channels of DF as source areas (b) Cross-section of DF (Fossa Lattara site), showing its characteristic U-shaped debris-flow profile (approximately 2 to 3 m of channel erosion).

The deposits, commonly designated as diamicts, are characterized by their poor sorting and absence of stratification (Figure 2.5). Matrix-supported amalgamations of clay to boulder-sized clasts are prevalent, with the fine fraction serving as the cohesive agent. In contrast to fluvial deposits, DF sediments are typically massive and structureless, reflecting the bulk transport dynamics of the flow rather than selective sedimentary processes (Costa, 1984; Pierson, 1981).

The fine-grained matrix serves an indispensable function, imparting both cohesion and buoyancy to coarser clasts. As Pierson (1981) articulated, a confluence of mechanisms including cohesion, buoyant uplift, dispersive pressure, and structural support within the particle framework facilitates the transportation of boulders exceeding 10 meters in diameter over distances spanning several kilometers by DFs.

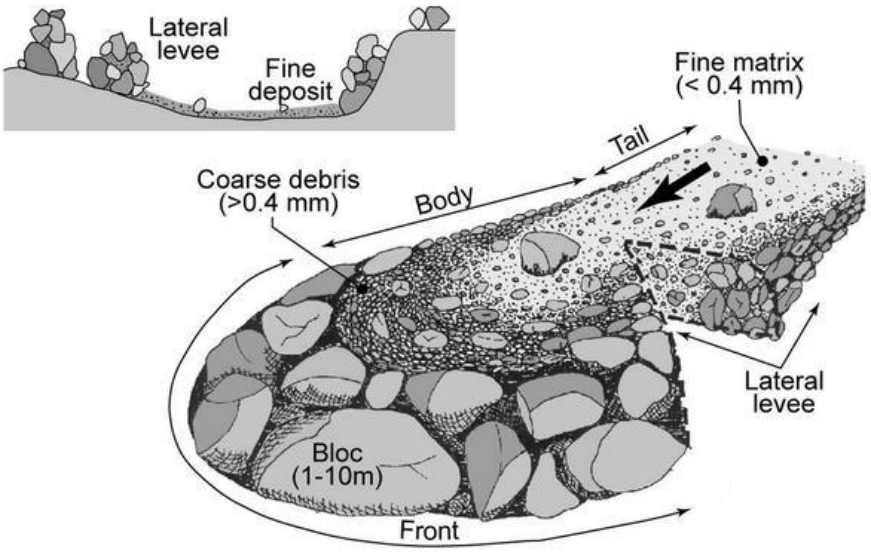

Figure 2.3. Schematic representation of debris flow body and deposits (modified after Bardou, 2002).

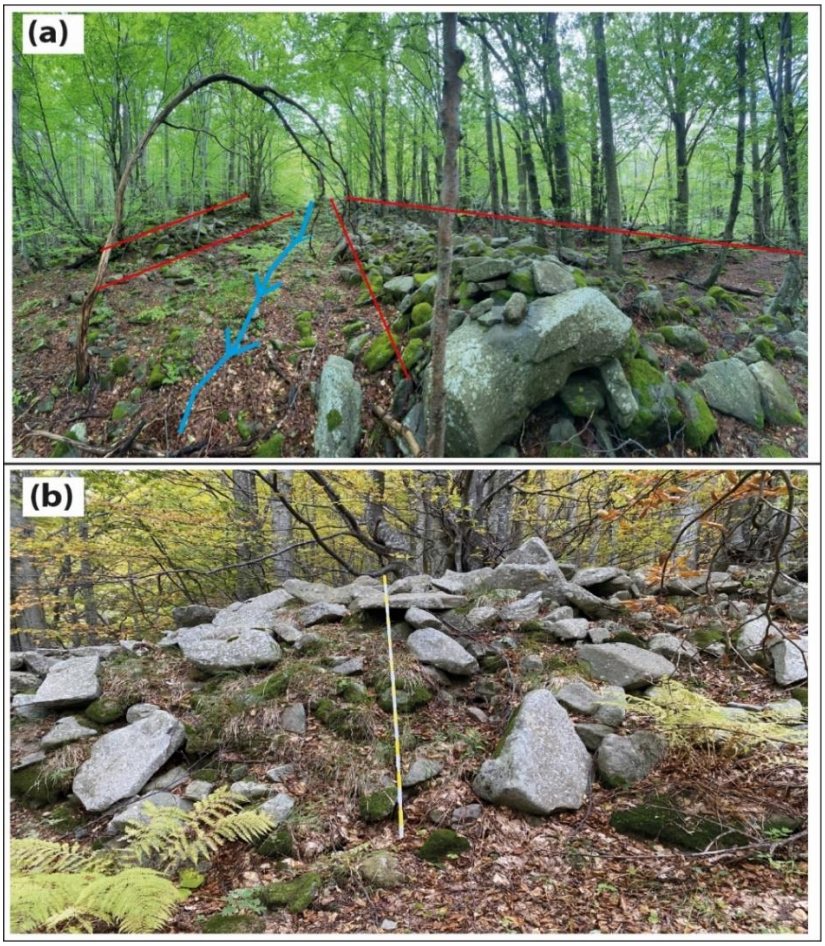

Figure 2.4. (a) Levees formed by DF deposits; (b) Levee height. Red line is showing the DF deposits (the stick is 1.30 m long).

Figure 2.5. Illustration of poor sorting and lack of stratification in debris-flow deposits (the length of the stick is 1.30 meters).

The dynamic behavior exhibited by DFs is indicative of their rheological characteristics as non-Newtonian, visco-plastic fluids (Lorenzini, 2004). Their movement combines features of both fluid dynamics and granular mechanics, resulting in unique surge like patterns. Documented velocities exhibit considerable variability, ranging from less than 1 m/s to exceeding 20 m/s, contingent upon slope and material properties (Pierson, 1980a). Flows infrequently progress as a continuous surge; rather, they propagate in a series of discrete pulses. For instance, a DF that occurred in the USSR in 1921 was comprised of 80 surges (Nosov et al., 2006), whereas a subsequent event in China recorded over 200 surges (Li & Luo, 1981). Each surge characteristically presents a coarse bouldery front succeeded by more fluid, fine-rich phases.

Rheological models such as the Bingham plastic and Coulomb-viscous frameworks are often applied to describe the complex motion of DFs (Melo et al., 2018). These models capture the role of yield strength the critical stress that must be exceeded for movement to begin, which arises from the combined effects of cohesion, internal friction, and viscosity (Johnson, 1970). Importantly, viscosity is not constant: it increases with sediment concentration and with the relative abundance of cohesive particles such as clays compared to non-cohesive sands and gravels (Fisher, 1971). This relationship (Figure 2.6) highlights why DFs behave very differently from clear-water floods.

Depending on particle size distribution and sediment concentration, their flow may shift between Newtonian (water-like) and non-Newtonian (slurry-like) behavior.

One of the most striking characteristics of DFs are their capacity to move large clasts, sometimes boulders weighing 30 to 40 tons over considerable distances. This ability is explained by four key support mechanisms that act together during transport:

1. Fine-grained clay fractions provide cohesion to bond the mass.
2. Buoyancy reduces the weight of larger clasts in the dense slurry.
3. Dispersive pressure from particle collisions lift larger particles upward in the flow.
4. Structural support, which involves interconnecting particles forming temporary frameworks capable of carrying massive blocks (Pierson, 1981).

Together, these mechanisms enable DFs to transport material far beyond the capacity of normal streamflow, underscoring their role as both powerful geomorphic agents and significant natural hazards.

For hazard and risk assessment, such complex processes are often simplified into depth-averaged numerical models that capture the bulk rheology of the flow. Among the most widely used is the Rapid Mass Movements Simulation (RAMMS-DF), developed by the Swiss Federal Institute for Forest, Snow and Landscape Research (WSL). RAMMS-DF is based on shallow-layer flow equations and employs the modified Voellmy–Salm rheological model (Salm et al., 1990; Bartelt et al., 2017). This formulation expresses basal shear stress (τ) as the sum of a Coulomb-type friction term and a velocity-dependent turbulent term:

$$S = \mu\rho gh\cos(\phi) + \frac{\rho g v^2}{\xi} \qquad (2.1)$$

where S represents the frictional resistance [Pa], μ is the basal friction coefficient, ρ is the density of the DF, h is the flow height (or flow depth), g is the gravitational acceleration, ϕ is the slope angle, v represents the velocity of the flow and ξ represents the turbulent friction coefficient.

The first term represents basal resistance due to dry friction, largely controlling depositional behavior and runout distance, while the second term accounts for velocity-dependent stresses

related to turbulence and collisional interactions, influencing flow velocity and energy dissipation (Hungr & Evans, 1996; Pudasaini & Hutter, 2007). Calibration of these parameters is critical: low values of μ typically represent highly mobile, saturated flows, whereas higher ξ values reflect enhanced collisional stresses in fast, dilute surges (Vicari, 2018).

In practice, RAMMS allows single or multiple release areas, integrates with GIS terrain models, and produces outputs such as flow height, velocity, and runout distance (Matjaž & Bezak, 2021; Cabral et al., 2023). These outputs are fundamental for hazard assessment, enabling researchers and practitioners to evaluate potential impacts on communities, infrastructure, and land use under different scenarios. By combining the conceptual understanding of DF rheology with the applied framework of the Voellmy–Salm model, RAMMS offers a flexible and physically grounded tool for predicting DF behavior at local to regional scales.

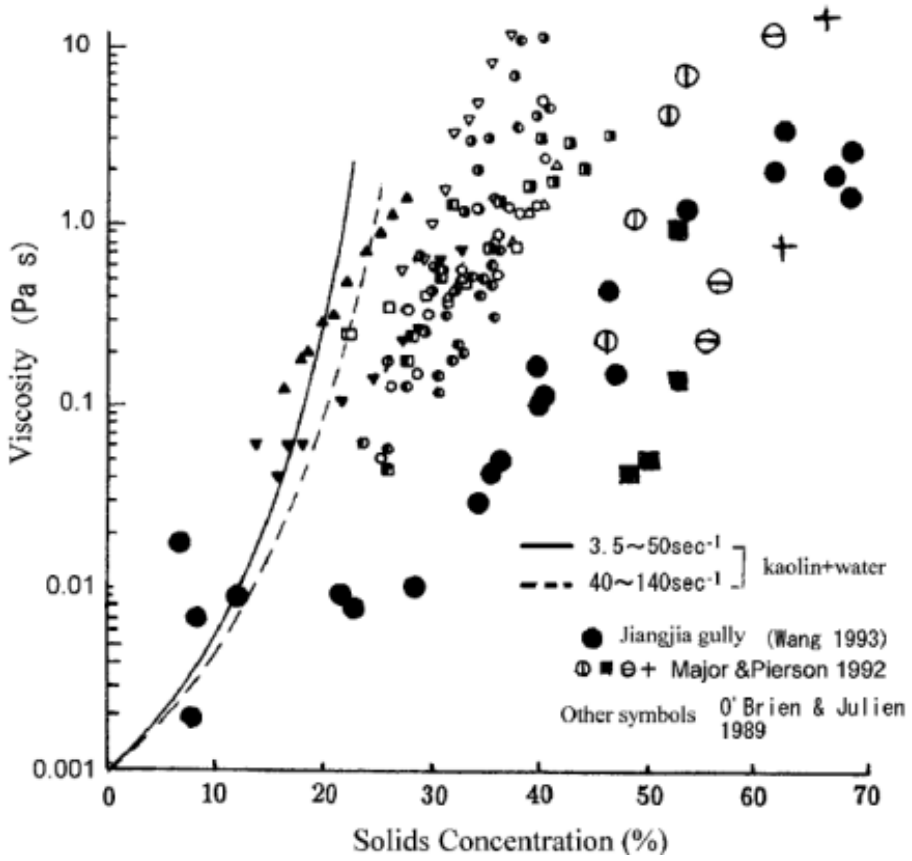

Figure 2.6. Viscosity trends showing increase with rising solid concentrations (Takahashi, 2014).

DFs exert shear stresses that can attain magnitude up to six times greater than those associated with clear-water floods of comparable depth, a phenomenon attributed to their enhanced density and thickness (Pierson, 1980b). Their impact forces may surpass 4000 N/m², a magnitude sufficient for the demolition of structures, the displacement of infrastructure, and the uprooting of trees (Takahashi, 1981). In addition to their role in transporting substantial sediment loads, they exhibit the capability to incise deeply into channels, destabilize valley slopes, and fundamentally transform entire drainage networks within a matter of hours.

In conclusion, DFs are one of the most formidable geomorphic events within mountainous environments. Their erosive capacity, coupled with their ability to transport extensive sediment loads and exert destructive forces on human infrastructure, highlight their dual role as both landscape modifying processes and significant natural hazards.

2.4 Overview of DFs in Italy

DFs constitute one of the most prevalent and hazardous geomorphic phenomena within the Italian mountainous regions, particularly evident in the Alpine and Apennine ranges (Guzzetti et al., 2005). Their occurrence is closely linked to steep topographical gradients, weak lithologies, and intense or short-duration precipitation events, frequently producing in abrupt and catastrophic occurrences.

Public and scientific awareness of landslide and debris-flow hazards in Italy increased markedly following the Sarno event in 1998, when rainfall-triggered landslides and debris flows caused severe casualties and widespread destruction in southern Italy (Crosta & Negro, 20023). This disaster highlighted the potential impact of rapid mass movements in densely populated areas and represented a key moment in the development of national strategies for landslide hazard assessment, mapping, and risk mitigation.

In the years that followed, the need for a systematic and homogeneous national dataset led to the development of the Inventario dei Fenomeni Franosi in Italia (IFFI). The IFFI project provides a standardized inventory of landslides, including debris flows, at the national scale and has become a fundamental reference for regional and national analyses (ISPRA, 2008). It supports susceptibility and hazard mapping, land-use planning, and comparative studies across different geological and

climatic settings, and it has strongly influenced how landslide and debris-flow hazards are assessed in Italy over the last decades.

In northeastern Italy, systematic documentation of over 800 debris flows across 537 basins highlights both their frequency and geomorphic impact, with volumes varying from several hundred to several hundred thousand cubic meters (Marchi et al., 2019). These events are typically triggered by convective storm systems that deliver extreme rainfall within a condensed timeframe, conditions that are increasingly prevalent in the context of climate variability (Marchi et al., 2019; Nikolopoulos et al., 2015).

Within the Emilia-Romagna Apennines, DFs are highly destructive due to their rapid initiation and substantial energy release. For instance, storm clusters occurring in 2014 and 2015 resulted in the generation of over a hundred debris flows within the provinces of Parma and Piacenza, severe damage on infrastructure and modifying slope-channel dynamics (Corsini et al., 2015; Berti et al., 2025; Ciccarese et al., 2021).

Central Italy, particularly in the context of the Sibillini Mountains, provides further evidence of DF activity, wherein seismic sequences have acted as additional triggering mechanism. The earthquakes that occurred in the Central Apennines during 2016 to 2017 not only triggered co-seismic landslides but also reactivated pre-existing DF channels, engendering complex interactions among seismic shaking, slope instability, and precipitation events (Farabollini et al., 2021). These phenomena illustrate how natural hazards in Italy frequently intersect, thereby amplifying the risks posed to local communities.

In summary, DFs in Italy demonstrate the interaction of geological, topographical, and climatic extremes. They serve as important role in sediment movement from headwater basins to valley floors, but they also pose enormous threats to infrastructure, human settlements, and lives. Recent advancement in geomorphological mapping, dendrogeomorphology, and numerical modeling have facilitated the development of more comprehensive frameworks for understanding their frequency, volume, and spatial distribution (Marchi et al., 2019; Ciccarese et al., 2021; Farabollini et al., 2021). Nonetheless, the increasing frequency of extreme rainfall events and the cumulative effects of seismic activity suggest that DFs will remain a significant hazard influencing the geological landscape of the Italian highlands in the future (Peruccacci et al., 2023; Nikolopoulos et al., 2015).

3. General Characteristics of Study Area and Regional scale

3.1 Geographical Framework

The Alpe di Succiso is located within the Reggio Emilia Apennines, a subsection of the Northern Apennines that spans approximately 1,100 km² in the province of Reggio Emilia (Figure 3.1). This mountainous region extends in a northwest–southeast direction, from the Lagastrello Pass (1,198 m a.s.l.), which separates it from the Parma Apennines to Monte Giovarello (1,760 m a.s.l.), where it borders the Modena Apennines. To the north, it descends into the Po Plain, while to the south, it borders the Garfagnana region.

From the main Apennine ridge, numerous secondary ridges extend contributing to the region's highly complex topography. Some of these secondary ridges reach elevations even higher than the main crest itself, Monte Ventasso (1,727 m a.s.l.) being a notable example. The highest peak in the area is Monte Cusna (2,121 m a.s.l.), which rises just north of the Tuscan-Emilian watershed, marking the boundary between the provinces of Reggio Emilia and Massa-Carrara. Other prominent peaks within this section of the Northern Apennines include Monte Prado (2,053 m a.s.l.), Alpe di Succiso (2,017 m a.s.l.), Monte Vecchio (1,981 m a.s.l.), Monte Alto (1,904 m a.s.l.), and Monte La Nuda (1,894 m a.s.l.). These peaks define the rugged skyline of the Reggio Emilia Apennines and form part of the Tuscan-Emilian Apennines National Park, known for its high ecological and geomorphological value. All of these lie within the Tuscan-Emilian Apennines National Park, an area of high environmental value and natural beauty (ISPRA, 2015).

Hydrographically, the region is defined by several important valleys. The Enza Torrent valley, shared with the Parma Apennines, and the Secchia River valley, shared with the Modena Apennines, are the two major basins. Other notable valleys include those of the Liocca Torrent (a right tributary of the Enza), and the Ozola, Dolo, and Secchiello Torrents, which all feed into the Secchia River. These waterways flow predominantly from south-west to northeast and ultimately contribute to the Po River basin.

The study area lies between 960 m a.s.l. and 2,017 m a.s.l. elevation and is centered on Alpe di Succiso, a prominent peak situated between the Lagastrello Pass and the Cerreto Pass, in the municipality of Ventasso (RE), in the western sector of the Reggio Emilia Apennines (Figure 3.2).

The study area consisted by a dense network of small hydrographic basins, which represent the fundamental geomorphic units linking hillslopes to the main valley systems. In the Northern Apennines, small basins often appear steep and deeply incised, as their morphology reflects both the tectonic imprint of regional-scale structures and the subsequent incision processes driven by Quaternary climate fluctuations (Carlini et al., 2016; Carlini et al., 2017). At the local scale, the basins feeding the Enza, Secchia, and Liocca valleys exhibit narrow headwaters situated between 1,600 and 1,900 m a.s.l., where steep slopes (30–40°) converge into V-shaped hollows. These areas coincide with zones of high Topographic Wetness Index (TWI) and Terrain Ruggedness Index (TRI) values (Rashid et al., 2024), which favor water accumulation and mass-movement initiation. At the regional scale, small basins across the Reggio Emilia Apennines display steep slopes and incised morphologies that strongly condition slope instability. Previous studies have documented how these morphometric settings, combined with structural controls, favor the widespread activity of DFs and large complex landslides in the area (Bertolini & Pellegrini, 2001; Carlini et al., 2017). Their hydrographic role is therefore twofold: they act as efficient sediment source areas and transfer zones for DF material, while at the same time recording the imprint of structural, climatic, and geomorphological processes that shape the Northern Apennines.

To the east, Alpe di Succiso is flanked by its notable forepeak, Monte Casarola (1,978 m). The Secchia River originates on its southern slopes, while the Liocca Torrent emerges from its northwestern side. The mountain also serves as a watershed divide between the Val Secchia and the Alta Val d’Enza.

Figure 3.1. Figure (a) illustrates the Reggio Emilia Apennine area location within Italy, highlighted by a red rectangle Reggio Emilia Apennines. Figure (b) offers a detailed map with the names of the main mountains, streams and lakes. The red rectangle represents study area location in the Northern Apennines (EPSG: 25832—ETRS89/UTM zone 32N coordinate system).

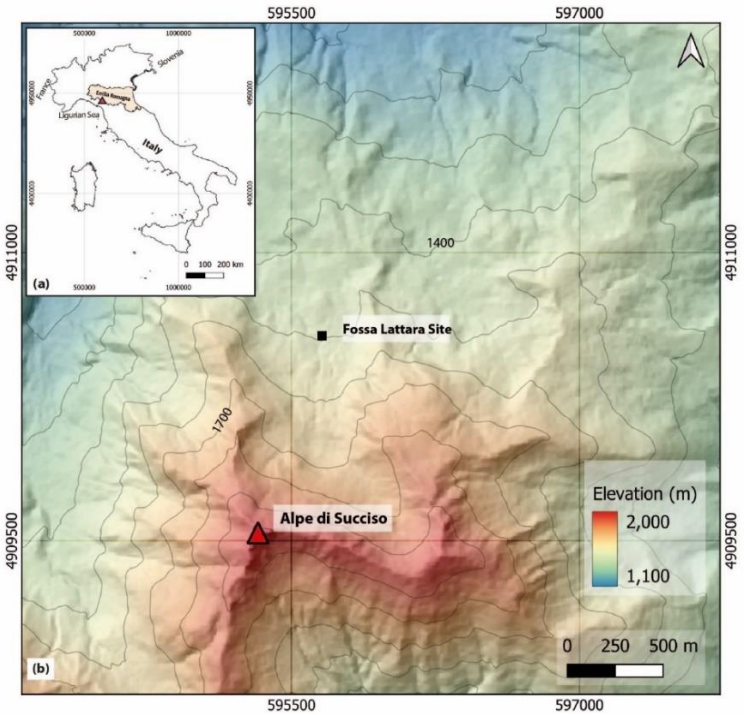

Figure 3.2: Figure (a) illustrates the study area location within Italy, highlighted by a red triangle. Figure (b) offers a detailed topographic map of the Alpe di Succiso mountain and its surroundings (5m DEM), with the peak also indicated by a red triangle. Contour lines show elevation changes, and the study area's coordinates are provided using the EPSG: 25832—ETRS89/UTM zone 32N coordinate system.

3.2 Geological Framework

The Northern Apennines represent a tectonically complex segment of the Mediterranean orogenic system, formed through the convergence and collision between the European and African plates, involving the Adriatic (Apulian) microplate and the Ligurian-Piedmontese oceanic crust (Boccaletti et al., 1971; Vai & Martini, 2001; Marroni et al., 2010). This convergence, which initiated during the Late Cretaceous and intensified through the Paleogene and Neogene, resulted in the eastward tectonic stacking of distinct paleogeographic domains (giving rise to a thick nappe pile observable throughout the range (Principi & Treves, 1984).

Two broad domains dominate the structural framework:

- The Internal Oceanic Units, corresponding to the Ligurian Domain (Vannucchi et al., 2012), and
- The External Continental Units, encompassing the Tuscan Domain and the Umbro-Marchigiano Domain (Bosellini, 2017; Vannucchi et al., 2012).

3.2.1 Ligurian and Subligurian Units

Within the Ligurian Domain, a fundamental subdivision is recognized between the Internal and External Ligurian Units (Figure 3.3) (Marroni et al., 2002). The Internal Units consist of ophiolitic sequences representing remnants of the Piedmont–Ligurian oceanic crust, including basalts, serpentinites, and radiolarian cherts, whereas the External Units comprise complex deposits and olistostromes with both oceanic and continental blocks in pelitic matrices (Remitti et al., 2007; Bettelli & Vannucchi, 2003). These successions are tectonically emplaced as part of the broader Ligurian nappe (Treves, 1984; Molli & Malavieille, 2010). The Canetolo Unit, belonging to the Subligurian Domain, records deposition at the ocean-continent transition and consists of highly deformed calcareous and marly successions (Elter et al., 1997; Vannucchi et al., 2012).

The two units are in tectonic contact, forming part of a broader Ligurian nappe that now rests structurally above the continental margin successions (Treves, 1984; Molli & Malavieille, 2010). It is composed of a highly tectonized and sheared succession, with significant lithological variability including calcareous, marly, and pelitic deposits, often difficult to interpret due to deformation during incorporation into the Apennine orogenic accretionary prism (Vannucchi et al., 2012).

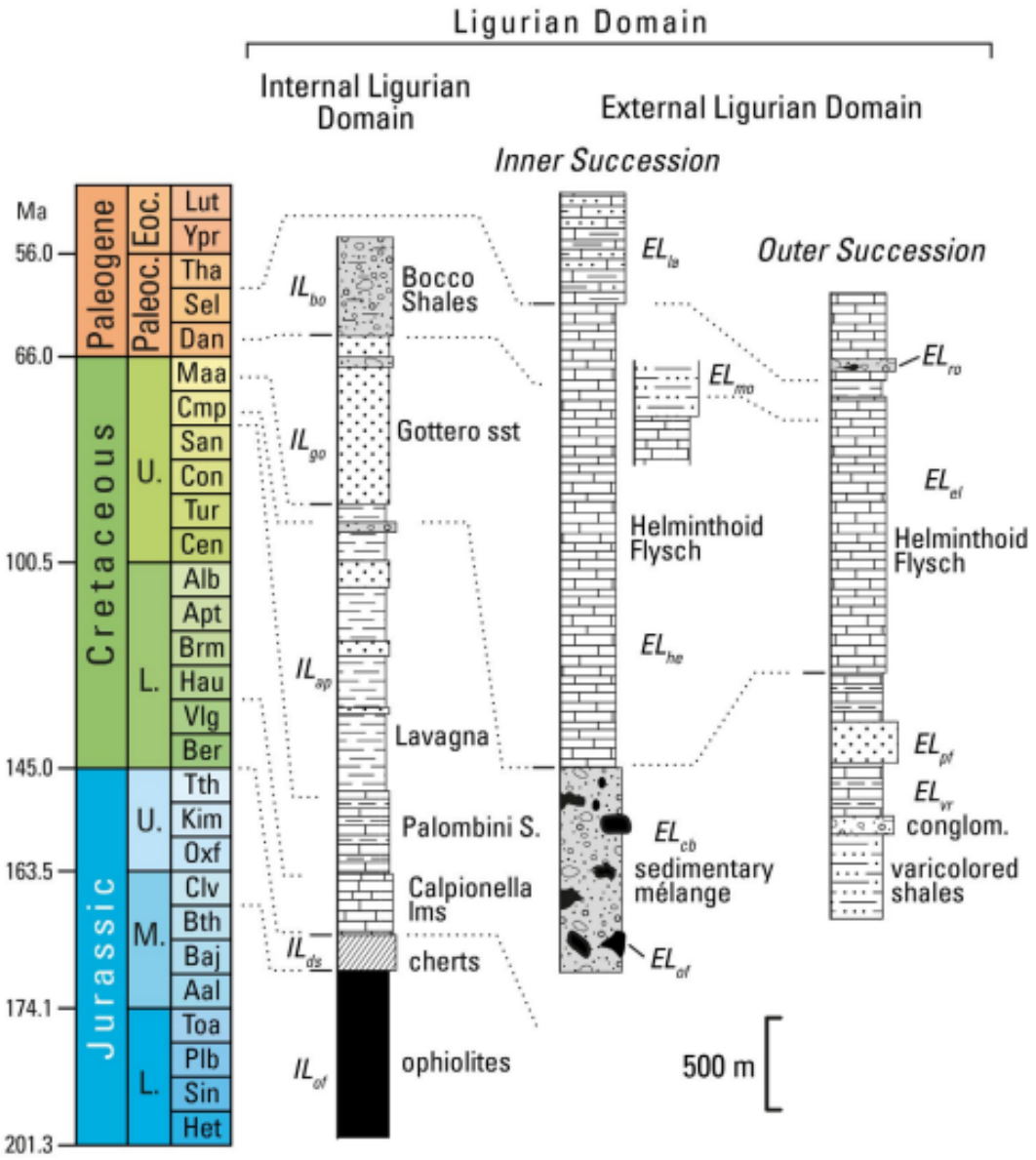

Figure 3.3: Stratigraphy of the Ligurian Domain, after Marroni et al., (2001, 2017) (adopted from Conti et al., 2020).

3.2.2 Tuscan Domain and Foredeep Evolution

The Tuscan Domain, forming the middle layer of the structural stack, includes both non-metamorphic sedimentary successions and metamorphosed equivalents (Figure 3.4) (Ricci Lucchi, 1986; Plesi, 2002). The non-metamorphic sequence ranges from the Upper Triassic evaporites (e.g., anhydrites and dolostones) to Oligo-Miocene foredeep turbidites. During the Jurassic, extensional

tectonics fragmented the carbonate platform, leading to the deposition of hemipelagic and pelagic marls and limestones, which evolved into increasing pelitic deposits during the Cretaceous (Palombini Clays, Maiolica, Scaglia Toscana) (Conti et al., 2020).

The foredeep sedimentation phase began in the Oligocene with the development of the Apennine foredeep basin, which received large volumes of siliciclastic sediments. These are partly preserved in the Macigno Formation and the Monte Modino Sandstones, both of which are well-exposed in the study area (Puccinelli et al., 2015). The Macigno (Upper Oligocene-Lower Miocene) is a thick succession of medium- to coarse-grained turbiditic sandstones and subordinate shales, interpreted as having been deposited by deep-sea gravity flows. The Monte Modino Sandstones (Upper Oligocene-Lower Miocene), by contrast, are somewhat younger and overlie the Macigno, though their contact is still debated (Elter et al., 2005).

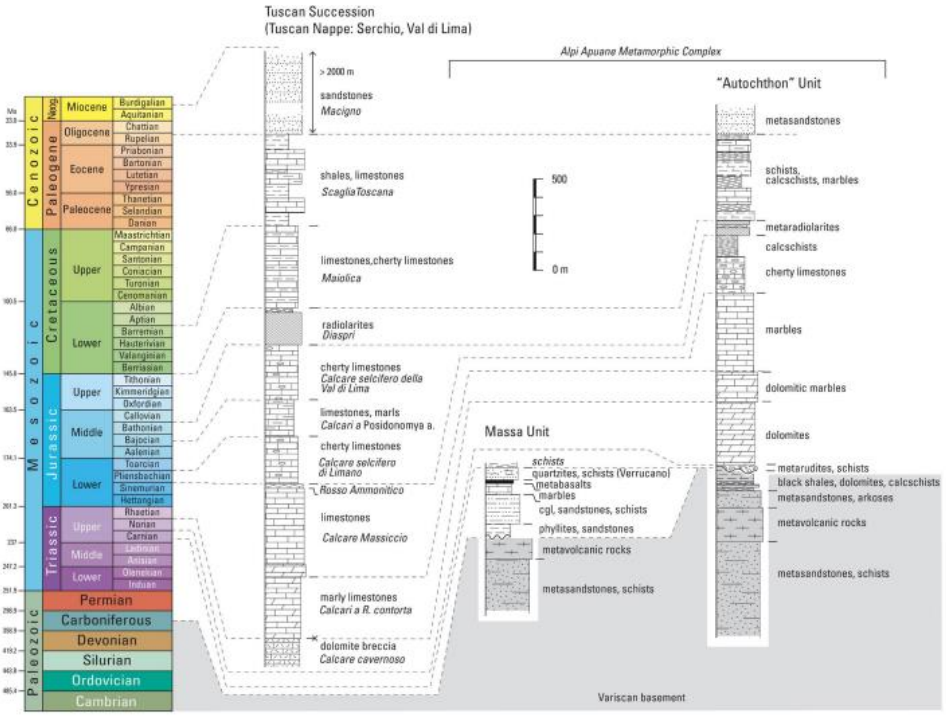

Figure 3.4: Stratigraphic logs of the Tuscan Succession (Tuscan Nappe) and Tuscan Metamorphic Successions in the Alpi Apuane area (adopted from Conti et al., 2020).

3.2.3 Local Stratigraphy at Alpe di Succiso

At Alpe di Succiso, formations are exposed, all part of the Tuscan Nappe and composed primarily of Oligocene-Miocene turbiditic deposits (Cerrina Feroni et al., 2002; Puccinelli et al., 2015) (Figure 3.5). The formations include:

1. Canetolo Clays and Limestone (Upper Paleocene - Middle Eocene)
2. Monte Modino Sandstones (Upper Oligocene - Lower Miocene)
3. Clayey Limestone Succession (Lower Cretaceous - Upper Cretaceous)
4. Macigno Sandstone (Upper Oligocene - Lower Miocene)
5. Cavernoso Limestone (Upper Triassic)
6. Rivaccia Quartzite (Upper Triassic)

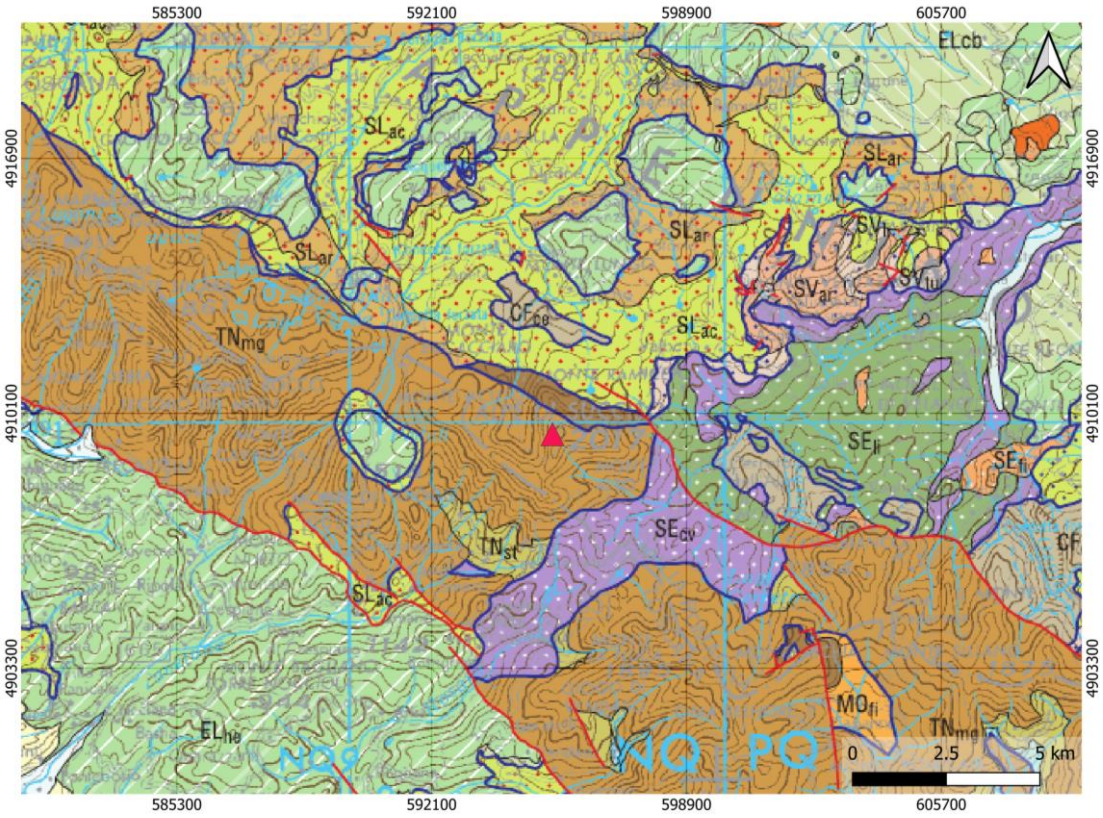

Figure 3.5: Geological map of the study area illustrating the spatial distribution of lithological units (map scale 1: 250,000). The red triangle indicates the location of the study area. Lithological units include turbiditic sandstones and siltstones (TNmg), volcaniclastic-rich sandstones (SLac), Helminthoides Flysch limestones (ELhe), breccias and polygenic conglomerates (SEcv, ELcb).

3.2.4 Structural Framework and Regional Geodynamics

From the Late Cretaceous to the Miocene epoch, the region underwent systematic nappe stacking and thrust propagation toward the foreland, resulting in the formation of a composite accretionary prism comprising both oceanic (Ligurian) and continental margin units (Tuscan and Umbro-Marchigiano) (Principi & Treves, 1984; Vannucchi et al., 2012). This tectonic evolution was followed

by major deformation processes that resulted in folds, thrusts, shear zones, and a complex network of discontinuities in the underlying bedrock (Carmignani & Kligfield, 1990).

The placement of the Ligurian and Subligurian nappes overlying the Tuscan Domain was accomplished by complex subduction channel mechanisms. Geological units such as the Sestola-Vidiciatico and Subligurian successions show evidence of multiple slip surfaces and laminar tectonic flow, indicating erosive subduction edges (Remitti et al., 2007; Bettelli & Vannucchi, 2003; Vannucchi et al., 2012). This kind of deformation resulted in the development of highly tectonized formations characterized by block-in-matrix fabrics, cleavage, and pervasive networks of fractures, which now influence the behavior of rock masses and the stability of slopes (Elter et al., 1997).

During the late Miocene to Pliocene, contractional tectonics continued to enable the uplift and exhumation of the orogenic wedge, whereas extensional tectonics formed at shallower structural levels (Carlini et al., 2013; Clemenzi et al., 2014). High-angle normal faults overlapped older thrust-related antiformal structures, leading in the formation of tectonic windows and differential uplift zones, particularly in the Reggio Emilia Apennines (Bernini et al., 1997). The superimposition of various tectonic regimes resulted in a complex network of discontinuities, faults, joints, and bedding-plane weaknesses that reduced the mechanical integrity of rock masses (Bertolini and Pellegrini, 2001; Mandrone, 2004).

At the outcrop scale, tectonic discontinuities have both passive and active effects on geomorphic processes (Carlini et al., 2016). Fractures, faults, and shear zones act as potential failure surfaces for mass movements, demonstrating the passive influence. Regional uplift and topographic escalation, on the other hand, have an active influence since they push hill slopes toward threshold angles, increasing their sensitivity to failure when precipitation or snowmelt occurs (Carlini et al., 2016, 2017). The spatial distribution of several large complex landslides in the Northern Apennines has been shown to correlate with late-orogenic antiforms and extensional fault zones, demonstrating the complex relationship between tectonics and slope instability (Chelli et al., 2013; Carlini et al., 2016).

The rock mass in the study area (Figure 3.6) is heavily pre-fractured by the multi-stage tectonic evolution of the Northern Apennines, which has produced orthogonal to oblique joint systems and fault-damage zones that locally increase fracture density and reduce rock-mass integrity.

Figure 3.6: Fractured Macigno Sandstone rock near Alpe di Succiso. A person (~1.80 m tall) is shown for scale.

In summary, the structural framework and geodynamics of the Northern Apennines reflect the complex tectonic history of mountain chain. These processes produced a pervasive system of tectonic discontinuities that condition both the morphology and slope stability of the range. As a result, the geomorphic evolution of the Alpe di Succiso area and the Northern Apennines more broadly cannot be understood without recognizing the fundamental role of tectonic stress and deformation in shaping both the bedrock fabric and the distribution of DFs.

3.3 Geomorphological Framework

The geomorphological framework of the Northern Apennines is characterized by a complex interaction of tectonic evolution, lithological heterogeneity, climatic factors, and erosional processes (Ricci Lucchi, 1986; CNR Geomorphology Research Group, 1982). The Apennine ridge serves as the primary morphological boundary separating two major drainage systems: the Emilian sector, which directs its hydrological flow northeastward into the Po River basin, and the Tuscan sector, which discharges toward the Ligurian Sea via the Magra and Serchio river systems (Puccinelli et al., 2015; CNR Geomorphology Research Group, 1982).

A crucial factor influencing the geomorphology of the area is its litho-structural framework. Relatively competent lithological units, such as the arenaceous sequences of the Macigno Formation

and other turbiditic sandstones (including the Monte Modino Formation), favour the development of steep slopes and prominent landforms, particularly where these units are exposed along structural highs or valley flanks (Emilia-Romagna Region, Natura 2000 Network, 2016). These sandstone-dominated successions commonly form high ridges and cliffs, where discontinuities such as joints and bedding planes predispose the rock mass to planar and wedge failures.

In contrast, slopes developed on clay-rich or tectonically disrupted units, such as the Canetolo and Subligurian units, exhibit more subdued morphologies and are frequently associated with landslides, debris flows, and plastic deformation processes (Remitti et al., 2007). These units have undergone intense shearing related to subduction and nappe stacking, which has significantly reduced their mechanical strength and favoured the development of deep-seated earth flows and complex landslides (Bertolini et al., 2005, 2017). The contrast between competent sandstones and weak, highly deformed units results in marked spatial variability in slope stability and geomorphic expression.

Structural control is also evident at the valley and catchment scale. Major drainage networks, including the Enza, Secchia, and Dolo streams, commonly follow fault-controlled lineaments or zones of lithological contrast, reflecting the strong influence of tectonic structures on landscape organisation (Conti et al., 2020). In the Valmozzola sector, for example, the Ghiare antiform and associated fault systems have been shown to localise large landslides, with tension cracks, counter-slope scarps, and failure surfaces closely corresponding to mapped fracture and joint sets (Carlini et al., 2016). These observations indicate that debris flows and related mass-movement processes can be interpreted not only as geomorphic responses to climatic forcing, but also as indicators of active or recently reactivated tectonic structures within the Northern Apennines (Crosta & Clague, 2006; Carlini et al., 2017).

From the perspective of glacial geomorphology, the region presents compelling evidence of significant Quaternary glaciations. Cirques (Figure 3.7a), moraines (Figure 3.7b), and glacial troughs predominantly characterize elevations exceeding 1,500 m. The Alpe di Succiso, along with Monte Acuto and Monte La Nuda, contains well-preserved cirques and moraine deposits, which are remnants from the Last Glacial Maximum (LGM), during which an extensive system of glaciers occupied the inner regions of the principal valleys (Federici & Tellini, 1983; Baroni et al., 2018). These

glacial features, generally retained on north-facing slopes between 700 and 2,000 m, highlight the asymmetric glaciation pattern prevalent within the Northern Apennines. The geomorphological map of the study area was produced for the first time as part of this research, providing a detailed and systematic representation of landforms and surface processes. This map offers new insights into the spatial organization of geomorphological features. A comprehensive description and interpretation of the mapped units, together with the applied mapping methodology, are presented in Chapter 4**.**

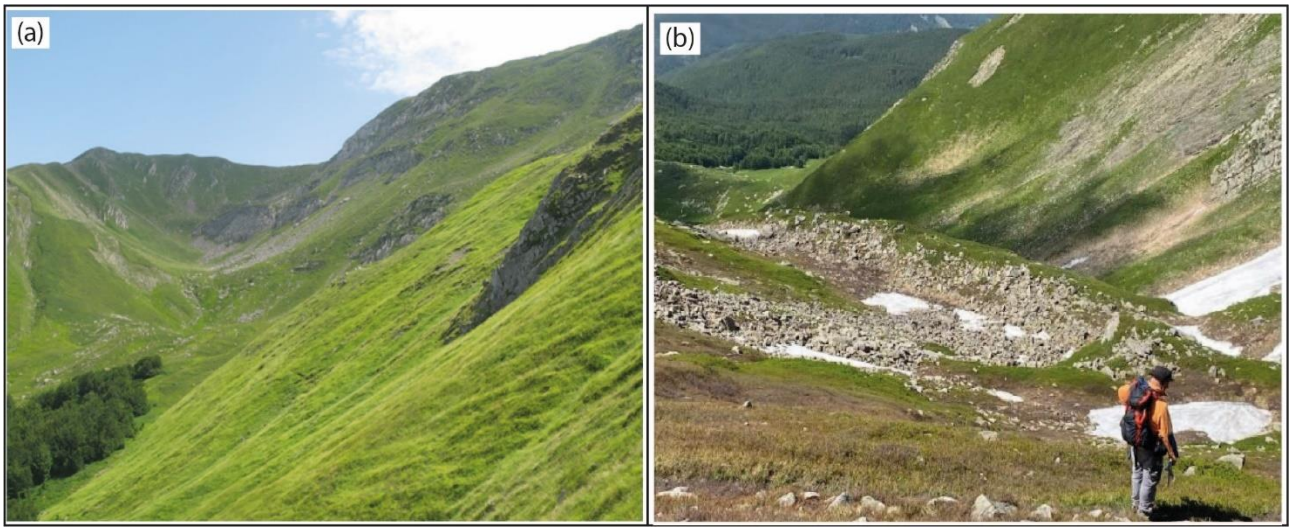

Figure 3.7: (a) Large Glacial cirque located between Alpe di Succiso and Monte Casarola; (b) Frontal moraine, oriented NS, located within the large glacial cirque between Alpe di Succiso and monte Casarola, along the northern slope.

The geomorphological dynamics of these glacial occurrences encompass the development of glacial lakes, which are frequently impounded by terminal moraines or glacial deposits, as evidenced in the Liocca and Secchia valleys. During the LGM, glaciers originating from cirques situated between Monte Acuto and Alpe di Succiso converged into a single glacier tongue, advancing into the Liocca Valley, while an additional glacier traversed the upper Secchia Valley, extending as far as Cerreto Alpi (Giraudi, 2004).

Following glacial and periglacial morphogenesis, the landscape has undergone further additional alteration. Features such as nivation hollows, frost-shattered debris fields, and gelifluction lobes are common features, especially at higher elevations and in areas without forest cover (CNR

Geomorphology Research Group, 1982). These periglacial processes were particularly active during the colder periods of the Late Pleistocene and Holocene.

Mass wasting and river erosion have dominated geomorphic processes throughout the Holocene and into the present day. Landslides of varying magnitudes occur often and represent ongoing risks in the region, owing to a mix of steep slopes, water saturation, weak lithologies, and active tectonics (Elter et al., 1997; Puccinelli et al., 2015). Areas with flysch, clay, and mélange units are more vulnerable. Back-tilted slopes, scarps, counter slopes, and interrupted drainage networks all provide evidence of historical and active landslides. Landslide-prone formations include the Canetolo Clays and the Ottone Flysch (Bertolini & Pellegrini, 2001).

In conclusion, the geomorphology of the Northern Apennines illustrates the interaction of tectonics, differential erosion, glaciation, periglacial and paraglacial (Ballantyne et al., 2002), and modern fluvial and gravitational processes. These forces have created a complex terrain in which ancient orogenic features coexist with dynamic surface processes, making it an ideal setting for researching mountain landscape formation in a tectonically active environment (Marroni et al., 2010; Baroni et al., 2018).

4. Quantitative characterization of geomorphological and topographical features of debris-flow channels at the Alpe di Succiso mountain, Northern Apennines (Italy)

Muhammad Ahsan Rashid*, Giovanni Leonelli, Alessandro Chelli

Department of Chemistry, Life Sciences & Environmental Sustainability, University of Parma, Parco Area delle Scienze, 157/a 43124 Parma, Italy

* Corresponding author: muhammadahsan.rashid@unipr.it

The paper corresponding to the content of this chapter has been published in Journal of Maps in 2024

4.1 Abstract

This paper proposes the combination of the traditional method of geological and geomorphological mapping with a quantitative approach on landforms and channels formed by debris flows by means of GIS software. The landforms around the Alpe di Succiso (Northern Apennines, Italy) are, in general, characterized by glacial and cryoclastic landforms and deposits, slope landforms and deposits due to gravity (particularly DF) and running waters. This work presents a geomorphological map of the area with the various landform features reported in a GIS environment using a high-resolution DEM (5 m). It enhances geomorphological analysis and mapping by utilizing geomorphometric parameters to quantitatively compare the parameters of channels for susceptibility and hazard mapping. The methodology applied to the channels is based on the geomorphometric parameters derived from the DEM, including Topographic Wetness Index (TWI), Terrain Ruggedness Index (TRI), Slope Angle, and Elevation extracted every 10 m along each channel and grouping the channels in four classes based on their lengths. Within each class, multiple ranking criteria were employed for the identification of channels showing anomalous or common patterns

in the geomorphometric parameters. DFs channels exhibit anomalous patterns in the geomorphometric parameters considered in this study, indicating significant variations in their topographical characteristics. Through channel analysis of slope angles, it is observed that differences in deposition pattern between DFs and debris cones in the surroundings of the Alpe di Succiso influenced by slope angle.

Keywords

Geomorphological mapping, Debris flow, Topographic Wetness Index, Terrain Ruggedness Index, Slope Angle, GIS analysis

4.2 Introduction

Recent decades have seen an increasing use of geomorphological mapping in spatial planning and environmental studies (Macchi et al., 2023; Magliulo & Valente, 2020; Seijmonsbergen, 2013). According to Dykes (2008), geomorphological mapping is a fundamental tool for analyzing landforms at any spatial scale, as it can reveal evidence that may not be easily observed in the field. Modern geomorphological mapping technologies besides expert-based observations include GIS-based techniques, and the availability of aerial and satellite images (Bufalini et al., 2021). According to Dramis et al. (2011), geomorphological maps provide a standardized way to represent landforms, geomorphic processes, and near-surface materials by documenting the spatial distribution, shape, and relationships of features across a landscape. Apart from its scientific significance, geomorphological maps are an important tool for hazard assessment (Chelli et al., 2021; Parry, 2011), land management and planning (Devoto et al., 2012), and the visualization of landscape characteristics for tourism and education (Bollati et al., 2017).

In order to improve the interpretation of landforms and processes, manual mapping based on remote sensing and Digital Elevation Model (DEM) data is greatly aided by visualization approaches (Daxer, 2020). Important factors for the geomorphometric examination of channels in mountain environments include elevation, slope angle, Topographic Wetness Index (TWI), and Terrain Ruggedness Index (TRI) (Wilson & Bishop, 2013). Slope angle and elevation are primary geomorphometric parameters used to characterize slope instability (Çellek, 2020). TWI and TRI are

secondary geomorphometric parameters used to characterize and describe soil moisture patterns (Buchanan et al., 2014; Riihimäki et al., 2021; Winzeler et al., 2022) and local relief characteristics (Różycka et al., 2017). Chen & Lee, (2010) as well as Kang et al. (2017) analyzed DF initiation by examining topographic features, such as slope gradient, terrain curvature, TWI, and elevation, which influence where and how debris flows are triggered. Mueting et al. (2021) identified DF channels by segmenting channels into finer sections, allowing for more detailed analysis of the erosion, transport, and deposition of the debris along the flow path. For the identification of DF and landslides, the accuracy and resolution of a DEM impact on the terrain analysis, detection of landform features, and the ability to accurately model geomorphological processes (Tarolli & Fontana, 2009). High quality DEMs at spatial scale of 1-5 m are required to better recognize local morphology and to detect the topographical signature of DF incision (Purinton & Bookhagen, 2017; Roering et al., 2013). To observe the behavior of debris flows, a geomorphometric approach has considerable potential.

The present study through geomorphological mapping in a GIS environment, proposes a quantitative characterization of geomorphological features and assessment of common patterns and anomalies of geomorphometric parameters in channels (some of them presenting debris flows) developed around the Alpe di Succiso, Northern Apennines (Italy).

4.3 Study Area

The study area covers 32.54 km², and is centered around the Alpe di Succiso peak, extending from an altitude of 960 m a.s.l. to the altitude of 2017 m a.s.l. which corresponds to the elevation of the peak itself (Figure 4.1).

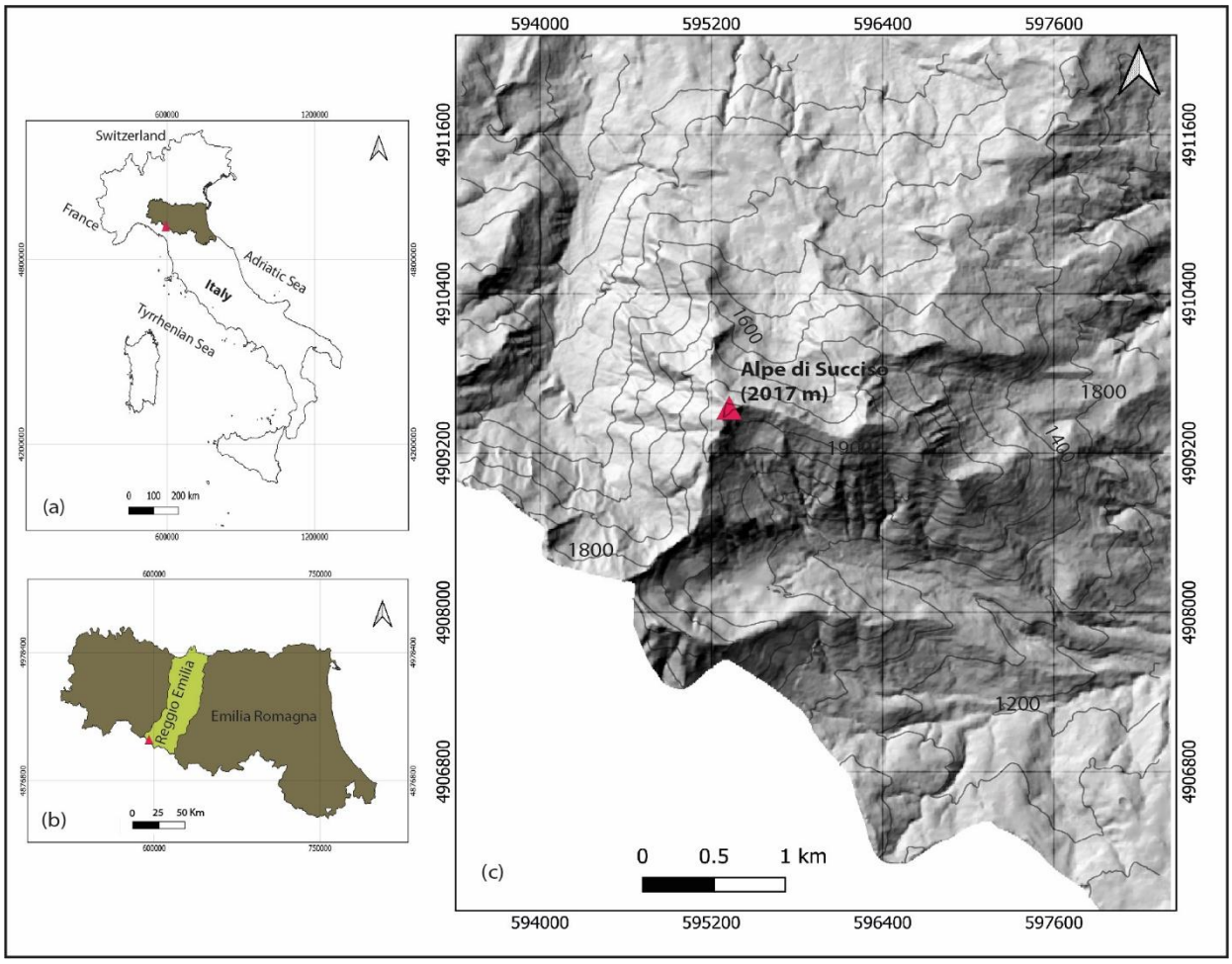

Figure 4.1: Figure (a) illustrates the study area location within Italy, highlighted by a red triangle. Figure (c) offers a detailed topographic map of the Alpe di Succiso mountain and its surroundings, with the peak also indicated by a red triangle. Contour lines show elevation changes, and the study area's coordinates are provided using the EPSG: 25832—ETRS89/UTM zone 32N coordinate system.

4.3.1 Geological and Geomorphological Setting

The landforms and deposits present in the surroundings of Alpe di Succiso are the product of different processes (glacial, gravitational, and due to running waters) which derived from the evolution of the morpho-climatic conditions that have affected the study area over the late Quaternary. The moraines and glacial cirques located at different altitudes are evidence of a stage-type retreat of the glaciers, as already highlighted for the Apennines (Federici, 1979; Federici and Tellini, 1983), which began after the Last Glacial Maximum (Giraudi, 2004) and presumably ended before the Holocene (Bertoldi et al., 2007). Baroni et al. (2018) also discussed the Last Local Glacial Maxima (LLGM) by ^{10}Be dating and found that this occurred 21,000 years ago in the Northern Apennines. In Alpe di Succiso area the LLGM occurred at 20,340 ± 820 years ago.

The morphology deposits found in the study area reveal that at least three valley glaciers shaped the area, which developed starting from the slopes of the Alpe di Succiso. Processes of gravity and running water are primarily responsible for contemporary and ongoing morphogenesis. The distribution of deposits is influenced by the physical and mechanical properties of the rocks and soils, in addition to the terrains morphology and slope steepness. The rocks are highly fractured and undergo mass movements.

According to the Geological Map (ISPRA, 2015), the studied area featured outcrops from the Canetolo Unit (Subligurian Domain) and to Tuscan Nappe (Tuscan Domain). *The Canetolo clay and limestone* (Upper Paleocene-Middle Eocene, Subligurian Domain) are black and dark grey argillites where calcilutites, calcarenites, arenites, siltites and turbiditic limestones or marly-limestones are intercalated. *The Canetolo clay and limestone* is a highly tectonized succession, due to the Apennine orogenic, and therefore makes it challenging to interpret. The Tectonic Unit of the Tuscan Nappe, which is part of the Tuscan Domain, described in the Geological Map (ISPRA, 2015), is represented by *Monte Modino* sandstone (Upper Oligocene- Lower Miocene), which are siliceous-clastic turbidites in thick beds with intercalation of metric to decametric sequences of calcilutites, arenites, and marls or argillites; the *Argillaceous limestone succession*(Lower Cretaceous-Upper Cretaceous), characterized by argillites interbedded with beds of limestones or marly limestones; the *Macigno* sandstone (Upper Oligocene-Lower Miocene), a turbiditic sequences with thick to very thick beds of limestone; *Cavernous limestone* (Upper Triassic), primarily composed of dolostones, dark dolomitic limestones, gypsum, anhydrites, and breccias; and *Rivaccia quartzite* (Upper Triassic), consisting of quarzitic sandstones.

4.4 Materials and methods

A Digital Elevation Model (DEM) with 5 m resolution was used as the base dataset for geomorphological mapping in a GIS environment (https://geoportale.regione.emilia-romagna.it/catalogo/dati-cartografici/altimetria/layer-2). Fieldwork was carried out to identify and characterize the geomorphological features in the surroundings of Alpe di Succiso. High resolution satellite imagery from Google Earth, a 1:10000 Regional Technical Map, and geological data taken from the Fivizzano sheet 234 geological map (ISPRA, 2015).

Following the acquisition in the field of geomorphological data, the maps were scanned at a high resolution (1200 dpi) to be digitalized and georeferenced in QGIS version 3.36.0. The mapping was carried out considering the guidelines (ISPRA, 2007; ISPRA & AIGeo, 2022) and the methods outlined in relevant geomorphological mapping literature (Farabollini et al., 2021; Campobasso et al., 2018; Chelli et al., 2015; Griffiths et al., 2011).

Once the geomorphological map was completed, it was redrawn on the hill shade DEM, and quantitative measurements of the geomorphological features surrounding Alpe di Succiso were taken with the help of QGIS (3.36.0) tools and additional plugins. Thus, for the characterization of landforms and deposits in the surroundings of the Alpe di Succiso, mean elevation was used to represent the height of the landforms, providing a central reference point for comparing the features across the study area, offering a clearer understanding of where most deposition occurs.

To characterize the channel features of the research area, a variety of data sources were used, including maps of the (see main map): (a) Topographic Wetness Index, (b) Terrain Ruggedness Index, (c) slope angle, and (d) elevation. The TWI predominantly relies on slope and is frequently utilized in research on superficial hydrological processes (Różycka et al., 2017). It serves as a valuable tool for predicting soil moisture levels and facilitates the examination of topographic influences on the hydrological response within a watershed. TWI (Dagdelenler et al., 2015; Gruber & Peckham, 2009; Różycka et al., 2017; Sørensen et al., 2006), can be calculated as Equation (4.1).

$$TWI = ln(\frac{a}{tan\beta}) \quad (4.1)$$

where a is the upslope catchment area and $tan\ \beta$ defines the tangent of local slope angle.

The Terrain Ruggedness Index (Equation 4.2) is used to measure how rugged the terrain is.

$$TRI_{r,c} = \sqrt{\sum_{i=r-1}^{r+1} \sum_{j=c-1}^{c+1} (e_{i,j} - e_{r,c})^2} \quad (4.2)$$

where $e_{r,c}$ is the elevation of the central grid cell at row r and column $e_{i,j}$ are the elevations of the surrounding cells within a 3×3 neighborhood. TRI is regarded as a morphometric index that characterizes the heterogeneous state of a land surface (Da Silva et al., 2019; Różycka et al., 2017, Riley et al., 1999).

The slope angle is the most important factor that affects slope stability (Çellek, 2020; Saleem et al., 2019; Yilmaz et al., 2012). Elevated slope values lead to heightened gravitational forces and enhanced shear stress, thereby facilitating the activation of materials through the destabilization of their equilibrium. Slope Angle may cause an increase in debris flow susceptibility and overall slope instability (Park et al., 2016).

Elevation is an important factor that may affect slope stability, especially in relation to rock weathering, rock degradation, and cryoclastic processes related to periglacial environments at the highest elevations. Researchers have discussed elevation effects on slope stability (Ahmed, 2015; Çellek, 2020; Park et al., 2016).

The study employed a comprehensive methodology to analyze geomorphometric parameters across the study area, utilizing advanced Geographic Information System techniques and statistical analyses. For extraction of geomorphometric parameters, QGIS function points along the geometry were used to measure the distance after every 10 m along the channels. Therefore, after every 10 m measurements of TWI, TRI, Slope Angle, and Elevation were taken for the quantitative analysis. The channels varied in length, which led to their division into four classes based on their length such as Class 1 (0-300 m), Class 2 (300-600 m), Class 3 (600-900 m) and Class 4 (900-1200 m). To facilitate comparative analysis, channel lengths within each class were normalized to the maximum observed length. This standardization allowed for a clearer interpretation of mean conditions and enhanced comparison analysis among channels by using multi ranking criteria.

Spline trend lines (cubic; order = 3) were fitted along each extrapolated channel to provide a smooth representation of variability in geomorphometric data over distance. For that, R (R Core Team, 2024) was used to extrapolate the channels as well as to take the readings of topographic variables every 10 m on the spline trend lines. For the detection of anomalous patterns, the standard deviation of each channel is calculated. The channels which show high standard deviations (> 1.3) are considered anomalous channels.

For the assessment of common patterns of channels, it was necessary to remove the anomalous channels. Based on multiple ranking criteria the channels were analyzed for each variable, allowing for the detection of both common and anomalous patterns within the different channel classes. The scoring system is as follows:

- 4: channel that shows mean conditions (common patterns), where the behavior across all selected parameters falls within a similar range, indicating consistent channel conditions.
- 3: channel that shows anomalous patterns for only one selected parameter while maintaining common pattern in the remaining parameters.
- 2: channel that shows anomalous patterns for two selected parameters.
- 1: channel that shows anomalous patterns for three selected parameters.
- 0: channel that shows anomalous patterns for all selected parameters, indicating a complete lack of conformity.

Moreover, the debris-flow source area was analyzed by using the previously mentioned geomorphometric parameters. Values were collected every 10 meters within the source area to identify the parameter values associated with debris flows triggering.

The analysis of channels is conducted to quantify their geomorphometric parameters, which are essential for understanding sediment transport processes and hydrological behavior. This assessment also aids in detecting anomalous channels. By categorizing channels into distinct ranks, the methodology allows for the targeted assessment of anomalous segments, which is crucial for understanding potential instability and sediment transport behavior.

4.5 Results and Discussion

4.5.1 Geomorphological mapping

The geomorphological map is produced on the DEM to collect quantitative data and information. The geomorphological map on the DEM has enhanced the accuracy of landforms. The total area covered by the map encompasses of 4.63 km². In our study area, the most frequent landforms are moraine deposits, covering 74% of the region, followed by landslide deposits at 9%, as depicted by the pie chart (main map (g)). Other notable features include deposits by water and relict scree slopes, each accounting for 4%, while debris cones (active and relict) constitute 3% and 0.5%, respectively. Debris flows make up 3%, deposits due to gravity account for 2%, and marsh deposits cover 0.3%. The least prominent feature is the active scree slope, representing just 0.2%. This

distribution highlights the dominant glacial and gravity-driven processes shaping the Alpe di Succiso area.

4.5.2 Glacial and cryoclastic landforms and deposits

In glacial and cryoclastic category, features such as glacial cirque scarp, moraine deposit, and denudational slopes are present. The cirques are forms of glacial erosion. The moraines deposits observed in the surrounding Alpe di Succiso are prominently featured in the geomorphological map, highlighting their spatial distribution and significance of landscape. These deposits are found on all sides of the peak, occupying both the bottom and flanks of the main valleys of the area and the bottom of the cirques in all directions. Moraine deposits are made up of clasts, from gravel to blocks, sandstone of the Macigno and Monte Modino formations and have a clastic support, with angular to rounded clasts, with a heterogeneous texture that varies from centimeter to meter. Mean elevation of features are used to provide consistent, generalized measures for comparing different geomorphological features across the study area. It helps to identify the typical elevation ranges where specific processes occur. The mean elevation of moraine deposits varies from 1200 to 1821 m a.s.l. in the surroundings of Alpe di Succiso.

The intense fracturing affecting the rocks outcropping in some slopes of the study area could be mainly due to the alternation of freeze thaw cycles (mechanical weathering). This intense fracturing, which characterizes denudational slopes of cryogenic origin, is observed on the northern slope of Alpe di Succiso at a mean elevation of 1815 m a.s.l.. The intense fracturing mainly related to the Pleistocene and Holocene as already observed in other parts of the Northern Apennines, as in the higher portion of Parma and Cedra valleys (Chelli & Tellini, 2001; Chelli & Tellini, 2002).

4.5.3 Slope landforms and deposits due to gravity

Multiple features of depositional and erosional landforms have been observed in the surroundings of Alpe di Succiso. The depositional landforms include debris cones, debris flows lobes and levees, areas affected by solifluction and deposit caused by gravity, like landslide and scree slopes. Erosional landform including scarps have been mapped. A total of twelve debris cones and four debris-flow channels were identified around the Alpe di Succiso area (main map). Among the twelve debris cones, two are not associated with any visible channel, four are connected to active debris-flow channels, and the remaining cones are related to relict channels. In addition, four debris-flow

channels currently show evidence of activity. The debris flows have been observed on the northern side of Alpe di Succiso (main map(f)). The features of debris flow at the Fossa Lattara site include levees (Figure 4.2a) and lobes (Figure 4.2b). The debris flows cones (Figure 4.2c) are made by coalescent lobes. The lobes are characterised by a steep to very steep frontal scarp, whereas smaller lobes are mainly concentrated within the lobe body and toward the distal tail, as observed at the Ghiaccioni site. They in general are elongated following the slope. Furthermore, in the northern side of the Alpe di Succiso, the debris flows are found on gentle slopes angles from 16° to 19° (main map(e)) while on the western slope the debris cones deposits are on steep slopes from 27° to 34°.

The variations in the mean elevation of the debris flow deposits provide important insights into the spatial distribution and activity level of the debris flow deposits. The mean elevation of active debris flow deposits varies from 1510 m a.s.l. to 1758 m a.s.l. on the northern and southern side respectively, suggest that material is still being actively transported and deposited at these elevations. The active debris cones on the northern and western side, ranging from 1221 m a.s.l. to 1755 m a.s.l. The wide range of elevations for these deposits reflect the changing intensity of flow events over time or variations in the volume of material being transported. The debris cones on the southern and northern flanks, occur between mean elevations of 1331 m a.s.l. and 1861 m a.s.l.. The lack of clear indicators of recent reworking, together with their well-defined cone morphology, suggests limited recent debris-flow activity; nevertheless, further geomorphic or biological indicators would be required to confirm stabilization of the deposited material.

Solifluction is responsible for the stepped shape of some slopes caused by the presence of small-size lobes and characterized by finer size of the material involved, from matrix supported pebbles to granules. This is observed on the northern side of the Alpe di Succiso peak (active) mean elevation varies from 1506 m to 1755 m, while the southern side has relict solifluction at a mean elevation of 1582 m.

A scree slope is present at the base of the cliff composed of highly jointed rock and is mainly developed on the southern side of the area. Although the morphoclimatic conditions favouring scree production (gravity-driven rockfall and cryonival processes) are still active, this scree slope shows limited evidence of recent material supply compared to the northern side. Its surface morphology, partial stabilization, and absence of fresh rockfall accumulations suggest a reduced or episodic activity rather than a fully active scree system (Figure 4.2d). The north side active scree slope

deposits are found at mean elevation of 1702 m a.s.l. to 1710 m a.s.l. while the southern side active scree slope observed at mean elevation from 1803 m to 1819 m. Relict scree slope on the northern side found at mean elevation 1799 m a.s.l. while on south side it varies from 1287 m a.s.l. to 1737 m a.s.l. The eastern side deposit was found at a mean elevation of 1338 m a.s.l.

Figure 4.2: Geomorphological Features (a) Debris Flow Heaps (Levee Deposits), (b) Debris Flows (Lobe Deposits), (c) Debris Cone, (d) Scree Slope.

On the northern flank of Alpe di Succiso, evidence of translational slide deposits is evident, while translational landslides are also observed at east and south direction. On the north side the landslide deposits are found at a mean elevation of 1291 m a.s.l., on the eastern side it varies from 1547 m a.s.l to 1699 m a.s.l., while on the southern side at a mean elevation of 1671 m. Gravity deposits were observed on the western slope at mean elevation varies from 1443 m a.s.l to 1604 m a.s.l.

A clearer pattern emerges where active geomorphological processes occur on the northern and western side of the Alpe di Succiso, suggesting ongoing material movement and instability in this direction. In contrast, the southern and eastern sides are characterized by relict or more stabilized deposits.

4.5.4 Deposits due to running waters

The deposits due to running waters are evident on the western side at mean elevation varies from 1210 m a.s.l. to 1284 m a.s.l. These deposits are the result of fluvial processes and formed by channelized water flow. They are at the end of short and steep channels and are mainly made by debris from pebbles to cobbles. These flows formed thick, poorly sorted sediment accumulations, reflecting high energy transport conditions and limited downstream reworking, while marsh deposits are found on the south side at mean elevation of 1505 m.

4.5.5 Classification of Channels Profiles

Geomorphological and hydrological modeling is an important application of DEMs (Wilson & Bishop, 2013), and channel network extraction is a necessary step before channel profile analysis (Purinton & Bookhagen, 2017). In Figure 4.3, the trends of TWI, TRI, Slope Angle, and Elevation of all four classes (depending on the channels lengths) can be observed. By analyzing 26 channels around the Alpe di Succiso, the mean conditions (common patterns) were identified while anomalous channels were excluded. It can be observed that the standard deviation of the anomalous channels (Table 4.1) is between 1.35 to 3.25 times higher than that of the mean conditions (common patterns) (Table 4.2), varying across different classes. The anomalous channels exhibited significant variations in standard deviations as well as exhibiting different trends, including sudden increases and decreases in the geomorphometric parameters over specified lengths due to erosion and deposition of rock and soil in the channels. These variations did not align with the common patterns. The TRI, Slope Angle, and Elevation show that with an increase of channel length, all three parameters decrease while TWI increases. A second order Polynomial function is observed on the mean condition of the trends in all classes.

Table 4.1: Assessment of Anomalous channels for various classes of geomorphometric parameters.

	TWI stedv	TRI stedv	Slope Angle (°) stedv	Elevation (m a.s.l.) stedv
Class 1	0.34	1.82	5.92	55.43
Class 2	1.69	1.94	6.54	232.60
Class 3	1.01	1.95	6.58	177.84
Class 4	1.03	2.28	8.34	92.47

Table 4.2: Assessment of mean Conditions (common patterns) for various classes of geomorphometric parameters.

	TWI stedv	TRI stedv	Slope Angle (°) stedv	Elevation (m) stedv
Class 1	0.22	0.82	2.51	30.67
Class 2	0.52	1.20	4.84	79.20
Class 3	0.78	1.23	4.34	96.78
Class 4	0.50	1.28	4.67	48.36

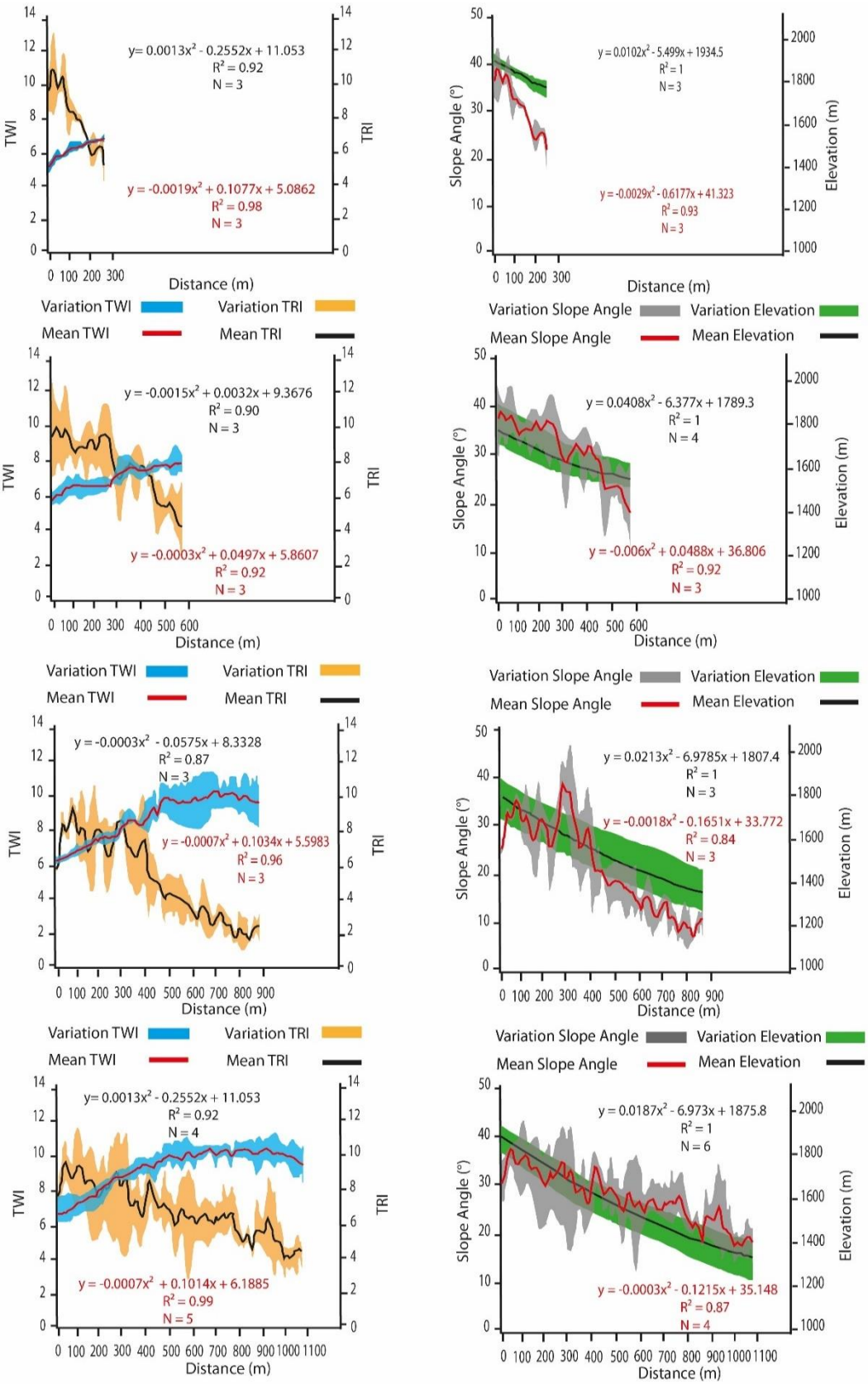

Figure 4.3: Channels Profiles: Class 1 (0-300 m) (figure a & b), Class 2 (0-600 m) (figure c & d), Class 3 (0-900 m) (figure e & f) and Class 4 (0-1200 m) (figure g & h). N is the number of channels which have been considered for the mean conditions (common patterns). The shaded region shows the variability of common patterns channels. Black and red lines showing the average of the common patterns.

4.5.6 Characterization of Channels based on ranking Criteria

Multi-ranking criteria was employed to analyze the channels (Figure 4.4), assigning scores based on the patterns observed in selected parameters (Table 4.3). The total rank of 4 is used for the multi-ranking criteria, corresponding to four parameters: TWI, TRI, slope angle and elevation. Each channel was evaluated across all four parameters. Channels that fell within the mean conditions (Common patterns envelop) were assigned a score of 1, while those outside the common patterns were assigned a score of 0. This technique simplifies channel assessment by quantifying and comparing multiple geomorphometric parameters, helping to identify which channels follow consistent patterns and which deviate. It provides a clear, objective way to detect anomalies and assess the stability or risk of individual channels.

Table 4.3: Multiple Ranking Criteria of channels. A score of 1 indicates that the channel adheres to the mean conditions (common patterns) while a score of 0 signifies that the channel exhibits anomalous behavior, deviating from the common patterns.

Channel No.		TWI	TRI	Slope Angle	Elevation	Total Rank
1	Active Debris Flow 1	1	1	1	1	4
3		1	1	1	1	4
17		1	1	1	1	4
2	Active Debris Flow 2	0	1	1	1	3
5		1	1	1	0	3
11	Inactive Debris Flow	1	1	1	0	3
18		1	1	1	0	3
6		1	0	0	1	2
8	Active Debris Flow 4	0	1	1	0	2
10	Inactive Debris Flow	1	0	0	1	2
15	Debris Flow Heaps 3	0	1	1	0	2
19		0	1	1	0	2
20		1	0	0	1	2

21	Inactive Debris Flow	1	0	0	1	2
24		1	0	0	1	2
25		1	0	0	1	2
7		1	0	0	0	1
9	Inactive Debris Flow	0	0	0	1	1
16		1	0	0	0	1
22	Inactive Debris Flow	0	0	0	1	1
23	Inactive Debris Flow	0	0	0	1	1
26		0	0	0	1	1
4	Active Debris Flow 3	0	0	0	0	0
12	Debris Flow Heaps 4	0	0	0	0	0
13	Debris Flow Heaps 1	0	0	0	0	0
14	Debris Flow Heaps 2	0	0	0	0	0

4.5.7 Mean conditions (Common Patterns) comparison with active debris flow channels

Różycka et al. (2017) employed TWI and TRI to characterize landslide terrains, whereas Da Silva et al. (2019) utilized spatial correlation analysis among TWI, TRI, and slope angle to establish the geomorphometric diversity index. Chen & Lee (2010) delineated the initiation of debris flows through the application of TWI and slope angle. It is an effective approach to check the debris flow channels in comparison to the mean conditions of other channels. Our study offers valuable insights into the geomorphometry of debris flow channels through the integration of diverse parameters such as TWI, TRI, slope angle, and elevation.

The debris flow channels are compared with the mean conditions of channels. Debris flow channels show variations with respect to the mean conditions (common patterns). Overall, 26 channels have been analyzed. As depicted in Fig. 4.4, changes in channels colors correspond to their respective rankings. It is observed that out of 8 active debris flow channels on the northern and western side of Alpe di Succiso, four channels are showing Rank 0, while two channels with rank 2, one channel

is with rank 3 while one channel is with rank 4. It can be observed that only debris flow channels exhibit rank 0 (i.e. 50% of the debris-flow channels in the study area). This suggests that debris flow channels undergo consistent erosion and deposition processes, which caused high st.dev. The other four debris-flow channels show higher ranks up to with rank 4 (one channel shows complete compliance with mean conditions of channels in the area).

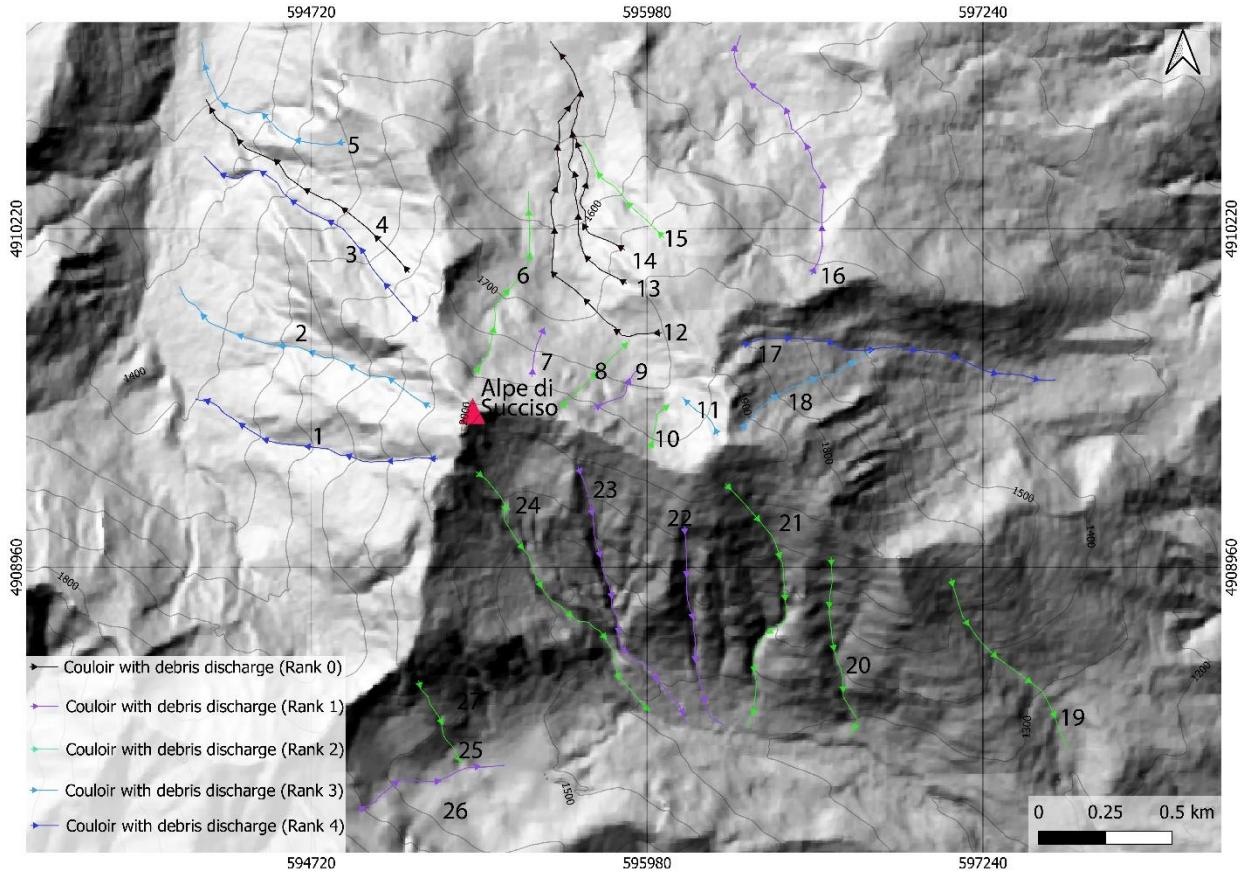

Figure 4.4: Multi-ranking criteria are employed to analyze the channels. The dark blue color (rank 4) indicates common patterns in all selected parameters in the selected group while light blue color (rank 3) exhibits anomalous patterns for only one selected parameter in the selected channel class. Moreover, green color (rank 2) shows anomalous patterns for two selected parameters in the selected group while purple color (rank 1) reveals anomalous patterns for three selected parameters in the selected group. Additionally, black color (rank 0) indicates anomalous patterns for all selected parameters in the selected group. Channels no. 1-26 refer to the same identifiers used in the text and table 4.3 (EPSG: 25832—ETRS89/UTM zone 32N coordinate system).

It is observed that channels that are classified as anomalous channels do not exhibit abnormality throughout the entire length; instead, certain segments of channels exhibit anomalous traits, which arise from specific irregularities within those segments. As a result, understanding the nature and location of these anomalies is crucial for accurately assessing the overall behavior of the channels.

This method can also be applied to design susceptibility maps which are necessary steps for hazard analysis. This approach is also beneficial in mitigation measures of debris flows.

4.5.8 Characterization of Debris Flow Source Zone

In this study, various topographic indices were employed to discern the relationship between geomorphological characteristics and the initiation of debris flow. According to Kang et al. (2017) slope is the most significant parameter in the debris flow initiation process. According to our obtained results, the mean values of slope of the source area is observed between 32° and 42° which is in the range of previous debris flow source area studies (Chen & Yu, 2011; Takahashi, 1981; Hungr et al., 1984; Rickenmann & Zimmermann, 1993). The TWI values for the source area of debris flow are highlighted in table 4.4. The results are aligned with previous research (Park et al., 2016; Chen & Lee, 2010). The TRI range in debris flow source area ranges from 8.13 to 11.16 while elevation varies from 1656 to 1929 m a.s.l.

Table 4.4: Mean values of topographical parameters in the source area of active debris flow with standard deviation (stedv). This table summarizes the average topographical characteristics of specific debris cones and debris flow heaps, calculated in the source area where these flows originate.

	TWI; stedv	TRI; stedv	Slope Angle (°); stedv	Elevation (m a.s.l.); stedv
Debris Cone 1	6.56; 0.54	9.02; 0.87	35.85; 2.77	1890.60; 19.83
Debris Cone 2	6.99; 0.20	8.81; 0.55	35.61; 1.82	1857.55; 21.23
Debris Cone 3	6.78; 0.25	8.98; 0.79	35.89; 2.71	1656.28; 21.25
Debris Cone 4	4.84; 0.24	11.16; 1.00	42.22; 2.33	1929.24; 15.72
Debris Flow Heaps 1	6.81; 0.30	8.19; 1.41	32.60; 4.82	1718.29; 18.97
Debris Flow Heaps 2	7.38; 0.23	8.32; 0.81	33.53; 2.72	1683.28; 16.70
Debris Flow Heaps 3	8.99; 0.17	8.13; 1.40	32.70; 4.60	1712.89; 20.22
Debris Flow Heaps 4	5.93; 0.19	8.27; 1.23	33.47; 2.54	1772.34; 22.56

4.6 Conclusions

The geomorphological map is a crucial tool for hazard assessment purposes. This study focuses on mapping all geomorphological landforms surrounding Alpe di Succiso, representing an initial approach to identifying and understanding the features and processes in the area. It is found that active debris flow activity dominates on the northern and western sides of the Alpe di Succiso. Geomorphological mapping data processed in a GIS environment together with a 5 m DEM, facilitates surface cover calculation, characterization of landforms and deposits based on mean elevation and subsequent channel analysis. Channels were categorized into four classes based on length, and the mean conditions of each class across four geomorphometric parameters were evaluated. Polynomial trends were observed in channels. To assess the channel characteristics, mean conditions and detect anomalous channels, multiple ranking criteria were employed. Mean conditions of channels compared with debris flow channels revealing that only the Debris Flow Cone 1 channel fell within the range of mean conditions across all geomorphometric parameters while the other seven debris flow channels show abnormality in different parameters. It is interesting to note that in 26 channels only debris flow channels exhibit rank 0, indicating significant erosion and deposition. Consequently, these channels differ from the common envelope. This differentiation underscores the importance of monitoring these anomalous channels to assess potential risks associated with debris flows and informs future research and management efforts aimed at understanding and mitigation geomorphological hazards. It has been observed that the slope angle is the cause of difference in the deposition pattern between debris flows (16° to 19°) on the northern side of Alpe di Succiso and debris cones (27° to 34°) on the west side of Alpe di Succiso. Additionally, analysis of the source area of debris flow channels was observed by using all geomorphometric parameters to analyze the factors that cause the debris flows around the Alpe di Succiso. Furthermore, a detailed study of channels is required to analyze the anomalous parts of debris flow channels to enhance the understanding of the mechanism of debris flows in channels.

Software

QGIS 3.36.0 software is applied to process the geomorphological map, area calculation of geomorphological landforms, and channel analysis. For extrapolation of channels RStudio software is used.

Funding

This work has benefited from the framework of the COMP-HUB and COMP-R initiative of the University of Parma, funded by the 'Departments of Excellence' program of the Italian Ministry for Education, University and Research (MIUR, 2018-2022 and 2023-2027). This work has been also financed by the European Union – Next Generation EU / PRIN-PNRR, PRIN 2022 PNRR - Projects of Great National Interest: project DECC - Debris flow hazard and climate change in the Northern Apennines: reconstructing and modelling past and future environmental scenarios, CUP D53D23022810001, and University of Parma-PhD School of Earth Sciences, research fund XXXVIII_SCIENZE_TERRA_QUOTA10.

Geological and Geomorphological Map of Alpe di Succiso (Northern Apennines, Italy)

Muhammad Ahsan Rashid, Giovanni Leonelli, Alessandro Chelli
Department of Chemistry, Life Sciences & Environmental Sustainability,
University of Parma, Parco Area delle Scienze, 157/a 43124 Parma, Italy

Bedrock

- Canetolo Clays and Limestone (Upper Paleocene - Middle Eocene)
- Monte Modino Sandstone (Upper Oligocene - Lower Miocene)
- Clayey Limestone Succession (Lower Cretaceous - Upper Cretaceous)
- Macigno Sandstone (Upper Oligocene - Lower Miocene)
- Cavernoso Limestone (Upper Triassic)
- Rivacca Quartzite (Upper Triassic)

Structural Data

- Lithologic Boundary
- Bed Attitude

Glacial and Cryoclastic landforms and deposits (relict)

- Scarp of Cirque
- Moraine Deposit
- Denudational slope of cryoclastic origin

Slope Landforms and Deposits due to Gravity

- Degradational and/or Landslide Slope (active)
- Scarp of Debris Flow (active)
- Debris Cone (active)
- Debris Cone (relict)
- Couloir with debris discharge (active)
- Couloir with debris discharge (relict)
- Stream
- Scree Slope (active)
- Scree Slope (relict)
- Deposit by gravity (active)
- Translational slide body (relict)
- Debris flow heaps (active)
- Area affected by solifluction (active)
- Area affected by solifluction (relict)

Deposits due to Running Water (active)

- Deposit by Running water
- Marsh deposit

Coordinate system

EPSG: 25832 -ETRS89/UTM zone 32N

Location Map

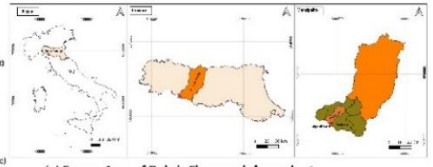

(e) Source Area of Debris Flows and channels at Fossa Lattara site, viewed from (h) in the SE direction

(f) Debris Flows deposits in Fossa Lattara site

(g) Quantitative Assessment of Landforms

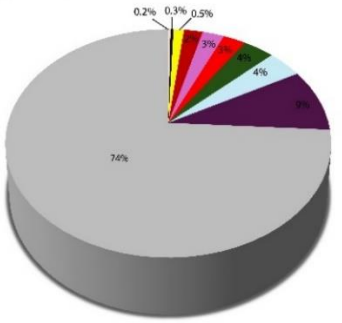

Geomorphometric parameters (a) TWI; (b) TRI; (c) Slope Angle; (d) Elevation

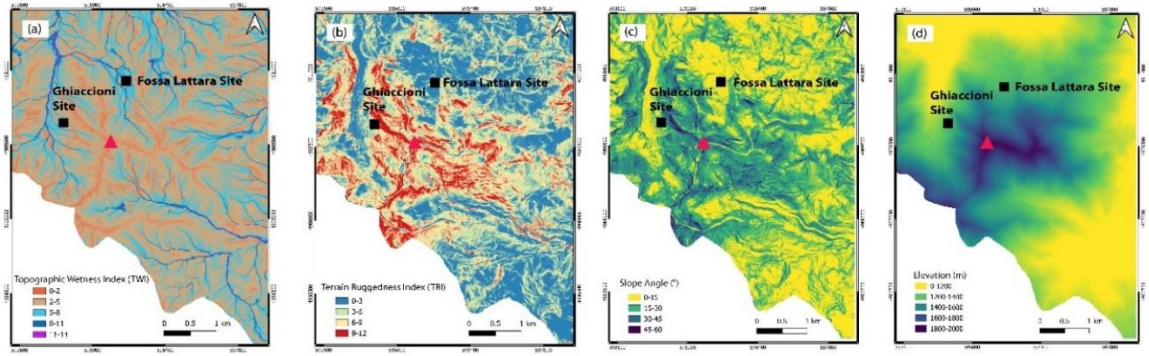

5. Multi-disciplinary reconstruction of debris flow events and dynamics in the Northern Apennines, Italy: A multi-scale approach linking ground evidence with climatic triggers

Muhammad Ahsan Rashid[1], Alessandro Chelli[1], Emma Petrella[1], Sara Pescio[1], Jacopo Melada[2], Veronica Manara[2], Bruno Arcuri[2], Maurizio Maugeri[2], Michele Brunetti[3], Luca Trombino[4], Anna Masseroli[5], Giovanni Leonelli[1]

[1] Department of Chemistry, Life Sciences and Environmental Sustainability, University of Parma, Parco Area delle Scienze, 11/a, 43124 Parma, Italy

[2] Department of Environmental Sciences and Policy, University of Milano, Via Celoria 2, 20133 Milano

[3] Institute of Atmospheric Sciences and Climate (CNR-ISAC), Bologna, Via P. Gobetti 101 40129

[4] Department of Earth Sciences, University of Milano, via Mangiagalli 34, 20133 Milano

[5] Department of Agricultural and Environmental Sciences, University of Milano, via Celoria 2, 20133 Milano

*Corresponding author

E-mail address: muhammadahsan.rashid@unipr.it

This chapter was published in Catena in 2026.

5.1 Graphical Abstract

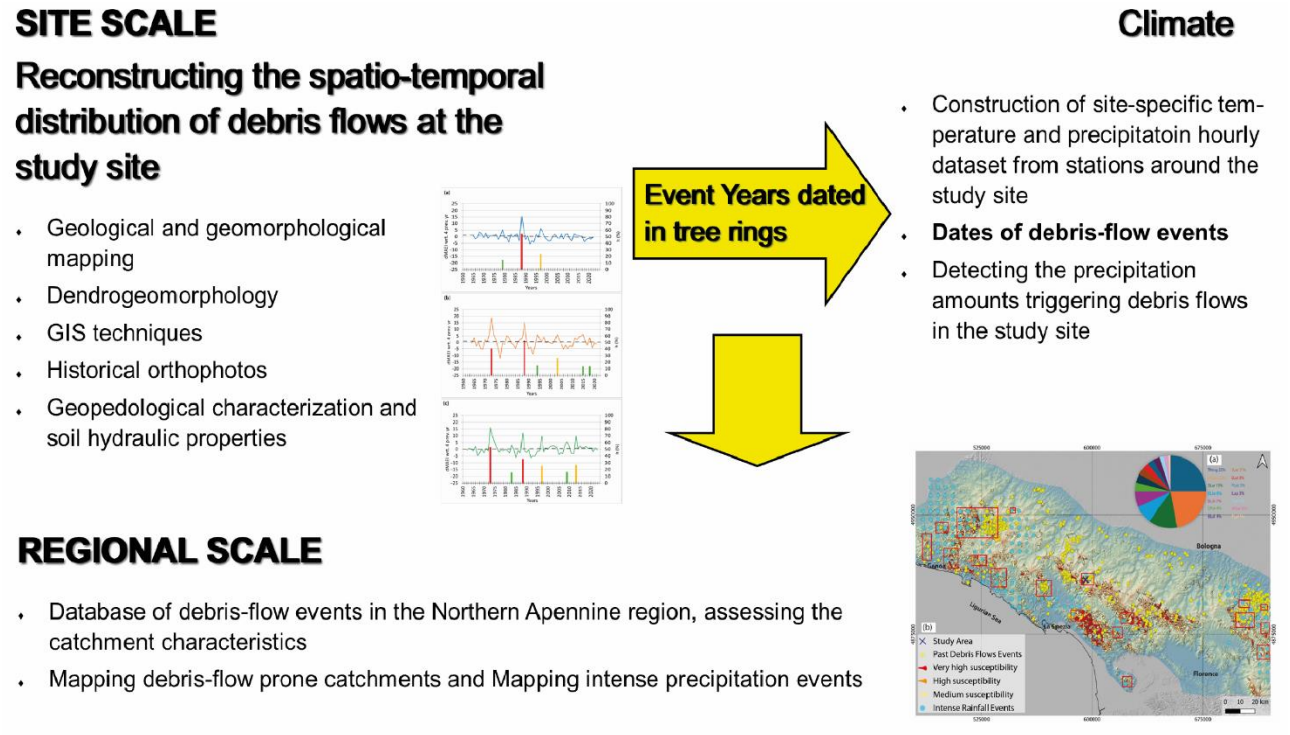

5.2 Highlights

- Reconstructed six decades of debris flows (DFs) events using tree-rings, geomorphic and climatic data
- Identified major and intermediate DF events based on dendrogeomorphological evidence
- Linked (dendro-identified) event years with hourly precipitation to determine DFs dates and triggering conditions
- Regional integration of DF-prone areas with spatial pattern of intense rainfall to identify DF hotspots

5.3 ABSTRACT

A multidisciplinary approach is used to reconstruct debris flow (DF) events and extent through time in a remote (data scarce) site located in the Northern Apennines, Italy. Field-based techniques such as geomorphological mapping of the area, dendrogeomorphological dating and the characterization of soils and water infiltration processes were integrated with the analysis of precipitation triggers and temperatures to reconstruct the sequence of DF events over the last 70 years. Major DF events detected by comparing the dendrochronological evidence and climatic data, occurred in 1972 and 1987 disturbing up to 54 % of the sampled trees, whereas intermediate events occurred in the years 1996, 2003 and 2013 with 20–30 % of disturbed trees. Minor events were characterized by less than 20 % of disturbed trees, indicating limited geomorphic impact and localized disturbance. Historical orthophotos analysis directly confirmed most of the events in chronology as well as their spatial patterns. The analysis of the site-specific hourly precipitation records highlighted that not all high rainfall events resulted in DFs occurrence. Such chronologies are valuable because DF inventories often lack nondamaging events. A database of approximately 500 DFs occurred in the region of the Northern Apennines was analyzed using composite susceptibility index (CSI) and lithology to provide broader context. Results highlight three main situations in the investigated region: i) areas of intense precipitation and corresponding DF-prone catchments and observed DFs, along the Northern Apennine ridge in East and West sectors; ii) areas of intense precipitation events over non-DF-prone catchments and without observed DF in the far-West sector; iii) areas along the mountain ridge where DFs are observed despite the absence of intense precipitation in the central sector. By integrating a multi-disciplinary approach to analyze the DFs, this study advances understanding of DF dynamics and provides a framework for improved hazard assessment in mountain environments.

Keywords: Debris flow; Dendrogeomorphology; Climate change; Intense precipitation; Soil saturation, Northern Apennines

5.4 Introduction

Debris flows (DFs) are among the most destructive geohazards in mountainous regions worldwide, characterized by the rapid entrainment and transport of sediments, water and air, either in a pseudo one-phase (Wang et al., 2015) or in a solid-liquid two-phase flow (Bout et al., 2018). DFs pose significant threats to human life, property, and infrastructure because of their high velocity, large sediment loads, and sudden onset (Mikoš and Bezak, 2021). DFs are triggered by factors such as intense precipitation and/or rapid snowmelt, earthquakes, and anthropogenic activities like unplanned development of infrastructures, mining, rock blasting, and slope deforestation, these slope processes may cause widespread socio-economic and environmental impacts (Segoni et al., 2024). DFs often occur in small catchments and may initiate from the slopes (hillslope DF) or through the reactivation and mobilization of in-channel sediment deposits (channelized DF), typically under the influence of extreme rainfall events (e.g., Du et al., 2021; Forte et al., 2025). Countries such as Switzerland, Italy, China, Japan, Colombia and Peru, present regions prone to geomorphic instability and face significant DF risks (Zhang et al., 2024).

DFs have a close relationship with climate and mostly are triggered by prolonged and/or intense rainfalls (Chen and Chen, 2022). Water infiltration and soil saturation are becoming increasingly critical issues under changing climate conditions. Rapid infiltration of prolonged intense rainfall causes soil saturation and a transient increase in pore-water pressure, which has important implications for slope DF initiation (Stoffel et al., 2024). Climate has several impacts on slope stability, and reconstruction of past DFs may be analyzed for detecting the climatic triggering factors on a variety of time scales. Increase in intense rainfall, under climate change may alter the frequency of DFs. It is vital to have a better understanding of how the frequency of DFs may change in the future, particularly for planning decisions in such mountainous environments, where settlements are often located on alluvial fans.

A number of researchers have worked on the interaction of DFs and precipitation (e.g., Grimsley et al., 2016; Tichavský et al., 2022; Šilhán et al., 2023). According to Myhre et al. (2019) a doubling of heavy precipitation events per degree of warming has been observed over Europe, mostly due to both increasing frequency (number of events/year) and an increase in intensity, the first one being the leading driver. However, several studies focusing on specific smaller regions do not confirm the same tendency. Specifically, Ulbrich et al. (2012) reported that no coherent signals emerge

throughout the whole Mediterranean basin; Scherrer et al. (2016) highlighted an increase in some indices of daily precipitation extremes starting from the beginning of the 20th century for Switzerland. Brugnara and Maugeri (2019) documented important regional differences in intense precipitation trends across the Alpine area; Pavan et al. (2019) found a very heterogeneous tendency in Northern Italy, both in precipitation intensity and in 90-th percentile events.

Where interacting with forests, DFs may damage trees causing scars on the stems and anomalies in the growth processes: with appropriate tree-ring analysis it is therefore possible to assess the spatial distribution of DF events through time in specific sites. Dendrogeomorphology aims at reconstructing the sequence of instability events by yearly dating them on the mid- to long-time scales, by analyzing trees that are affected by geomorphological processes. DFs may cause sudden physical stress on trees, such as reduced tree-ring widths after stem burial, eccentric growth due to stem tilting, up to the formation of reaction wood (Wistuba et al., 2013). The analysis of tree rings may play a critical role in hazard assessment, providing essential information on past activity and relative spatial distribution, especially in forested sites where other techniques may fail (Leonelli and Pelfini, 2013; Wistuba et al., 2013; Stoffel et al., 2014; Šilhán and Stoffel, 2015; Germain et al., 2018; Leonelli et al., 2021; Ballesteros-Cánovas et al., 2023; Tichavský, 2023; Šilhán et al., 2024).

Reconstructing the sequence of past DF events through time (by dating them), opens the possibility of analyzing the corresponding precipitation events, thus providing significant insights for modeling DF dynamics with precisely detected inflow amounts. By reconstructing event chronologies with high temporal resolution, typically annual and sometimes seasonal or monthly, researchers can link these events to specific extreme hydrometeorological conditions, as proposed by Schläppy et al., (2016) with avalanches. There are different ways to analyze the link between geomorphic activity and hydrometeorological triggers which require diverse analytical approaches, and each has its own strengths and limitations. Site monitoring is considered as the most precise approach for real-time observation; however, it is often impeded by deficiencies in past data, making it less effective for long-term studies (Hürlimann et al., 2019).

The study area (Alpe di Succiso, Northern Apennines) has experienced numerous DF events, making it a key site for geomorphic studies as it is under semi-natural conditions. Densely traversed by hiking trails, the area attracts mountaineers, hikers, and visitors, emphasizing the need to

understand the spatial and temporal distribution of this hazard also in relation to the precipitation events. These implications are crucial for risk assessment and for implementing effective safety measures to protect both the natural environment and the people who visit it.

This study employs a multi-disciplinary framework to analyze geomorphic activity and its underlying triggers, by applying site-scale investigations with overview of broader regional analyses. At the study site of Fossa Lattara, geological and geomorphological mapping, dendrogeomorphology, GIS techniques, historical orthophotos, geopedological characterization and soil hydraulic properties have been integrated with the analysis of precipitation data, delivering a comprehensive understanding of spatio-temporal patterns and environmental interactions. This multi-disciplinary combination has ensured cross-validation of results, enabling precise and detailed reconstructions despite the absence of prior temporal and spatial information of DFs in the study area.

At the regional level, a database of documented DFs has been set up for the Northern Apennines to provide a broader context for DF hazard assessment. Numerous researchers have investigated DEM-derived indices to assess DF susceptibility (Bertrand et al., 2013; Ilinca, 2021; Jakob et al., 2022). This study conducted an extensive geomorphometric analysis including Melton Ruggedness Index (MRI), Hypsometric Integral (HI), average slope, and channel gradient indices together with the hydro-geomorphological Stream Power Index (SPI) to analyze DFs drainage basins in the Northern Apennines. This methodology provides a quantitative basis for the regional assessment of catchment susceptibility and supports the development of more efficient risk mitigation strategies.

The overall objective is to bridge multiple disciplines to gain valuable insights that advance both academic knowledge and practical knowledge for DF hazard management strategies. The main objective is to characterize the spatial and temporal distribution of DFs through a multi-disciplinary approach. Another secondary objective is to assess DF catchment critical areas in the Northern Apennines by integrating the distribution of intense precipitation (last 70 years data), catchment characteristics, and lithology.

5.5 Study Area

The Alpe di Succiso mountain (2017 m a.s.l.) lies within the National Park of the Tuscan-Emilian Apennines (Figure 5.1). Beyond this site, a regional scale assessment of catchment susceptibility and lithological analysis was conducted across the Northern Apennines, spanning from Genoa to Florence.

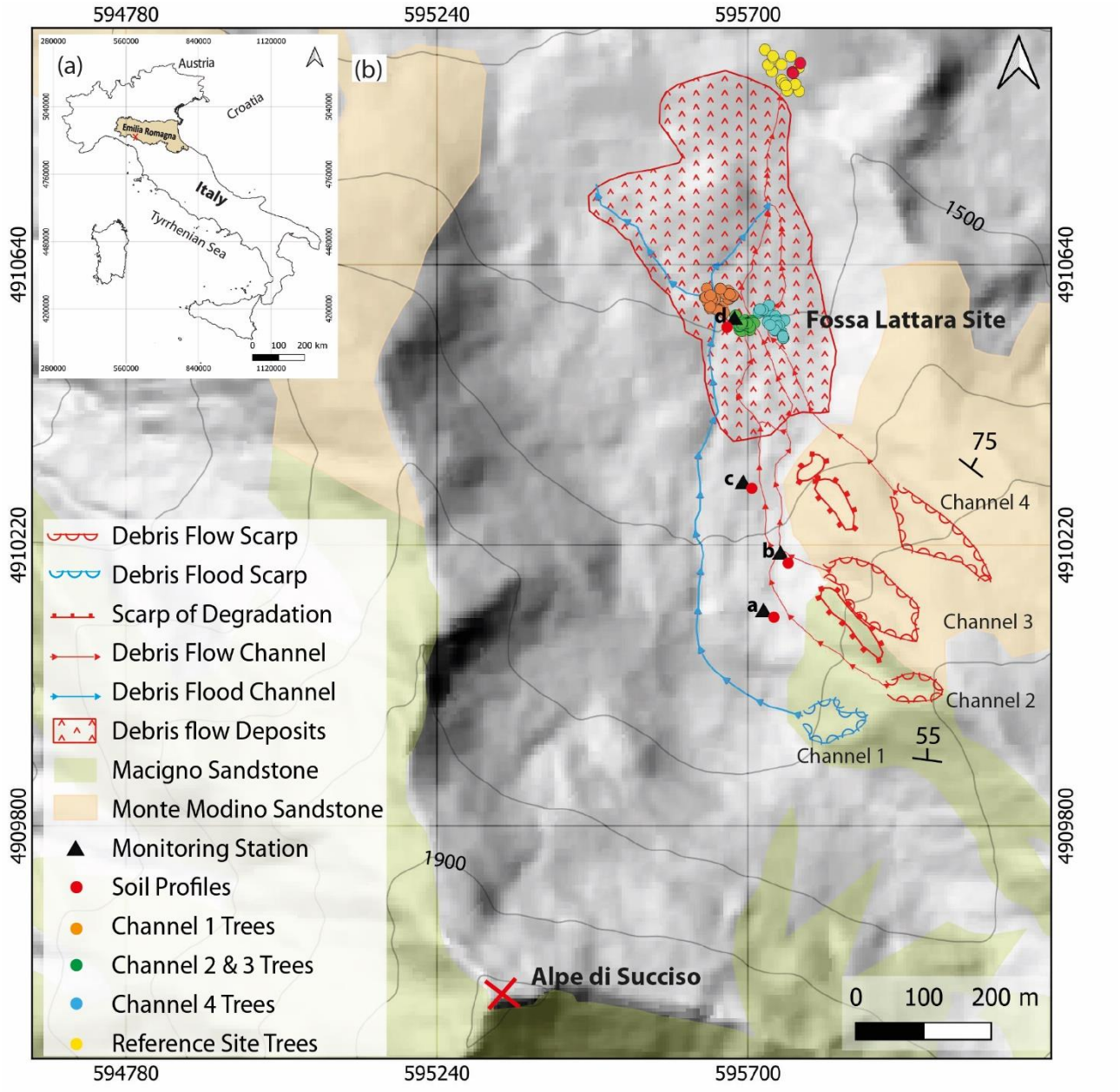

Figure 5.1: Location of the study area in Italy (a) Alpe di Succiso marked by a X. (b) Geological and geomorphological mapping of debris flows (DFs) and debris flood along with the sampled trees (colored points). Soil profiles in the DF area coincide with monitoring stations, other profiles are in the reference site outside the study site (see text). For more details of geology and geomorphology of the study area, see Rashid et al. (2024).

The landforms and deposits surrounding Alpe di Succiso have been shaped by a combination of geomorphic processes, including glacial, gravitational, and fluvial activities. These features signify the evolution of morpho-climatic conditions that have impacted the region throughout the late Quaternary period (Rashid et al., 2024). The geological framework of the Fossa Lattara site (44°20′31″N, 10°12′03″E) is characterized by the Tuscan Nappe Tectonic Unit, which is a component of the Tuscan Domain, as outlined in the Geological Map (ISPRA, 2015). This includes Monte Modino sandstone (Upper Oligocene–Lower Miocene), characterized by siliceous-clastic turbidites interbedded with sequences of calcilutites, arenites, marls, and argillites, and Macigno sandstone (Upper Oligocene–Lower Miocene), consisting of thick to very thick turbiditic strata with interspersed turbiditic limestone layers.

At the Fossa Lattara site distinct geomorphological features indicative of DFs activity have been identified, including prominent lobes (Figure 5.2a) and levees (Figure 5.2b). The levees are formed by DF deposits. These features highlight the dynamic processes that shape the landscape over time. Numerous DF events have been recorded at Fossa Lattara, with four distinct channels identified. All channels contain deposition material confined within the channels. Channel 1, notably, does not exhibit visible DF deposits in the deposition area (Figure 5.2c) probably indicating debris flood activity while debris is confined within the channel (Figure 5.2d), whereas Channels 2, 3, and 4 reveal typical characteristics of DF activity. Initial triggers, such as debris and material degradation, frequently evolve into flows that create distinct channels and deposit material along their paths. The deposits are composed of clasts ranging in size from gravel to large boulders, predominantly sourced from outcrops of weathered sandstone formations of the Macigno and Monte Modino units. Channels 1 and 2 originate from Macigno sandstone, whereas Channels 3 and 4 are associated with Monte Modino sandstone. These clasts display a heterogeneous texture, with sizes ranging from a few centimeters to several meters and shapes spanning from angular to subangular (see Rashid et al., 2024).

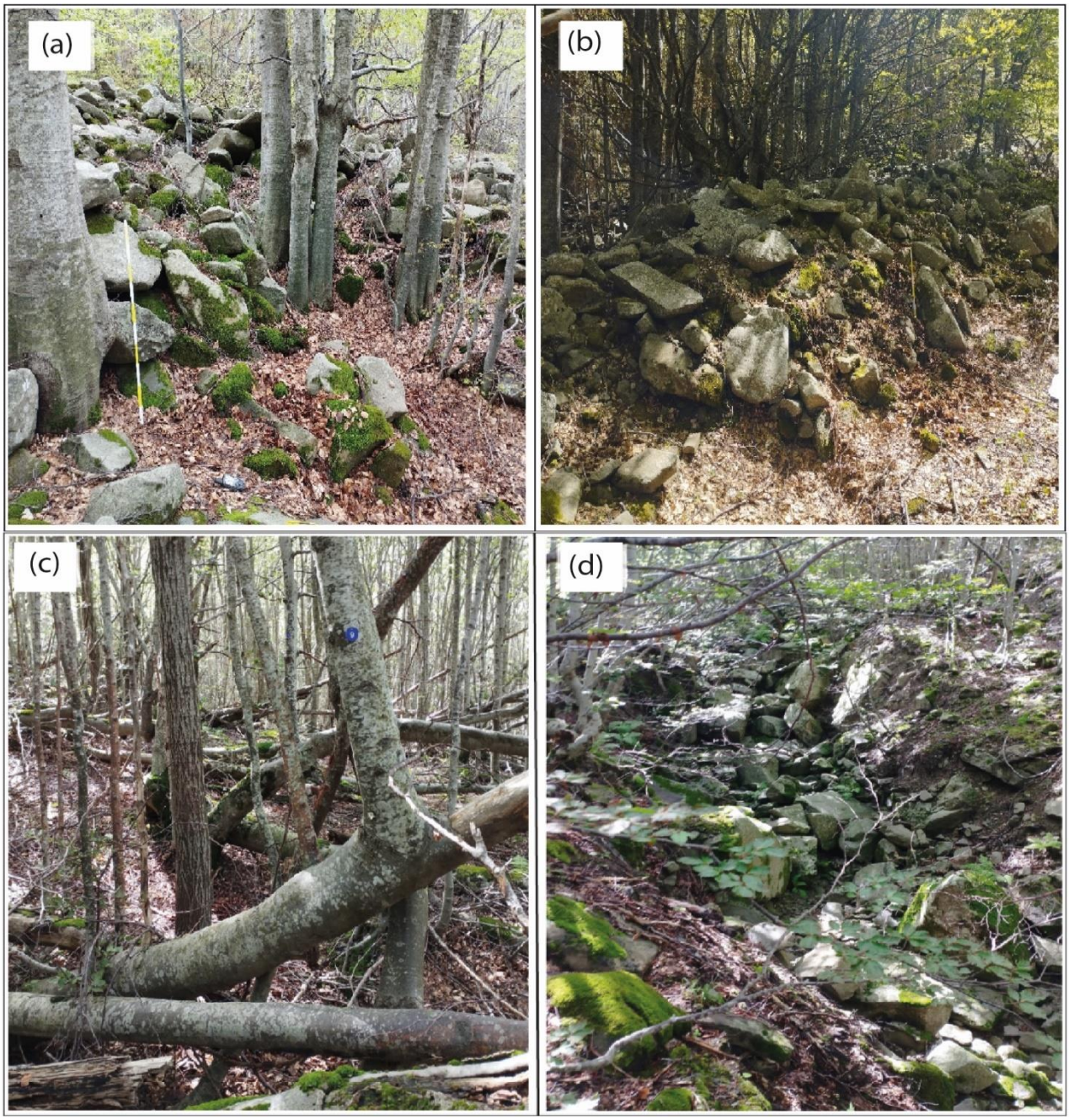

Figure 5.2: Geomorphological features in Channel 2 and 3 and Channel 4 (a) Lobe deposits, (b) Levee Deposits (c) Tilted stems and vertical adventitious branches caused by debris flood in channel 1, and (d) Debris material observed within the channel 1. Image of G.L. and M.A.R (2023). The stick is 1.30 m long.

A forest of European beech (*Fagus sylvatica L.*) characterizes the study area and plays significant importance in dendrochronological research because these trees are quite sensitive to changes in the environment, particularly those changes related to climatic variability and geomorphic disturbances. European beech growth is constrained by aridity in southern Europe and spring frosts in northern regions, with an increasing susceptibility to drought stress induced by climate change

(Eilmann et al., 2014). The radial growth of this species is profoundly affected by temperature and precipitation, particularly in Italy, where periods of summer drought significantly influence its longevity and growth dynamics (Tognetti et al., 2019). From a geopedological point of view, the Succiso area is mainly characterized by the presence of Leptosols (i.e. Umbric Leptosols) and Cambisols (i.e. Humic Cambisols), and to a lesser extent by Podzols (i.e. Haplic Podzols) (Servizio Cartografico – Ufficio Pedologico, 1994). These soils range from those that are poorly developed (Leptosols, i.e.: “Thin or with many coarse fragments” - IUSS Working Group WRB. 2022), to “Moderately developed” (Cambisols - IUSS Working Group WRB, 2022), to those that are undergoing biochemical alteration (Podzols, i.e., with “Subsoil accumulation of humus and/or oxides” - IUSS Working Group WRB, 2022).

Given the high spatial coherence of temperature variability and trends, the long-term evolution of the surface temperature in the study area can be reconstructed by interpolating the centennial temperature series available from a dense stations’ network available for the Italian territory. The temperature series reconstructed for the study site (Figure 5.3) highlights a temperature increase of 0.12°C/10-years over the period 1801-2024, with a progressive intensification of the phenomenon when the most recent period is considered. The increase is in fact 0.19°C/10-years over the 1901-2024 period, 0.35°C/10-years over the 1951-2024 period and 0.52°C/10-years over the 1981-2024 period.

Yearly total precipitation highlights strong gradients around the study site, as shown by the 1991-2020 normals of the stations in the data set presented in section 5.6 and by their projection onto a 30-arc-second grid by means of the method presented in Crespi et al. (2018) (Figure 5.4). The yearly 1991-2020 normal estimated for the Fossa Lattara site is 2143 mm, with maximum precipitation in autumn (36% of yearly precipitation falls from September to November) and minimum precipitation in summer (12% of yearly precipitation falls from June to August). The main divide of the Tuscan-Emilian Apennines turns out to be among the wettest areas in Italy because of strong orographic precipitation when atmospheric disturbances cause the advection of moist air masses from the Tyrrhenian Sea.

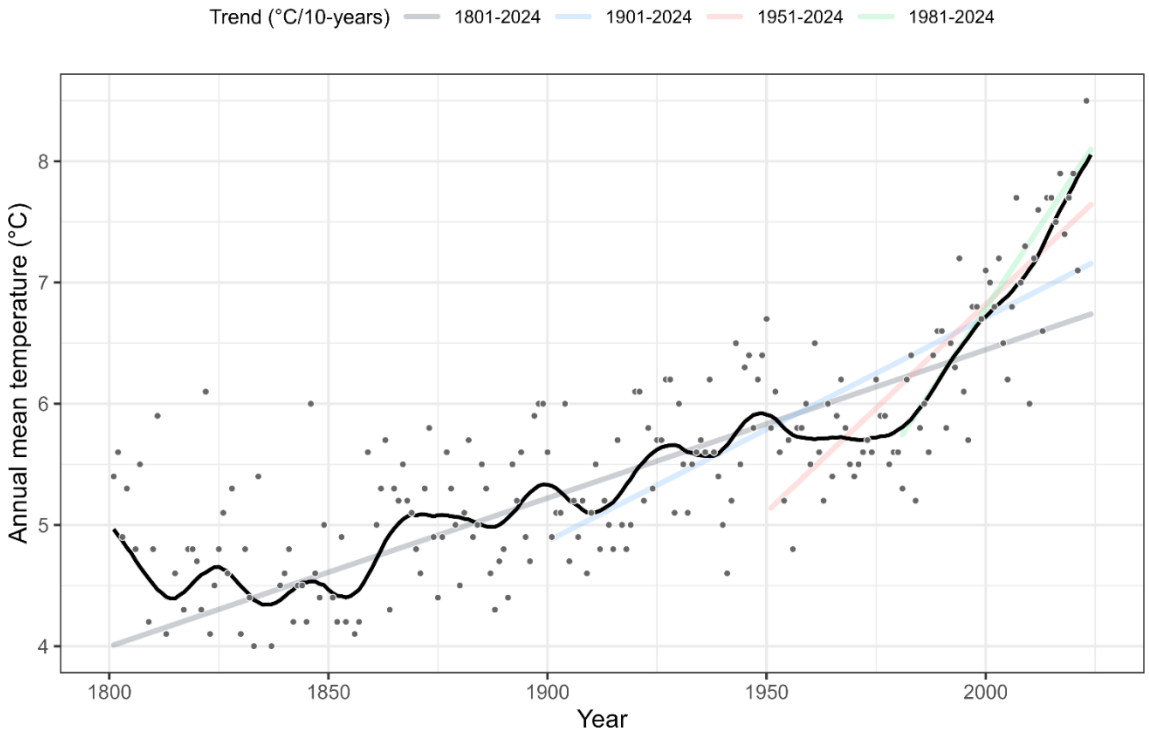

Figure 5.3: Long-term trend of the yearly average temperature (°C) at the Fossa Lattara site over the period of 1800 - 2024 plotted together with a Gaussian low-pass filter (5-year standard deviation; 21-year window).

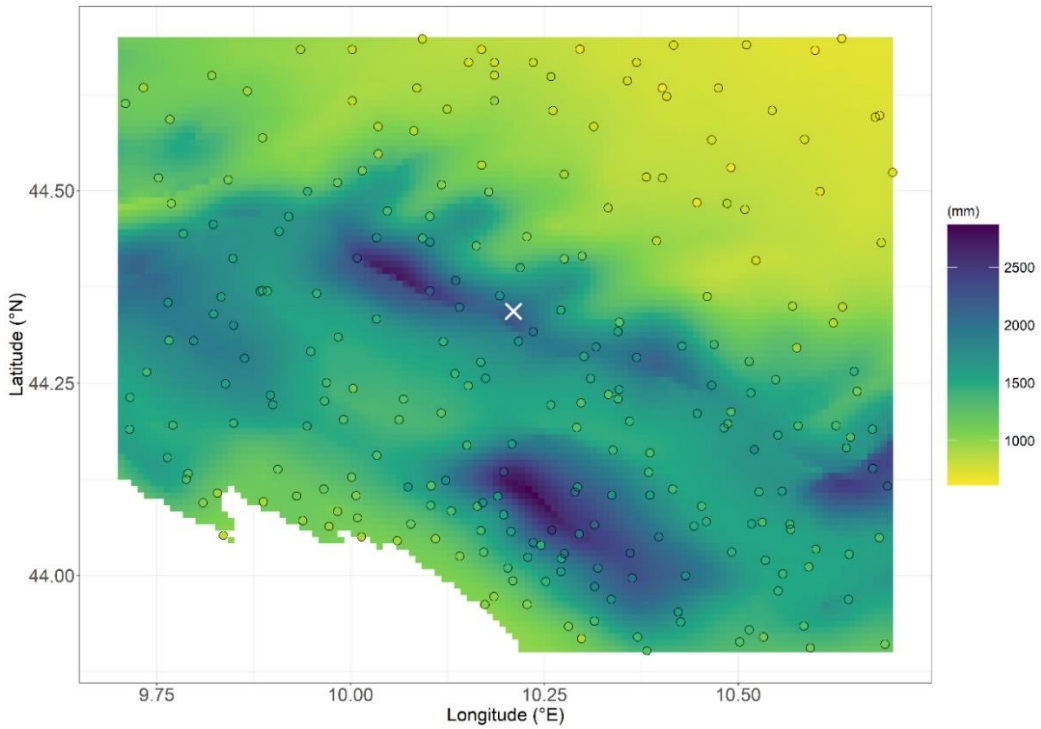

Figure 5.4: Position of the stations in the study area (circles) plotted together with the spatial distribution of the 1991-2020 yearly precipitation normals over the study area and the corresponding station normals. The white cross sign shows the Fossara Lattara site.

5.6 Materials and method

The methodological framework is designed to reconstruct DF events and their dynamics by integrating geomorphic evidence, dendrogeomorphological records, climatic triggers, soil and hydrological conditions, and catchments susceptibility and lithological analyses (Figure 5.5). To reconstruct DF events and dynamics, multiple datasets were assembled providing complementary sources of evidence at the site and regional scale. Each dataset is summarized below with its source, temporal coverage, resolution, and purpose:

- Topographic data: A Digital Elevation Model (DEM) with 5 m resolution (Rashid et al., 2024) and a 1:10,000 Regional Technical Map were used for geomorphological mapping while 10 m DEM (Tarquini et al., 2023) for susceptibility analysis.

- Geological data: Geological Map Sheet 234-Fivizzano (ISPRA, 2015) was used to characterize lithology at the site, while the 1:250,000 regional geological map (Conti et al., 2020) supported regional lithological analysis.

- Dendrochronological data: 73 European beech (*Fagus sylvatica L.*) trees were cored in the Fossa Lattara site to analyze growth disturbance and date DF events, and 15 trees from an undisturbed reference site to build a reference chronology.

- Orthophotos: Historical orthophotos (1944, 1978, 1988, 2003, 2014) were acquired from the Emilia-Romagna and Tuscany regional repositories (https://www.regione.emilia-romagna.it/; https://www502.regione.toscana.it/geoscopio/ortofoto.html). These were georeferenced in QGIS 3.36.0 and used to delineate DF extents and assess changes through time.

- Precipitation data: Daily records from 1951–2023 were retrieved from SCIA (ISPRA) and regional networks (Dext3r, SIRAL, SIR). ARCIS gridded precipitation (5 km, 1961–present) was also used, along with sub-daily extremes from Italian Hydrographic Service Yearbooks. These datasets were analyzed for trends and to identify DF-triggering events.

- Temperature data: A secular temperature anomaly record representative of the study site was constructed from the Brunetti et al. (2006, 2009) dataset.

- Soil and hydrological data: Eight soil profiles (four in DF-affected areas, four in a reference site) were excavated and described (Servizio Cartografico - Ufficio Pedologico, 1994). Four monitoring

stations with Teros probes (Meter Group) recorded soil moisture, matric potential, and temperature from June–November 2024.

- Regional DF inventory: A dataset of 511 DF initiation points compiled from Moratti and Pellegrini (1972), ISPRA (2019), Ciccarese et al. (2020, 2021), Peruccacci et al. (2023), Rashid et al. (2024), Berti et al. (2025), and the Emilia-Romagna Geoportal (https://geoportale.regione.emilia-romagna.it; accessed 27 May 2025). The purpose of the data set was to give an overview of DFs and to identify critical areas in Northern Apennines.

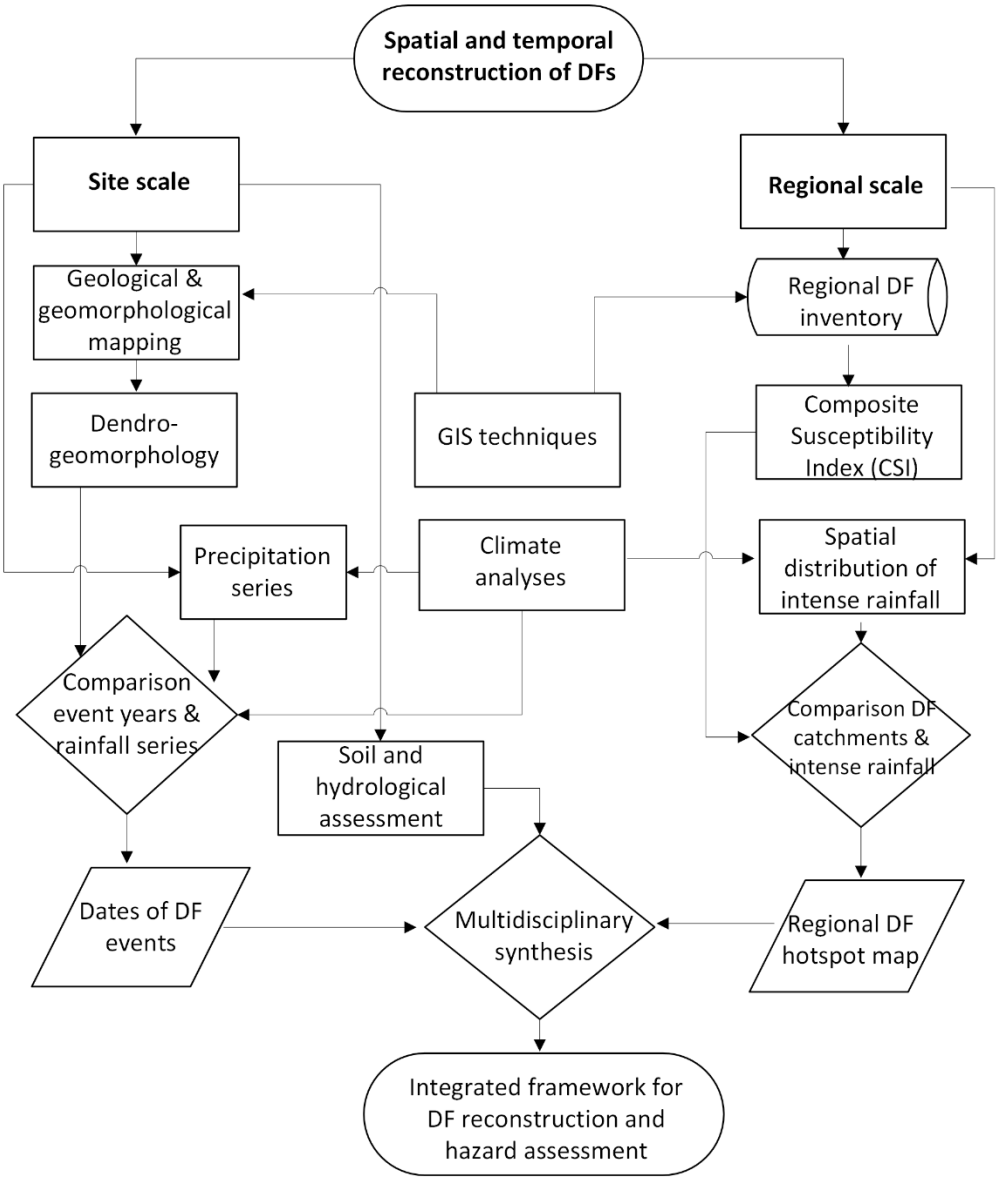

Figure 5.5: Overview of the applied methodological framework. The research was developed through site-scale and regional approaches to reconstruct debris-flow (DF) events and assess their spatial and temporal dynamics in the Northern Apennines. Oval, start/end; rectangle, process; cylinder, geodatabase; parallelogram, document output; diamond, decision.

5.6.1 Geomorphic evidence, dendrogeomorphological analysis, GIS analysis and assessment of DF extents

The study site was chosen based on field observations, and a different series of aerial photographs. Field work was carried out to identify the features of DFs such as scarps, lobes, levees, and channels. Fieldwork was conducted to identify and characterize the DFs source area, deposit areas, and channels in the Fossa Lattara site. The Fossa Lattara site was selected for detailed analysis, identifying four channels as sources of DFs as detailed in section 5.5.

A dendrogeomorphological analysis was carried out during field investigations to assess past DF activity within the forested area of the study site. Suitable trees were selected based on their location and their direct interaction with DFs. The acquired dendrochronological data were organized using GIS software to incorporate field data effectively. Trees were sampled from both DF-affected locations and an undisturbed reference site, which was then used to support the interpretation of disturbed trees, detect missing rings, and avoid misinterpreting growth changes caused by climatic variability as events of DFs. For climatic influences, an initial reference chronology was created using 15 trees growing in a reference site about 400 meters north of the study area, which served as a baseline of undisturbed growth. At the study site, specifically, 29 trees were sampled from Channel 1, 24 trees from Channels 2 and 3, and 20 trees from Channel 4. Tree cores were extracted from the trunks of tilted trees, to observe the growth anomalies and assess the dendrochronologically-detected event years. All sampled trees from the study site were georeferenced using the Trimble DA2 GNSS antenna, ensuring high-precision coordinate acquisition (Trimble, 2023). This accurate spatial positioning was essential for spatial reconstruction of DF extent and for relating tree locations to geomorphic disturbance patterns.

After collecting samples from the field, lab activities were performed to date the DF events. Laboratory preparation of samples followed standardized methods (Stokes and Smiley, 1968), with tree-ring widths measured using TSAP-WIN software by using microscope. The quality of cross-dating was verified using COFECHA (growth series from the stems of disturbed trees against reference trees), and TSAP-WIN was employed for graphical representation. A reference chronology was created using ARSTAN software (Cook, 1985).

Since bent trees were very frequent in the study area, most of DF events were dated by analyzing abrupt growth change initiations, and eccentric growth patterns. These analyses considered stem

deformation, including tilting and bending, that occurred after multiple DFs. Additional parameters, such as the Eccentricity Index (EI) and its annual variations, were calculated to identify and date historical DF events. The detection of tree-ring growth disturbances was conducted annually using a normalized difference EI, previously applied in studies such as Gattinoni et al. (2019) and Leonelli et al. (2021).

The Mean Absolute Eccentricity Index (MAEI) was employed for event dating and to identify significant geomorphic activities. Thresholds were defined to categorize DF events by MAEI values exceeding 1.5 standard deviations above the reference chronology. Many events were detected near the threshold, leading to further categorization into major, intermediate, and minor events on the basis of standard event-response (I_t) index (Shroder, 1978). Thresholds for the percentage of disturbed trees were established to strengthen the classification of event magnitudes. Major events were identified when at least 30% of trees displayed disturbances, indicating widespread impact. Intermediate events were associated with disturbance levels ranging from 20% to 30% of sampled trees. The minor events are defined as those that exhibit a disturbance level less than 20%. The thresholds were derived from the proportion of sampled trees showing growth disturbance, supported by the observed geomorphic extent of DF deposits and the spatial distribution of disturbed trees. This approach highlights the correlation between statistical thresholds and ecological responses, offering a robust framework for analyzing DF dynamics.

Additional methodologies were employed to enhance the reliability of DFs event dating. Cores extracted from vertical adventitious branches growing from horizontally tilted stems (candelabra growth) were analyzed to determine the first year of adventitious branch growth, serving for time-constraint of the tilting. This multi-faceted approach, combining tree-ring eccentricity indices with branch-core analysis, strengthens the temporal resolution and accuracy of event reconstruction. Finally, given the dormant period in trees during fall and winter months, all event years in the tree rings were compared to the climate series from August of the previous year to July of the current year in order to detect the most reliable dates of the DF events.

To ascertain the years of significant past DF events and to delineate their magnitude, an analysis of historical orthophotos was conducted allowing for accurate identification of affected trees during significant event years.

5.6.2 Site-specific precipitation dataset

Multiple datasets of precipitation records were used to define the precipitation climatology of the study site, to investigate long-term trends in precipitation-related variables and to identify precipitation patterns that could trigger DFs.

Specifically, a data set of station records was compiled for the period 1951-2023 by retrieving and integrating data from various sources, including regional and national meteorological networks, to obtain daily precipitation records from local weather stations. Data were retrieved from SCIA – the National System for the collection, processing and dissemination of climate data - of the Italian Institute for Environmental Protection and Research (ISPRA) as well as from the data sets Dext3r, SIRAL and SIR provided by the regional services of Emilia-Romagna, Liguria and Tuscany, respectively. The stations in this data set are shown in Figure 5.4, where the data set is presented more in detail and the long-term trends of precipitation, maximum 1-day precipitation, number of rainy days and precipitation intensity are presented.

The station record data set was then accompanied by the ARCIS gridded data set, covering the years after 1961, which provides daily precipitation records for Northern and Central Italy on a regular grid with a spatial resolution of 5 km, specifically developed for climatological analyses over Italy.

Finally, sub daily data concerning high-intensity precipitation events were obtained from the Yearbooks issued by the Italian Hydrographic Service (*Annali idrologici*), which provide, for some selected stations, the highest values recorded for each year over 1, 3, 6, 12 and 24 hours. The sub daily data, however, is frequently missing in the Yearbooks.

5.6.3 Geopedological characterization and hydraulic soil properties

To characterize the soil variability of the study area, eight soil profiles were excavated, observed and described. Three of these profiles (ST a, ST b and ST c) were dug above the tree line (between 1590 and 1640 m a.s.l.) on a slope covered by herbaceous and shrub vegetation. These were selected in close proximity to the DF channels 2 and 3 (Figure 5.1), while a fourth profile (ST d) was located in the DF deposition area (Figure 3), in a forest dominated by beech trees. In addition, four soil profiles (CONTR01, CONTR02, CONTR03 and CONTR04) were selected in the reference site

outside the study area, on a slope not affected by DFs at an elevation of approximately 1450 m a.s.l., in a beech forest.

Moreover, four monitoring stations were located in different representative areas affected by DFs to understand soil hydraulic properties and thus characterize the water infiltration processes. In detail, the spots consider the different land use of the area (forest vs. grassland), and the different positions related to the DF morphology (flank, steep slope, near flat area, between two DF channels) at altitudes that span from 1510 to 1640 m a.s.l. Two different types of sensors were installed in each station at two different depths along the soil. In more detail, Teros 12 (Meter) probes were used for measuring Volumetric Water Content and Bulk EC, and Teros 21 probes (Meter) for Temperature and Matric potential. The monitoring period spans from June to the middle of November 2024 including a summer-to-fall period and allowing to study water infiltration processes during the first intense precipitations after a dry period.

5.6.4 Composite susceptibility index (CSI) analysis of the catchments hosting DFs at the regional level

The Northern Apennines, extending from Genoa to Florence, were analyzed to quantify and interpret the DFs at the regional level. In this region, a dataset of 511 DF-initiation points has been compiled from a range of published sources and official databases. Each DF point was georeferenced, and associated depositional areas were delineated using topographic maps and high-resolution imagery. These depositional zones allowed for accurate delineation of DF prone catchments, which are necessary for calculating terrain-based indices. To ensure comparability among indices with different scales and units, the values of each index were normalized to 0-1 range using min-max scaling to eliminate scale effects (Wang et al., 2025a). This mean of the normalization allowed us to integrate the average value from 0-1 of MRI, HI, channel gradient, average slope and SPI. For each DF, all the indices of the corresponding catchment were computed to quantify the morphometric controls on DF initiation and assess the overview of regional susceptibility. These indices are commonly used in geomorphometric and topographic studies. The higher values of them usually indicate steep, high-energy catchments that are susceptible to the development of DFs (Wilford et al., 2004; Ilinca, 2021).

After calculating all the indices for documented DFs catchments, the lowest CSI normalized value of 0.38 was determined and subsequently adopted as the reference threshold. Using a 10 m

resolution DEM and the r.watershed tool in QGIS, catchments with a minimum area of 0.02 km² were delineated to ensure inclusion of smaller, DF prone catchments. Subsequently, all catchments across the Northern Apennines (from Liguria to the border between Emilia-Romagna and Tuscany regions) were considered to identify regions with elevated morphometric and hydro-geomorphological index values. To further analyze the most susceptible areas, the catchments were classified into five categories using a percentile-based approach. This classification ranked catchments relative to one another based on their CSI value, thereby highlighting spatial patterns in DF vulnerability. The percentile thresholds were set as follows: 0–20% (very low), 20–40% (low), 40–60% (medium), 60–80% (high), and 80–100% (very high). This classification was used to map catchments with increasing potential for DF occurrence, forming the basis for spatial hazard analysis within the Northern Apennines. Moreover, the classification was validated against the DF inventory, showing that past events are well represented at the catchment scale analysis.

To further characterize the terrain conditions under which DFs are triggered, a geological assessment was conducted using the same 511 DF initiation points. The geological units at each initiation site were analyzed based on the regional lithological map (Conti et al., 2020).

5.7 Results

5.7.1 Climate and extreme precipitation events at the study site

We have subjected the daily and monthly precipitation records presented in section 5.6.2 to several analyses to investigate long-term trends from the 1950s (Figures 5.6-5.17). Overall, the results highlight a slight and often non-significant drying mainly driven by a reduction in rainfall frequency, particularly during summer, while maximum 1-day precipitation and rainfall intensity have remained stable, contributing to the persistence of relatively constant annual precipitation totals despite some minor seasonal shifts. We have also analyzed the records of the yearly highest precipitation over 1-3-6-12-24 hours at the Succiso and Lago Paduli stations, which are both located within 5 km from the Fossa Lattara site. Even though this analysis is partially hampered by a significant fraction of missing values, it is worth noticing that no one of these records gives evidence of significant trends.

Beside to subjecting the records to trend analysis, we have also ranked stations (only stations with less than 20% of missing data in the 1962-2023 period were considered) and gridded daily precipitation data in order to identify the dates with highest amount. The most relevant event occurred 11 September 1972. This event ranks first both for the grid cell of the ARCIS data set including the Fossa Lattara site and for the three stations within 10 km from the site (Succiso, Paduli-Diga, and Collagna). All other events ranking within position 6 at the Fossa Lattara ARCIS grid cell and/or in at least one of the stations within less than 10 km from the Fossa Lattara site are listed in Table 5.1. The event on 11 September 1972 is consistently the highest in all records, reaching 376.8 mm at Succiso, 371.2 mm at Paduli-Diga, 301.0 mm at Collagna, and 314.1 mm according to the ARCIS gridded data (all ranked first for their respective series). Another noteworthy episode occurred on 11 December 2017, with daily totals of 305.4 mm at Succiso (rank 2), 203.0 mm at Paduli-Diga (rank 7), 204.8 mm at Collagna (rank 3), and 266.5 mm from ARCIS (rank 2).

Despite a general consistency in event timing among the three stations and the ARCIS dataset, significant spatial variability in daily totals occasionally emerges. For instance, on 25 August 1987, Collagna recorded its second-highest daily precipitation (220.6 mm), whereas Paduli-Diga ranked the same day only 109th (104.2 mm). Comparison with ARCIS grid data confirms that extreme precipitation signals are captured consistently in both station measurements and the gridded product, although magnitudes can differ by up to several tens of millimeters, reflecting the inherent uncertainties in spatial interpolation and the localized nature of convective storms.

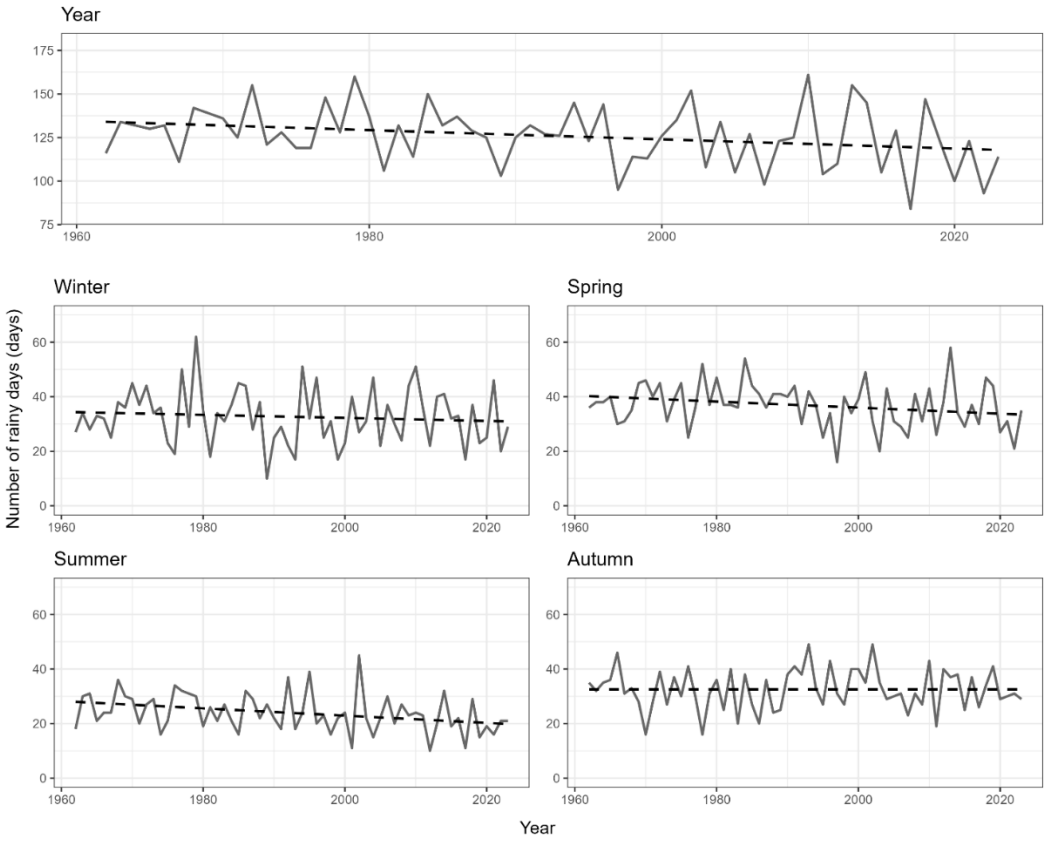

Figure 5.6: Long-term trend of yearly and seasonal precipitation (mm) at the Fossa Lattara site plotted together with a Gaussian low-pass filter (3-year standard deviation; 11-year window).

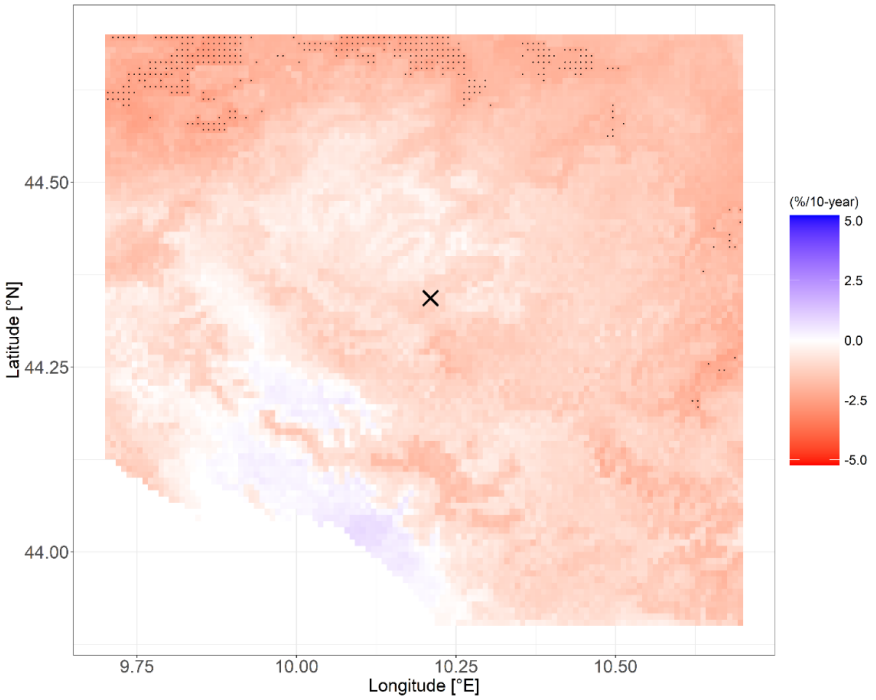

Figure 5.7: Spatial distribution of yearly precipitation trends (%/10-years) in the study area. Significant trends (p-value ≤ 0.05) are represented with a black dot.

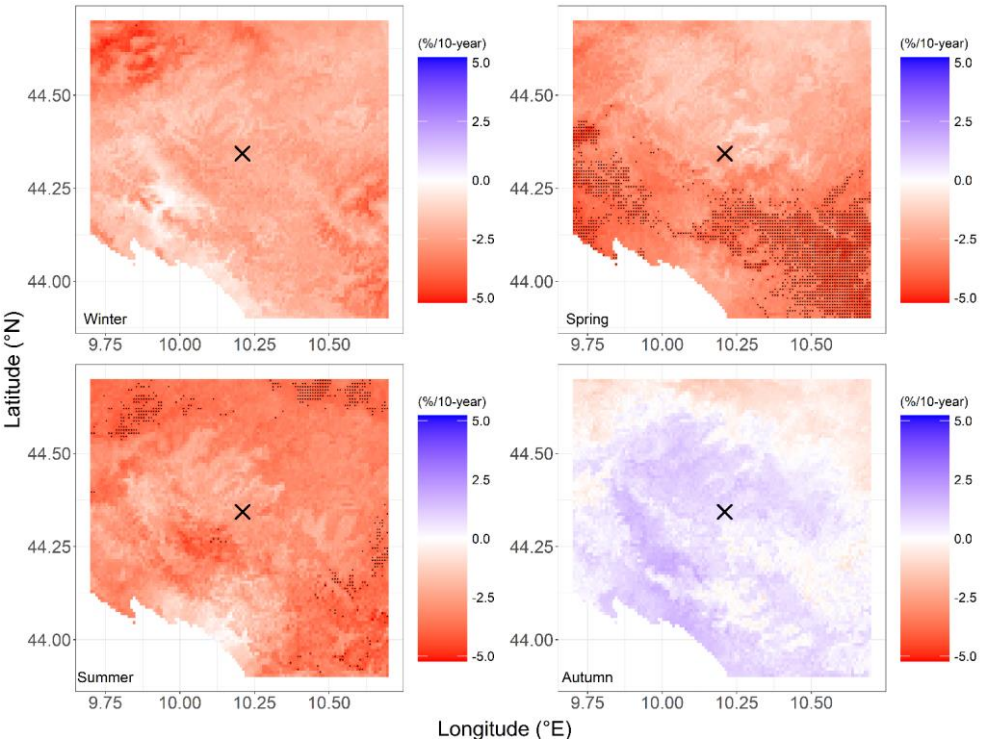

Figure 5.8: Spatial distribution of seasonal precipitation trends (%/10-years) in the study area. Significant trends (p-value ≤ 0.05) are represented with a black dot.

Also, for yearly maximum 1-day precipitation the trends turn out to be weak and non-significant both at the Fossa Lattara site and at most points of the study area. In this case the analyses were performed on the 1962-2023 period (Figures 5.9-5.11).

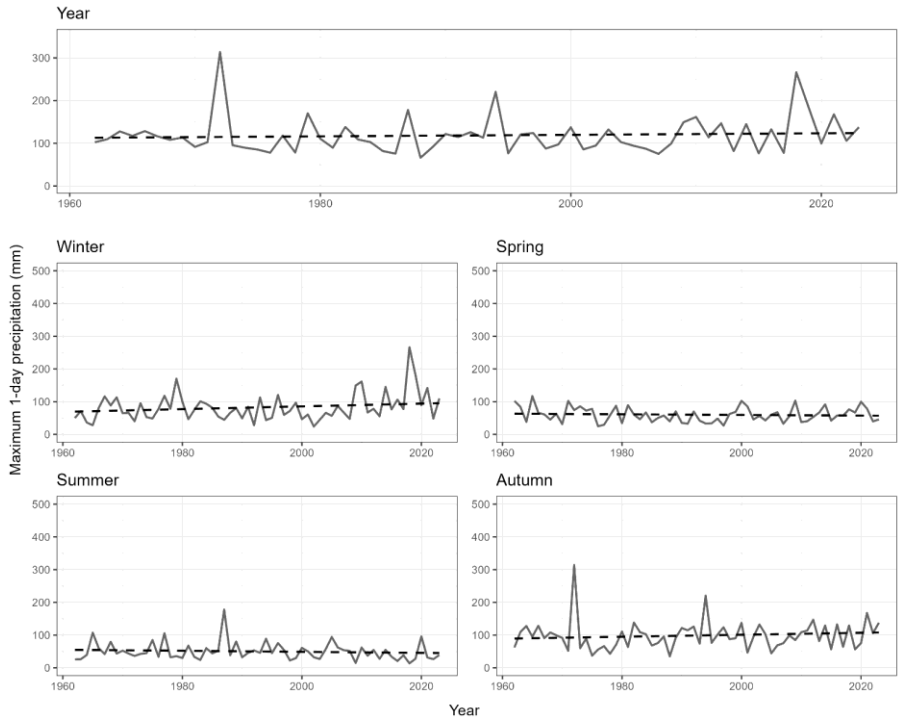

Figure 5.9: Spatial distribution of maximum 1-day precipitation trends (%/10-years) at the Fossara Lattara site, plotted together with corresponding interpolation lines.

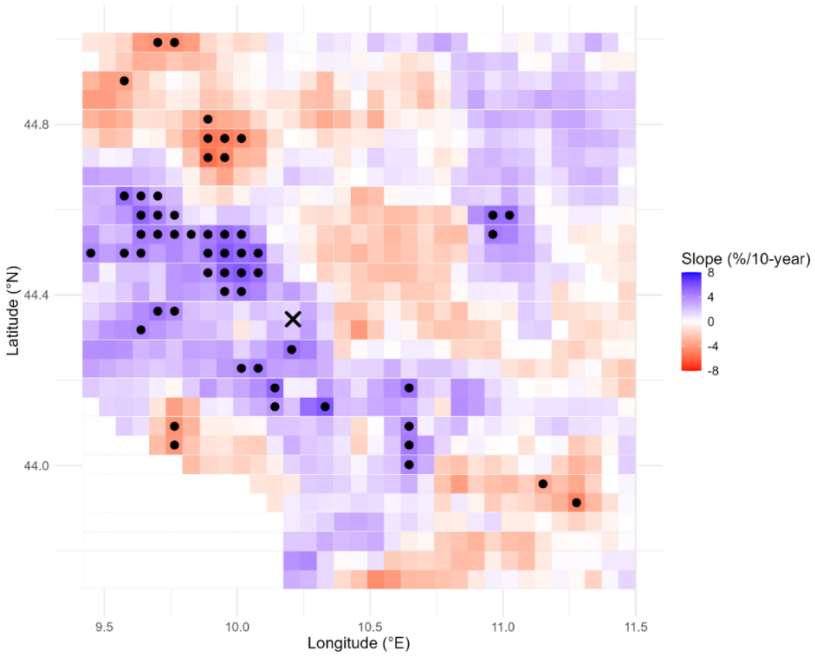

Figure 5.10: Spatial distribution of maximum 1-day precipitation trends (%/10-years) in the study area. Significant trends (p-value ≤ 0.05) are represented with a black dot.

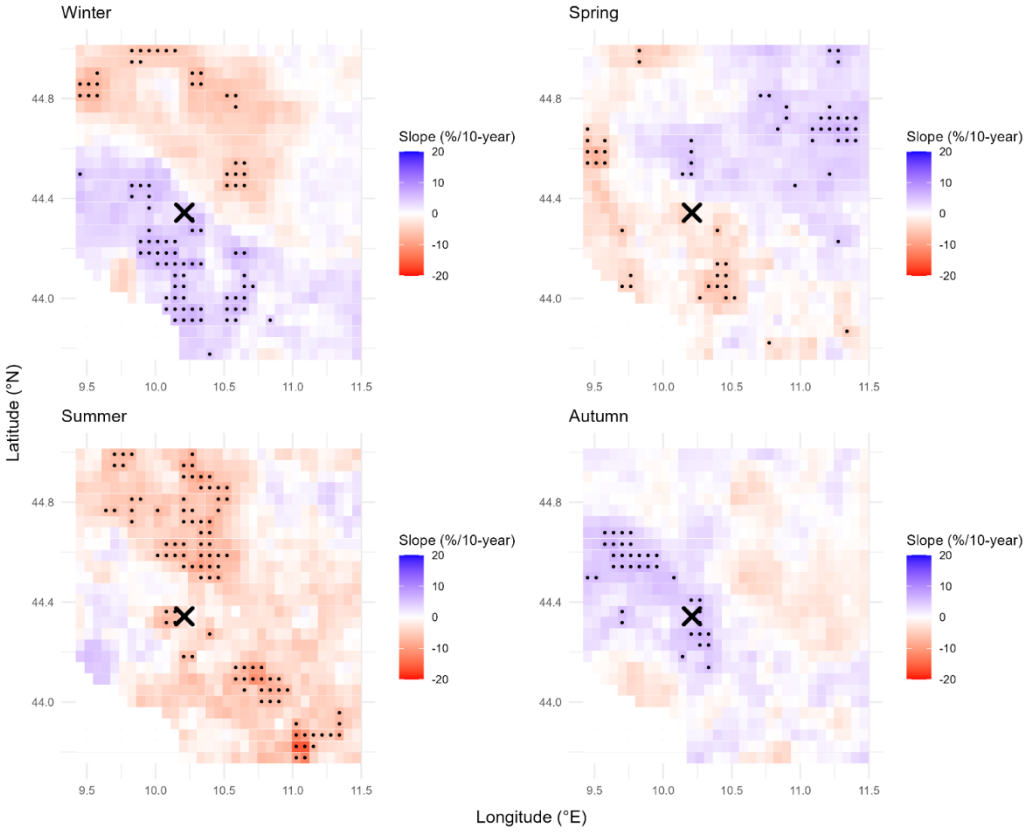

Figure 5.11: Spatial distribution of seasonal maximum 1-day precipitation trends (%/10-years) in the study area. Significant trends (p-value ≤ 0.05) are represented with a black dot.

The most significant tendency of the precipitation records concerns the number of rainy days. A general tendency towards a reduction in wet days is observed both at the Fossa Lattara site and over the entire study area, particularly during summer (Figures 5.12-5.14). On average, summer shows decrease of approximately –0.8 days/10-years over the study area, with several grid points displaying statistically significant trends. Smaller, localized decreases are also present in spring, while winter and autumn show limited or no significant changes, with trends close to zero and high interannual variability.

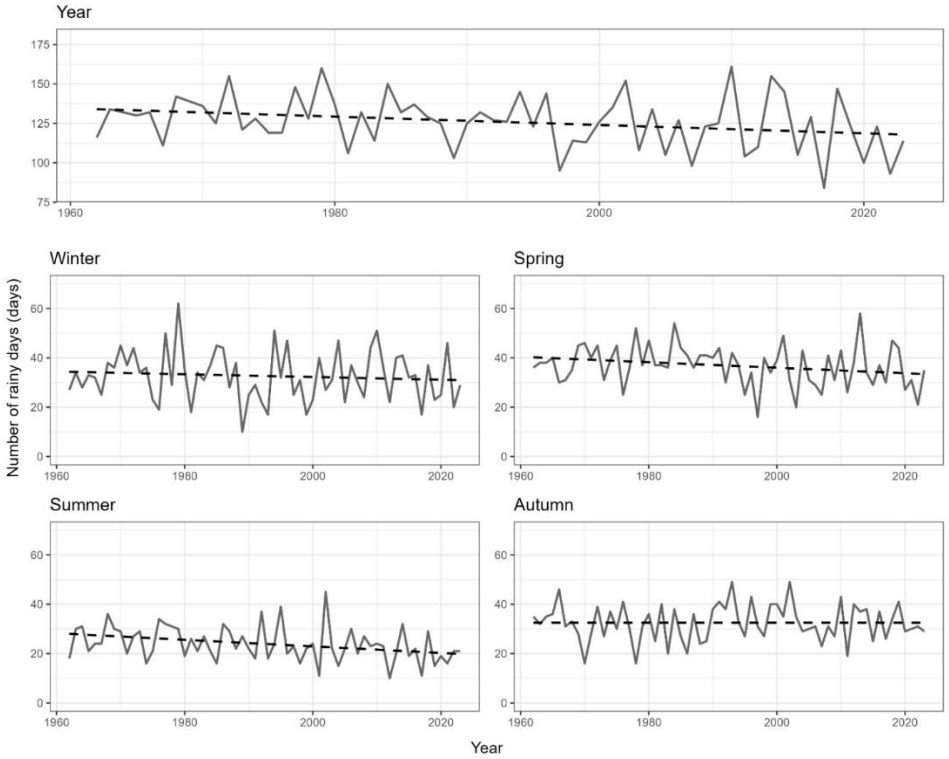

Figure 5.12: Long-term evolution of the of the number of rainy days at the Fossa Lattara site, plotted together with corresponding interpolation lines.

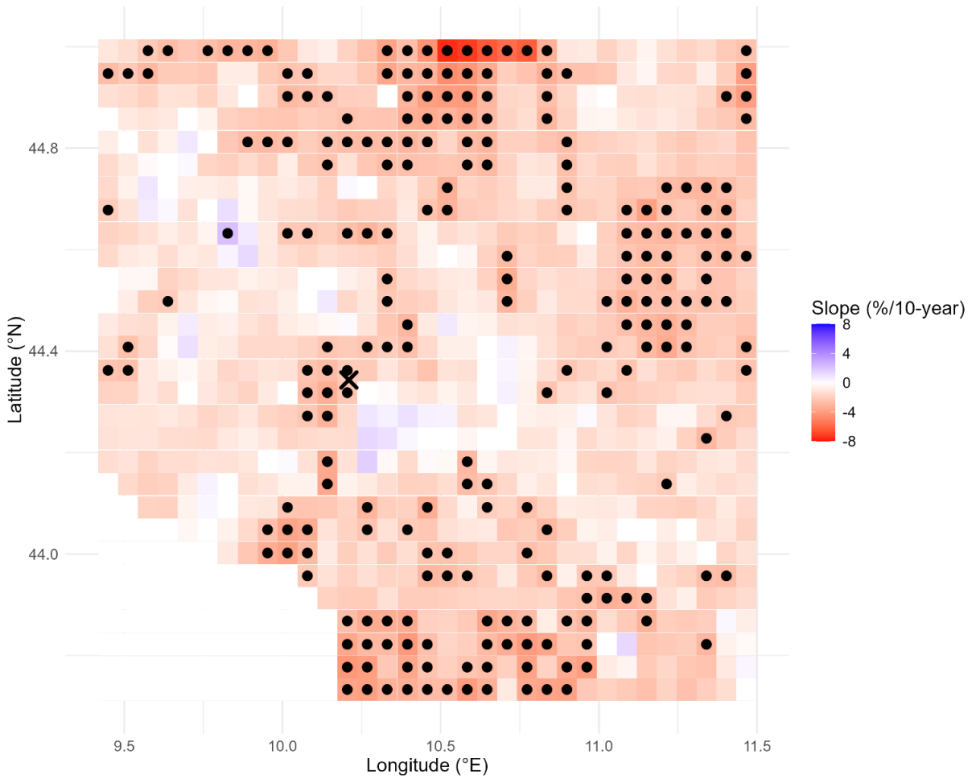

Figure 5.13: Spatial distribution of the number of rainy days trends (%/10-years) in the study area. Significant trends (p-value ≤ 0.05) are represented with a black dot.

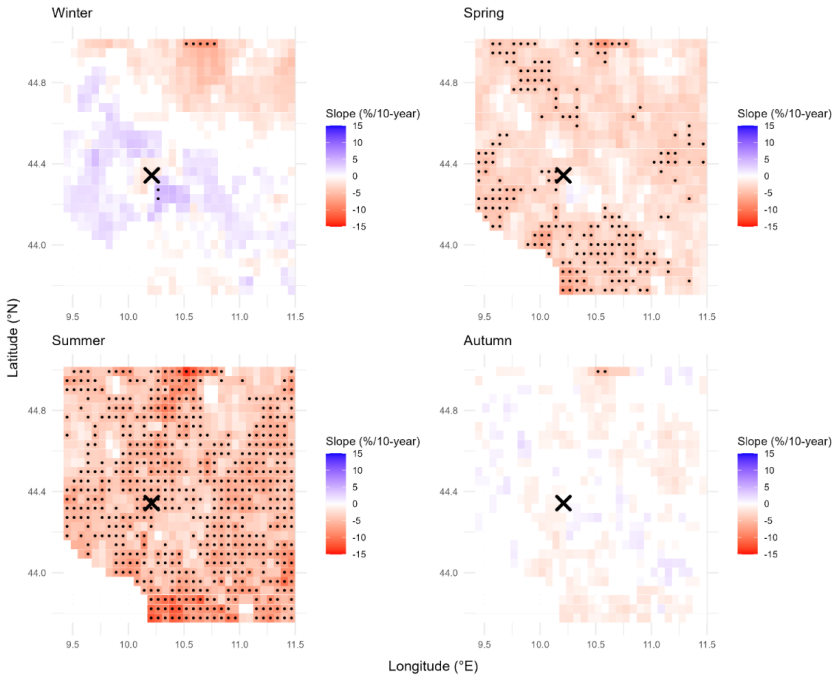

Figure 5.14: Spatial distribution of seasonal number of rainy days trends (%/10-years) in the study area. Significant trends (p-value ≤ 0.05) are represented with a black dot.

The analysis of precipitation intensity from 1962 to 2023 indicates clear stationarity at yearly scale at the Fossa Lattara site, whereas at seasonal level there is positive trend (not significant) in winter (Figure 5.15). Also the study area does not give evidence of a clear pattern both at annual and seasonal scales, with scattered points showing positive or negative trends (Figures 5.16-5.17).

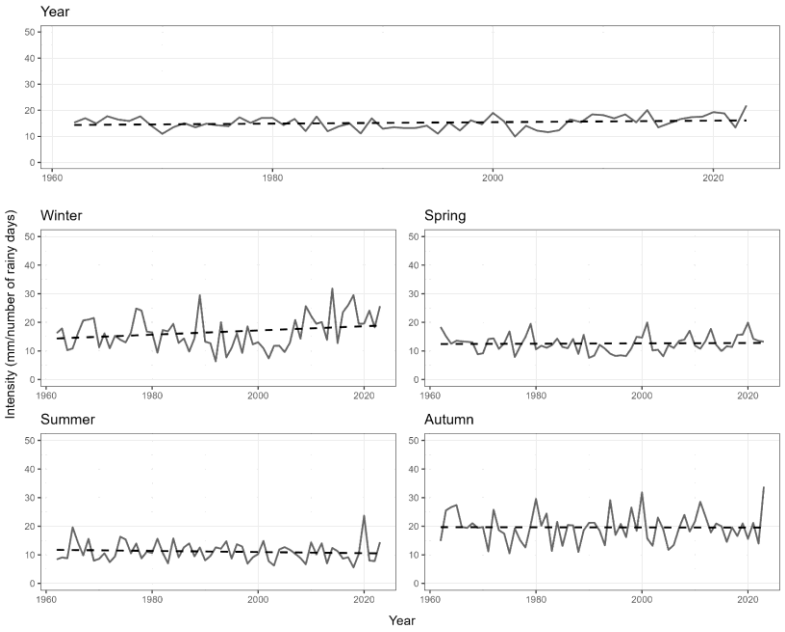

Figure 5.15: Long-term evolution of the precipitation's intensity at the Fossa Lattara site.

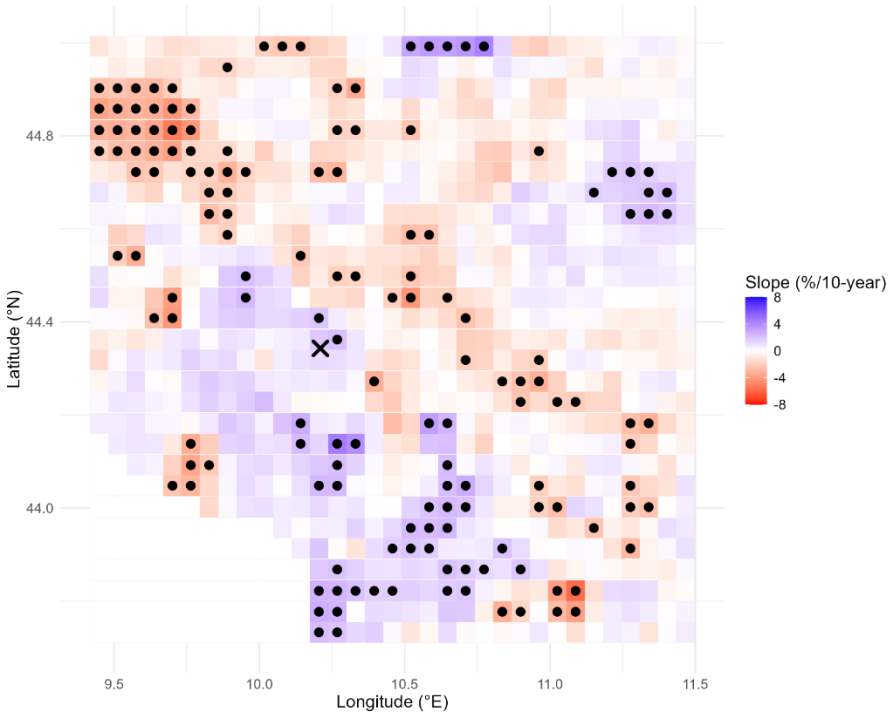

Figure 5.16: Spatial distribution of the precipitation's intensity trends (%/10-years) in the study area. Significant trends (p-value ≤ 0.05) are represented with a black dot.

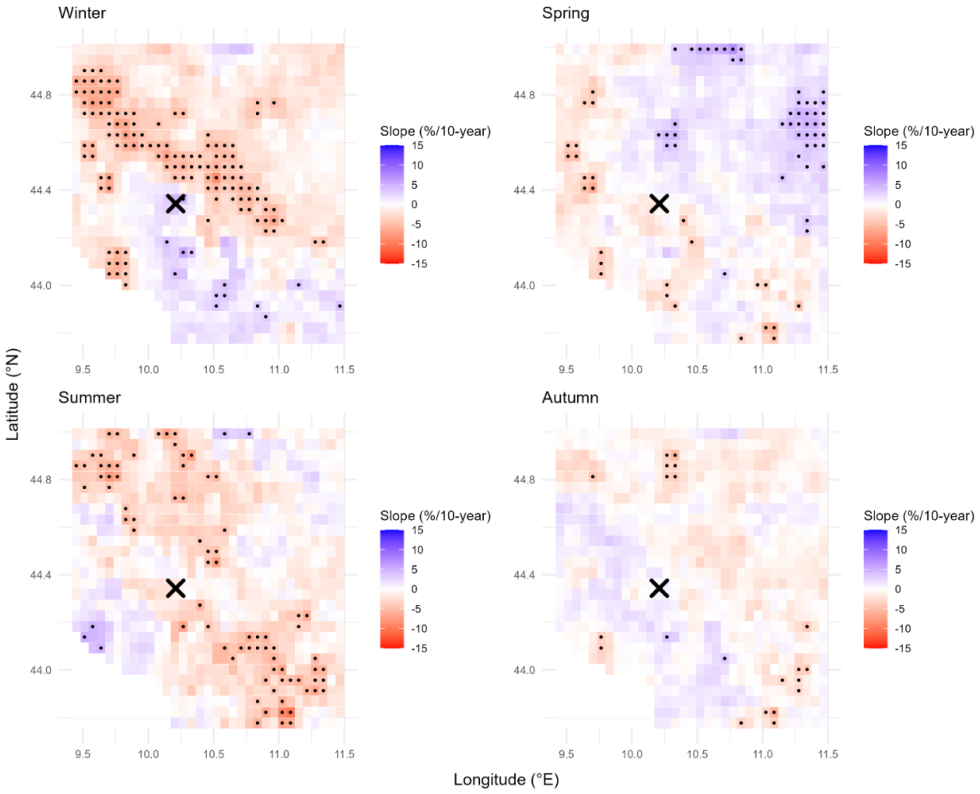

Figure 5.17: Spatial distribution of seasonal precipitation's intensity trends (%/10-years) in the study area. Significant trends (p-value ≤ 0.05) are represented with a black dot.

Table 5.1: Daily precipitation for the Fossa Lattara ARCIS grid cell and for the Succiso, Lago Paduli and Collagna stations for all the dates in which at least one of the values ranks within position 6 within its ordered record. The table also reports the positions of the reported values in the ordered records. Bold characters for dates indicate an identified DF after comparison with the dendrochronological evidences.

Date	SUCCISO		PADULI DIGA		COLLAGNA		ARCIS	
	Rank	Precp. (mm/day)	Rank	Precp. (mm/day)	Rank	Precp. (mm/day)	Rank	Precp. (mm/day)
11/09/1972	**1**	376.8	**1**	371.2	**1**	301	**1**	314.1
28/01/1979	6	201	45	122	26	106	6	170.3
09/11/1982	24	142.4	4	217.8	40	100	13	138.4
25/08/1987	8	178.6	86	104.2	**2**	220.6	5	178.1
02/09/1994	**3**	238.6	**3**	223.4	5	162.4	**3**	220.5
27/12/1995	36	133.6	6	210	65	84	31	120.8

12/10/2000	17	150.6	5	212.4	111	71	15	137.5
05/12/2008	33	134.8	26	140	6	161.4	32	120.7
05/11/2014	5	201.2	9	190	7	136.6	21	129.3
08/12/2017	18	150.2	63	110.6	4	177.6	16	137.3
11/12/2017	**2**	305.4	7	203	**3**	204.8	**2**	266.5
01/02/2019	4	214.8	18	161.2	17	116.2	4	182.6
16/09/2021	7	187.2	**2**	247	27	105	7	167.9

5.7.2 Tree-ring dating of growth anomalies and dates of precipitation inputs triggering DFs

Multiple dendrochronological methods were employed to date growth anomalies induced by DF events. Initially, all tree cores were compared against the reference chronology to cross-date all growth series and identify any reduction in tree-ring growth, indicative of environmental stress. EI was calculated for each couple of cores to further refine the dating process and mean absolute EI (MAEI) was calculated for each channel (Figure 5.18).

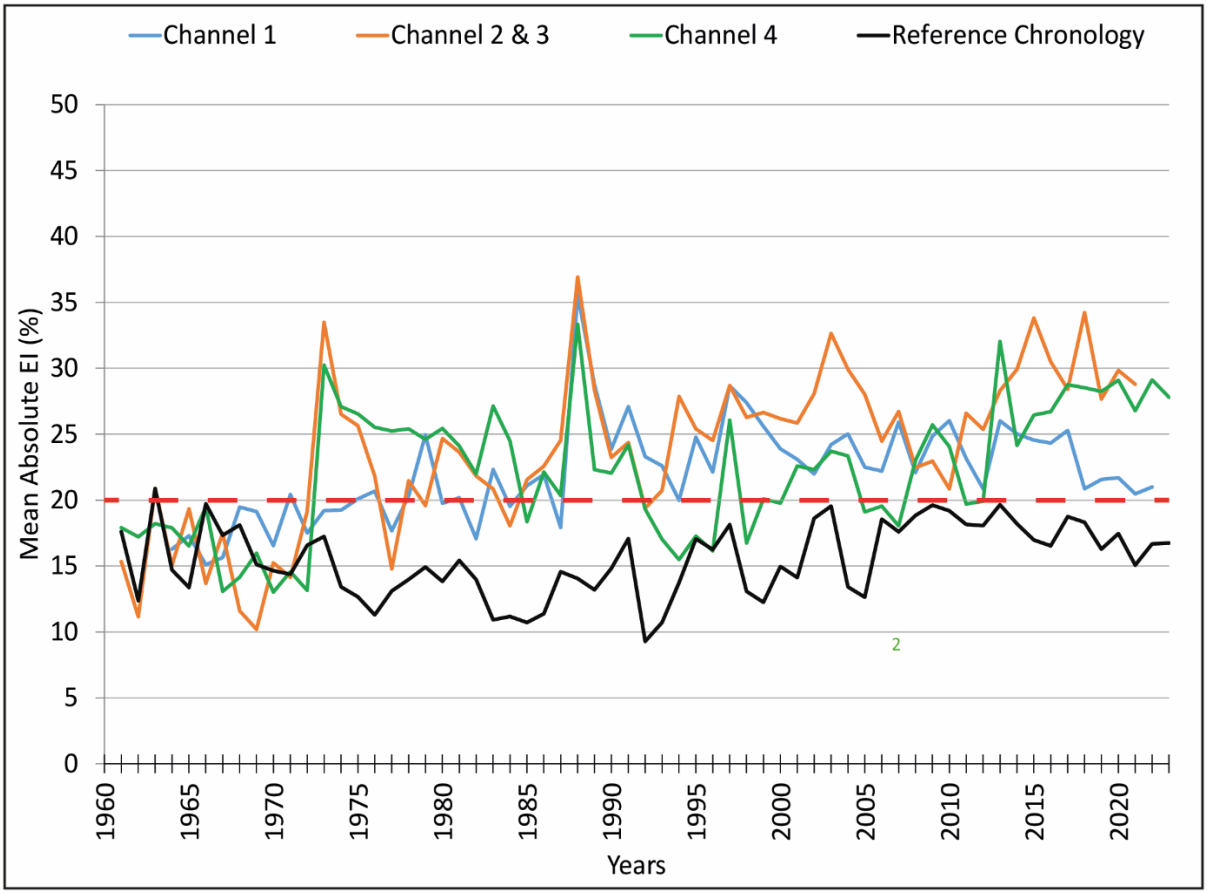

Figure 5.18: MAEI index expressed as percentage with trend lines. Threshold is set on 1.5 StDev of reference site (red dashed line).

Event years, defined by exceeding 1.5 standard deviation in MAEI from the reference chronology, demonstrate temporal patterns and reveal spatial variability when tree responses are marked across the study area. The modeled trends help highlight shifts in geomorphological activity, particularly around major events in 1973 and 1988, supporting a broader interpretation of temporal changes in geomorphic disturbances. Higher MAEI values of all channels compared to the reference site suggest a strong eccentricity response to DF disturbances. The trend in Channel 4's MAEI is likely associated to the milder impact of DF compared to Channels 1, 2, and 3. In Channel 4, trees were primarily tilted but remained intact, resulting in relatively stable MAEI values over time.

To further assess the impact of DFs in a given year, the dMAEI (difference of MAEI values in a given year with respect to previous four years) was calculated and compared with the event-response index (I_t) (Figure 5.19).

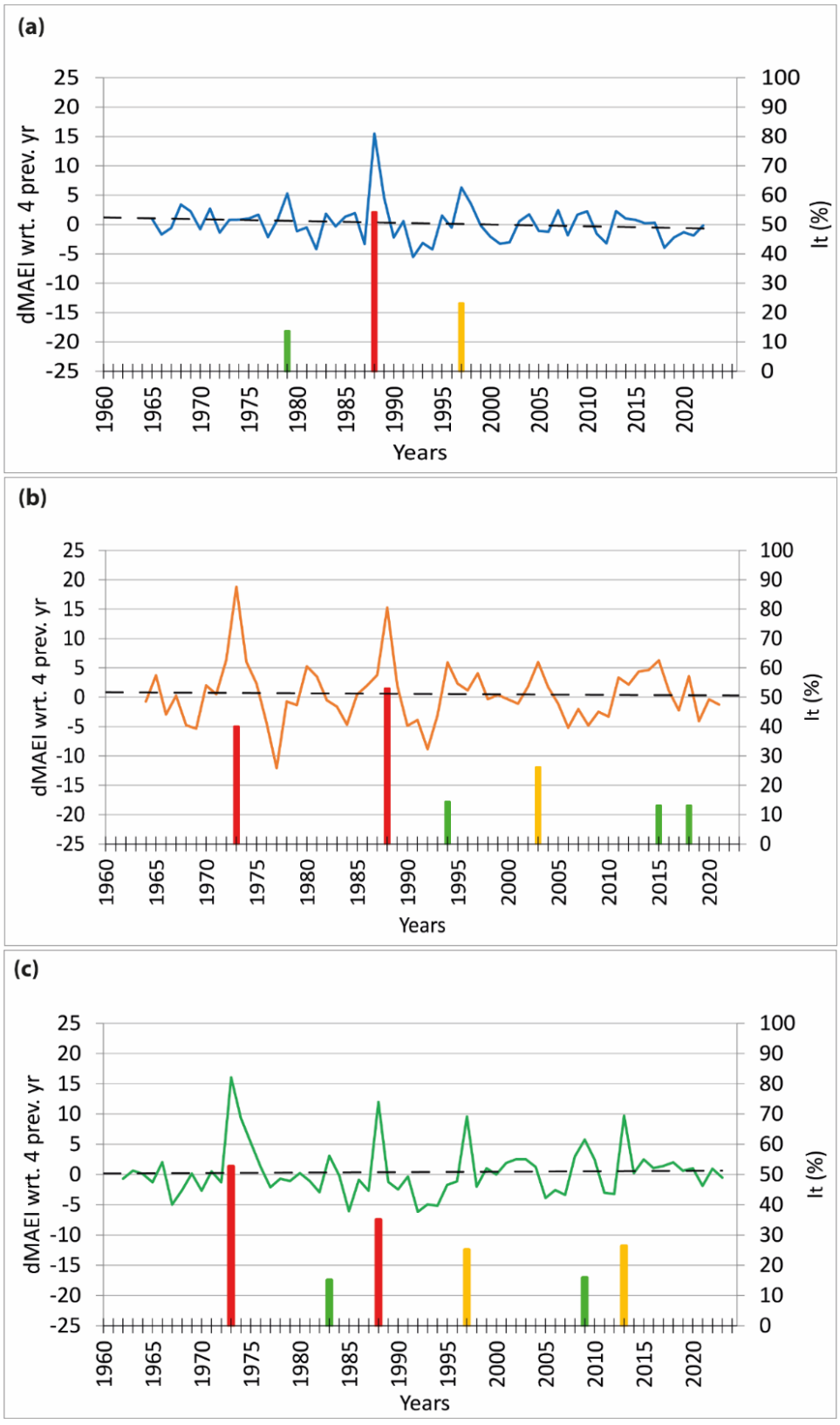

Figure 5.19: dMAEI values over the common period 1961–2023 and detection of event years in the tree-rings. Channel 1 (a); Channel 2 & 3 (b); Channel 4 (c). The secondary axis reports the trees event-response index (I_t) in given years. Red bars indicate major events, yellow bars represent intermediate events, and green bars show minor events. Dashed horizontal lines depict linear trend in the dMAEI series at each channel. This dual-axis approach highlights not only the frequency but also the intensity of DF events over time.

Higher percentage of disturbed trees were associated to major DF events, compared to less pervasive events. Channel 1 (Figure 5.19a) exhibited a single major event year in 1988, while Channels 2 and 3 (Figure 5.19b) recorded major event years in both 1973 and 1988. Although scars were also observed in the field, only few were analyzed as a comprehensive analysis would have required stems sections (disks) and tree fell (Figure 5.20). Similarly, Channel 4 (Figure 5.19c) recorded significant event years in 1973 and 1988.

In Channel 1, the 1988 dendrochronologically detected event year resulted in 54% of sampled trees exhibiting disturbance in their tree rings, underscoring the event's severity. In Channels 2 and 3, the observed tilted trees indicate that 1973 and 1988 event years were characterized by varying levels of disturbance. Notably, the 1988 event year in Channels 2 and 3 led to disturbances in 53% of the trees. Channel 4, while impacted during the same events, primarily showed 53 % trees disturbance in 1973 while 35 % in 1988. These observations emphasize that Channel 2 and 3 experienced the most intense geomorphic activity, followed by Channel 1, with Channel 4 exhibiting comparatively lower impacts. The varying severity across channels underscores the importance of site-specific geomorphic conditions and channel dynamics in influencing DF impacts and associated ecological disturbances.

The dendro-event years were further corrected by observing the daily climatic series to get the most probable dates of the DF events and their precipitation amounts (Table 5.2). The combination of multiple dating methods and statistical thresholds provided a robust framework for reconstructing the chronology of DF events, offering valuable insights into their temporal patterns and environmental consequences.

Figure 5.20: (a) Debris flow event scar on tree sample. The DF occurred on September 11, 1972; (b) Evidence of the debris flow event of August 25, 1987, indicated by eccentric tree ring growth one year later.

Table 5.2: Daily maximum precipitation (mm/day) and corresponding recurrence intervals recorded at the Succiso, Paduli Diga, and Collagna stations for each dendrochronologically dated debris flow year (some years exhibit a delayed signal in the tree rings, appearing one year later with respect to the rainfall event). For each year, the table reports the date of Dendro-Event year, probable date of DF event on the basis of precipitation, and its recurrence based on the full series (1950–2023).

	Dendro - Event Year	Station	Probable date of DF event	Precipitation (mm/day)	Recurrence
Major events	1973	Succiso	11 September 1972	376.8	0
		Paduli Diga	11 September 1972	371.2	0
		Collagna	11 September 1972	301	0
	1988	Succiso	25 August 1987	178.6	7
		Paduli Diga	25 August 1987	104.2	110
		Collagna	25 August 1987	220.6	1
Intermediate events	1997	Succiso	09 October 1996	109	83
		Paduli Diga	09 October 1996	91.8	169
		Collagna	09 October 1996	86	66
	2003	Succiso	03 April 2003	62.4	415
		Paduli Diga	22 October 2002	118.4	66
		Collagna	22 October 2002	74.6	109
	2013	Succiso	18 March 2013	134.6	39
		Paduli Diga	18 March 2013	120.2	59
		Collagna	02 February 2013	85.6	68

Minor events		Succiso	28 January 1979	201	5
	1979	Paduli Diga	28 January 1979	122	54
		Collagna	28 January 1979	106	29
		Succiso	09 November 1982	142.4	27
	1983	Paduli Diga	09 November 1982	217.8	4
		Collagna	14 November 1982	133.6	8
		Succiso	03 October1993	90.9	148
	1994	Paduli Diga	12 June 1994	101.8	122
		Collagna	12 June 1994	94.7	55
		Succiso	20 January 2009	171	10
	2009	Paduli Diga	20 January 2009	142.6	26
		Collagna	05 December 2008	161.4	5
		Succiso	05 November 2014	201.2	4
	2015	Paduli Diga	05 November 2014	190	10
		Collagna	05 November 2014	136.6	7
		Succiso	11 December 2017	305.4	1
	2018	Paduli Diga	11 December 2017	203	8
		Collagna	11 December 2017	204.8	2

5.7.3 Spatial distribution of past debris flow events

To complement the dendrogeomorphological analysis and the DF events dating, a series of historical orthophotos were collected to examine the changes in the study area and assess the extent and severity of DF events. The available orthophotos spanned the years 1944, 1976, 1988, 2003, and 2014 (Figure 5.21). These images were utilized to delineate the visual extent of DFs, identify active source areas, and evaluate the impact on vegetation, particularly the disturbed trees identified through tree-ring analysis. Trees affected by specific event years are marked on each orthophoto, along with active source areas identified during those events. Additionally, the extent of disturbances is delineated based on orthophoto analysis, providing a clear representation of the spatial impact of each DF event. The only 1943 event was detected solely through the 1944 orthophoto, supported by rainfall record from the preceding two years. Subsequent tree-ring analysis indicated that most trees in the study area are younger, dating back only to the 1950s and 1960s, thus supporting the observation that the 1943 event had a destructive impact on the earlier forest. Furthermore, all subsequent events were first detected by dendrogeomorphology and then validated using rainfall data and orthophotos. Together, these methods increase reliability, as each compensates for the limitations of the others.

A major DF event identified dated 1972 and was recorded in 1973 in the tree rings. Although no orthophoto from 1972 was available, the 1976 orthophoto provided clear evidence of significant geomorphic changes, with the extent and active source areas of the DF event being marked.

The extent and source areas of the 1987 DF event were delineated using the 1988 orthophoto. The imagery revealed extensive forest damage, particularly in Channels 1, 2, and 3, where the DF had demolished large sections of vegetation. The tilted trees observed during fieldwork were directly linked to the 1987 event, emphasizing its severe impact.

For subsequent intermediate DF events in 1996, 2003, and 2013, the 2003 orthophoto provided a post-event view, enabling the delineation of the 1996 and 2003 DF extents and source areas. Similarly, the 2014 orthophoto highlights the 2013 DF event, capturing its impact. Major events caused severe and clearly observable damage in the depositional areas on orthophotos, whereas intermediate events produced only limited and less distinct disturbance. The minor events are not included in this analysis due to the very low number of disturbed trees and very low impact. Each orthophoto was also cross-referenced with the locations of disturbed trees identified through dendrogeomorphology to validate and enhance the spatial accuracy of the marked DFs.

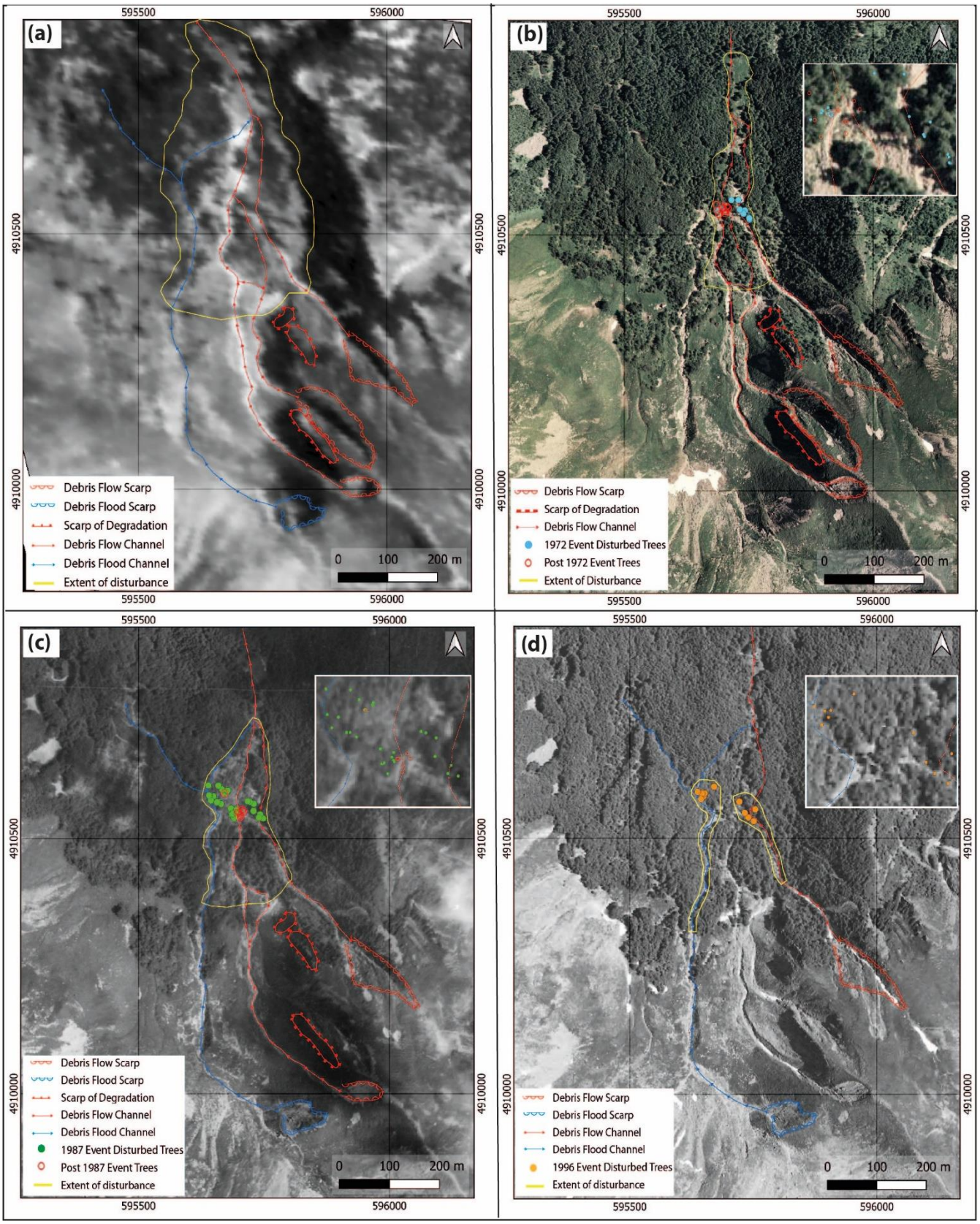
(a)
595500
596000
4910500
4910000
Debris Flow Scarp
Debris Flood Scarp
Scarp of Degradation
Debris Flow Channel
Debris Flood Channel
Extent of disturbance
0 100 200 m
(b)
Debris Flow Scarp
Scarp of Degradation
Debris Flow Channel
1972 Event Disturbed Trees
Post 1972 Event Trees
Extent of Disturbance
(c)
Debris Flow Scarp
Debris Flood Scarp
Scarp of Degradation
Debris Flow Channel
Debris Flood Channel
1987 Event Disturbed Trees
Post 1987 Event Trees
Extent of disturbance
(d)
Debris Flow Scarp
Debris Flood Scarp
Debris Flow Channel
Debris Flood Channel
1996 Event Disturbed Trees
Extent of disturbance

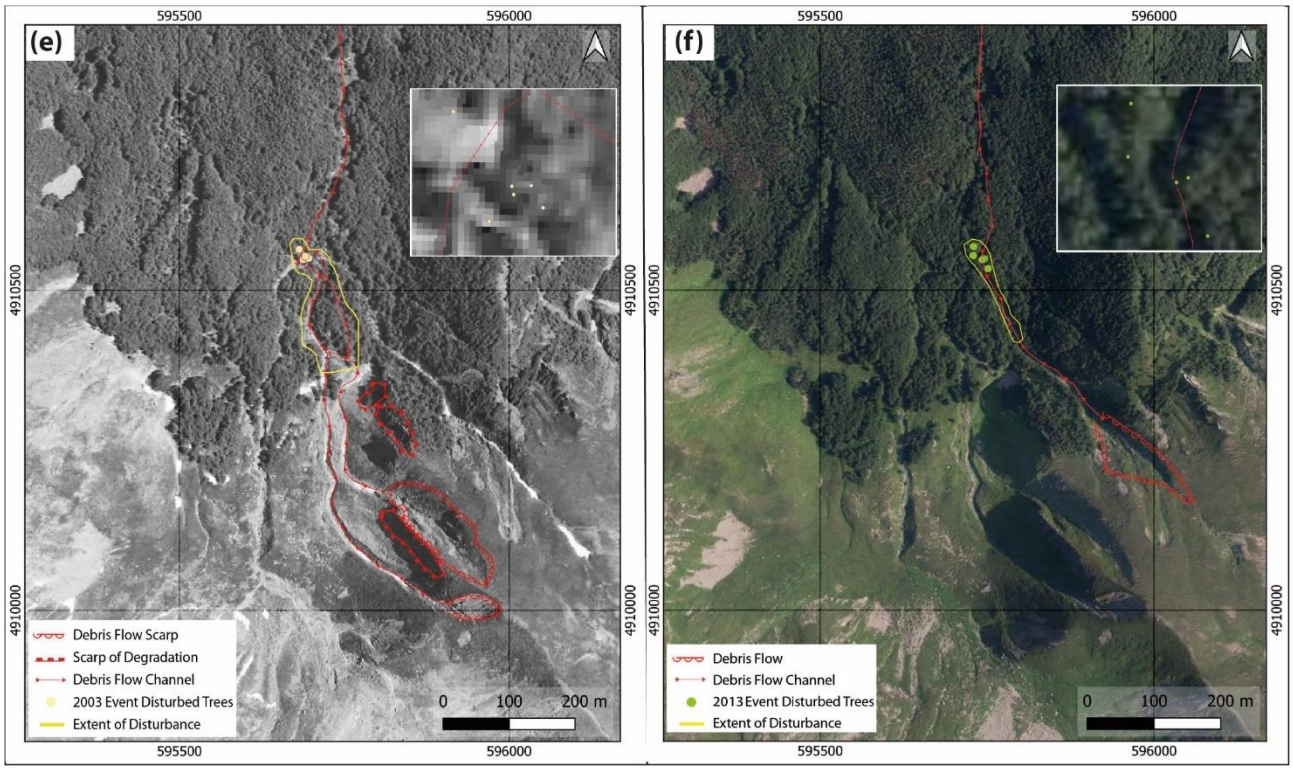

Figure 5.21: Historical orthophotos illustrating DF events: (a) 1943 (orthophoto 1944); (b) 1972 (orthophoto 1978); (c) 1987 (orthophoto 1988); (d) 1996 (orthophoto 2003); (e) 2003 (orthophoto 2003); (f) 2013 (orthophoto 2014).

5.7.4 Geopedological conditions and soil hydraulic properties

In the study area, slight differences are observable when comparing the soils described at the reference site with those found along the slope affected by DFs. Notwithstanding the limited thickness of all the described profiles, the soils in the reference site appear relatively more developed. Soil texture is loam (Figure 5.22) in most soil horizons, but an increase in the sand fraction is observed in profiles located along the slope affected by DFs (ST a, ST b, ST c, and ST d). More specifically, the profile with the highest sand content is the profile ST d located in the DFs deposition area.

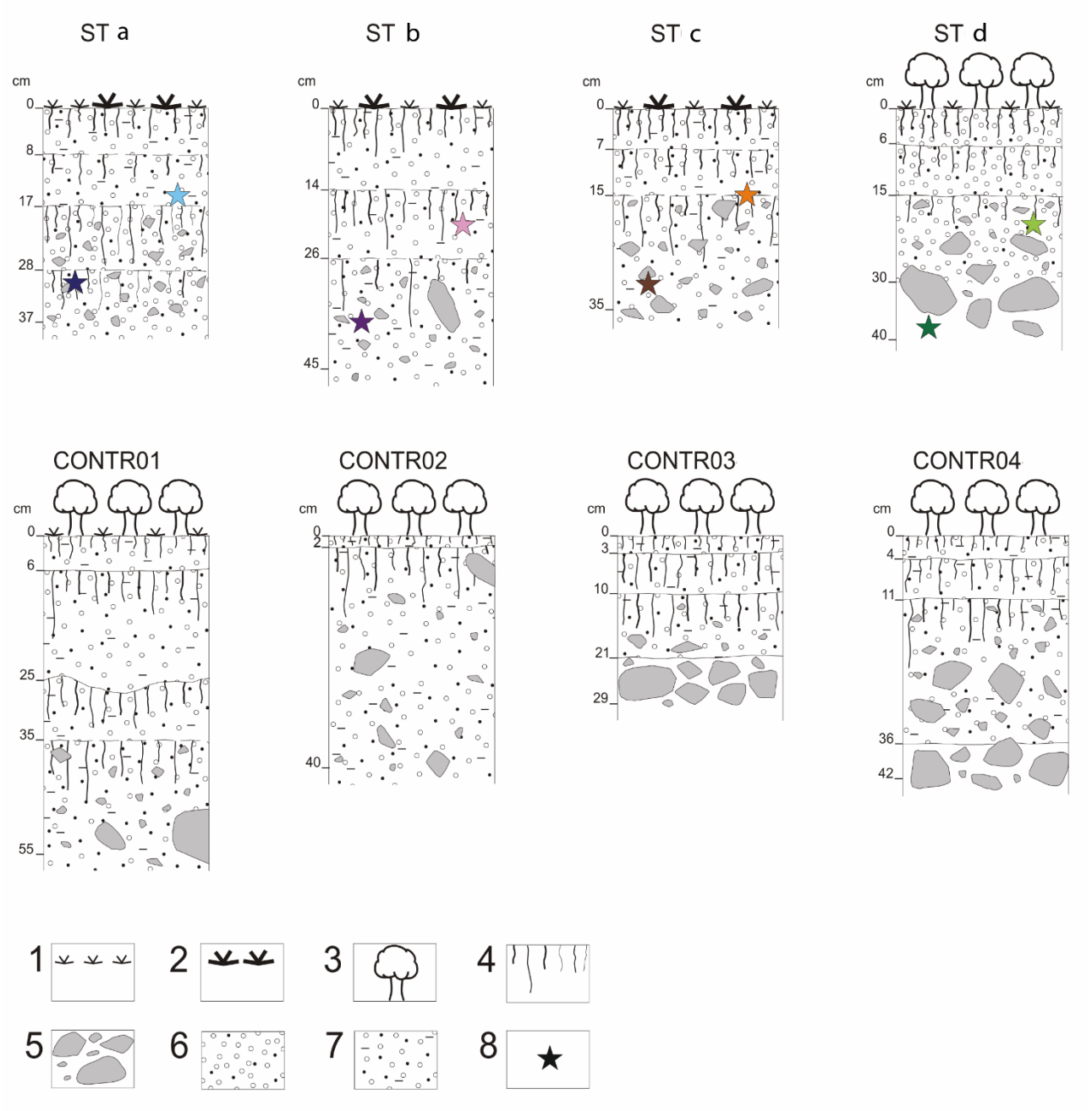

Figure 5.22: Sketch of the investigated soil profiles and position of sensors for soil monitoring parameters. Soil profiles ST a, ST b and ST c are located along the slope affected by DFs and ST d in the DFs deposition area; soil profiles CONTR01, CONTR02, CONTR03 and CONTR04 were dug in the reference site outside the study site. In legend: 1) Grass. 2) Shrubs. 3) Trees. 4) Roots. 5) Stones and gravel. 6) Sandy loam. 7) Loam. 8) Sensors.

The soil hydraulic data from in situ monitoring stations demonstrates a pronounced seasonal pattern. Summer is characterized by sporadic precipitation events and warm soil temperatures (>10°C, Figure 5.23a) that generate several wetting/drying cycles, while fall is marked by frequent

precipitation and lower soil temperatures (<10°C), which result in sustained higher moisture levels with shorter recovery periods (Figure 5.23b; 5.23c and 5.23d). Soil depth significantly affected responses, with shallow layers (15-20 cm) showing rapid and intense reactions to meteorological changes, while deeper layers (30-38 cm) exhibited greater stability and delayed responses of each parameter monitored. Station location slightly influences the hydraulic parameters of soil, even if some minor differences can be found. In all the stations, during the summer, the scarce precipitation and the high air temperatures (up to 35 °C) allow the soil to get dry after the infiltration event. In contrast, in autumn, the intense and continuous rainfall, combined with a drastic drop in air temperatures, causes the soil to remain constantly moist, which could favor the onset of DF processes.

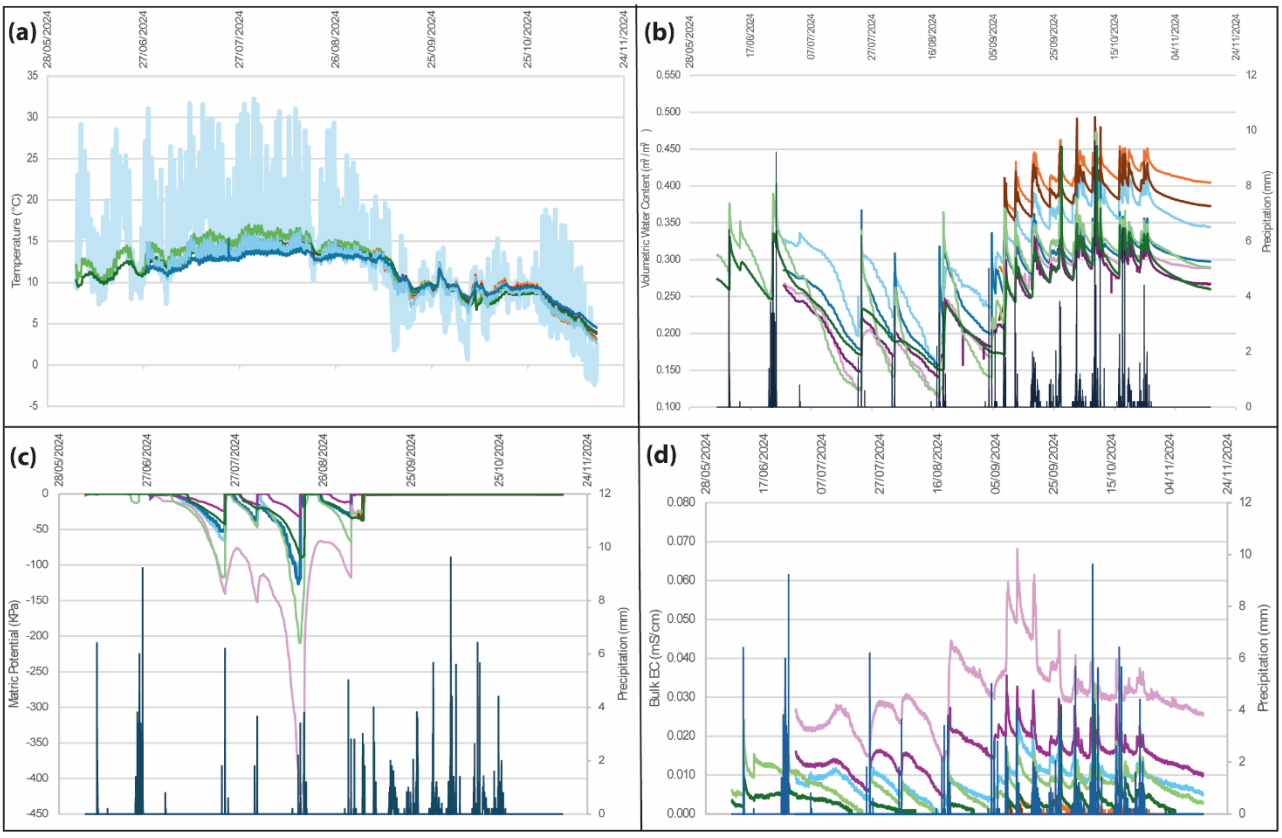

Figure 5.23: a) Soil temperature; b) Volumetric water content in soil; c) Matric Potential in soil; d) Bulk EC in soil. Legend: Lines) Light blue: ST a at 15cm depth; Dark blue: ST a at 30cm depth; Pink: ST b at 20cm depth; Purple: ST b at 37cm depth; Orange: ST c at 15cm depth; Brown: ST c at 30cm depth; Light green: ST d at 20cm depth; Dark green: ST d at 38cm depth. Blue bars) Precipitation

5.7.5 Regional scale assessment of debris flows

Sandstone is the dominant lithology in the Northern Apennines and represents the primary source material for DF initiation (Figure 5.24a). Other rocks like limestone, shales, siltstone, claystone and marlstones were also found where DF initiated, but less often. Furthermore, it is assessed that quaternary deposits may be also present in the source areas, being involved in DFs processes in Northern Apennines. A geological map was used to indicate areas more prone to DFs because it provides underlying bedrock, and the type of bedrock influences slope stability, weathering rates, and hydrological behavior, which affects DFs susceptibility. Overall, these findings show that the type of ground material plays an important role in DF activity, especially in complex and active mountain regions such as the Northern Apennines.

The CSI classification facilitated the mapping of catchments with moderate to very high potential susceptibility for DF activity. Furthermore, the 511 past DFs are cross validated with the catchment scale classification. It is observed that 82% of the past DFs are validated, while only 18% remain unclassified, as their source areas do not fall within the defined catchment classification (Table 5.3). Out of a total of 36,626 small catchments analyzed across the region, 5,904 were classified moderate to very high susceptibility. Areas marked with red rectangles represent critical zones where high CSI catchments coincide with intense rainfall areas, highlighting their potential for DF activity (Figure 5.24).

Table 5.3: Classification of catchments based on CSI (very low to very high) based on the composite index integrating four morphometric and one hydro-geomorphological parameter.

Class	Percentile	Composite Susceptibility Index	Count	Percentage (%)
Unclassified		< 0.38	93	18
Very Low Susceptibility	< 20	0.38-0.41	167	33
Low Susceptibility	20-40	0.41-0.43	85	36
Medium Susceptibility	40-60	0.43-0.46	71	14
High Susceptibility	60-80	0.46-0.51	34	7
Very high Susceptibility	> 80	> 0.51	61	12

5.8 Discussion

The DFs at the Alpe di Succiso site demonstrate significant complexity due to the interaction of various geological and geomorphic processes. These include rock weathering, progressive rock degradation, channelized flows, rockfalls, and the subsequent mobilization of debris. The complex dynamics are further affected by climatic change, hydrological inputs, variations in slope morphology, and material composition, resulting in a system where each process interacts to shape the landscape. Understanding each of these processes is essential for evaluating the site's geomorphic evolution and assessing the associated risks in the perspective of a changing climate.

The DF deposits at the study site are distributed over an area of approximately 0.14 km^2. In the Northern Apennines several major precipitation events, including short duration and high intensity precipitation, which have triggered DFs have been documented by previous researchers (Moratti and Pellegrini,1972; Corsini et al., 2019; Ciccarese et al., 2020; Berti et al., 2025). Corsini et al. (2019) investigated the severe event of DFs in October 2014 in Val Parma and Val Baganza, when the Marra rain-gauge (ARPAE network) recorded 308.6 mm precipitation in 24 hours. Ciccarese et al. (2020) conducted an analysis of the storms of 2014 and 2015 within the Emilia-Romagna region, observed over 130 DFs, with maximum 1-hour rainfall intensities exceeded over 100 mm. Berti et al. (2025) have detailed the DF events in Emilia-Romagna in May 2023, where two consecutive storm events yielded rainfall accumulations up to 250 mm within a span of 48 hours, resulting in the initiation of over 80,000 shallow landslides, predominantly DFs and debris slides throughout the region.

A fundamental aspect of our multi-disciplinary methodology is its ability to determine the dates of DF events within a multi-decadal temporal framework. The present work also aims to compile a dataset of past debris-flow events in a relatively remote mountain area. Existing debris-flow inventories are often concentrated in regions of high socio-economic relevance or dense population, where events are more likely to be documented following damaging or catastrophic occurrences. As a result, debris-flow activity in less accessible areas is frequently underrepresented or poorly documented. In this context, the dataset presented here represents a valuable contribution, particularly when compared with previous debris-flow datasets that primarily record events after major disasters (Moratti and Pellegrini,1972; Ciccarese et al., 2020 and 2021; Berti et al., 2025).

The integrated multi-disciplinary approach here proposed, by combining dendrogeomorphology, orthophoto analysis and climate data, has provided a comprehensive reconstruction of DF history in the study area at the multi-decadal scale. This methodology, by integrating ground evidences and climatic triggers, has determined the probable dates, magnitude, and intensity of the DF events at the study site. Identifying the precise temporal occurrences of past DF events is not only critical for understanding hazard frequency but also holds practical implications for DF modeling. Accurate event dates enhance the calibration and validation processes of numerical simulations that model inflow and outflow dynamics, sediment entrainment, and deposition processes (Mergili et al., 2018). Our dataset substantially contributes such modeling efforts by providing a validated temporal sequence of DFs events, which can be correlated with model outputs, thereby allowing for scenario assessments under climate change and geomorphic conditions. Moreover, this study offers a forward-looking viewpoint: the possible utilization of multi-decadal reconstructions to enhance regional hazard mapping, model validation and predictive assessments in future climate scenarios, in addition to historical analysis.

5.8.1 Research Implications and Limitations

Overall, the applied methods allowed us to determine the dates of DF events, however some limitations to such reconstruction exist. DF deposits from prior events can be reactivated by intense or prolonged precipitation, resulting to secondary disturbances in the tree rings that may not indicate new DF events. Dendrogeomorphology, while invaluable for analyzing long-term disturbances in the tree rings, has limitations including the dependency on the availability of suitable trees (and only trees that survived DF events are available). Other limitations include challenges in precise events dating in areas with complex geomorphic processes (Stoffel et al., 2013), and the risk for misinterpretation of growth disturbances caused by non-DF factors such as disease, defoliation or adverse climatic conditions such as drought or low temperature (e.g., Šilhán and Stoffel, 2015), which however do not cause eccentricity and usually impact the whole growth process in the trees. The temporal resolution of EI is limited to the annual scale, and overlapping disturbances across consecutive years may obscure individual events. Some DFs may not generate detectable eccentricity signals, while in other cases tree recovery growth patterns can dampen the response, leading to underestimation of event frequency. Moreover, event years detected by means of dendrogeomorphological techniques can be adjusted by comparison with meteorological climatic series in order to find the most probable date of the DF event. The adjustment of the

seasonal resolution of the dendrochronological date allows to detect the amount of precipitation that has triggered a given DF, a key point that may be critical for modeling the DF dynamics with exact inflows in the catchment. However, this link remains probabilistic unless the event is independently documented.

Rainfall data is essential for understanding the environmental triggers of DFs; however, it is frequently inadequate in capturing localized disturbance impacts and its temporal resolution is often insufficient to detect sub-daily high-intensity events. Moreover, gaps in data availability pose substantial challenges, making it difficult to establish precise correlations between rainfall events and DF occurrences. Finally, as we could demonstrate, not all the intense precipitation events correspond to evidence of DF in a given site (see also Qie et al., 2025).

Thus, relying only on one methodology may lead to misinterpretation of DF events. Each scientific discipline has its limitations, but integrating multiple methodologies and data can provide a more comprehensive understanding of DF events, detecting the dates of DF events and their magnitudes.

5.8.2 Field evidence of geomorphic processes across channels

The channels of DFs at the study site are attributed to differences in geomorphic dynamics. In Channel 1, no visible DF deposits were observed in the disturbed area, yet many trees were found tilted to the ground, indicating a high-energy event probably consistent with a debris flood. The debris material was observed in Channel 1, but it remained within the channel boundaries, indicating that water overflowed beyond the channel with some portion of debris, which caused this destruction in adjacent areas. In Channels 2 and 3, patchy deposition of material was observed; some trees were associated with DF deposits, while others were not. Several trees in these channels were also tilted, indicating a combination of flow dynamics. In Channel 4, deposition material was clearly observed, and stem tilting caused by the interaction with DF deposits. Channel 2 and 3 showed both DF and debris flood processes, while Channel 1 was probably affected only by debris flood. Moreover, field observations revealed the presence of DF material within the channel and across the deposition area, indicating active sediment transport and potential reactivation of previously deposited material.

5.8.3 Precipitation patterns and their role in triggering debris flows

At the study site after the assessment of major events by dendrogeomorphology approach, the two major event years related to DFs were 1973 and 1988, that were associated with the extreme rainfall events occurring in 1972 and 1987. The 1972 rainfall event concerned September 10 and September 11. It ranks as the most intense event for 1-3-6-12-24-hour durations for Succiso and Lago Paduli stations, with up to about 100 mm in 1 hour and about 450 mm in 24 hours. The 1987 rainfall event occurred on August 25. It ranks as the second event (after the 1972 event) for Collagna station (about 6 km from the Fossa Lattara site) and it ranks also in the first 10 events both for the cell of the ARCIS data set including the Fossa Lattara site and for the Succiso station. This event also ranks third (after the 1972 event and an event in 1994) for Succiso station 6-hour precipitation.

Our dendrochronological study revealed DF activity in 1997, 2003, and 2013; however, these events are related to lower precipitation amounts when compared to major events as those in 1972 and 1987. Rainfall on 9 October 1996 might be related to the 1997 event year in the tree rings. The precipitation events on 22 October 2002, or 3 April 2003, may be the source of the 2003 event year in the tree rings. Rainfall on 18 March 2013 may be related to the 2013 event year in the tree rings. The existence of these intermediate events is confirmed by tree-ring data, although short-duration, intense rainfall may not be the only factor responsible for the DF initiation. Instead, the DF events can be the result of pre-existing soil moisture conditions, moderate but persistent precipitation (Hirschberg et al. 2019), or the reactivation of previously deposited debris within the catchment area (Qie et al., 2024).

The minor event years recorded by trees in 1979, 1983, 1994, 2009, 2015, and 2018 may be associated with intense precipitation events, respectively, on 28 January 1979, 9 November 1982, 3 October 1993, 5 December 2008, 5 November 2014, and 11 December 2017. These events impacted on only a small percentage of trees and are likely due to reactivations of previously deposited material inside the channels rather than new deposits.

The analysis of daily and hourly extremes reveals notable differences in the temporal structure of rainfall events. For instance, while the 11 September 1972 event is the highest daily record across all stations, its hourly intensities are comparable to other events, such as the 20 October 2013 event, which exhibits particularly high 1-hour and 3-hour intensities. This suggests that an extreme

daily event may result from a prolonged period of moderately high rainfall, whereas intense short-duration bursts reflected in the hourly data can occur in events with lower overall daily totals.

These findings emphasize that severe rainfall does not necessarily lead to DFs, highlighting the importance of other parameters such as soil temperature and soil saturation that influence slope stability by affecting infiltration and runoff dynamics. Furthermore, the lack or availability of loose debris in channels or slopes is also one of the most important factors in establishing whether heavy rainfall may cause a DF event. Extreme rainfall, however, emerges as the most significant parameter in triggering DFs. The results of our analysis emphasize that short-duration, high-intensity rainfall is a critical factor for DFs during major events.

This analysis exhibits the necessity for integrated models that account for rainfall intensity, duration, and environmental factors to accurately anticipate and mitigate DF risks. Moreover, the study demonstrates the importance of integrating historical data, dendrochronological evidence, and modern analytical methods to understand the frequency, intensity, and impact of DF events in the study area.

5.8.4 Geopedological and Hydrological Controls on slope stability

Soil development in mountain environments is strongly influenced by slope stability, with active processes often limiting pedogenesis through rejuvenation or subsequent soil burial (Masseroli et al., 2023). In the study area, soils at DF site are less developed and have higher sand content in the DF deposition area (ST d) is due to coarse material accumulation from the upper part of the slope. In contrast, the reference site shows more developed profiles, confirming its geomorphic stability and suitability as a control for dendrochronological analysis.

The contrast between dry summer conditions and rainy fall periods is one of key seasonal variation in soil dynamics. The surface soil (15-20 cm below the ground) shows greater soil parameters fluctuation compared to deeper layers (30-38 cm below the ground), reflecting higher sensitivity to short-term atmospheric changes as observed in several different study cases (i.e. Rocchi et al., 2020; Bordoni et al., 2021; Fusco et al., 2022, Wang et al., 2025b). There were slight differences across sites because of local soil composition, topography and sunlight insulation, but these did not substantially change the dynamics of infiltration. For example: lower stations (ST d) recorded higher temperatures during summer, whereas flat areas (ST c) maintained higher water content and lower

electrical conductivity values, suggesting small differences in soil composition in this portion. Although there is considerable heterogeneity, our results indicate that overall infiltration mechanisms are fairly constant along the slope where the DF occurred, suggesting that seasonal moisture conditions rather than spatial diversity in soil hydraulics may have a greater impact on slope stability. The observed soil parameters are consistent with those obtained from other study areas with similar elevation characteristics (Eccel et al., 2015).

5.8.5 Regional scale DF related phenomena and predisposing factors

Numerous authors (Baroni et al., 2000; Corsini et al., 2017; Ciccarese et al., 2021; Peruccacci et al., 2023; Rashid et al., 2024; Berti et al., 2025;) have conducted investigations on DFs within Northern Apennines and the Apuan Alps. However, due to extensive area and complex topography of the region, the task of identifying every DFs remains a significant challenge. As a result, regional scale assessments are essential as the current study. Such mapping provides essential support for hazard assessment, early warning systems, and the prioritization of field assessments in under-monitored areas.

The integration of the spatial distribution of DF-prone catchments with the spatial distribution of intense precipitation events that occurred over the wider region in the last 70 years, delineates the areas potentially exposed to DF hazards across the region. Extreme rainfall in the Northern Apennines usually occurs in early October because of warm Mediterranean-triggered convective storms, whereas summers are dry and winters bring light rains (Rosso and Ceppi, 2023). Eastern Liguria and northern Tuscany are "wet hotspots," which are frequently hit by severe storms and flash flooding (Bartolini et al., 2014; Brunetti et al., 2019). Emilia-Romagna's mountainous parts are influenced by Ligurian spillovers or isolated cyclonic systems, with peak events occurring in early fall or winter (Nigro et al., 2024).

This analysis allowed us to determine areas of intense precipitation and corresponding DF-prone catchments and observed DFs (E and W sectors). These areas represent critical zones for DF hazard, as they meet both higher CSI values and climatic conditions that cause DF initiation. Roughly three-quarters of threshold-breaking storms strike the Ligurian-to-north-Tuscan maritime belt, where steep, debris-rich slopes align with extreme Tyrrhenian rainfall to form a continuous DF hotspot that dwindles sharply east of the Apennine divide.

This analysis delineates also areas of intense precipitation over non-DF-prone catchments and without observed DF (far-W sectors). These areas suggest more stable slopes, lower slope gradients and less erodible soil despite intense rainfall. Moreover, especially along the mountain ridge and the Apuan Alps (Baroni et al., 2000) there are areas where no intense precipitation events occurred but that are presenting DF-prone catchments and DFs (ISPRA, 2019) as well. This suggests that in these areas, moderate but prolonged rainfall, and less intense event can be sufficient to trigger DFs. Numerous studies have documented that non extreme precipitation was enough to initiate DFs in highly susceptible basins (e.g. presenting very steep slopes with abundant loose debris, or areas with reduced vegetation cover), in these contexts the rainfall threshold required for triggering DFs are much lower (Tiranti et al., 2021).

Although earthquakes have been identified as potential triggers of DFs, in the Northern Apennines (Zei et al., 2024), no correlation was found in our study area, where intense precipitation remains the dominant triggering factor. The geological context further enhances the vulnerability of DFs. The existence of Macigno sandstone (TNmg) formation covered by Quaternary deposits plays a critical role because this formation is associated with a high number of DFs in the region (Conti et al., 2020).

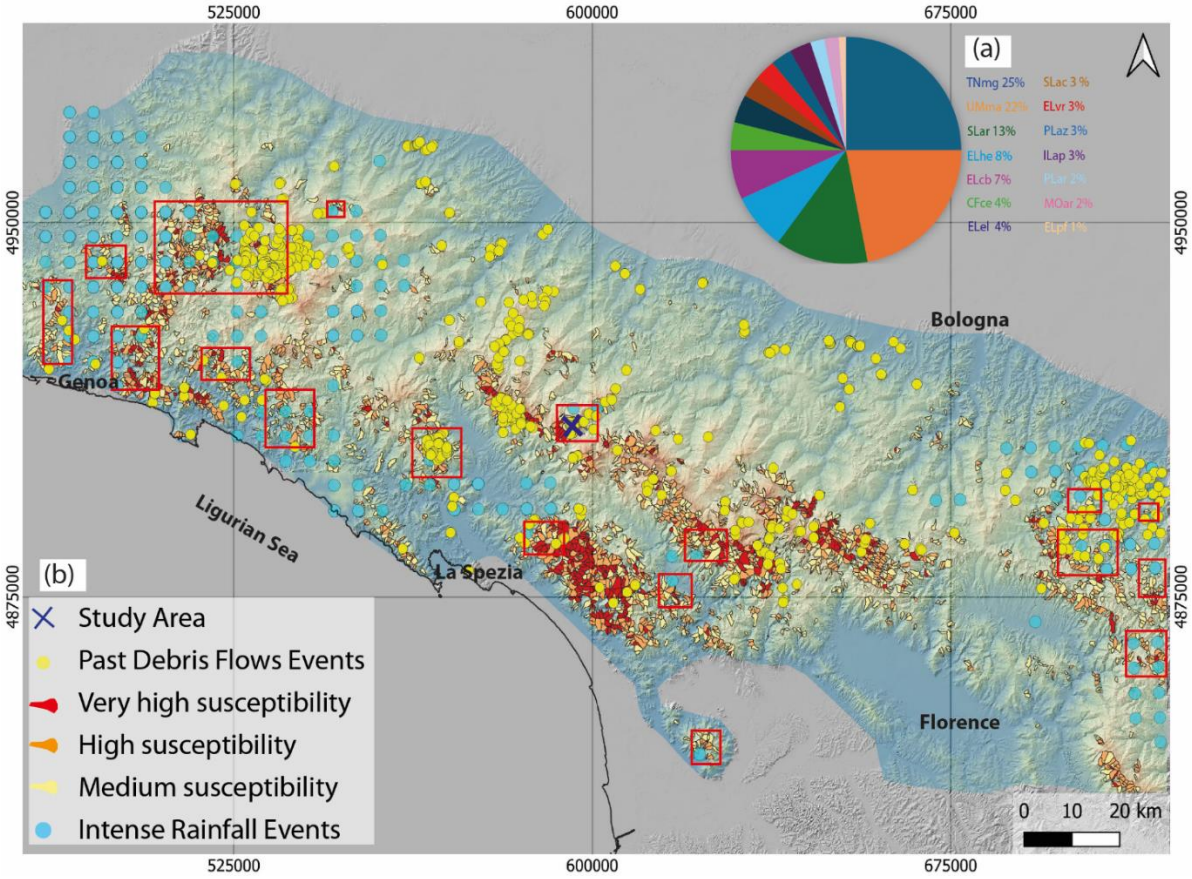

Figure 5.24: (a) Distribution of DFs in relation to lithological units. Key units include TNmg (Turbidite sandstones and siltstones); UMma (Turbiditic sandstones and siltstones); the full list is provided in online material table S1. (b) Regional-scale assessment of extreme precipitation events, and DF-prone catchments based on the composite susceptibility index (integrating four morphometric indices including MRI, HI, slope, channel gradient and one hydro-geomorphological index, SPI), together DFs reported in literature considering the northern portion of the Northern Apennines. The red rectangles indicate regions with high susceptible values and intense precipitation, marking zones predisposed to elevated DF hazard (EPSG: 25832—ETRS89/UTM zone 32N coordinate system).

5.9 Conclusions

The temporal and spatial characteristics of DFs have been effectively analyzed, through the integration of multi-disciplinary methodologies. This extensive assessment has facilitated the determination of the most probable dates when DF events were triggered, including 24 November 1943, 11 September 1972, 25 August 1987, 09 October 1996, 22 October 2002, or 3 April 2003, and 18 March 2013. The identification of these specific dates also highlights the significance of precise event dates in reconstructing past geomorphic activity and evaluating the triggers of such occurrences, contributing to enhance hazard management and mitigation strategies.

The multi-disciplinary approach revealed that major events had a widespread impact across the area, significantly transforming the terrain. Conversely, intermediate and minor events resulted in localized effects. These minor disturbances did not contribute significant new sediments but rather reactivated pre-existing deposits within the channels. This distinction highlights the importance of event magnitude in influencing geomorphic processes and emphasizes the complex interaction among rainfall intensity, sediment availability, and topographic factors in driving DF dynamics. This study suggests that not all extreme rainfall events necessarily trigger significant DFs, highlighting both the complexity and unpredictability of DF occurrence.

The regional analysis of DFs highlights potential geomorphic activity by integrating multiple indices with the distribution of intense precipitation events from long-term rainfall records. This combined approach provides a strong basis for identifying high-risk catchments and contributes to future hazard mitigation and land-use planning in the Northern Apennines.

This study highlights the complex correlation between geomorphic processes and environmental factors in influencing DFs, emphasizing the need for further investigation in key areas. Future research will focus on detailed grain-size analysis to refine our understanding of sediment transport and depositional dynamics in DF events. Moreover, geotechnical modeling will be conducted to explore the mechanical and physical processes that govern the initiation, movement, and deposition of DFs. Filling these research gaps will significantly enhance the comprehension of DF mechanisms and their variability over time and space. The outcomes will contribute to the development of advanced geomorphic models, facilitating precise reconstructions of historical events and supporting the sustainable management of regions prone to DF activity.

Authorship contribution statement

M. A. Rashid led the multidisciplinary analysis, contributing to geomorphology, dendrogeomorphology, orthophoto interpretation, and regional susceptibility mapping. He coordinated rainfall data correlation with debris flows years and played a key role in drafting the manuscript. **A. Chelli** provided continuous scientific guidance throughout the research and contributed significantly to the geomorphological analysis, interpretation of results, and the structuring and revision of the manuscript. **J. Melada, V. Manara, and B. Arcuri** were involved in the assessment and processing of rainfall and temperature data. **M. Brunetti** contributed to the analysis and interpretation of rainfall and temperature data. **M. Maugeri** contributed to the

development and interpretation of climatic data and assisted in manuscript writing and revision, coordinating the University of Milano unit in the DECC project. **S. Pescio, L. Trombino, and A. Masseroli** worked on the characterization of geopedological conditions of the soil and GIS for managing the geodatabase. **E. Petrella** analyzed soil hydraulic properties and participated in manuscript writing. **G. Leonelli**, principal investigator of the DECC project, provided overall coordination and strategic direction for the research. He offered substantial input in the interpretation of results and the writing and critical revision of the manuscript.

Declaration of Competing Interest

The authors declare that there are no competing financial interests or personal relationships that could have influenced the outcomes or interpretations of the work presented in this paper.

Acknowledgements

This research was conducted within the framework of the COMP-HUB and COMP-R initiatives at the University of Parma, supported by the 'Departments of Excellence' program of the Italian Ministry for Education, University, and Research (MIUR) for the periods 2018–2022 and 2023–2027. Additional funding was provided by the European Union – Next Generation EU / PRIN-PNRR through the PRIN 2022 PNRR – Projects of Great National Interest, specifically the DECC project (Debris flow hazard and climate change in the Northern Apennines: reconstructing and modeling past and future environmental scenarios), CUP D53D23022810001. This work was also supported by the University of Parma's PhD School of Earth Sciences, research fund XXXVIII_SCIENZE_TERRA_QUOTA10

6. Catchment scale reconstruction of debris flow dynamics in the Northern Apennines (Italy) using geomorphometry and field constrained numerical modeling

Muhammad Ahsan Rashid[1], Giovanni Leonelli[1], Roberto Valentino[1], Emma Petrella[1], Nazarena Bruno[2], Maurizio Maugeri[3], Veronica Manara[3], Alessandro Chelli[1]

[1] Department of Chemistry, Life Sciences and Environmental Sustainability, University of Parma, Parco Area delle Scienze, 11/a, 43124 Parma, Italy

[2] Department of Engineering and Architecture, University of Parma, Parco Area delle Scienze, 181/a, 43124 Parma, Italy

[3] Department of Environmental Sciences and Policy, University of Milano, Via Celoria 2, 20133 Milano, Italy

*Corresponding authors

E-mail address: M.A. Rashid muhammadahsan.rashid@unipr.it; G. Leonelli (giovanni.leonelli@unipr.it)

This chapter is under review in Engineering Geology Journal.

6.1 Abstract

This study investigates debris-flow (DF) dynamics in a remote and data-scarce catchment of the Northern Apennines (Italy) using an integrated approach. The analysis combines geomorphometric data, numerical modeling, sedimentological evidence, tree-ring disturbance records and ortho-photo interpretation. A key novelty of this work lies in the quantitative integration of multiple independent field-based datasets for reconstructing and validating historical DF dynamics in the absence of direct instrumental observations. The research focuses on the 1987 debris-flow (DF) event, one of the largest documented in the catchment, resulting in substantial sediment deposits and severe forest destruction. The event was triggered by an intense rainfall storm on 25 August 1987, with daily precipitation reaching ~220 mm at nearby monitoring stations (Collagna and Succiso). Sedimentological studies indicated distinct grain-size segregation, characterized by steep levee gradients (31°–41°) and more gradual lobe slopes (12°–30°), reflecting spatial variations in flow energy and depositional processes. The 1987 event was reconstructed using the RAMMS-DF (Rapid Mass Movement Simulation) model, calibrated through multiple scenarios including release volume, and Voellmy rheological parameters, and constrained by delineated depositional boundaries alongside detailed channel morphology. Model performance was validated by comparing simulated and observed runout distances, flow thicknesses, levee heights, and the spatial distribution of dendrogeomorphological disturbance signals, supported by precipitation and infiltration conditions. The findings demonstrate that robust reconstructions of debris-flow (DF) dynamics in data-scarce mountain regions can be achieved through a multidisciplinary, field-constrained modeling framework, highlighting the critical role of local hydrological and geomorphic controls and supporting engineering hazard assessment and risk-mitigation.

Keywords

Debris Flow Modelling, Dendrogeomorphology, Sedimentology, Channel Analysis, Geomorphometry

Highlights

- Geomorphometry and RAMMS-DF modeling was used to reconstruct debris-flow (DF) dynamics at catchment scale.
- High-resolution mapping and sedimentological evidence enabled realistic model calibration.
- Model validation through field data, tree-ring signals, soil properties, precipitation and infiltration processes.

6.2 Introduction

Debris flows (DFs) are rapid, gravity-driven flows of water-saturated sediments that can be triggered by intense precipitation, seismic disturbances, or rapid snowmelt, resulting in destructive effects on both infrastructure and human settlements (Matjaž & Bezak, 2021; Hungr et al., 2014; Takahashi, 2007). Understanding of DF dynamics is essential for effective hazard assessment and mitigation strategies, as the back-analysis of past debris flow (DF) events provides valuable understanding of flow behavior (Rickenmann et al., 2006). Rainfall thresholds, which identify critical precipitation levels that trigger DF events, serve as key predictive tools for hazard assessment and early warning systems (Guzzetti et al., 2007).

Numerical modeling has emerged as an influential approach for simulating the dynamics of DFs, providing critical details into the processes of flow initiation, transport, and deposition (Dos Santos Corrêa et al., 2024; Cabral et al., 2023).

A comprehensive understanding of DF dynamics, particularly in remote and un-monitored areas, can be achieved by employing multi-disciplinary approaches. Dendrogeomorphology serves as a powerful tool for reconstructing the frequency, and spatial extent of DF events over mid to long term timescales with annual resolution by analyzing trees impacted by geomorphological processes and their position (Rashid et al., 2026; Šilhán et al., 2023; Tichavský, 2023; Leonelli et al., 2021; Šilhán & Stoffel, 2015). The mechanical impact of DFs on the stems exerts stress within trees, creating eccentric growth patterns due to tilting trees up to the development of reaction wood in more extreme tilting (e.g., Curioni et al., 2024). These disturbances additionally damage stems, and generate asymmetrical growth anomalies that act as signal of past DFs events (Wistuba et al., 2013; Guida et al., 2008). This analysis may be used for validating models simulating DF dynamics and

their areal extension, beyond providing the possibility of detecting the dates of the rainfall event triggering the DF.

The identification and subsequent analysis of DF channels requires the utilization of high-resolution terrain data alongside advanced geomorphometric techniques. Mueting et al. (2021) undertook the segmentation of DF channels into finer sections, facilitating a more detailed investigation of erosion, deposition, and sediment transport dynamics along the flow path. In mountain terrains, parameters such as elevation and slope angle are critical in geomorphometric analysis, as they affect slope stability and the probability of DF initiation (Çellek, 2020; Wilson & Bishop, 2013).

Sedimentological analysis is essential for improving the understanding DF dynamics, particularly through the assessment of grain size distributions and depositional structures. DFs characteristically exhibit a poorly sorted, matrix-supported texture, with large boulders embedded within finer sediments, indicative of high energy transport and rapid deposition (Blair & McPherson, 1994). In numerous documented events, boulders exceeding 1 m in diameter are transported over considerable distances due to the high density and bulk strength of DFs mixtures, which sharply contrast with fluvial deposits that tend to exhibit better sorting, stratification, and clast imbrication (Blair, 2002; Whipple & Dunne, 1992; Pierson, 1980; Bluck, 1979). Tiranti et al. (2008) observed DF deposits in 12 basins and used depositional morphologies and sediment properties to divide catchments into three groups (carbonate basins with cohesive flows, fine grained metamorphic basins with frequent mud-rich flows, and coarse grained igneous/metamorphic basins dominated by non-cohesive DFs) based on sedimentology and rheology.

To support hazard and risk assessment, a range of numerical models have been developed and widely applied, such as RAMMS-DF (Matjaž & Bezak, 2021), RASH3D (Pirulli & Sorbino, 2008), r.avaflow (Baggio et al., 2021), FLO-2D (Armento et al., 2007) and DebrisFlow Predictor (Guthrie & Befus, 2021). These models allow for the simulation of key DF parameters such as velocity, volume, height, and runout distance, allowing for a more detailed assessment of their potential impacts on infrastructure, exposed communities, and land use. Model performance depends on the integration of topographic and hydrological data, along with friction coefficients, flow characteristics, and climatic variables, to simulate DF runout across both spatial and temporal domains (Martini et al., 2023). The spatial resolution of topographic data significantly influences

the computational power required and the accuracy of the model outputs (Bühler et al., 2018). Among these models, Rapid Mass Movements Simulation (RAMMS-DF), developed by the Swiss Federal Institute of Technology Zurich and the WSL (Bartelt et al., 2017; Gan & Zhang, 2020), is one of the most widely used for DF back-analysis and hazard assessment. The model outputs, particularly DF heights, are commonly employed in hazard assessment studies to explore different hazard scenarios and mitigation strategies (Zou et al., 2016).

The main objective of this study is to reconstruct and model DF dynamics in a data-scarce mountain catchment of the Northern Apennines (Italy), focusing on a single DF event. A numerical modeling was performed using the RAMMS-DF model, supported by geomorphometric and sedimentological analyses to quantify triggering and depositional mechanisms, and flow behavior. Model validation of the 1987 DF event was performed by combining dendrogeomorphological evidences, geomorphic observations, ortho-photos interpretation, soil properties, precipitation data and infiltration processes.

6.3 Study Area

The study area, ranging in elevation from 960 m a.s.l. to 2,017 m a.s.l., is centered around the Mount Alpe di Succiso, in the Northern Apennines, slightly north of the main Apennine ridge (Figure 6.1). The area falls entirely within the Tuscan-Emilian Apennines National Park.

A detailed characterization of the climatic setting of the study area, including long-term precipitation and temperature trends and extreme rainfall analysis, is presented in a related study (Rashid et al., 2026). Geologically, the DFs originate from the Macigno and Monte Modino sandstone formations. The transported material spans a wide range of grain size varies from fine clay particles to sizable blocks, reflecting the high energy and intensity of DF events. Sedimentological study of the depositional zones highlighted characteristic features of DFs, such as matrix-supported lobes, coarse-grained levees, and sharp depositional boundaries (Rashid et al., 2024; Rashid et al., 2026). These characteristics provide a key evidence for reconstructing flow dynamics and depositional processes.

The geomorphological setting of the study area is highly complex and strongly influenced by past glacial activity. Glacial landforms associated with glacier development during the Last Glacial

Maximum (LGM) (Baroni et al., 2018) and modified by multiple interacting processes including bedrock weathering, gravitational slope processes, and repeated DFs activity following glacier retreat. A detailed description of geological and geomorphological features of the research area have been detailed in Rashid et al. (2024). The area is predominantly influenced by active DF processes, with all four DF channels (Figure 6.1) containing remnants of earlier DFs indicating repeated flow events over time (Rashid et al., 2026).

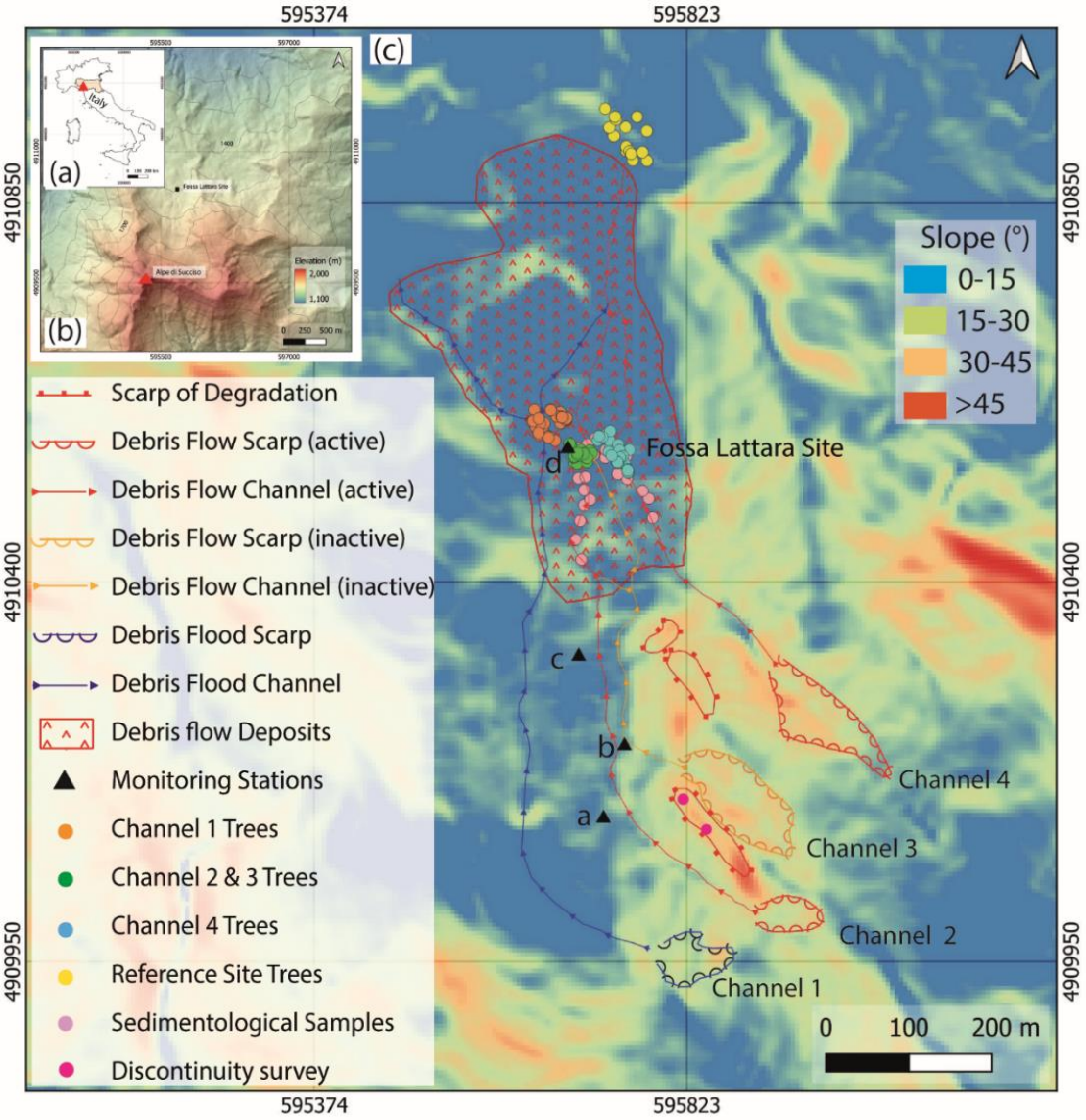

Figure 6.1: (a) Location of the study area in Italy; (b) elevation map of the study area; (c) slope angle map showing DFs landforms and channels (channels 2, 3 and 4) and the debris flood channel (channel 1). The location of sampled trees and sedimentological survey sites (shown as light pink points), while hydraulic monitoring stations (a, b, c and d) are also shown (see text for details).

In DF Channel 1, deposits are primarily confined within the channel boundaries. Despite this, significant destruction was noted along the channel's margins, where no direct debris deposits were observed. Importantly, a considerable number of trees exhibited severe damage, indicating that a debris floods provoked destruction without substantial deposition, thus indicating concentrated flow energy and lateral outflow. DF Channel 2 exhibits characteristics of both DFs and debris flood. In some sectors, depositional features such as coarse material and matrix-supported sediments are present, whereas in other areas trees are tilted or uprooted in the absence of deposits. This damage may partly reflect debris-flood effects associated with outflow from Channel 1. DF Channel 3 was inactive during the 1987 event (Rashid et al., 2026), and no geomorphological evidence of recent debris transport was identified. Conversely, DF Channel 4 revealed typical impact features of DF, including well-defined lobes and lateral levees. The trees in this vicinity are primarily damaged due to direct debris impact and sediment accumulation.

6.4 Materials and Methods

6.4.1 Data and Reconstruction Approach

A comprehensive, multi-method reconstruction framework was developed to analyze DF dynamics through integrated field, laboratory, and computational data sets. The adopted methodologies collectively enabled the reconstruction of the 1987 DF dynamics and its geomorphic impacts. The source, temporal coverage, resolution, and purpose of each dataset are outlined below.

Model input data:

- Photogrammetric data. Three high-resolution aerial images dated 1976 (i.e. the first available year before the 1987 event) were obtained from the Regione Toscana (https://www502.regione.toscana.it/geoscopio/ortofoto.html) and processed through a standard photogrammetric workflow using Agisoft Metashape v. 2.2.1. The block was constrained with Ground Control Points (GCPs) derived from the Regional Technical Cartography (CTR) and then validated using GNSS-measured Check Points (CPs), yielding an average horizontal accuracy of approximately 4 m. From the photogrammetric processing a georeferenced Digital Elevation Model (DEM) with 1 m resolution was obtained and employed as basis for the subsequent analyses. The achieved accuracy was considered

enough for DF modeling, although the related uncertainty was accounted for during model interpretation and spatial analysis.

- Channel Morphometric Analysis. The DEM obtained from the photogrammetric process was analyzed in a GIS environment to derive longitudinal profiles of slope and elevation along flow paths at 10 m intervals. The analysis was used to classify the source, transport, and depositional zones, highlighting zones influencing DF triggering, energy dissipation, and sediment deposition.
- Orthophotos data. To investigate the 1987 debris flow (DF) event, historical orthophotos from 1976 to 1988, before and after the event were directly acquired from the Regione Toscana geoportal (the ortophotos can be viewed at https://www502.regione.toscana.it/geoscopio/ortofoto.html and acquired under request). These images were georeferenced and analyzed using QGIS 3.36.0 to assess vegetation disturbances and spatial impacts resulting from the 1987 event. This analysis contributed to delineating the extent of the event and supported the reconstruction of geomorphic changes.
- Grain-size analysis. Grain size distribution over levees, lobes, and matrix zones was characterized through field studies and lab studies. Fine fractions (<16 mm) were analyzed using sieve and laser granulometry techniques while coarse fractions (>16 mm and <1000 mm) were measured in 35 in-situ 1 m^2 grids to document clast size variability. The count method was used to analyze the big clasts above 1000 mm. This analysis allowed to investigate sediment sorting, segregation, and flow-related depositional mechanism.

Model calibration:

RAMMS Modelling: The RAMMS-DF model was calibrated through back analysis using mapped depositional extents, channels morphology and release volume scenarios. Multiple rheological parameter scenarios were tested to identify the best-fit conditions reproducing observed flow behavior, run-out distances and depositional patterns.

Model Validation:

- The model was validated by comparing modeled and measured levee heights, by integrating dendrogeomorphological evidence, orthophoto vegetation loss footprint, sedimentological analysis, precipitation and infiltration processes.

- Precipitation and Rainfall data. Daily records from 1951 to 2023 were retrieved from SCIA (ISPRA) and regional networks (Dext3r, SIRAL, SIR). ARCIS gridded precipitation (5 km, 1961–present) was also used, along with sub-daily extremes from Italian Hydrographic Service Yearbooks. For further details of rainfall and temperature data refer to (Rashid et al., 2026 and Brunetti et al., 2009 & 2006).
- Soil hydraulic properties and infiltration monitoring. Soil hydraulic characteristics and infiltration were evaluated at four instrumented stations in geomorphic areas impacted by DFs. Continuous measurements of volumetric water content, matric potential, soil temperature, and bulk electrical conductivity at various depths were employed to evaluate infiltration processes and pre-existing moisture levels relevant to DF activity.

6.4.2 Channel analysis and sedimentological analysis

To investigate the morphometric controls on DF dynamics, slope angle and elevation were analyzed along the flow paths. These were derived from a high-resolution Digital Elevation Model (1 m/pix resolution) using the terrain analysis tools available in QGIS 3.36.0. The "Points along geometry" tool was employed to generate sampling points at regular 10 m intervals along the centerlines of DF channels, from the source areas to the deposition zones (Mueting et al., 2021). This approach allowed the construction of detailed longitudinal profiles for each DF path, highlighting critical slope segments and elevation changes that influenced flow behavior and depositional patterns.

Field investigations were carried out in DF-affected areas to characterize grain size distribution. Two channels of DF were investigated and sediment samples were collected to capture the full range of transported material. For fine to medium fractions (≤16 mm), approximately 1 kg of sample was collected at each site from a total of 16 locations, including flow lobes, levees, and matrix-supported deposits. The <2 mm fraction was analyzed using laser granulometry (Storti & Balsamo, 2010), while the 2–16 mm fraction was processed through standard sieve analysis following ASTM D6913/D6913M-17. Results from both methods were combined to construct a continuous grain size distribution curve covering the range (0.0005–16 mm).

Coarse fractions (>16 mm) were analyzed in the field using a grid-based measurement approach. In total, 35 randomly positioned 1 m^2 window frames (Khan & Valentino, 2022) were established across different DF deposits. Within each window, the intermediate axis (Blair & McPherson, 2009)

of all exposed clasts were measured and classified into three grain size classes: 16–64 mm, 64–256 mm, and 256–1000 mm. Particles exceeding 1000 mm were manually counted across the entire DF deposit.

The further classification of DFs deposits was performed using the Blair and McPherson (1999) chart. In addition, the fine-grained fraction (0.0005–16 mm) was compared with previously published datasets to evaluate consistency with established DF sedimentological characteristics.

6.4.3 Debris flow modelling

DF dynamics were simulated using the RAMMS-DF (Rapid Mass Movement Simulation) numerical model. Prior to using a numerical model, it was necessary to prepare an appropriate digital elevation model (DEM) to be used as data input. A 1-meter resolution DEM, representing the terrain conditions before the 1987 DF, was utilized as the primary topographic input for the simulations (Matjaž & Bezak, 2021; Frank et al., 2017; Schraml et al., 2015; Scheidl et al., 2012; Cesca & D'Agostino, 2008).

Field observations and event classification through field investigations were conducted to map DF channels, assess deposit thickness, and pinpoint areas of source areas, channels and deposition areas. Elevated precision Trimble GPS Antenna enabled the height measurement of DFs deposits at different locations. Channel 2 and channel 4 were chosen because of the significance of geomorphic evidence.

Debris flow simulations were performed using the RAMMS-DF model, a two-dimensional depth-averaged numerical model created by the WSL Institute (WSL, 2022). RAMMS-DF operates on shallow-layer flow equations and employs the modified Voellmy-Salm model (Salm et al., 1990), incorporating turbulence coefficients to better reflect real-world conditions and integrating seamlessly with GIS-based analyses (Gan & Zhang, 2020). This model takes into consideration both Coulomb-type and turbulent resistance components and is designed for granular flows. The frictional resistance (S) is calculated through the following equation:

$$S = \mu \cdot \rho \cdot g \cdot h \cdot cos(\phi) + \frac{\rho \cdot g \cdot v^2}{\xi} \qquad (6.1)$$

where S represents the frictional resistance [Pa], μ is the basal friction coefficient, ρ is the density of the DF, h is the flow height (or flow depth), g is the gravitational acceleration, ϕ is the slope angle of the channel bed, v represents the velocity of the flow and ξ represents the turbulent friction coefficient. RAMMS-DF model allows for single or multiple release areas within a simulation, with flexible parameters tailored to the specific characteristics of the study area (Liu et al., 2021).

Numerical modeling was conducted for both Channel 2 and Channel 4, utilizing site-specific DF parameters obtained from field observations and literature (Matjaž & Bezak, 2021). The input parameters, which are reported in Table 6.1, have been selected based on back-analysis in both channels. In particular, a material density of 2000 kg/m³ is fixed because by changing the density (1800-2200 kg/m³) there was no significant effect on the debris flows simulations, a basal friction coefficient (μ) equal to 0.10, 0.14, 0.18, 0.22 and 0.26, and a turbulent friction coefficient (ξ) fluctuating from 120, 170, 220, 270 m/s² were used in the analysis. The values can be compared with those reported in previous studies (Matjaž & Bezak, 2021). The simulation period was not predetermined but adjusted during scenario testing. Various time intervals were assessed across distinct input volumes. Seven distinct release volume scenarios (based on field-mapped source areas) were assessed for each channel: Channel 2 (Table 6.2) exhibited release volumes between 6987 m³ to 20654 m³, whereas Channel 4 (Table 6.3) ranged from 5889 m³ to 16343 m³. Model calibration was conducted by methodically comparing the generated deposition extents and flow heights with field-observed data. Two simulation phases were conducted to calibrate the rheological parameters in RAMMS. During the initial phase, the turbulent friction coefficient (ξ) was maintained at a constant value of 170 m/s², while the Coulomb friction coefficient (μ) was altered within the range of 0.10 to 0.26. This step helped to determine the μ value that is most coherent with the observed deposition patterns and flow heights. In the second phase, the ideal μ value derived from the first phase was maintained constant, while the ξ values were adjusted within a range of 120 to 260 m/s² to assess their impact on flow behavior and refine model performance. This two-step sensitivity analysis facilitated a calibration of the Voellmy rheology parameters under localized settings (Cabral et al., 2023).

Table 6.1: Details of input parameter of RAMMS model

Input	**Source**	**Numerical Parameter**
Topographic data	1:1000	1 m
Release area	Scars from Aerial Photos (1976 and 1988); and Field surveys	-
Release volume	Back analysis, field surveys	Table 6.2 & 6.3
Calculation domain	Field surveys and aerial pics	-
Debris Flow duration	Back analysis	180 seconds for channel 2 and 140 second for channel 4
Material density	Literature and back analysis (Matjaž & Bezak, 2021)	2000 kg/m³
Coulomb friction coefficient (μ)	Back analysis	Table 6.2 & 6.3
Turbulent friction coefficient (ξ)	Back analysis	Table 6.2 & 6.3

Table 6.2: Calibration and scenario analysis parameters for RAMMS-DF software for Channel 2

Analysis	Source volume (m^3)	Friction Coefficient (μ)	Turbulent Coefficient (ξ) (m/s^2)	Flow Height (m)	DEM (m)
I	20654	0.22	170	6.4	1
II	14263	0.22	170	6.1	1
III	12352	0.22	170	5.7	1
IV	9103	0.22	170	5.1	1
V	8238	0.22	170	4.8	1
VI	7555	0.22	170	4.6	1
VII	6987	0.22	170	4.2	1

Table 6.3: Calibration and scenario analysis parameters for RAMMS-DF software for Channel 4

Analysis	Source volume (m^3)	Friction Coefficient (μ)	Turbulent Coefficient (ξ) (m/s^2)	Flow Height (m)	DEM (m)
I	16343	0.22	170	7.2	1
II	11523	0.22	170	6.8	1
III	9541	0.22	170	6.1	1
IV	7982	0.22	170	5.7	1
V	7335	0.22	170	5.3	1
VI	6654	0.22	170	4.8	1
VII	5889	0.22	170	4.6	1

6.4.4 Hydraulic properties of soil

Four monitoring stations were installed in representative areas affected by DFs to investigate soil hydraulic properties and analyses the water infiltration processes (Figure 6.1). Going into detail, the selected sites reflect variation in land use of the area (forest vs. grassland), different geomorphological positions related to the DF system (flank, steep slope, near flat area, between two DF channels) at elevations ranging from 1510 to 1640 m a.s.l. Each station was instrumented with two different types of sensors at two different soil depths: Teros 12 probes (Meter Group) for Volumetric Water Content and Bulk Electrical Conductivity, and Teros 21 probes (Meter Group) for Temperature and Matric Potential. Monitoring was conducted from middle of June to the middle of November 2024 to record the response of the hydraulic parameters during the first major rainfall events in autumn, after the summer dry season.

6.5 Results

6.5.1 Site characterization and sedimentological analysis

Two channels in the study area showed distinct DF deposits within their depositional zones. One channel presented deposits that were confined to the channel boundaries, with no indications of deposition in the adjacent regions. The identification of channel 3 was recognized as inactive during the 1987 event and was validated by historical orthophotos. The three levees that were observed in the study area (Figure 6.2) ranged in height from approximately 1 to 3.5 m at different locations.

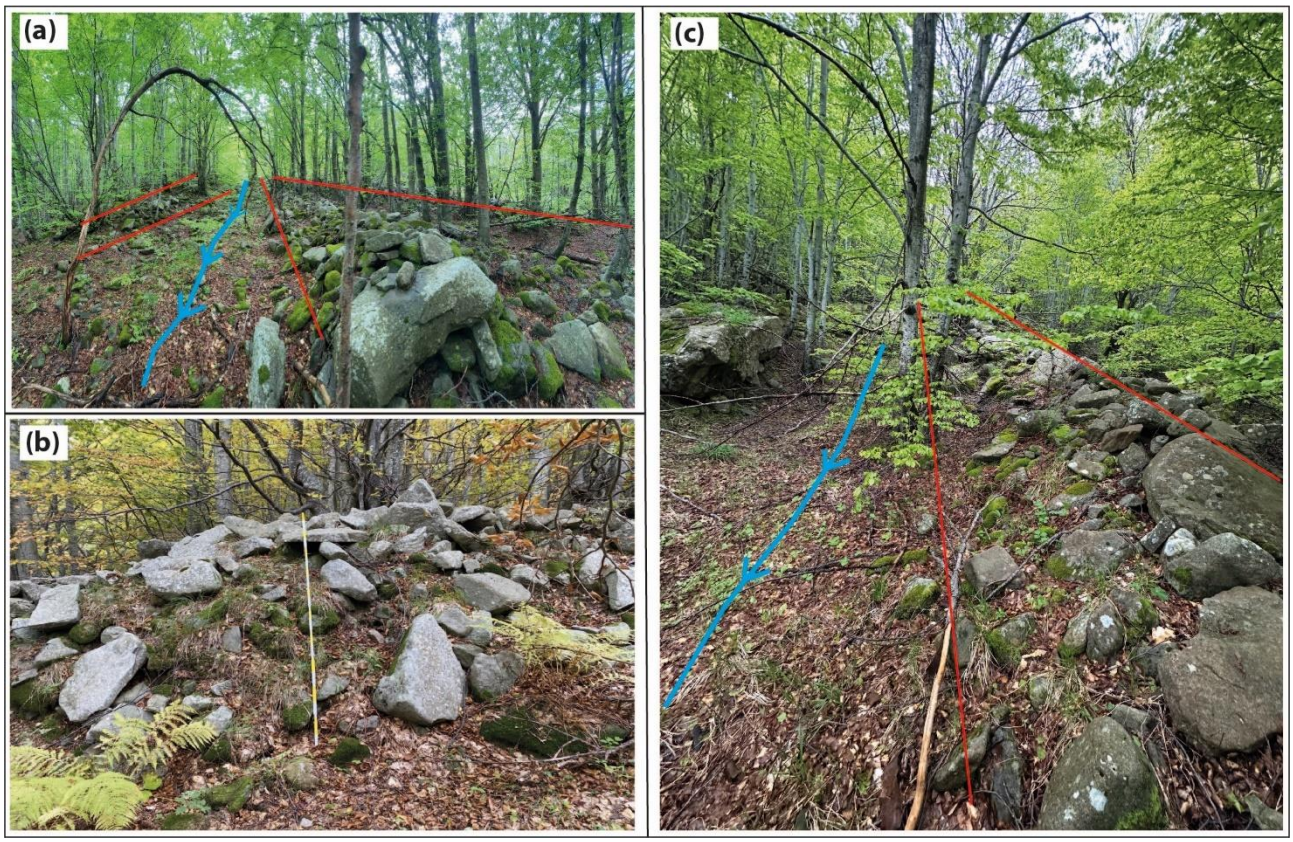

Figure 6.2: (a) Two levees (highlighted in red) formed by Channel 4 (highlighted in pale blue) deposits; (b) Levee height (the length of stick meter is 200 cm) (c) Levee deposits (highlighted in red) from Channel 2 (highlighted in pale blue).

The sedimentological analysis indicates distinct patterns in particle sorting and slope angles between lobe and levee deposits. In lobe deposits, larger particles consistently occur at the front side, transitioning to finer particles towards the back (Bardou, 2002). Conversely, levee deposits exhibit vertical sorting, with larger particles predominantly at the top and finer particles at the bottom. Additionally, slope angles significantly differ between these depositional forms: levees demonstrate steeper slopes ranging from approximately 31° to 41°, whereas lobes have comparatively gentler slopes between 12° and 30° (Table 6.4). These findings align with existing literature, suggesting that levee steepness is related to confinement and sediment transport dynamics, while gentler slopes in lobes result from sediment spreading and gradual loss of kinetic energy, facilitating deposition (Blair & McPherson, 2009; Major & Iverson, 1999).

Table 6.4: Detailed observations of DF deposits involved in modelling across ten distinct sections revealed varying sediment characteristics and geomorphological features. For further details of location refer to section 6.5.5.

Sections	Type	Height (m)	Particle Shape	Particle Size Distribution	Structure	Deposits Angle
Section 1	Lobe	2.2	Angular to Sub-angular	Front: 25-140 cm, Upper: 8-29 cm	Open work top, matrix supported below	20-22
Section 2	Levee	2.9	Angular to Sub-angular	Upper: 77-155 cm, Lower: 1-21 cm Back: 2-23 cm	Massive	34-36
Section 3	Lobe	2.8	Angular to Sub-angular	Front: 21-180 cm, Back: 1-22 cm	Massive	20-25
Section 4	Lobe	3.1	Angular to Sub-angular	Front: 50-130 cm, Lower:1-23	Open work top, matrix supported below	28-30
Section 5	Levee	3.2	Angular to Sub-angular	Top: 34-70 cm, Bottom: 1-12 cm	Massive	31-33
Section 6	Levee	1.7	Angular to Sub-angular	Top: 12-70 cm, Bottom: 2-7 cm	Massive	32-35
Section 7	Lobe	2.2	Angular to Sub-angular	Front: 20-75 cm, Bottom: 3-12 cm	Open work top, matrix supported below	12-15
Section 8	Levee	3.3	Angular to Sub-angular	Top: 15-90 cm, Bottom: 2-6 cm	Open work top, matrix supported below	38-41
Section 9	Lobe	3.1	Angular to Sub-angular	Front: 14-110 cm, Bottom: 11-22 cm	Massive	27-30
Section 10	Lobe	2.3	Angular to Sub-angular	Front: 11-98 cm, Bottom: 3-17 cm	Massive	26-28

The grain-size sorting shows predominantly coarser, angular to subangular particles, particularly in the upper part of the levees, with a gradual transition downward into finer, matrix-supported sediments. This vertical and lateral sorting reflects the dynamic energy conditions during DF propagation, highlighting variations in flow energy strongly control sediment transport and deposition. The lack of well-developed sedimentary structures further highlights the deposition environment characteristics of DF processes, affirming grain size and sedimentological characteristics as key indicators for interpreting flow dynamics and depositional mechanisms.

Larger boulders and coarse particles are observed at steep surge fronts, resulting in the development of lateral levees through high frictional interactions and flow dynamics. In contrast, depositional lobes form as frictional resistance at the flow fronts halts debris movement, resulting in finer materials accumulation behind the coarser front deposits (Figure 6.3). This grain-size segregation process (Bardou, 2002) produces steeply inclined levees and more gently sloping lobes, which is consistent with field observations from the present study.

Figure 6.3: Schematic representation of debris flow body and deposits (the length of stick meter is 100 cm) (modified after Bardou, 2002).

Grain size variations are summarized in Figure 6.4a. The minimum, maximum, and mean values from all grain size curves were used to construct a representative mean distribution, which was compared with published datasets from previous DF studies (Figure 6.4b) (D'Agostino et al., 2010; Hu et al., 2011; Liu et al., 2024; Scheidl et al., 2012; Wang et al., 2018; Yang et al., 2020; VAW, 1992). The grain size distribution in the 35 square window frames analyzed, indicates a granular DF, characterized by the following size counts: 420 particles in the 16–64 mm range, 250 particles in the 64–256 mm range, and 180 particles in the 256–1000 mm range (Figure 6.4c). Clasts larger than 1000 mm were recorded separately across DF area, with approximately 1030 grains identified. These data are illustrated using a bar chart to emphasize the relative contribution of each size class.

Furthermore, the grain-size distribution in the study area was compared with the grain-size classification proposed by Blair and McPherson (1999). The results reveal that the deposits range from clay-sized particles to blocks reaching up to 6 meters in diameter (Figure 6.5), indicating a highly heterogeneous and poorly sorted material. This wide range spectrum further supports the interpretation of the event as a granular DF. The presence of such large blocks alongside finer sediments suggests high-energy transport conditions capable of mobilizing and depositing coarse material over significant distances. This broad distribution also reflects the dynamic depositional environment and complex flow behavior typical of DFs in steep mountainous terrains.

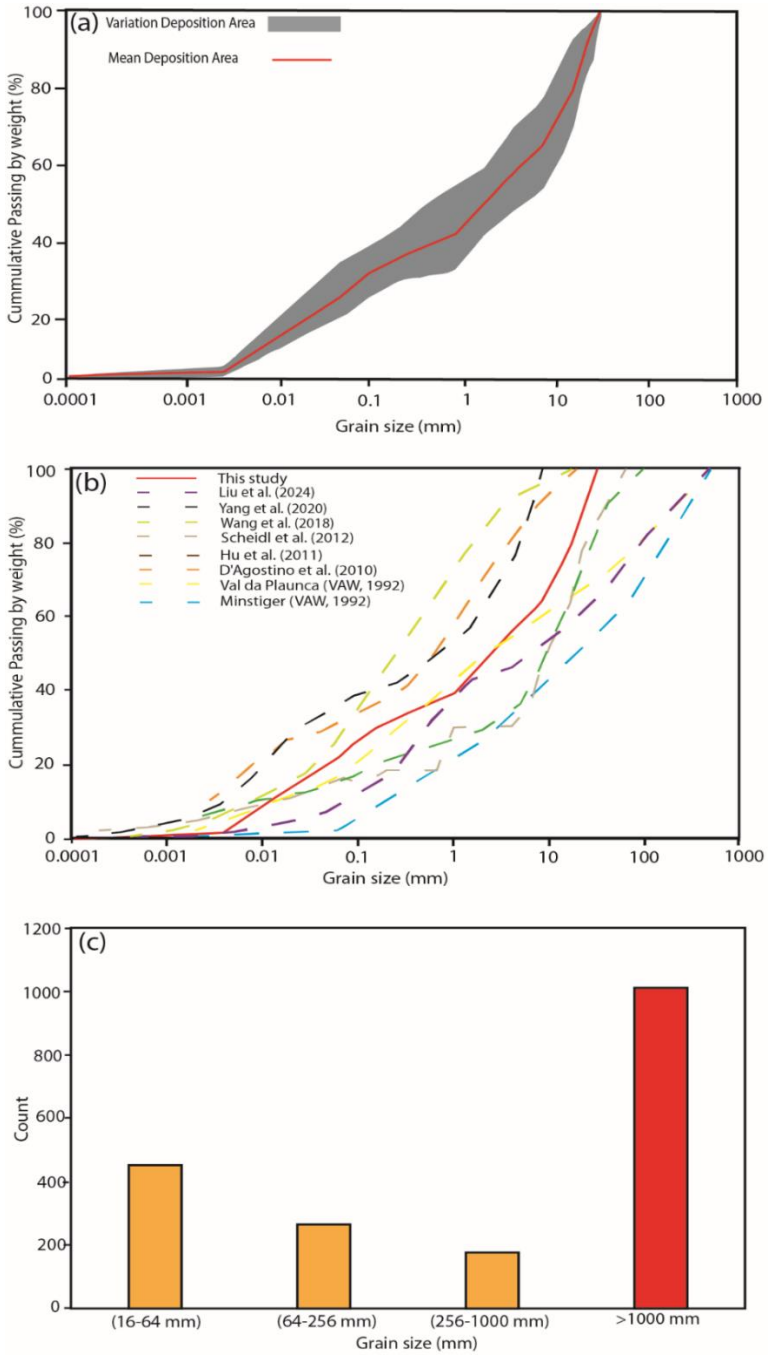

Figure 6.4: Grain size distribution in the deposition area: (a) mean grain size curve of fine particles; (b) comparison between the grain size distribution curve of this study with curves from other case studies; (c) frequency of counted large particles: the orange histograms refer to the DF deposit area in 35 m^2 window; the red shading indicates the overall distribution of grains over 1 m.

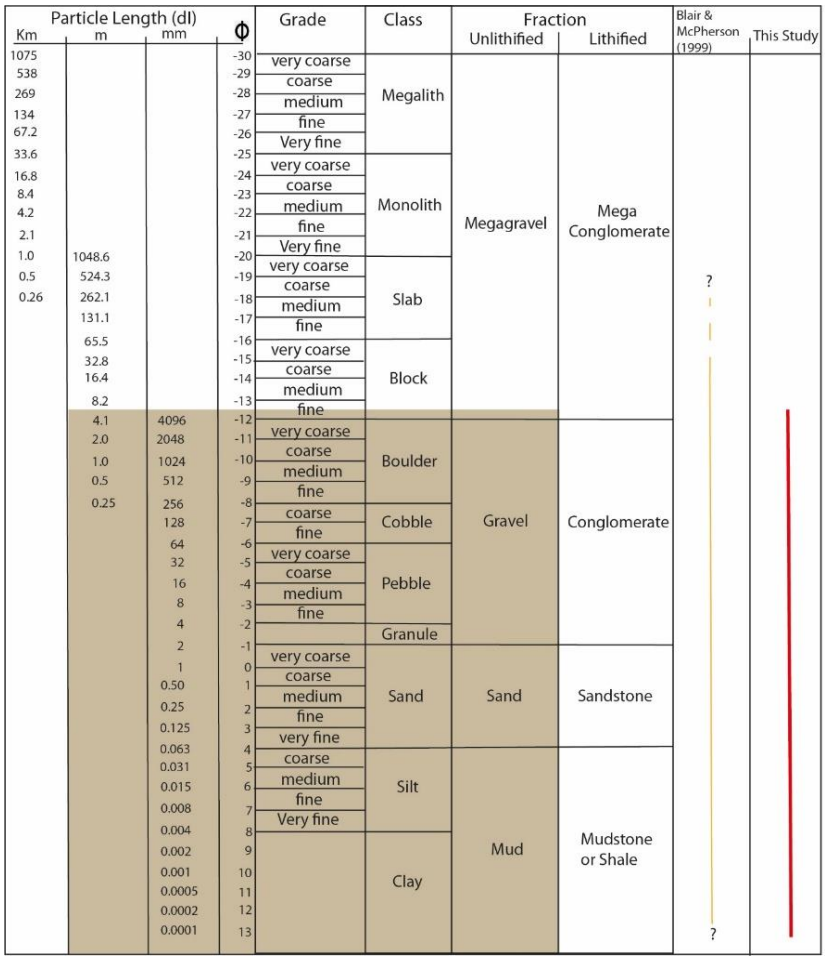

Figure 6.5: Grain-size classification terminology adapted from Blair and McPherson (1999).

6.5.2 Hydro-geomorphic evidence and reconstruction of the 1987 DF event

Detailed dendrogeomorphological dating and analyses of DF event chronology in the study area are presented in a related publication (Rashid et al., 2026).

The catchment study area experienced a heavy rainfall storm on August 25, 1987 (Figure 6.6), with marked magnitudes at neighboring stations. On the same day, the Succiso station recorded 178.6 mm of precipitation, while the Collagna station recorded its second highest (1950-2023) daily total of 220.6 mm. Both stations continuously recorded the same event signal despite these spatial variations, indicating its regional relevance. This interpretation is correlated by comparison with ARCIS (Archivio Climatologico per l'Italia centro-Settentrionale) gridded data, which shows that the 1987 event is in the top ten daily events in the 1961-2023 period for both the Collagna and Succiso stations and the ARCIS cell that includes the Fossa Lattara location. In the 1987 precipitation record,

a sudden and exceptional increase in rainfall is observed on 25 August 1987, far exceeding the values recorded during the rest of the year (Figure 6.7). This intense precipitation event acted as the primary triggering factor for DF activity, highlighting the strong hydro-meteorological control on slope instability in the study area.

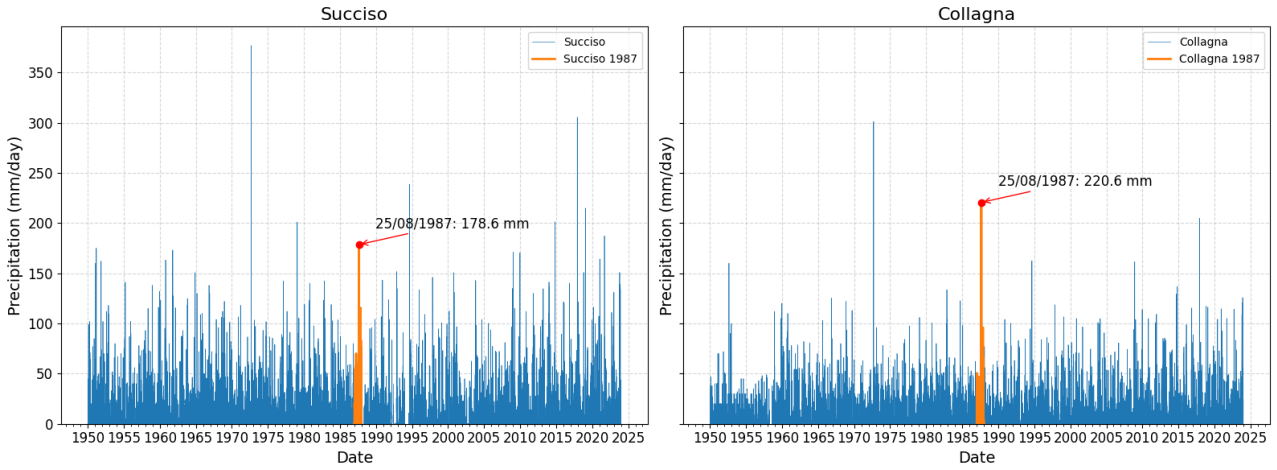

Figure 6.6: The rainfall event of August 25, 1987 in nearby stations of study area (from 1950-2024), was not the highest daily event recorded at that stations. Instead, it ranks as the second-highest event at the Collagna station and within the top ten events at the Succiso station.

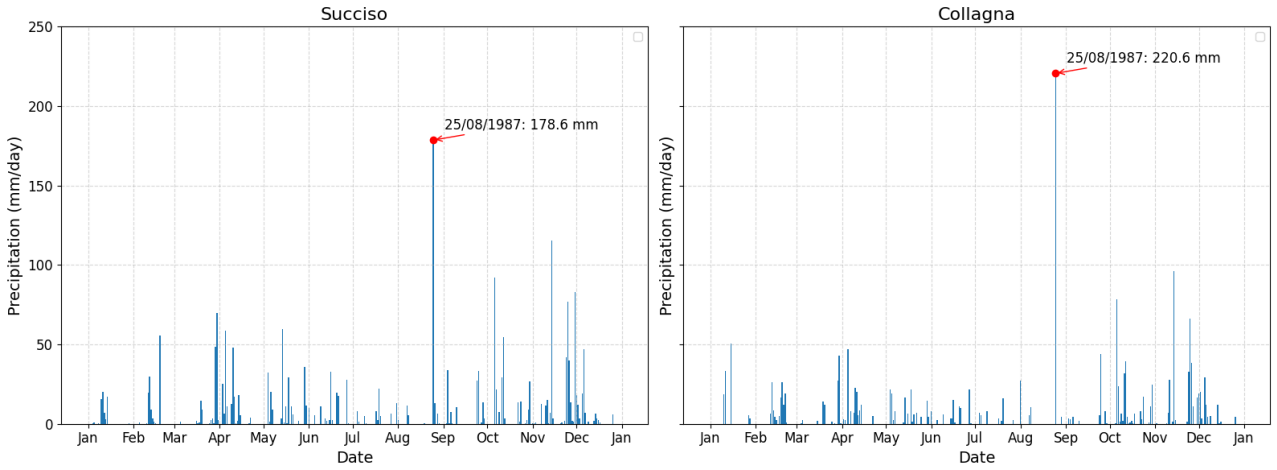

Figure 6.7: Daily rainfall in the nearby stations of study area for the year 1987.

After confirming the year of the DF event, trees exhibiting signs of disturbance corresponding to that year were identified and mapped. Using a historical orthophoto from 1988 (just after the event), the channel and extent of the DF were delineated (Figure 6.8). The image indicates extensive vegetation destruction, with numerous trees showing severe damage. This spatial pattern

delineates the DF impact zone, and highlighting the intensity of the event and its effect on the forested landscape, which covers an area of approximately 17000 m^2.

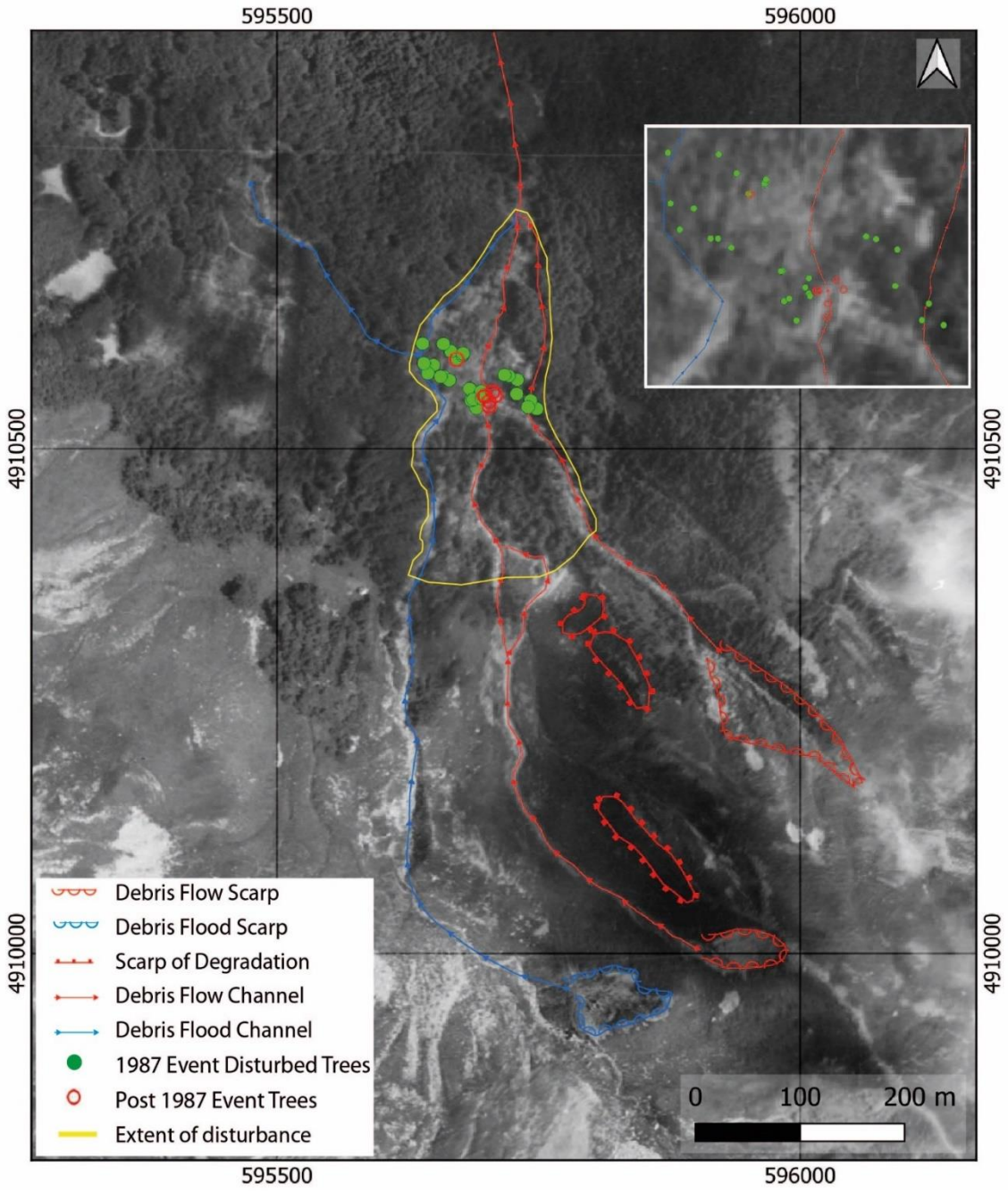

Figure 6.8: Historical orthophotos illustrating the DF event of 1987 (orthophoto 1988).

6.5.3 Slope-based zonation of DF channels

In Channel 2 (Figure 6.9), distinct slope-based zones associated with DF dynamics were identified. The source area is characterized by steep slopes ranging from 38° to 33°, reflecting areas where DFs are triggered primarily due to gravitational forces with intense rainfall. Downstream, the transport zone displayed a progressive decrease in slope from 30° to 15°, representing an intermediate sector where sediment transport occurs effectively. Further downstream, slopes reduced to less than 15°, defining the deposition zone, where flow velocities decrease and facilitating sediment accumulation becomes dominant.

A similar zonation was observed in channel 4, although source area exhibited steeper slopes, ranging between 30° to 40°, indicative of a larger and more dynamic triggering area. The transport zone is defined by gradual reduction in slope from 27° to 16°, allowing sustained sediment transport. The deposition zone is characterized by gentler gradients below 15°, providing favorable conditions for sediment accumulation and deposition of DF.

This slope-based zonation reflects geomorphic processes across the source, transport, and depositional domains. Steep gradients in the source zones are critical for debris mobilization, moderate slopes in the transport zone facilitate sediment transport, and low gradients (Table 6.5) in the deposition zone promote sediment accumulation. These systematic variations in slope angles provide important details into DF behavior and highlights its significant role in influencing channel morphology. Rock-mass conditions indicate only minor, structurally controlled failures, with a limited contribution to sediment supply locally; details are shown in Figures 6.10 and 6.11. The discontinuity survey (within the study area demonstrated Rock Mass Rating (RMR) values ranging between 45 and 56, thereby classifying it as rock of moderate quality, whereas Rock Quality Designation (RQD) values fluctuated from 44% to 65%, indicating a range from poor to fair quality. The structural assessment revealed significant sets of discontinuities J1 (NW) and J2 (SW), along which failures were observed. Wedge-type failures were detected as a result of the interaction of joint sets J1 and J2, while planar failures predominantly manifested along joint set J2.

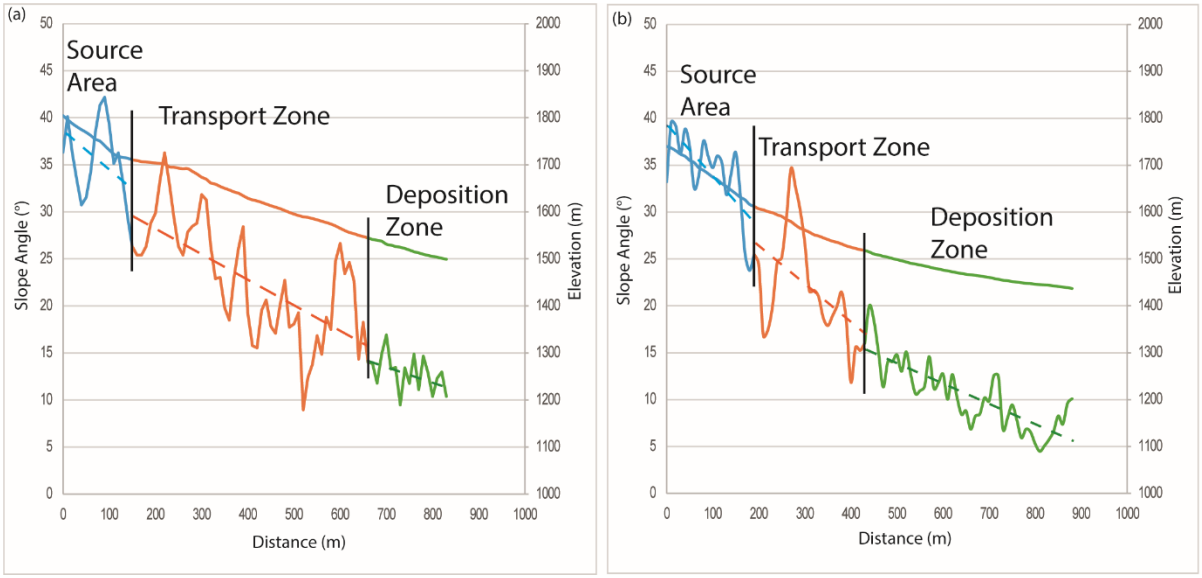

Figure 6.9: Logitudal profile of elevation and slope angle of the Channel 2 (a) and Channel 4 (b).

Table 6.5: The gradient (Δh / Δx) of DF channels

Channel number	Source Zone (Δh / Δx)	Transport Zone (Δh / Δx)	Deposition zone (Δh / Δx)
2	0.62	0.32	0.26
4	0.67	0.40	0.17

Figure 6.10: Discontinuity survey in the study area (see figure 1 of main manuscript) (11/08/2023).

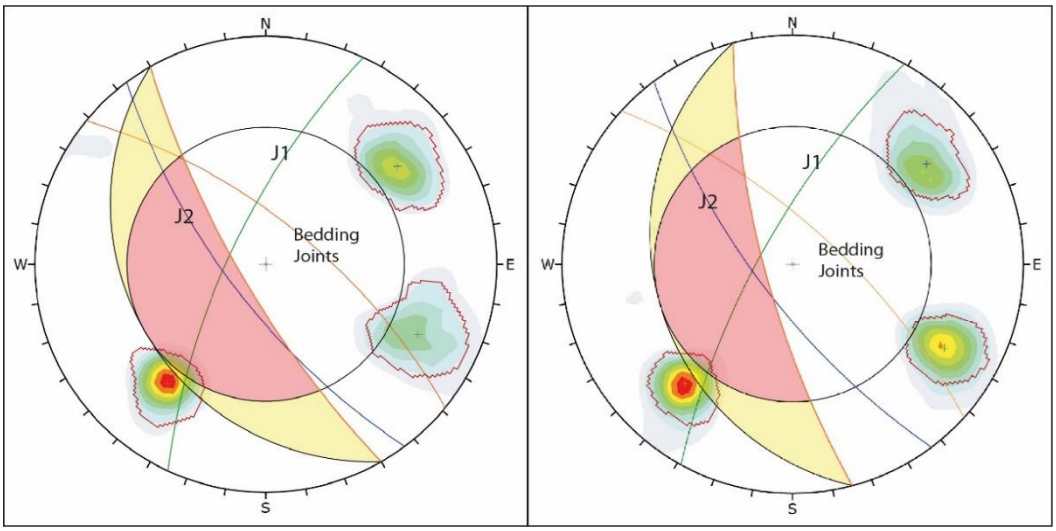

Figure 6.11: Discontinuity survey in the vicinity of the study area, indicating the presence of wedge failures.

6.5.4 Hydraulic properties of soil

The hydraulic data collected from the field monitoring stations reveal a clear seasonal pattern (Figure 6.12 a-d). During summer, sporadic rainfall combined with warm air and soil temperatures produces multiple wetting–drying soil cycles. In contrast, the fall season is characterized by more frequent precipitation and cooler soil temperatures (<10 °C), leading to persistently higher moisture levels and shorter drying or recovery intervals.

Soil depth ranges from a few centimeters to approximately half a meter affecting the soil response to meteorological parameters. The upper soil layer (15–20 cm below the surface) exhibits greater variability in soil hydraulic parameters compared with the deeper horizons (30–38 cm), reflecting its stronger and more immediate connection with atmospheric conditions. For instance, soil temperature in the surface horizon tends to show higher summer and lower winter values compared to the deeper soil horizon. It also evident a time lag of about 12 hours relative to air temperature. In contrast, the deeper horizon (30–38 cm) displays a much more stable thermal regime: daily oscillations are strongly dampened, and thermal propagation through the soil profile is slower. During the dry season (summer), temperature signals at this depth can lag those at the surface by approximately 2–3 days (Figure 6.12 e). A similar depth-dependent response is also observed for soil moisture. The Volumetric Water Content (VWC) increases almost instantaneously after major rainfall events, but with distinct timings across the soil profile. For example, at ST4, during the rainfall event on 9 June 2024 (14.6mm daily rainfall depth), a sharp rise in VWC begins about 2 hours after the

onset of precipitation in the shallowest soil layer, whereas the deepest sensor records the increase with a 4-hour delay (Figure 6.12 f). In wet season (Autumn), persistent and intense rainfall, together with a marked decline in air temperatures, keeps the soil continuously moist, creating favorable conditions for the initiation of DF processes.

Across the monitoring sites, the soil system exhibits a remarkably fast hydrological response: even moderate rainfall triggers rapid increases in VWC, first in the upper horizons and shortly after in the deeper layers. This behavior reflects a highly permeable and well-connected soil structure capable of quickly routing precipitation into the subsurface.

Minor differences were observed among the stations, mainly due to variations in soil composition, slope gradient and solar exposure. However, these factors did not significantly alter infiltration dynamics. In fact, the infiltration processes remain relatively consistent along the slope where DF occurred, implying that seasonal moisture variations may influence slope stability more than spatial differences in soil hydraulic properties.

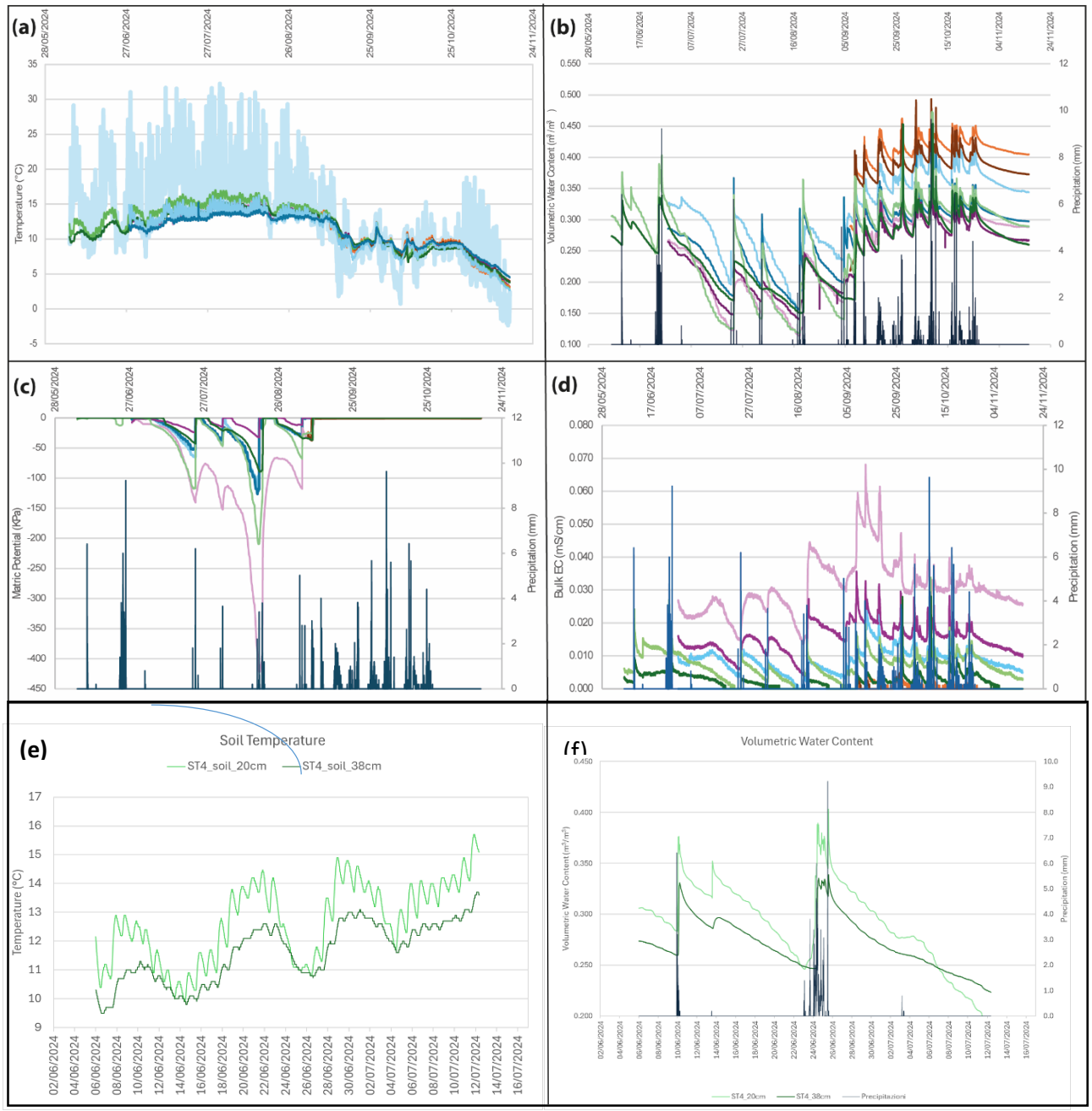

Figure 6.12: Soil hydraulic parameters monitored at the four stations: a) Soil temperature; b) Volumetric water content in soil; c) Matric Potential in soil; d) Bulk EC in soil; e) Detail of temperature variation at ST4; f) Detail of VWC variation at ST4. Legend: Lines) Light blue: ST1 at 15cm depth; Dark blue: ST1 at 30cm depth; Pink: ST2 at 20cm depth; Purple: ST2 at 37cm depth; Orange: ST3 at 15cm depth; Brown: ST3 at 30cm depth; Light green: ST4 at 20cm depth; Dark green: ST4 at 38cm depth. Blue bars: Precipitation. a) b) c) and d) are from Rashid et al. (2026).

6.5.5 DF modeling and validation of 1987 event dynamics

The numerical modelling of DF for the 1987 event was carried out to reconstruct its dynamics and spatial extent. The source areas for Channel 2 and Channel 4 (Figure 6.13a) were defined through detailed field surveys combined with analysis of historical aerial orthophotos from 1988, which were captured immediately after the event. These orthophotos were crucial in delineating the initiation zones, transport pathways, and deposition areas, and provided an essential banchmark for comparing model outputs with observed geomorphic evidence.

For Channel 2 (Figure 6.13b), the simulation that most realistically reflected field conditions, utilized a source volume of 9,103 m^3, effectively exhibiting the observed extent and thickness of deposits. Similarly, in Channel 4 (Figure 6.13c), a source volume of 7,335 m^3 appropriately represented the runout distance, flow direction, and deposit heights, in accordance with field observations and the 1988 orthophoto. The combined simulation of both channels (Figure 6.13d) illustrated an interaction between DFs and further supports the consistency of the selected input parameters.

The modeling results indicate that the DFs followed the channel paths, and the deposition zones closely matched with field-mapped deposits and post-event orthophoto evidence, inluding zones of trees disturbance and location of surveyed cross sections (Figure 6.14). In both channels, the material was predominantly deposited downslope, forming three distinct levees along the margins of the deposit (Figure 6.15). These levees were clearly observable in the RAMMS output as zones of maximum heights (black lines). Furthermore, an area highlighted in orange exhibited an absence of DF deposits. This area is associated with a debris flood from Channel 1, characterized by high flow energy but limited sediment transport. As a result, vegetation damage and surface disruption occurred without the formation of significant deposits. Additional supporting evidence for this interpretation is provided in Figure 6.16. Overall, the comparison between simulated and field observed depositional patterns shows the spatial reliability of the model.

To further validate the the modelling results, 10 field measured cross-sections (Table 6.6) were documented (height of DF deposits) and compared with RAMMS DF simulations. The comparison revealed a significant correspondance between flow height, although some local differences still remain. Given the complexity of the modeled phenomenon and the extension of the study area, this consistency between field measurements and model results could be considered satisfactory.

Overall, the results support the robustness of the chosen input parameters and confirm the model's efficiency to realistically reprroduce DF dynamics in complex terrain.

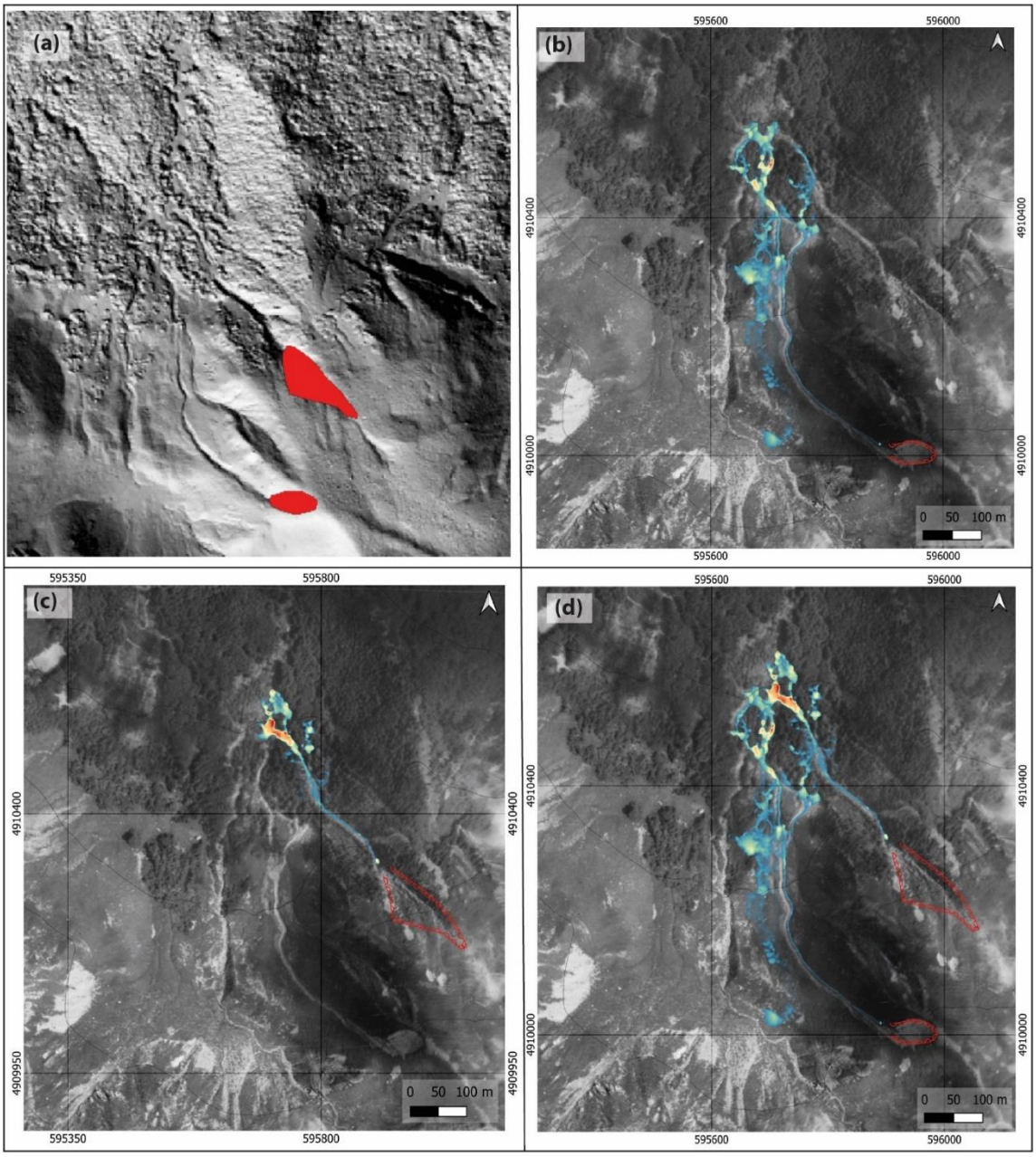

Figure 6.13: (a) Identified source areas of debris flows (red polygons); (b) Flow simulation results for Channel 2 (red line shows the source area); (c) Flow simulation results for Channel 4; (d) Combined simulation showing interaction of debris flows from both channels.

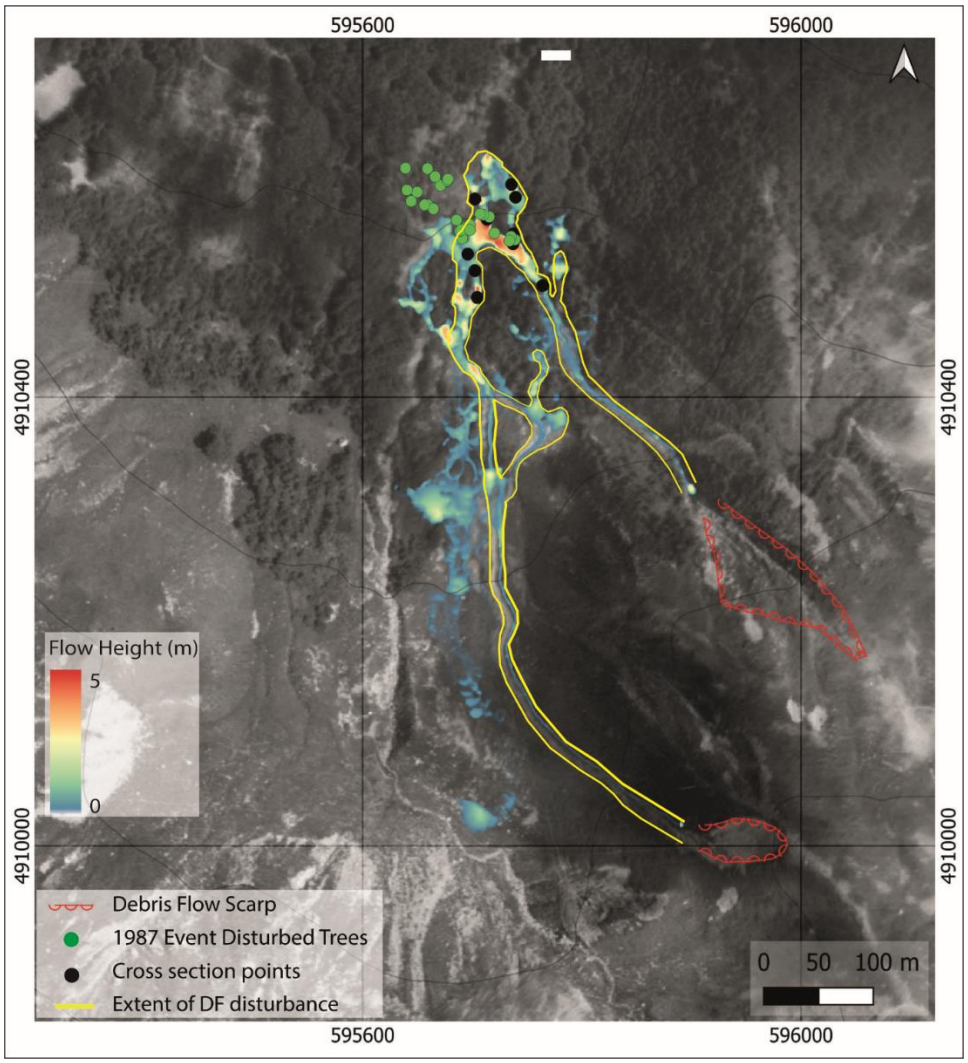

Figure 6.14: (a) Overview of the simulated DF of 1987 from source area to deposition area showing the locations of disturbed trees and cross-section points and yellow color indicating the extent of DF

Table 6.6. Cross section of field observations with simulation results

Deposit Number	Field Observations (Height)	Simulation results (Height)	Difference
section number 1	2.20 m	1.40 m	+0.8 m
section number 2	2.90 m	4.50 m	- 1.60 m
section number 3	2.80 m	2.60 m	+0.20 m
section number 4	3.10 m	2. 20 m	+0.90 m
section number 5	3.20 m	4.60 m	-1.40 m

section number 6	1.70 m	2.20 m	-0.50 m
section number 7	2.20 m	2.50 m	-0.30 m
section number 8	3.30 m	5.10 m	-1.80 m
section number 9	3.10 m	2.60 m	+0.50 m
section number 10	2.30 m	0.60 m	+1.70 m

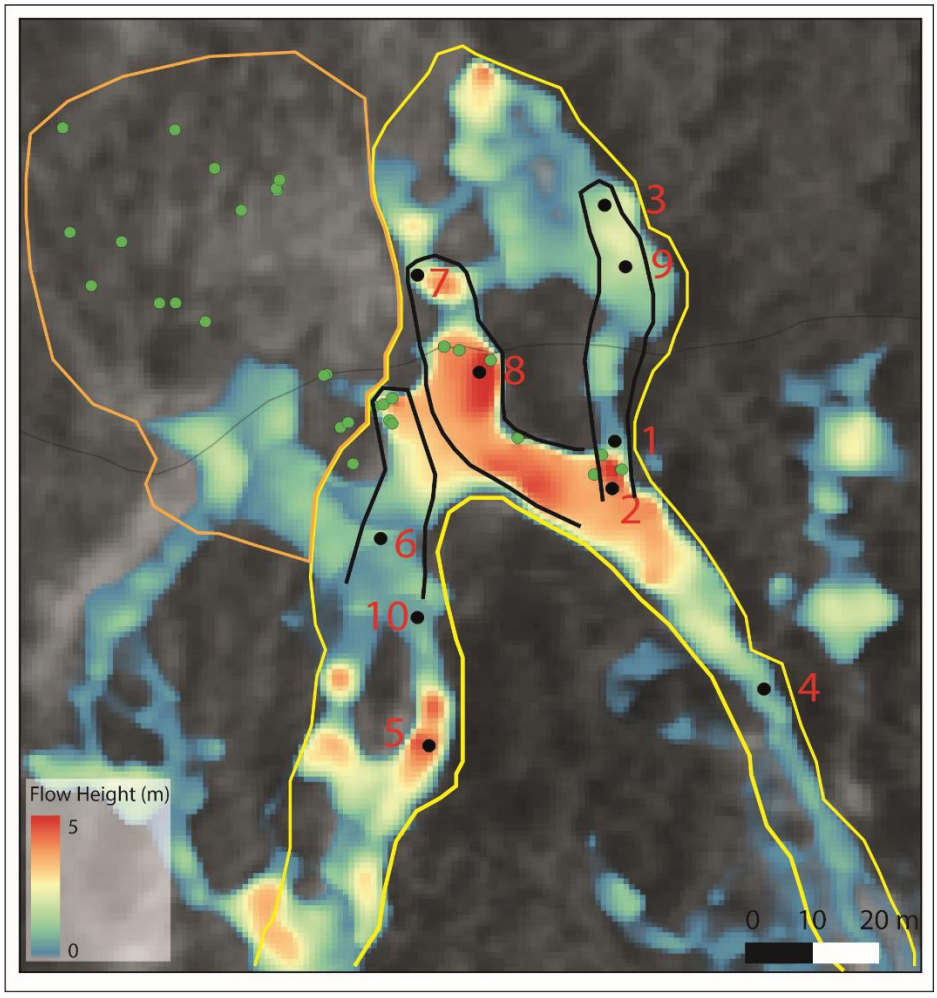

Figure 6.15: Overview of the DF and debris flood deposition extents. The orange-marked zone indicates an area with no visible debris flow deposits, suggesting that the observed disturbances are likely associated with a debris flood event originating from Channel 1. The extent of DF deposits is delineated by the yellow line, while the positions of three levees are indicated by black lines. Numbers and black dots represent sedimentological survey points. Green points indicate trees disturbed during the 1987 event.

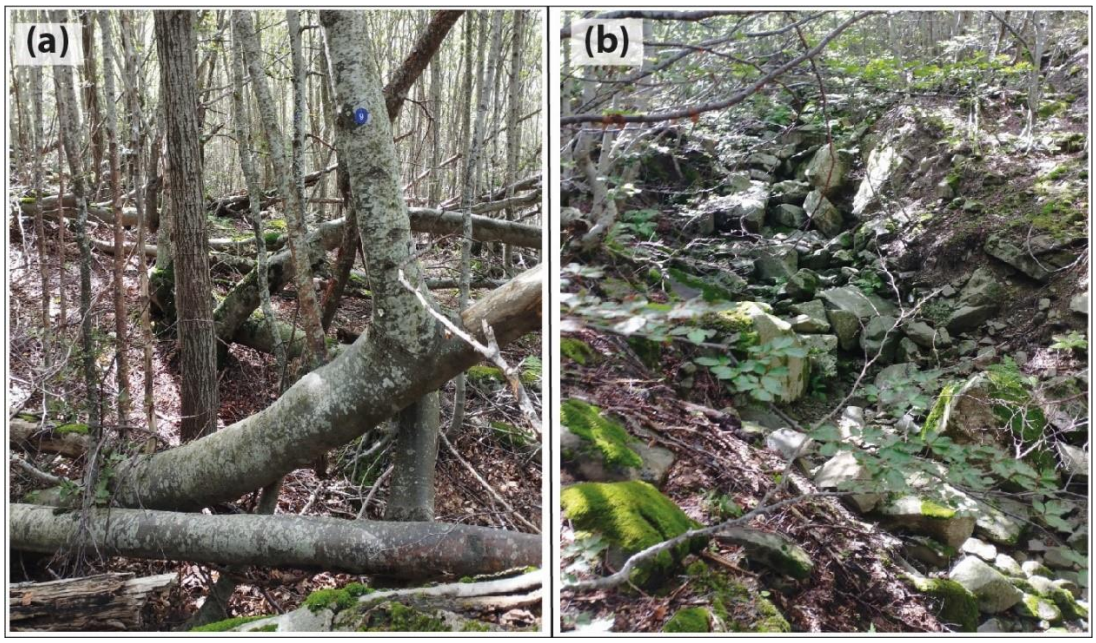

Figure 6.16. Debris flood at Channel 1 deposition area (a) Tilted stems and vertical adventitious branches caused by debris flood, and (b) Debris material observed within the Channel 1. (14/05/2024)

To evaluate the efficiancy of the RAMMS simulation, an analysis was conducted with the observed maximum flow heights (h_{max}) represented on the x-axis and the simulated h_{max} values illustrated on the y-axis (Figure 6.17). Furthermore, dashed lines delineating a ±1 meter tolerance range surrounding the 1:1 line were added to enhance the visualization of model precision. Among the 10 data points analyzed, 6 points (60%) were observed within the ±1 m tolerance range, signifying a correlation between the simulated and surveyed values. The remaining 4 points were marginally outside the acceptable bounds, indicating potential localized discrepancies, which may be attributed to the complexities of the terrain, constraints inherent in the resolution of the input data as well as some minor and intermediate events after 1987 (Rashid et al., 2026).

The RAMMS simulation's performance was evaluated using statistical indices such as Mean Absolute Error (MAE), Root Mean Square Error (RMSE), and Mean Bias Error (MBE). The results indicate a good agreement between simulated and observed maximum flow heights (h_{max}), with an average deviation (MAE) of 0.97 m and an RMSE of 1.13 m. The MBE value of +0.15 m demonstrates a minor positive bias, implying that the model marginally overestimates flow heights while staying within acceptable ranges for DF simulations in complex Apennine terrain.

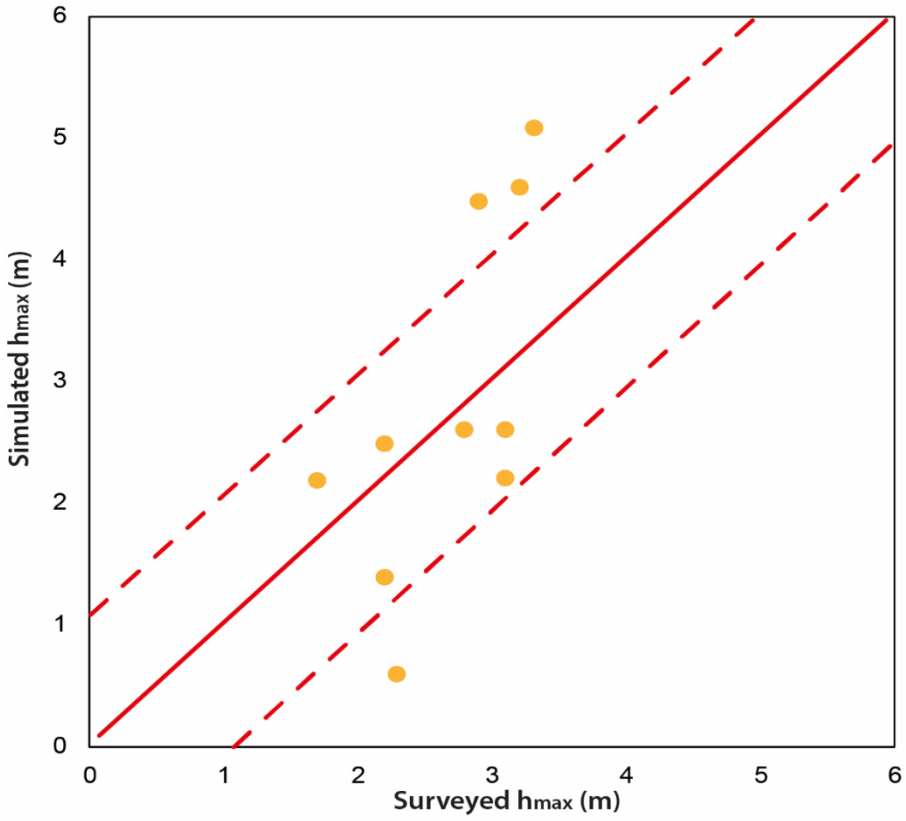

Figure 6.17: The relation between surveyed hmax (m) (x-axis) with the simulated hmax (m) (y-axis). The dashed lines show a ±1 meter tolerence rage around the solid 1:1 line.

6.6 Discussion

This research introduces an innovative and multidisciplinary framework for reconstructing and evaluating DF dynamics in data-scarce mountain regions by integrating field mapping, sedimentology, dendrogeomorphology, orthophoto interpretation, hydrological monitoring and physically based numerical modelling. In mountain regions, the limited availability of event records often prevents robust back-analysis and leads to high uncertainty in the estimation of controlling parameters such as release volume and flow rheology (Rickenmann et al., 2006). In this framework, the integration of independent field-based datasets offers the essential physical constraints to interpret model outputs and correctly attribute processes (Baggio et al., 2021).

The field evidence suggests that the 1987 event involved high-energy mass movement which formed distinct levees and lobes, characterized by strong grain-size segregation typical of granular DF deposition. These deposits are poorly sorted (Figure 6.18), matrix-supported mixtures in which

flow margins and snouts become enriched with coarse clasts while finer fractions dominate the more internal zones, reflecting progressive energy dissipation and sorting during deposition (Blair & McPherson, 1999; Major & Iverson, 1999; Bardou, 2002). The segmentation of channels further supports this interpretation: steep slopes initiate mobilization, intermediate slopes facilitate transport, and slope breaks enhance deposition (Hungr et al., 2008; Çellek, 2020).

A significant finding of the study is that the event cannot be characterized as a uniform process across the catchment. Notably, the area linked with Channel 1 shows severe tree disturbance but lacks DFs deposits, likely to indicate a debris-flood process rather than a depositional DF. This observation is critical because it highlights the importance of numerical model against multiple independent datasets, depending on a single method risks misclassifying the process and misinterpreting the spatial impact of the event (Gan & Zhang, 2020).

Figure 6.18: Illustration of poor sorting and lack of stratification in debris-flow deposits in channel 4 (the length of stick meter is 130 cm) (12/04/2023)

6.6.1 Model efficacy in reconstructing DF dynamics

The RAMMS-DF simulations effectively reconstruct the characteristics of the 1987 DFs event in Channels 2 and 4, particularly runout distance, flow routing, and depositional extent. This correlation indicates that the model captured the dominant first-order controls, particularly channel morphology and slope distribution, which are known to significantly influence DF mobility and deposition (Hungr et al., 2008). The utilization of a pre-event DEM is important in this context, as it

enables the model to represent channel geometry prior to the event while reducing bias linked with post-event surface changes.

Model efficacy is also reflected in the spatial coherence of the results. Deposition is mainly concentrated in areas where field evidence indicates slope reduction and channel widening, and the model reproduces the formation of depositional lobes and marginal levees in the expected areas. Importantly, the simulations also correctly indicate exclusion areas where DF deposition is unlikely. This supports the interpretation that not all disturbed areas are depositional DFs. This is particularly evident in Channel 1, where severe vegetation disturbance is observed despite the absence of DF deposits.

In terms of flow thickness, the model performs well. The overall differences between simulated and measured deposit thickness is within the range reported for DF simulations in complex terrain, where errors can arise from DEM limitations, local microtopography, and natural heterogeneity of sediment concentration and grain-size composition along the flow path (La Porta et al., 2024). Given these factors, the model outcomes provide a robust reconstruction of DF when interpreted together with field evidence.

6.6.2 Physically constrained model calibration

Model calibration was carried out by back-analysing the 1987 event by through a series of simulations that tested different combinations of release volumes and Voellmy rheological parameters (μ and ξ) within RAMMS-DF framework (Bartelt et al., 2017; Matjaž & Bezak, 2021). Rather than relying solely on numerical fitting; the calibration was constrained by independent field evidence, including mapped deposit boundaries, channel morphology, and observed grain-size characteristics. This strategy is important because release volume and rheological parameters can compensate for each other, leading to similar model outcomes, particularly when direct historical measurements are unavailable (Rickenmann et al., 2006). By incorporating geomorphic and sedimentological constraints, the study aimed to reduce this uncertainty and ensure physically realistic model settings.

Channel morphometry was used as a first-order bounds for model calibration by identifying slope ranges associated with initiation areas (>30°), transport zones (15–30°), and deposition sectors

(<15°), where slope reduction promotes rapid energy dissipation and sediment accumulation (Hungr et al., 2008). Model scenarios were therefore assessed by the runout distance, also by whether they deposited material in the correct geomorphic areas. This physically based approach helps to reduce an apparent “good fit” through unrealistic parameter combinations.

Sedimentological evidence further supported the selected parameters. Field observations revealed poorly sorted, matrix-supported textures with abundant coarse clasts, which are characteristics of frictional granular flows (Blair & McPherson, 1999; Major & Iverson, 1999; Tiranti et al., 2008). These features justify the use of rheological parameter ranges consistent with granular DFs, in line with previous RAMMS based studies (Matjaž & Bezak, 2021).

6.6.3 Model validation through multiple datasets

Model validation was primarily based on direct comparisons between observed field measurements and simulated model outputs, particularly flow depths and depositional patterns. The core validation approach was complemented by independent datasets constrain different aspects of the event, including dendrogeomorphological evidence, orthophoto interpretation, sedimentological observations, and the precipitation-hydrological context.

6.6.3.1 Comparison between modelled and observed DF characteristics

The results show that the RAMMS-DF model is able to realistically reproduce the spatial extent, flow paths, and depositional patterns of the 1987 DF event when supported by detailed field observations and post-event orthophotos. The close correspondence between simulated deposits, observed levees, and measured flow heights indicates that the chosen source volumes and friction parameters are appropriate, in line with previous back-analyses in alpine and Apennine settings (Matjaž & Bezak, 2021). Most simulated flow heights fall within a ±1 m tolerance of field measurements, a level of agreement comparable to that reported in similar DF studies in complex mountain terrain (La Porta et al., 2024). The remaining local discrepancies are likely related to small-scale topographic variability, post-event surface modifications, and DEM resolution limits (Bühler et al., 2018). The slight tendency of the model to overestimate flow heights has also been observed in earlier applications and is generally considered acceptable for hazard assessment purposes (La Porta et al., 2024).

6.6.3.2 Dendrogeomorphological evidence and orthophoto-based validation

Dendrogeomorphological evidence provides spatially explicit information on impact zones and disturbance intensity, and thus offers a powerful independent validation dataset for model validation, particularly when direct observations of past events are lacking (Leonelli et al., 2021; Šilhán & Tichavský, 2016). Disturbed trees are mainly clustered within the modeled flow paths and depositional zones, while undisturbed trees characterize the areas outside the simulated runout. This spatial correspondence supports the reliability of the modeled routing and depositional boundaries.

Historical orthophotos acquired before and after the 1987 event provide an additional, independent means of validating the spatial extent of disturbance and deposition. Patterns of vegetation damage and geomorphic change observed in the orthophotos show good agreement with the modeled depositional footprints and channel routing. This consistency strengthens confidence in the reconstructed runout geometry and is in line with previous DF back-analyses that have successfully combined numerical modeling with orthophoto interpretation (Huang et al., 2022).

6.6.3.3 Sedimentological and depositional morphology

Sedimentological and morphological observations further support model validation by constraining process attribution. Field evidence shows well-developed levees and lobes, poor sorting, matrix-supported textures, and the presence of coarse clasts, all of which are characteristic of granular debris-flow dynamics (Tiranti et al., 2008; Bardou, 2002; Blair & McPherson, 1999). In addition, field-mapped levees and measured deposit thicknesses provide direct ground truth for evaluating simulated flow heights. This step is essential, as a model may reproduce runout distance while still misrepresenting the depositional process if not validated against deposit properties and internal structure.

6.6.3.4 Precipitation and hydrological preconditioning

Precipitation records and soil hydrological conditions provide important context for validating the triggering and mobility of the event. Rapid infiltration responses and persistently high soil moisture during rainfall indicate favorable preconditioning for DF initiation and propagation. These

observations support the interpretation that DF activity in the study area is controlled not only by rainfall intensity, but also by antecedent hydrological conditions, consistent with previous studies (Lee et al., 2024; Scognamiglio et al., 2016).

6.7 Limitations of the Study

- The research employed various methodologies to examine the grain size distribution of debris flows, plotting the grain size ranging from 0.005 to 16 mm, while simultaneously utilizing an alternative approach for higher ranges. A single curve was not implemented in this investigation due to the considerable variability in grain size, which can pose a risk of both overestimation and underestimation.
- The 1976 DEM was used as input parameter but dense forest cover in depositional areas further affect terrain detail, potentially introducing elevation inaccuracies and reducing the precision of the modeled flow paths and deposition zones.
- The numerical model assumes uniform rheological properties (e.g., density, friction angle, turbulence coefficients) throughout the flow path. However, as recently highlighted by some authors (Cuomo et al., 2025a; 2025b) natural debris flows are highly heterogeneous, and variations in sediment concentration, water content, and clast size distribution can cause localized differences in flow behavior that are not captured in the proposed simulation.
- The RAMMS model cannot account for trees resistance, so the simulated flow may overestimate runout distance or deposit thickness.
- The RAMMS model was applied without activating entrainment or erosion modules, resulting in a fixed flow volume throughout the simulation. This excludes the potential for sediments along the flow path, which is relevant in steep or unconsolidated sections and may lead to underestimation of final flow volume and runout extent.
- The minor and intermediate events that followed the 1987 DF were not destructive, but they might have altered or added to the material deposited in 1987. This poses a challenge for interpreting sedimentological and field data collected in 2024.
- High-resolution post-event surveys (e.g., LiDAR or drone imagery) were not available for the 1987 event, restricting the ability to assess model accuracy in terms of spatial deposition patterns and flow depth.

6.8 Conclusions

This study demonstrates the effectiveness of a multidisciplinary methodology in reconstructing and modeling a significant DF event in the Northern Apennines. By combining dendrogeomorphology, sedimentological observations, geomorphological mapping, and numerical modelling, it was possible to reconstruct DF dynamics in a remote and data-limited catchment.

The year 1987 was identified as the last major DF event in the study area. Field surveys and tree-ring data, supported by historical orthophotos, allowed robust constraints of DF timing, runout extents and depositional patterns, enabling independent validation of numerical simulations. Beyond its traditional role in event dating, dendrochronology evolved into a quantitative dataset for model validation, thereby aiding in the enhancement of flow simulations and improving confidence in reconstructed event dynamics.

Sedimentological observations revealed systematic grain-size sorting and structural differences between levees and lobes, indicative of differential flow energy and depositional mechanisms. These findings demonstrate the significant impact of terrain and sediment properties on DF movement and deposition in steep, confined channels, when combined with morphometric controls like slope gradients.

Numerical modeling with RAMMS-DF effectively reproduced the observed deposition height and runout extents, showing strong correspondence with field evidence, supporting the capability of process-based models to realistically represent DF behavior in complex mountain environments. Although calibrated rheological parameters are site-specific, the proposed multidisciplinary methodological framework is transferable to similar geomorphic settings and provides a robust basis for DF hazard assessment.

Overall, this research signifies the importance of multidisciplinary approaches in DF studies and highlights their potential to improve hazard characterization, risk mitigation strategies, and landscape management in mountainous regions vulnerable to DFs hazard.

Credit authorship contribution statement

M. A. Rashid led the multi-disciplinary analysis, contributing to dendrogeomorphology, morphometric assessment, sedimentological analysis, and debris-flow modelling. He also

coordinated the integration of field, laboratory, and modelling datasets to ensure methodological consistency throughout the study. **G. Leonelli**, principal investigator of the DECC project, provided overall coordination and strategic direction, and offered substantial input in data interpretation as well as in the writing and critical revision of the manuscript. **R. Valentino** supported the sedimentological investigations and debris-flow modelling, and contributed to the writing and revision of the manuscript. **E. Petrella** analyzed soil hydraulic properties and contributed to the revision of the manuscript. **N. Bruno** assisted in the development of the digital elevation model and participated in manuscript revision. **M. Maugeri** and **V. Manara** contributed to the development and interpretation of climatic data, assisted in writing and revising the manuscript, and coordinated the University of Milano unit within the DECC project. **A. Chelli** provided continuous scientific guidance, contributing substantially to interpretation of results, and the overall structuring and revision of the manuscript. He also ensured the coherence of the methodological framework and its alignment with the project's scientific objectives.

Declaration of Competing Interest

The authors declare that there are no competing financial interests or personal relationships that could have influenced the outcomes or interpretations of the work presented in this paper.

Data availability

The data supporting this study will be made available by the authors upon request.

Acknowledgements

This research was conducted within the framework of the COMP-HUB and COMP-R initiatives at the University of Parma, supported by the 'Departments of Excellence' program of the Italian Ministry for Education, University, and Research (MIUR) for the periods 2018–2022 and 2023–2027. Additional funding was provided by the European Union – Next Generation EU / PRIN-PNRR through the PRIN 2022 PNRR – Projects of Great National Interest, specifically the DECC project (Debris flow hazard and climate change in the Northern Apennines: reconstructing and modeling past and future environmental scenarios), CUP D53D23022810001. This work was also supported by the University of Parma's PhD School of Earth Sciences, research fund XXXVIII_SCIENZE_TERRA_QUOTA10.

7. Overall Discussion and Conclusions

Debris flows (DFs) are a widespread geomorphic process in the Northern Apennines, somewhere posing substantial threats to infrastructure, human settlements, and ecological systems. Notwithstanding extensive prior investigations performed in this region, documenting DF occurrence, magnitude, and triggering mechanisms, no comprehensive study has integrated diverse lines of evidence such as field-based geomorphology, dendrogeomorphology, sedimentology, channel morphometry, catchment susceptibility, GIS and remote sensing, climate analysis and numerical modeling into a singular, cohesive framework. This research addresses that gap, concentrating on the Alpe di Succiso site and its adjacent DF-prone catchments, while analyzing events across both temporal and spatial scales.

Through the integration of dendrochronological data, sedimentological and orthophoto analyses, it was possible to reconstruct the chronology, magnitude, and spatial distribution of antecedent DF occurrences, including the significant flow events of 1972 and 1987. Geographic Information System (GIS)-driven catchment analysis coupled with hydrological data further revealed critical zones susceptible to flow initiation, while RAMMS-DF simulations displayed quantitative information into flow channels, runout distances, and depositional patterns. The results deriving from the integration of different methodologies (Figure 7.1) highlight the interrelated nature of climatic, geomorphic, and lithological determinants influencing DF behavior, thereby illustrating the capacity of multidisciplinary approaches can enhance both understanding and predictive accuracy. These findings yield novel perspectives for hazard assessment, risk management, and policy formulation, providing actionable guidance for territories susceptible to DFs.

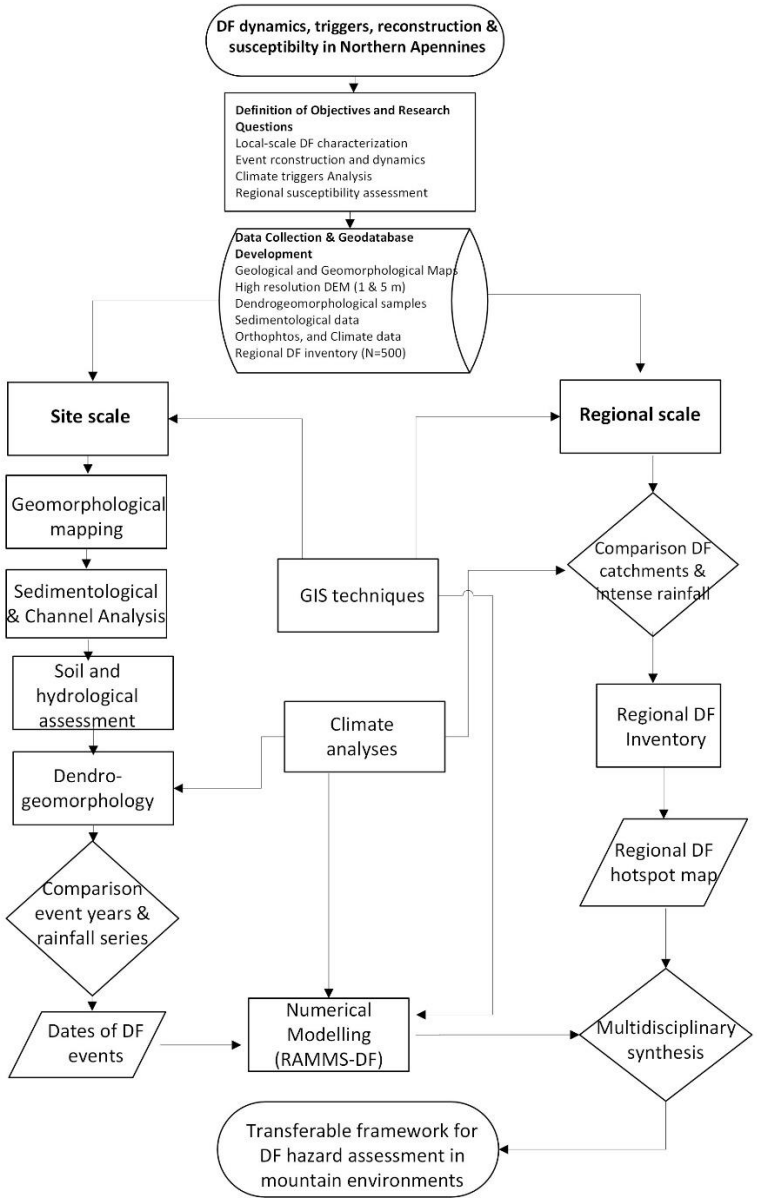

Figure 7.1: Conceptual representation of the integrated and transferable framework proposed in this thesis for debris-flow (DF) hazard assessment. The approach bridges site-scale process reconstruction and regional-scale susceptibility analysis through the combined use of geomorphological mapping, sedimentological and dendrogeomorphological evidence, climate analyses, GIS techniques, and numerical modelling (RAMMS-DF), applied to the Northern Apennines.

7.1 Scientific Contributions

7.1.1 Advancing Multidisciplinary Integration

A central strength of the present study lies in its multidisciplinary approach and is beneficial where no prior monitoring data is available for natural hazards such as DFs. This study developed a framework capable of reconstructing past DF events with good temporal and spatial precisions. This research contributed a distinct layer of information: dendrogeomorphology delineated the timing of events, sedimentology revealed rheological characteristics and depositional processes, rainfall data indicated the amount of rainfall which triggered the events and numerical modeling quantified flow mechanics and runout behavior. This integration is valuable in data-scarce mountainous terrain, where no single method could independently capture the full complexity of DF phenomena.

The interaction between dendrochronological datasets and RAMMS modeling provided a distinctive opportunity to directly calibrate the DF model utilizing tree-ring data indicative of historical flow disturbances for the DF event of 1987 (chosen considering its impacts in all channels in the study catchment as well as last major event). The spatial distribution and intensity of growth anomalies recorded in trees such as tilting, or abrupt growth suppression were systematically compared with the simulated flow depth, velocity, and impact zones produced by RAMMS. This comparative analysis allowed for the refinement of rheological parameters (e.g., friction and turbulence coefficients) to achieve a closer alignment with the observed patterns of tree disturbance in the field. In this way, dendrochronology transcended its conventional function as a chronological tool and evolved into a quantitative dataset for model validation, thereby aiding in the enhancement of flow simulations and improving confidence in reconstructed event dynamics. The study framework is transferable to other regions of the Northern Apennines, as the calibrated numerical modeling parameters such as friction coefficient of 0.22 and a turbulent coefficient of 170 (Matjaž & Bezak, 2021) can serve as reliable reference values for similar geomorphic settings. Similarly, geomorphological mapping and grain-size analysis contributed to the determination of rheological parameters, reducing the uncertainty often associated with numerical simulations.

7.1.2 Geomorphology, Dendrogeomorphology and Rainfall Analysis

The Northern Apennines geomorphology is the consequence of tectonics, erosion, glaciation, and continuous fluvial and gravitational processes, all of which have complex and dynamic mountain landscape. This dynamic interaction results in steep and unstable slopes where DFs are triggered by intense rainfall, making the region ideal for investigating the link between climate, geomorphology and slope instability.

The dendrogeomorphological study revealed that the major event years occurred in 1973 and 1988, while intermediate events were identified in 1997, 2003 and 2013. The temporal occurrences identified through dendrogeomorphological analysis were subsequently refined by comparison with meteorological datasets, thereby confirming that the major DFs events occurred in the years 1972 and 1987, while intermediate events were recognized in 1996, 2002, and 2013. These events had not been documented in previous studies, thus highlighting the efficacy of dendrogeomorphology in reconstructing the frequency and temporal distribution of DF activity in regions characterized by limited data availability, such as mountainous terrains. This methodological framework not only extends the historical record of DF occurrences but also provides essential insights into the episodic dynamics of DF processes and their correlation with intense precipitation events within the Northern Apennines. After adjusting dendrochronological dates due to seasonal resolution and supporting field and climatic evidence, the multidisciplinary approach demonstrates that DFs in the surroundings of Alpe di Succiso is episodic, linked to high-magnitude rainfall events, but also related with antecedent conditions and sediment availability. Major DF events in 1972 and 1987 correspond to extreme rainfall intensities. At the site scale, the 11-12 September 1972 event ranks first, while 25 August 1987 ranks among top events at Collagna and Succiso (ARCIS/ station analyses). The study also documents intermediate and minor events where rainfall alone was insufficient to explain DFs. These events highlight the importance of preconditioning factors, including soil moisture conditions, moderate but persistent precipitation, snowmelt, and the availability of pre-existing deposits within the catchment area that have been widely recognized in previous studies (Hirschberg et al. 2019), (Qie et al., 2024).

This study establishes a multi-decadal chronology of DF occurrence with temporal and spatial resolution for the Alpe di Succiso sector. Such chronologies are valuable because DF inventories often lack non-damaging events. Furthermore, linking dendrochronological evidence to precise

precipitation records enhances the calibration of models and supports the validation of numerical simulations. Importantly, this dataset reveals that not all intense rainfall events result in DFs as already observed by Tiranti et al., (2021), challenging simplified hazard assessments that rely on rainfall thresholds since antecedent soil moisture, sediment supply availability, and slope morphology also play important role in controlling DF initiation. Furthermore, the study shows the importance of combining historical information, dendrochronological evidence, and analytical techniques in order to understand the frequency, intensity, and significance of DF events in the study area. The findings of the performed analysis highlight that short-duration, high-intensity rainfall is a critical factor for DFs during significant events.

7.1.3 Numerical Modeling (RAMMS-DF), channel analysis and sedimentology

The recognized 1987 DF event serves as a key case study in this research. By employing RAMMS-DF simulations, the reconstruction of the flow dynamics, runout distances, and deposition patterns were linked to this high-magnitude event. Debris-flow modelling with RAMMS, calibrated against tree-ring evidence of past flow disturbance identified through dendrogeomorphology, offers an innovative, field-grounded approach. The model accurately predicted flow paths and depositional levees. The simulations highlighted that intense rainfall, recorded during 1987 event (187 mm), was a critical trigger for the event, aligning with findings from Ciccarese et al. (2020) and Berti et al. (2025), who documented similar climatic patterns influencing DFs in the region. The current modeling provides a process-based viewpoint by connecting recorded rainfall to the mechanical behavior, runout, and deposition of DFs, whereas prior studies concentrated on defining rainfall thresholds and mapping event distributions. This event highlights the importance of accurately modeling precipitation-driven flow initiation and the need to refine numerical simulations by including additional factors such as vegetation drag in future studies.

The sedimentological study demonstrates the complexities of DF processes in steep mountainous catchments. Channel slope analysis highlight a distinct zonation pattern: source zones (>30°) facilitate the triggering of DFs, transport zones (15–30°) maintain flow energy, and deposition zones (<15°) allow sediment accumulation. Sedimentological data related to characteristic DF attributes, including poorly sorted, angular to sub-angular particles and open-work structures, in accordance

with granular flow dynamics as observe by numerous authors (Blair & McPherson, 1999; Major & Iverson, 1999).

Field-based sedimentological observations validate that DFs in this region are characterized by granular flows with poorly sorted, matrix-supported textures and abundant large clasts, consistent with high-energy, gravity-driven processes. The difference in slope between levees (31°–41°) and lobes (12°–30°) illustrate spatial variations in flow energy and depositional mechanics. Larger boulders and coarse particles tend to accumulate at steep surge, forming lateral levees due to high frictional interaction and flow dynamics, whereas depositional lobes form as frictional resistance at the flow fronts halts debris movement, resulting in finer materials accumulating behind coarser front deposits. This segregation process results in steeply inclined levees and gently sloping lobes, as exhibited in the study (Bardou, 2002). The grain size distribution in study area, varying from clay size to blocks over 6 meters, further emphasizing the high-energy, complex characteristics of the event.

7.1.4 Regional Context and Morphometric Controls

Regional scale assessments such as the present study, are necessary for the purposes of hazard mapping, and the prioritization of field investigations in areas that are less frequently monitored. Through the spatial distribution of catchments susceptible to DFs and the occurrence of intense precipitation events over the preceding seven decades, we have delineated critical zones characterized by a high hazard for DFs, particularly within the Ligurian to Tuscan mountain belt. The occurrence of extreme rainfall is attributable to Mediterranean storms during the early autumn season, while regions exhibiting steep slopes and a presence of loose debris demonstrate increased vulnerability to DFs, even with the occurrence of moderate rainfall. The geological framework, which encompasses the presence of Macigno sandstone and Quaternary deposits, further amplifies the risk associated with DFs. Although seismic events have also potential triggers for DFs, our investigation exhibits the conclusion that intense precipitation continues to be the predominant factor influencing this phenomenon within the region.

At the regional level, morphometric thresholds have emerged as critical indicators of susceptibility to DFs. The majority of DF events are initiated on slopes that exhibit steepness between 25–40°, which aligns with findings from previous studies (Chen & Yu, 2011; Hungr et al., 1984; Rickenmann

& Zimmermann, 1993; Takahashi, 1981), at altitudes surpassing 500 m, and within TRI values that denote rugged terrain ranging from 4 to 11. TWI values in the vicinity of 4–6 are consistently correlated with initiation events, highlighting the significance of concentrated subsurface water convergence in the destabilization of debris. The Alpe di Succiso site, characterized by initiation slopes exceeding 32° and TRI values greater than 8, lies at the upper limits of these specified ranges, thereby confirming its high sensitivity to the initiation of DFs.

The combination of localized field observations and regional-scale inventories strengthens hazard assessment by contextualizing site-specific processes within larger geomorphic frameworks. This dual-scale analysis demonstrates that the central Apennine ridge is the primary hotspot for DFs, where extreme precipitation from the Tyrrhenian Sea converges with steep, debris-laden slopes. The identification of both precipitation-dominated and sediment supply-dominated catchments allows for a more comprehensive understanding of hazard distribution across the Northern Apennines. This finding expands on the observations of Ciccarese et al. (2021), who linked heavy convective rainfall to DF initiation in the northwestern Apennines, but refines their interpretation by defining the ridge as a climatic-geomorphic convergence zone. The recognition of both precipitation-dominated and sediment-supply-dominated catchments provide the regional variability of DF hazard in the Northern Apennines. This research advances the understanding of regional DF dynamics and provides a basis for targeted hazard assessment.

7.1.5 Implications, Limitations, and Future Directions

The findings of this study provide valuable insights into the timing, magnitude, and dynamics of DFs highlighting the importance of integrating multiple methodologies including dendrogeomorphology, sediment analysis, rainfall data, and numerical modeling for a comprehensive understanding of these events. However, several limitations remain. Dendrogeomorphology is constrained by tree availability, potential non-debris-flow growth disturbances, and annual-scale resolution, which may obscure consecutive events or underrepresent event frequency (Stoffel et al., 2013; Šilhán and Stoffel, 2015). Rainfall records, while critical, often lack sufficient temporal and spatial resolution to capture localized high-intensity events, and not all extreme precipitation leads to observable debris-flow activity (Qie et al., 2025).

Numerical modeling using RAMMS provided useful reconstructions of flow paths and dynamics even if it assumed uniform rheological properties and excluded erosion or entrainment, potentially underestimating flow volumes and deposition extents. Terrain inaccuracies due to the 1976 DEM and dense forest cover also limited spatial precision. Sediment analysis was similarly constrained by the wide variability in grain size, requiring separate curves to avoid over- or underestimation.

Future research will be aimed at advanced computational approaches, including machine learning and deep learning techniques, which could be applied to automatically identify and classify DF occurrences across the region, improving detection efficiency and predictive capabilities. Addressing these gaps will enhance hazard prediction, enable more accurate reconstruction of past events, and support sustainable management strategies in DF-prone areas.

7.1.6 Conclusions

This investigation demonstrates that a multidisciplinary methodology is not solely additive but also transformative, providing a comprehensive understanding of debris-flow (DF) processes at both local and regional scales. Through the integration of geomorphological mapping, dendrogeomorphology, sedimentology, rainfall analysis, and numerical modeling, this research establishes a connection between short-term event reconstruction and long-term hazard assessment. The findings provide a cohesive perspective that associates detailed local reconstructions, such as the high-magnitude occurrences of 1987 and 1972 at the vicinity of Alpe di Succiso.

The results indicate that DFs are episodic phenomena, predominantly triggered by intense rainfall events, and also influenced by antecedent soil moisture levels, sediment supply availability, and slope morphology characteristics. These interconnected factors emphasize the complexity of DF initiation and propagation within a climatically sensitive mountainous environment.

In addition to reconstructing individual events, this research established a comprehensive framework for integrated hazard assessment, which is applicable in other mountainous regions characterized by limited data availability. Ultimately, the multidisciplinary framework developed through this Ph.D. research enhances both scientific understanding and practical risk management strategies. It contributes not only to the theoretical knowledge of DF dynamics but also to the advancement of hazard mapping, early warning systems (by delineate high hazard channels and simulate potential runout scenarios which is essential components of DF early warning and

management), and mitigation strategies within mountainous landscapes that are increasingly subjected to hydroclimatic extremes.

References

AGSS-RER (Area Geologia, Suoli e Sismica, Regione Emilia-Romagna), 1986. Carta Geologica dell'Appennino emiliano-romagnolo, scala 1:10.000, https://geoportale.regione.emilia-romagna.it/ (last access: 27 May 2025)

Ahmed, B. 2015. Landslide susceptibility mapping using multi-criteria evaluation techniques in Chittagong Metropolitan Area, Bangladesh. Landslides, 12(6), 1077–1095. https://doi.org/10.1007/s10346-014-0521-x

APAT Servizio geologico d'Italia. 2015. Foglio 234: Fivizzano / APAT, Agenzia per la protezione dell'ambiente e per i servizi tecnici, Dipartimento difesa del suolo, Servizio Geologico d'Italia [Map]. ISPRA.

Argnani, A., Barbacini, G., Bernini, M., Camurri, F., Ghielmi, M., Papani, G., Rizzini, F., Rogledi, S. and Torelli, L., 2003. Gravity tectonics driven by Quaternary uplift in the Northern Apennines: insights from the La Spezia-Reggio Emilia geo-transect. Quaternary International, 101, 13-26.

Armento, M. C., Genevois, R., & Tecca, P. R., 2007. Comparison of numerical models of two debris flows in the Cortina d' Ampezzo area, Dolomites, Italy. Landslides, 5(1), Article 1. https://doi.org/10.1007/s10346-007-0111-2

ASTM International., 2017. Standard Test Methods for Particle-Size Distribution (Gradation) of Soils Using Sieve Analysis (ASTM D6913/D6913M-17). ASTM International, West Conshohocken, PA. https://doi.org/10.1520/D6913_D6913M-17

Baggio, T., Mergili, M., & D'Agostino, V., 2021. Advances in the simulation of debris flow erosion: The case study of the Rio Gere (Italy) event of the 4th August 2017. Geomorphology, 381, 107664. https://doi.org/10.1016/j.geomorph.2021.107664

Ballantyne, C., Hall, K. and French, H., 2002. Paraglacial geomorphology: processes and paraglacial context. Geomorphology, 95, pp.1-2.

Ballesteros-Cánovas, J.A., Kariya, Y., Imaizumi, F., Manchado, A.M.T., Nishii, R., Matsuoka, N., Stoffel, M., 2023. Debris-flow activity in the Japanese Alps is controlled by extreme precipitation and ENSO – Evidence from multi-centennial tree-ring records. Global and Planetary Change 231(6). https://doi.org/10.1016/j.gloplacha.2023.104296

Bardou, E.: Méthodologie de diagnostic des laves torrentielles sur un bassin versant alpin, EPFL, Lausanne., 2002.

Baroni, C., Bruschi, G., & Ribolini, A., 2000. Human-induced hazardous debris flows in Carrara marble basins (Tuscany, Italy). Earth Surface Processes and Landforms: The Journal of the British Geomorphological Research Group, 25(1), 93-103. https://doi.org/10.1002/(SICI)1096-9837(200001)25:1<93::AID-ESP53>3.0.CO;2-0.

Baroni, C., Guidobaldi, G., Salvatore, M. C., Christl, M., & Ivy-Ochs, S., 2018. Last glacial maximum glaciers in the Northern Apennines reflect primarily the influence of southerly storm-tracks in the western Mediterranean. Quaternary Science Reviews, 197, 352–367. https://doi.org/10.1016/j.quascirev.2018.07.003.

Bartelt, P., Bieler, C., Bühler, Y., Christen, M., Deubelbeiss, Y., Graf, C., McArdell, B. W., Salz, M., & Schneider, M., 2017. User Manual V1. 7.0 Debris Flow. User Manual v1.7.0 Debris Flow. Scopus.

Bartolini, G., Messeri, A., Grifoni, D., Mannini, D., Orlandini, S., 2014. Recent trends in seasonal and annual precipitation indices in Tuscany (Italy). Theor Appl Climatol 118, 147–157. https://doi.org/10.1007/s00704-013-1053-3

Beaty, C.B., 1974. Debris flows, alluvial fans and a revitalized catastrophism Z. Geomorpho1 21:39-51

Bernini, M., Vescovi, P., Zanzucchi, G., 1997. Schema strutturale dell''Appennino Nord- Occidentale. Acta Natur. Aten.-Parm. 33, 43–54.

Berti, M., Pizziolo, M., Scaroni, M., Generali, M., Critelli, V., Mulas, M., Tondo, M., Lelli, F., Fabbiani, C., Ronchetti, F., Ciccarese, G., Dal Seno, N., Ioriatti, E., Rani, R., Zuccarini, A., Simonelli, T., Corsini, A. 2025. RER2023: The landslide inventory dataset of the May 2023 Emilia-Romagna meteorological event. Earth System Science Data, 17(3), 1055–1074. https://doi.org/10.5194/essd-17-1055-2025

Bertoldi, R., Chelli, A., & Roma, R., 2007. New data from Northern Apennines (Italy) pollen sequence spanning the last 30,000 yrs. Il Quaternario, 20, 3–20

Bertolini, G., Pellegrini, M., 2001. The landslides of Emilia Apennines (northern Italy) with reference to those which resumed activity in the 1994–1999 period and required Civil Protection interventions. Quad. Geol. 8 (1), 27–74.

Bertolini, G., Guida, M., Pizziolo, M., 2005. Landslides in Emilia-Romagna region (Italy): strategies for hazard assessment and risk management. Landslides 2, 302–312. http://dx.doi.org/10.1007/s10346-005-0020-1.

Bertolini, G., Corsini, A., Tellini, C., 2017. Fingerprints of Large-Scale Landslides in the Landscape of the Emilia Apennines. In: Soldati M., Marchetti M. (eds) Landscapes and Landforms of Italy. World Geomorphological Landscapes. Springer, Cham, pp 215-224

Bertrand, M., Liébault, F., Piégay, H. 2013. Debris-flow susceptibility of upland catchments. Natural Hazards, 67(2), 497–511. https://doi.org/10.1007/s11069-013-0575-4

Bettelli, G. & Vannucchi, P., 2003. Structural style of the offscraped Ligurian oceanic sequences of the Northern Apennines: new hypothesis concerning the development of melange block-in-matrix fabric. Journal of Structural Geology, 25 (3), 371-388.

Blair T. C., McPhereson J. G., 1994. Alluvial Fans and their Natural Distinction from Rivers Based on Morphology, Hydraulic Processes, Sedimentary Processes, and Facies Assemblages. SEPM Journal of Sedimentary Research, 64A. https://doi.org/10.1306/D4267DDE-2B26-11D7-8648000102C1865D

Blair, T. C., McPherson, J.G., 1999. Grain-size and textural classification of coarse sedimentary particles. Journal of Sedimentary Research 69: 6–19. https://doi.org/10.2110/jsr.69.6

Blair, T. C., 2002. Sedimentology of the debris-flow-dominated Warm Spring Canyon alluvial fan, Death Valley, California. Sedimentology, 46(5), 941–965. Scopus. https://doi.org/10.1046/j.1365-3091.1999.00260.x

Blair, T. C., & McPherson, J. G., 2009. Processes and Forms of Alluvial Fans. In A. J. Parsons & A. D. Abrahams (Eds.), Geomorphology of Desert Environments (pp. 413–467). Springer Netherlands. https://doi.org/10.1007/978-1-4020-5719-9_14

Bluck, B. J. 1979. Structure of coarse grained braided stream alluvium. Transactions of the Royal Society of Edinburgh, 70(10–12), 181–221. Scopus. https://doi.org/10.1017/S0080456800012795

Boccaletti, M., Elter, P. & Guazzone, G., 1971. Plate Tectonics Models for the development of the Western Alps and Nothern Apennines. Nature Physical Science, 234, 108-111.

Bollati, I., Della Seta, M., Pelfini, M., Del Monte, M., Fredi, P., & Lupia Palmieri, E., 2012. Dendrochronological and geomorphological investigations to assess water erosion and mass wasting processes in the Apennines of Southern Tuscany (Italy). CATENA, 90, 1–17. https://doi.org/10.1016/j.catena.2011.11.005

Bollati, I. M., Lenz, B., Enrico, Z., & Pelfini, M., 2017. Geomorphological mapping for the valorization of the Alpine environment. The case study of the Loana Valley (Western Italian Alps). Journal of Mountain Science, 14, 1023–1038. https://doi.org/10.1007/s11629-017-4427-7

Bollschweiler, M., Stoffel, M., Ehmisch, M., & Monbaron, M., 2007. Reconstructing spatio-temporal patterns of debris-flow activity using dendrogeomorphological methods. Geomorphology, 87(4), 337–351. https://doi.org/10.1016/j.geomorph.2006.10.002

Bordoni, M., Bittelli, M., Valentino, R., Vivaldi, V., Meisina, C., 2021. Observations on soil-atmosphere interactions after long-term monitoring at two sample sites subjected to shallow landslides. Bull Eng Geol Environ 80, 7467–7491. https://doi.org/10.1007/s10064-021-02334-y

Bosellini, A., 2017. Outline of the geology of Italy. In Landscapes and landforms of Italy, 21-27, Cham: Springer International Publishing. https://doi.org/10.1007/978-3-319-26194-2_3

Bout, B., Lombardo, L., van Westen, C.J., Jetten, V.G., 2018. Integration of two-phase solid fluid equations in a catchment model for flashfloods, debris flows and shallow slope failures. Environmental Modelling Software 105, 1–16. https://doi.org/10.1016/j.envsoft.2018.03.017

Brugnara, Y., Maugeri, M., 2019. Daily precipitation variability in the southern Alps since the late 19th century. International Journal of Climatology 39, 3492–3504. https://doi.org/10.1002/joc.6034

Brunetti, M., Maugeri, M., Monti, F., Nanni, T., 2006. Temperature and precipitation variability in Italy in the last two centuries from homogenised instrumental time series. International Journal of Climatology, 26(3), 345-381. https://doi.org/10.1002/joc.1251

Brunetti, M., Lentini, G., Maugeri, M., Nanni, T., Auer, I., Böhm, R., Schöner, W., 2009: Climate variability and change in the Greater Alpine Region over the last two centuries based on multi-variable analysis. Int. J. Climatol., 29, 2197-2225. https://doi.org/10.1002/joc.1857.

Brunetti, M., Bertolini, A., Soldati, M., Maugeri, M., 2019. High-resolution analysis of 1-day extreme precipitation in a wet area centered over eastern Liguria, Italy. Theor Appl Climatol 135, 341–353. https://doi.org/10.1007/s00704-018-2380-1

Buchanan, B. P., Fleming, M., Schneider, R. L., Richards, B. K., Archibald, J., Qiu, Z., & Walter, M. T., 2014. Evaluating topographic wetness indices across central New York agricultural landscapes, Hydrology and Earth System Sciences, 18, 3279–3299. https://doi.org/10.5194/hessd-10-14041-2013

Bufalini, M., Materazzi, M., De Amicis, M., & Pambianchi, G., 2021. From traditional to modern 'full coverage' geomorphological mapping: A study case in the Chienti river basin (Marche region, central Italy). Journal of Maps, 17, 1–12. https://doi.org/10.1080/17445647.2021.1904020

Bühler, Y., Christen, M., Kowalski, J., & Bartelt, P., 2018. Sensitivity of snow avalanche simulations to digital elevation model quality and resolution | Annals of Glaciology. Cambridge Core. https://doi.org/10.3189/172756411797252121

Cabral, V., Reis, F., Veloso, V., Ogura, A., & Zarfl, C., 2023. A multi-step hazard assessment for debris-flow prone areas influenced by hydroclimatic events. Engineering Geology, 313, 106961. https://doi.org/10.1016/j.enggeo.2022.106961

Campobasso, C., Carton, A., Chelli, A., D'Orefice, M., Dramis, F., Graciotti, R., Guida, D., Pambianchi, G., Peduto, F., & Pellegrini, L. (2018). Carta Geomorfologica d'Italia - 1:50.000 - Progetto CARG: Modifiche ed Integrazioni al Quaderno N. 4/1994. Quaderni del Servizio Geologico d'Italia, serie III, 13(I), 153.

Carlini, M., Artoni, A., Aldega, L., Balestrieri, M.L., Corrado, S., Vescovi, P., Bernini, M.,Torelli, L., 2013. Exhumation and reshaping of far travelled/allochthonous tectonic units in mountain belts. New insights for the relationships between shortening and coeval extension in the western Northern Apennines (Italy). Tectonophysics 608, 267–287. http://dx.doi.org/10.1016/j.tecto.2013.09.029.

Carlini, M., Chelli, A., Francese, R., Giacomelli, S., Giorgi, M., Quagliarini, A., Carpena, A., & Tellini, C., 2017. Landslides types controlled by tectonics-induced evolution of valley slopes (Northern Apennines, Italy). Landslides, 15(2), 283-296.

Carlini, M., Chelli, A., Vescovi, P., Artoni, A., Clemenzi, L., Tellini, C., Torelli C., 2016. Tectonic control on the development and distribution of large landslides in the Northern Apennines (Italy). Geomorphology 253:425–437

Carmignani L., & Kligfield R., 1990. Crustal extension in the Northern Apennines: the transition from compression to extension in the Alpi Apuane Core Complex. Tectonics, 9, 1257-1303.

Carton, A., Panizza, M. (eds.) (1988). Il paesaggio fisico dell'Alto Appennino Emiliano. Bologna: Grafis.

Çellek, S., 2020. Effect of the Slope Angle and Its Cclassification on Landslide. Natural Hazards and Earth System Sciences Discussions,1-23. https://doi.org/10.5194/nhess-2020-87

Cerrina Feroni, A., Ottria, G., Martinelli, P., Martelli, L. & Catanzaritir., 2002. Note Illustrative della Carta Geologico- Strutturale dell'Appennino Emiliano-Romagnolo, scala 1:250,000. Regione Emilia Romagna, Servizio Geologico, Sismico e dei Suoli, S.EL.CA., Florence

Cesca, M., & D'Agostino, V., 2008. Comparison between FLO-2D and RAMMS in debris-flow modelling: A case study in the Dolomites (p. 206). https://doi.org/10.2495/DEB080201

Chalupová, O., Chalupa, V., Šilhán, K., 2021. Vertical variability of tension wood formation in the stem of Fagus sylvatica L. affected by landslide movement. Trees, 35(6), 1863–1874. https://doi.org/10.1007/s00468-021-02156-1

Chelli, A., & Tellini, C., 2001. Scree slope deposits during a cold-damp climatic phase in the early Middle Ages in the Gulf of La Spezia (Liguria, Italy). Geografia Fisica e Dinamica Quaternaria, 24, 25-28

Chelli, A., & Tellini., 2002. Geomorphological features of the Bratica Valley (Northern Apennines, Italy). Geografia Fisica e Dinamica Quaternaria, 25, 45-60

Chelli, A., Ruffini, A., Vescovi, P., Tellini, C., 2013. Tectonics and large landslides in the Northern Apennines (Italy). Proceed. II World Landslide Forum, 3–7 October 2011, Rome (Italy). Springer-Verlag.

Chelli, A., Segadelli, S., Vescovi, P., & Tellini, C., 2015. Large-scale geomorphological mapping as a tool to detect structural features: The case of Mt. Prinzera ophiolite rock mass (Northern Apennines, Italy). Journal of Maps, 12 (5), 770-776. https://doi.org/10.1080/17445647.2015.1072115

Chelli, A., Bordoni, M., Cappadonia, C., Pepe, G., Rotigliano, E., & Smith, M., 2021. Geomorphological tools for mapping natural hazards. Journal of Maps, 17(3), 1–4. https://doi.org/10.1080/17445647.2021.1920794

Chen, C. Y., & Lee, W. J., 2010. Topographic features and the initiation of debris flows. 10th Congress INTERPRAEVENT, Taipei (Taiwan). 10.

Chen, C. Y., & Yu, F. C., 2011. Morphometric analysis of debris flows and their source areas using GIS. Geomorphology, 129(3–4), 387–397. https://doi.org/10.1016/j.geomorph.2011.03.002

Chen, H.-W., Chen, C.-Y., 2022. Warning Models for Landslide and Channelized Debris Flow under Climate Change Conditions in Taiwan. Water 14, 695. https://doi.org/10.3390/w14050695

Ciccarese, G., Mulas, M., Alberoni, P. P., Truffelli, G., & Corsini, A., 2020. Debris flows rainfall thresholds in the Apennines of Emilia-Romagna (Italy) derived by the analysis of recent severe rainstorms events and regional meteorological data. Geomorphology, 358, 107097. https://doi.org/10.1016/j.geomorph.2020.107097

Ciccarese, G., Mulas, M., & A., C., 2021. Combining spatial modelling and regionalization of rainfall thresholds for debris flows hazard mapping in the Emilia-Romagna Apennines (Italy). Landslides, 18(11), 3513–3529. https://doi.org/10.1007/s10346-021-01739-w

Clemenzi, L., Molli, G., Storti, F., Muchez, P., Swennen, R., Torelli, L., 2014. Extensional deformation structures within a convergent orogen: the Val di Lima low-angle normal fault system (Northern Apennines, Italy). J. Struct. Geol. 66, 205–222.

CNR Geomorphological Research Group (Gruppo Ricerca Geomorfologia CNR), 1982. Geomorphology of the Febbio territory between Mt. Cusna and the Secchia River (Emilian Apennines). Geografia Fisica e Dinamica Quaternaria, 5, 285–360.

Conti P., Cornamusini G. & Carmignani L., 2020. An outline of the geology of the Northern Apennines (Italy), with geological map at 1:250,000 scale. Italian Journal of Geosciences, 139 (2), 149–194. https://doi.org/10.3301/IJG.2019.25

Cook, E.R., 1985. A time series analysis approach to tree-ring standardization: Ph. D. Dissertation. University of Arizona, 1985.

Corsini, A., Ciccarese, G., Berti, M., Diena, M., Truffelli, G. 2015. Debris flows in Val Parma and Val Baganza (northern Apennines) during the October 2014 alluvial event in Parma Province (Italy). Rendiconti Online Della Società Geologica Italiana 35:85–88. https:// doi. org/ 10. 3301/ ROL. 2015. 70

Corsini, A., Ciccarese, G., Diena, M., Alberoni, P. P., and Amorati, R., 2017: Debris flows in Val Parma and Val Baganza (Northern Apennines) during the 13 october 2014 alluvial event in Parma province (Italy), Italian Journal of Engineering Geology and Environment, Special issue V National Congress of AIGA (Cagliari, Italy), 35/2015, 29–38, https://doi.org/10.4408/IJEGE.2017-01.S-03, 2017.

Corsini, A., Ciccarese, G., Truffelli, G., 2019. Unusual becoming Usual: Recent persistent-rainstorm events and their implications for debris flow risk management in the northern Apennines of Italy. Proceedings of the 4th Regional Symposium on Landslides in the Adriatic - Balkan Region, 13–18. https://doi.org/10.35123/resylab

Costa, J.E., 1984. Physical geomorphology of debris flows. In Developments and applications of geomorphology, 268-317. Berlin, Heidelberg: Springer Berlin Heidelberg.

Crespi, A., Brunetti, M., Lentini, G., Maugeri, M., 2018. 1961–1990 high-resolution monthly precipitation climatologies for Italy. International Journal of Climatology 38, 878–895. https://doi.org/10.1002/joc.5217

Crosta, G.B., Clague, J.J., 2006. Large landslides: dating, triggering, modelling, and hazard assessment. Eng. Geol. 83, 1–3.

Crosta, G.B. and Dal Negro, P.J.N.H., 2003. Observations and modelling of soil slip-debris flow initiation processes in pyroclastic deposits: the Sarno 1998 event. Natural Hazards and Earth System Sciences, 3(1/2), 53-69.

Cruden, D, M., Varnes, D, J., 1996. Landslides: Investigation and Mitigation. Chapter 3 - Landslide types and processes. Transportation Research Board Special Report

D'Agostino, V., Cesca, M., & Marchi, L., 2010. Field and laboratory investigations of runout distances of debris flows in the Dolomites (Eastern Italian Alps). Geomorphology, 115(3–4), 294–304. https://doi.org/10.1016/j.geomorph.2009.06.032

Da Silva, J. M. F., Santos, L. J. C., & Oka-Fiori, C., 2019. Spatial correlation analysis between topographic parameters for defining the geomorphometric diversity index: Application in the environmental protection area of the Serra da Esperança (state of Paraná, Brazil). Environmental Earth Sciences, 78(12), 356. https://doi.org/10.1007/s12665-019-8357-2

Dagdelenler, G., Nefeslioğlu, H., & Gokceoglu, C. (2015). Modification of seed cell sampling strategy for landslide susceptibility mapping: An application from the Eastern part of the Gallipoli Peninsula (Canakkale, Turkey). Bulletin of Engineering Geology and the Environment, 75, 575-590. https://doi.org/10.1007/s10064-015-0759-0

Daxer, C., 2020. Topographic Openness Maps and Red Relief Image Maps in QGIS. Technical Report, University of Innsbruck, Institute of Geology. https://doi.org/10.13140/RG.2.2.18958.31047

Devoto, S., Biolchi, S., Bruschi, V., Furlani, S., Mantovani, M., Piacentini, D., Pasuto, A., & Soldati, M. (2012). Geomorphological map of the NW Coast of the Island of Malta (Mediterranean Sea). Journal of Maps, 8(1), 33–40. https://doi.org/10.1080/17445647.2012.668425

Dikau R., Cavallin A., Jäger, S., 1996. Databases and GIS for landslide research in Europe. Geomorphology 15:227–239. https://doi.org/10.1016/0169-555X(95)00072-D

Dos Santos Corrêa, C. V., Reis, F. A. G. V., do Carmo Giordano, L., Cabral, V. C., Veloso, V. Q., & D'Affonseca, F. M., 2024. Numerical modeling of a high magnitude debris-flow event occurred in Brazil. Natural Hazards, 120(14), Article 14. https://doi.org/10.1007/s11069-024-06728-5

Dramis, F., Guida, D., & Cestari, A. (2011). Geomorphological Mapping: Methods and Applications. Developments in earth surface processes Nature and aims of geomorphological mapping. Smith M.J., Paron P. & Griffiths J.S. (eds.), 15, 39–73. https://doi.org/10.1016/B978-0-444-53446-0.00003-3

Du J., Fan Z.J., Xu W., Dong L.Y., 2021. Research Progress of Initial Mechanism on Debris Flow and Related Discrimination Methods: A Review. Front. Earth Sci. 9:629567. https://doi: 10.3389/feart.2021.629567

Dykes, A., 2008. Geomorphological maps of Irish peat landslides created using hand-held GPS. Journal of Maps, 4, 258-276 https://doi.org/10.4113/jom.2008.1029

Eccel, E., Cordano, E., Zottele, F., 2015. A project for climatologic mapping of soil water content in Trentino. Italian Journal of Agrometeorology, 1, 5-20.

Eilmann, B., Sterck, F., Wegner, L., Vries, S., Arx, V. G., Mohren, G.M.J., Ouden, J., Klaassen, S., U., 2014. Wood structural differences between northern and southern beech provenances growing at a moderate site. Tree Physiology 34, 882–893. https://doi.org/10.1093/treephys/tpu069

Elter, P., Lasagna, S., Marroni, M., Pandolfi, L., Vescovi, P. and Zanzucchi, G., 1997. Note Illustrative della Carta Geologica d'Italia alla scala 1: 50,000.

Elter, P., Lasagna, S., Marroni, M., Pandolfi, L., Vescovi, P. & Zanzucchi, G., 2005. Note Illustrative della Carta Geologica d'Italia alla scala 1:50,000, Foglio 215 "Bedonia". Servizio Geologico d'Italia-Regione Emilia Romagna, S. EL.CA., Firenze, 117.

Emilia-Romagna Region Natura 2000 Network, 2016. SIC/ZPS IT403000 Monte Acuto, Alpe di Succiso Cognitive framework. 318.

Farabollini, P., De Pari, P., Discenza, M. E., Minnillo, M., Carabella, C., Paglia, G., & Miccadei, E., 2021. Geomorphological evidence of debris flows and landslides in the Pescara del Tronto area (Sibillini Mts, Marche Region, Central Italy). Journal of Maps, 17(3), 90–99. https://doi.org/10.1080/17445647.2020.1827055

Federici, P.R., 1979. Una ipotesi di cronologia glaciale würmiana, tardo e post e würmiana nell'Appennino Centrale. Geogr. Fis. Din. Quaternaria 2, 196-202

Federici, P.R., Tellini, C., 1983. La geomorfologia dell'Alta val Parma (appennino settentrionale). Riv. Geogr. Ital. 90 (3-4), 393-428

Fisher, R.V., 1971. Features of coarse-grained, high concentration fluids and their deposits. J Sediment Petrol 41: 916-927

Forte, G., De Falco, M., Santo, A., Gautam, D., Santangelo, N., 2025. Flash flood impacts and vulnerability mapping at catchment scale: Insights from southern Apennines. Engineering Geology, 350, 107988. https://doi.org/10.1016/j.enggeo.2025.107988

Frank, F., McArdell, B., Oggier, N., Baer, P., Christen, M., & Vieli, A., 2017. Debris-flow modeling at Meretschibach and Bondasca catchments, Switzerland: Sensitivity testing of field-data-based entrainment model. Natural Hazards and Earth System Sciences, 17, 801–815. https://doi.org/10.5194/nhess-17-801-2017

Fusco, F., Bordoni, M., Tufano, R., Vivaldi, V., Meisina, C., Valentino, R., Bittelli, M., De Vita, P., 2022. Hydrological regimes in different slope environments and implications on rainfall thresholds triggering shallow landslides. Natural Hazards 114, 907–939. https://doi.org/10.1007/s11069-022-05417-5

Gan, J. J., & Zhang, Y. X., 2020. Numerical Simulation of Debris Flow Runout Using Ramms: A Case Study of Luzhuang Gully in China. Computer Modeling in Engineering and Sciences. https://doi.org/10.32604/cmes.2019.07337

Gattinoni, P., Consonni, M., Francani, V., Leonelli, G., Lorenzo, C., 2019. Tunnelling in landslide areas connected to deep seated gravitational deformations: An example in Central Alps (northern Italy). Tunnelling and Underground Space Technology 93(6). https://doi.org/10.1016/j.tust.2019.103100

Gelati, R., 2013. Storia geologica del paese Italia; Diabasis: Parma, Italy.

Germain, D., Dagenais-Du-Fort, É., Lajeunesse, P., Simard, M., 2018. Dendrogeomorphic reconstruction of the seasonal timing and rainfall threshold for debris slide occurrence in eastern Canada. Dendrochronologia 52, 57-66. https://doi.org/10.1016/j.dendro.2018.09.007

Giano, S. I., Pescatore, E., & Siervo, V., 2021. Morphometry and Debris-Flow Susceptibility Map in Mountain Drainage Basins of the Vallo di Diano, Southern Italy. Remote Sensing, 13(16), 3254. https://doi.org/10.3390/rs13163254

Giraudi, C., 2004. The Apennine glaciations in Italy. Quaternary Glaciations Extent and Chronology. Developments in Quaternary Science, 2 (1), 215-223. https://doi.org/10.1016/S1571-0866(04)80073-3

Griffiths, J. S., Smith, M. J., & Paron, P., 2011. Introduction to Applied Geomorphological Mapping. In: Smith M.J., Paron P. & Griffiths J.S. (eds.), Geomorphological Mapping methods and applications. Developments in Earth Surface Processes 15, 3–11. https://doi.org/10.1016/B978-0-444-53446-0.00001-X

Grimsley, K.J., Rathburn, S.L., Friedman, J.M., Mangano, J.F., 2016. Debris Flow Occurrence and Sediment Persistence, Upper Colorado River Valley, CO. Environmental Management 58, 76–92. https://doi.org/10.1007/s00267-016-0695-1

Gruber, S., & Peckham, S., 2009. Land-Surface Parameters and Objects in Hydrology. In Hengl T. & Reuter H. I. (eds.), Developments in Soil Science 33, 171–194. https://doi.org/10.1016/S0166-2481(08)00007-X

Guida, D., Pelfini, M., & Santilli, M., 2008. Geomorphological and dendrochronological analyses of a complex landslide in the southern apennines. Geografiska Annaler: Series A, Physical Geography, 90(3), 211–226. https://doi.org/10.1111/j.1468-0459.2008.340.x

Guthrie, R., & Befus, A., 2021. DebrisFlow Predictor: An agent-based runout program for shallow landslides. Natural Hazards and Earth System Sciences, 21(3), 1029–1049. https://doi.org/10.5194/nhess-21-1029-2021

Guzzetti, F., Reichenbach, P., Cardinali, M., Galli, M., Ardizzone, F., 2005. Probabilistic landslide hazard assessment at the basin scale. Geomorphology 72(1–4):272–299.

Guzzetti, F., Peruccacci, S., Rossi, M., & Stark, C. P., 2007. The rainfall intensity–duration control of shallow landslides and debris flows: An update. Landslides, 5(1), Article 1. https://doi.org/10.1007/s10346-007-0112-1

Hirschberg, J., McArdell, B. W., Badoux, A., Molnar, P., 2019. Analysis of rainfall and runoff for debris flows at the Illgraben catchment, Switzerland.

Hu, K., Wei, F., & Li, Y., 2011. Real-time measurement and preliminary analysis of debris-flow impact force at Jiangjia Ravine, China: REAL-TIME MEASUREMENT AND ANALYSIS OF DEBRIS-FLOW IMPACT FORCE. Earth Surface Processes and Landforms, 36(9), 1268–1278. https://doi.org/10.1002/esp.2155

Hungr, O., Morgan, G. C., & Kellerhals, P., 1984. Quantitative analysis of debris hazards for design of remedial measures. Canadian Geotechnical Journal, 21(4), 663–677. https://doi.org/10.1139/t84-073

Hungr, O., and Evans, S., 1996. Rock avalanche runout prediction using a dynamic model.Proceedings of the 7th International Symposium on Landslides, Trondheim, Norway. 21.

Hungr, O., Evans, S.G., Bovis, M. and Hutchinson, J., 2001. Review of the Classification of landslides of the flow type: Environmental and Engineering Geoscience. Geological Society of America and the Association of Engineering Geologists, 7(3), 231-228. https://doi.org/10.2113/gseegeosci.7.3.221

Hungr, O., Leroueil, S., & Picarelli, L., 2014. The Varnes classification of landslide types, an update. Landslides, 11(2), 167–194. https://doi.org/10.1007/s10346-013-0436-y

Hürlimann, M., Coviello, V., Bel, C., Guo, X., Berti, M., Graf, C., Hübl, J., Miyata, S., Smith, J.B., Yin, H.-Y., 2019. Debris-flow monitoring and warning: Review and examples. Earth-Science Reviews 199(1), 102981. https://doi.org/10.1016/j.earscirev.2019.102981

Hutchinson, J, N., 1988. General report: Morphological and geotechnical parameters of landslides in relation to geology and hydrogeology. pp 3–35

Ilinca, V., 2021. Using morphometrics to distinguish between debris flow, debris flood and flood (Southern Carpathians, Romania). CATENA, 197, 104982. https://doi.org/10.1016/j.catena.2020.104982

ISPRA., 2007. Guida alla rappresentazione cartografica della Carta Geomorfologica d'Italia in scala 1:50,000. Quaderni del Servizio Geologico Nazionale, Serie III, 10, 34

ISPRA, 2015. APAT Servizio geologico d'Italia. Foglio 234: Fivizzano / APAT, Agenzia per la protezione dell'ambiente e per i servizi tecnici, Dipartimento difesa del suolo, Servizio Geologico d'Italia [Map]

ISPRA, 2019. Frana EIT201900231. Inventario dei Fenomeni Franosi in Italia (IFFI). Retrieved May 19, 2025, from https://beta.idrogeo.isprambiente.it/app/iffi/e/EIT201900231

ISPRA-Trigila, A., Iadanza, C., Lastoria, B., Bussettini, M., & Barbano, A., 2021. Dissesto idrogeologico in Italia: pericolosità e indicatori di rischio-Edizione 2021. Rapporti, 356, 2021.

ISPRA & AIGEO., 2022. Aggiornamento ed integrazione delle linee guida della Carta Geomorfologica d'Italia in scala 1:50,000. Quaderni del Servizio Geologico Nazionale, Serie III, 15, I

IUSS Working Group WRB, 2022. World Reference Base for Soil Resources. International soil classification system for naming soils and creating legends for soil maps. 4th edition. International Union of Soil Sciences (IUSS), Vienna, Austria.

Iverson, R.M., Reid M.E., LaHusen, R.G., 1997. Debris-Flow Mobilization from Landslides. Annual Review of Earth and Planetary Sciences 25:85–138. https://doi.org/10.1146/annurev.earth.25.1.85

Iverson, R. M., & George, D. L., 2014. A depth-averaged debris-flow model that includes the effects of evolving dilatancy. I. Physical basis. Proceedings of the Royal Society A: Mathematical, Physical and Engineering Sciences, 470 (2170), 20130819. https://doi.org/10.1098/rspa.2013.0819

Jakob, M., Hungr, O. and Jakob, D.M., 2005. Debris-flow hazards and related phenomena 739, 700. Berlin: Springer.

Jakob, M., Davidson, S., Bullard, G., Busslinger, M., Collier-Pandya, B., Grover, P., Lau, C.-A. 2022. Debris-flood hazard assessments in steep streams. Water Resources Research, 58, e2021WR030907. https://doi.org/10.1029/2021WR030907

Jian, L., Defu, L., 1981. The formation and characteristics of mud flow and flood in the mountain area of the Dachao River and its prevention. Z Geomorphol 25:470-484

Johnson, A. M., 1970. Physical processes in geology. Freeman and Cooper, San Francisco, 577 p

Kang, S., Lee, S.-R., Vasu, N. N., Park, J.-Y., & Lee, D.-H., 2017. Development of an initiation criterion for debris flows based on local topographic properties and applicability assessment at a regional scale. Engineering Geology, 230, 64–76. https://doi.org/10.1016/j.enggeo.2017.09.017

Khan, U. A., & Valentino, R., 2022. Investigating the Granulometric Distribution of Fluvial Sediments through the Hybrid Technique: Case Study of the Baganza River (Italy). Water, 14(9), 1511. https://doi.org/10.3390/w14091511

La Porta, G., Leonardi, A., Pirulli, M., Cafaro, F., & Castelli, F., 2023. Time-resolved triggering and runout analysis of rainfall-induced shallow landslides. Acta Geotechnica, 19, 1–17. https://doi.org/10.1007/s11440-023-01996-0

Lee, S., An, H., Kim, M., Lee, D., Lee, J., 2024. Debris flows analysis through quantitative evaluation of soil depth distribution under limited data. Catena, 246 (2024), 108379. https://doi.org/10.1016/j.catena.2024.108379

Leonelli, G., Chelli, A., Consonni, M., Lorenzo, C., Gattinoni, P., 2021. Multi-decadal dating of surface slope movements in forested DSGSD areas of the European Alps: detecting precipitation triggering factors. Geografiska Annaler: Series A, Physical Geography 103, 8–32. https://doi.org/10.1080/04353676.2020.1813983

Leonelli, G., Pelfini, M., 2013. Past surface instability of Miage debris-covered glacier tongue (Mont Blanc Massif, Italy): a decadal-scale tree-ring-based reconstruction. Boreas 42, 613–622. https://doi.org/10.1111/j.1502-3885.2012.00291.x

Li J., Luo., 1981. The formation and characteristics of mudflow and flood in the mountain area of the Dachao River and its prevention. Z Geomorphology 25: 470–484

Liu, B., Hu, X., Ma, G., He, K., Wu, M., & Liu, D., 2021. Back calculation and hazard prediction of a debris flow in Wenchuan meizoseismal area, China. Bulletin of Engineering Geology and the Environment, 80(4), 3457–3474. Scopus. https://doi.org/10.1007/s10064-021-02127-3

Liu, M., Deng, M., Chen, N., Tian, S., & Wang, T., 2024. Analysis of the Low-Frequency Debris Flow Disaster Induced by a Local Rainstorm on 12 July 2022, in Pingwu County, China. Remote Sensing, 16(9), 1547. https://doi.org/10.3390/rs16091547

Lorenzini, G. and Mazza, N. eds., 2004. Debris flow: Phenomenology and rheological modelling. WIT press.

Macchi, G., Monegato, G., Pasuto, A., Boretto, G., Crema, S., Marchi, L., & Cavalli, M., 2023. Geomorphology of the Liera catchment (Dolomites, NE Italy): Understanding landscape response to an extreme event. Journal of Maps, 19, 1–8. https://doi.org/10.1080/17445647.2023.2165979

Magliulo, P., & Valente, A., 2020. GIS-Based Geomorphological Map of the Calore River Floodplain Near Benevento (Southern Italy) Overflooded by the 15th October 2015 Event. Water, 12, 148. https://doi.org/10.3390/w12010148

Major, J. J., & Iverson, R. M., 1999. Debris-flow deposition: Effects of pore-fluid pressure and friction concentrated at flow margins. Geological Society of America Bulletin, 111(10), 1424–1434. https://doi.org/10.1130/0016-7606(1999)111<1424:DFDEOP>2.3.CO;2

Mandrone, G., 2004. Assessing of geomechanical features of some of the most common heterogeneous rock units in the Northern Apennines. Quad. Geol. Appl. 11, 5–18.

Marchi, L., Brunetti, M.T., Cavalli, M. and Crema, S., 2019. Debris-flow volumes in northeastern Italy: Relationship with drainage area and size probability. Earth Surface Processes and Landforms, 44(4), pp.933-943.

Marroni, M., Molli, G., Ottria, G. and Pandolfi, L., 2001. Tectono-sedimentary evolution of the External Liguride units (Northern Apennines, Italy): Insights in the pre-collisional history of a fossil ocean-continent transition zone. Geodinamica Acta, 14(5), 307-320.

Marroni, M., Molli G., Montanini A., Ottria G., Pandolfi L. & Tribuzio R., 2002. The external Ligurian Units of the Northern Apennines, Italy: From rifting to convergence of a fossil oceancontinent transition zone. Ofioliti, 27, 119-132.

Marroni, M., Meneghini F., & Pandolfi L., 2010. Anatomy of the Ligure-Piemontese subduction system: evidence from Late Cretaceous-middle Eocene convergent margin deposits in the Northern Apennines, Italy. International Geology Review, 1-33. doi: 10.1080/00206810903545493.

Marroni, M., Meneghini, F. and Pandolfi, L., 2017. A revised subduction inception model to explain the Late Cretaceous, double-vergent orogen in the precollisional western Tethys: Evidence from the Northern Apennines. Tectonics, 36(10), pp.2227-2249.

Martini, M., Baggio, T., & D'Agostino, V., 2023. Comparison of two 2-D numerical models for snow avalanche simulation. Science of The Total Environment, 896, 165221. https://doi.org/10.1016/j.scitotenv.2023.165221

Masseroli A., Bollati I.M., La Licata M., Pelfini M., Trombino L., 2023. The relative imprint of forming factors on soil characteristics in a recently deglaciated area: concerns about chronosequences approach, Physical Geography, 44:6, 678-709. https://doi.org/10.1080/02723646.2022.2136600

Matjaž, M., & Bezak, N., 2021. Debris Flow Modelling Using RAMMS Model in the Alpine Environment With Focus on the Model Parameters and Main Characteristics. Frontiers in Earth Science, 8. https://doi.org/10.3389/feart.2020.605061

Melo, R., Van Asch, T. and Zêzere, J.L., 2018. Debris flow run-out simulation and analysis using a dynamic model. Natural Hazards and Earth System Sciences, 18(2), pp.555-570.

Mergili, M., Frank, B., Fischer, J.-T., Huggel, C., Pudasaini, S. P., 2018. Computational experiments on the 1962 and 1970 landslide events at Huascarán (Peru) with r.avaflow: Lessons learned for predictive mass flow simulations. Geomorphology, 322, 15–28. https://doi.org/10.1016/j.geomorph.2018.08.032

Mikoš, M., Bezak, N., 2021. Debris flow modelling using RAMMS model in the alpine environment with focus on the model parameters and main characteristics. Frontiers in Earth Science, 8, 605061.

Molli, G., & Malevieille J., 2010. Orogenic processes and the Corsica/Apennines geodynamic evolution: insights from Taiwan. Int. J. Earth Sci. (Geol. Rundsch.). doi: 10.1007/s00531-010-0598-y.

Moratti, L., Pellegrini, M., 1972. Caratteristiche delle alluvioni e dei dissesti verificatisi nei bacini dei fiumi Secchia e Panaro (Province di Modena e Reggio Emilia) nel settembre 1972. Atti della Società dei Naturalisti e Matematici di Modena, 103, 133–195. (Map used: "Carta dei dissesti e delle alluvioni del 10–16 settembre 1972", a cura di M. Pellegrini.)

Mueting, A., Bookhagen, B., & Strecker, M. R. (2021). Identification of Debris-Flow Channels Using High-Resolution Topographic Data: A Case Study in the Quebrada del Toro, NW Argentina. Journal of Geophysical Research: Earth Surface, 126(12), e2021JF006330. https://doi.org/10.1029/2021JF006330

Myhre, G., Alterskjær, K., Stjern, C., Hodnebrog, Ø., Marelle, L., Samset, B., Sillmann, J., Schaller, N., Fischer, E., Michael, S., Stohl, A., 2019. Frequency of extreme precipitation increases extensively with event rareness under global warming. Scientific Reports 9, 16063. https://doi.org/10.1038/s41598-019-52277-4

Nigro, M., Barsanti, M., Raco, B., Giannecchini, R., 2024. Investigating a Century of Rainfall: The Impact of Elevation on Precipitation Changes (Northern Tuscany, Italy). Water 16, 2866. https://doi.org/10.3390/w16192866

Nikolopoulos EI, Borga M, Marra F, Crema S, Marchi L. 2015. Debris flows in the eastern Italian Alps: seasonality and atmospheric circulation patterns. Natural Hazards and Earth System Sciences 15: 647–656. https://doi.org/10.5194/nhess-15-647-2015.

Nishiguchi, Y., Uchida T., 2022. Long-runout-landslide-induced debris flow: the role of fine sediment deposition processes in debris flow propagation. Journal Geophysics Res Earth Surf 127(2): e2021JF006452

Nosov, K.N., Chernomorets, S.S., Tutubalina, O.V. and Zaporozhchenko, E.V., 2006. Debris flow research in Russia and the Former Soviet Union: history and perspectives. WIT Transactions on Ecology and the Environment, 90.

Novellino, A., Pennington, C., Leeming, K., Taylor, S., Alvarez, I.G., McAllister, E., Arnhardt, C. and Winson, A., 2024. Mapping landslides from space: A review. Landslides, 21(5), pp.1041-1052.

Park, D. W., Lee, S. R., Vasu, N. N., Kang, S. H., & Park, J. Y., 2016. Coupled model for simulation of landslides and debris flows at local scale. Natural Hazards, 81(3), 1653–1682. https://doi.org/10.1007/s11069-016-2150-2

Parry, S., 2011. The Application of Geomorphological Mapping in the Assessment of Landslide Hazard in Hong Kong. In: Smith M.J., Paron P. & Griffiths J.S. (eds.), Developments in Earth Surface Processes, 15, 413-441. https://doi.org/10.1016/B978-0-444-53446-0.00015-X

Pavan, V., Antolini, G., Barbiero, R., Berni, N., Brunier, F., Cacciamani, C., Cagnati, A., Cazzuli, O., Cicogna, A., De Luigi, C. and Di Carlo, E., 2019. High resolution climate precipitation analysis for north-central Italy, 1961–2015. Climate Dynamics, 52(5), 3435-3453. https://doi.org/10.1007/s00382-018-4337-6

Peruccacci, S., Gariano, S.L., Melillo, M., Solimano, M., Guzzetti, F., Brunetti, M.T., 2023. The Italian rainfall-induced Landslides Catalogue, an extensive and accurate spatio-temporal catalogue of rainfall-induced landslides in Italy, Earth Syst. Sci. Data, 15, 2863–2877, https://doi.org/10.5194/essd-15-2863-2023

Pierson, T. C., 1980a. Erosion and deposition by debris flows at Mt Thomas, North Canterbury, New Zealand. Earth Surface Processes, 5(3), 227–247. https://doi.org/10.1002/esp.3760050302

Pierson, T. C., l980b. Debris flows. Rev 39 J Tussoch Grassl Mt Lands Inst: NZ, December, pp 3-14

Pierson, T. C., 1981. Dominate particle support mechanisms in debris flows at Mount Thomas, New Zealand, and implications for flow mobility. Sedimentology 28:49-60

Pierson, T. C., Costa, J., 1987. A rheologic classification of subaerial sediment-water flows. Geological Society of America

Pirulli, M., & Sorbino, G., 2008. Assessing potential debris flow runout: a comparison of two simulation models. NHESS, 8 (4), 961–971, 2008. https://doi.org/10.5194/nhess-8-961-2008.

Plesi, G., Galli M. & Daniele G., 2002. The Monti Rognosi ophiolitic unit (cfr. Calvana unit Auct.) paleogeography position in the external Ligurian domain, relationships with the tectonic units derived from the Adriatic margin. Boll. Soc. Geol. It., Special Volume, 1, 273-284.

Principi, G,. & Treves B., 1984. Il sistema corso-appenninico come prisma di accrezione. Riflessi sul problema generale del limite Alpi-Appennini. Mem. Soc. Geol. It., 28, 549-576.

Puccinelli, A., Avanzi G.D., Perilli N., 2015. Note Illustrative della Carta Geologica d'Italia alla scala 1:50.000, F. 233 Pontremoli, ISPRA - Serv. Geol. d'It., Roma. https://doi.org/ 10.15161/oar.it/212021

Pudasaini, S.P., and Hutter, K. 2007. Saint-Venant Equations and Friction Law for Modelling Self-Channeling Granular Flows: From Analogue to Numerical Simulation. Avalanche Dynamics. Springer, Berlin.

Purinton, B., & Bookhagen, B., 2017. Validation of digital elevation models (DEMs) and comparison of geomorphic metrics on the southern Central Andean Plateau. Earth Surface Dynamics, 5(2), 211–237. https://doi.org/10.5194/esurf-5-211-2017

QGIS Development Team, 2023. QGIS Geographic Information System. Open Source Geospatial Foundation Project, version 3.36.0. http://qgis.osgeo.org(open in a new window

Qie, J., Favillier, A., Liébault, Ballesteros Cánovas, J. A., Lopez-Saez, J., Guillet, S., Francon, L., Zhong, Y., Stoffel, M., Corona, C., 2024. A supply-limited torrent that does not feel the heat of climate change. Nature Communications 15, 9078. https://doi.org/10.1038/s41467-024-53316-z

Qie, J., Corona, C., Favillier, A., Gubler, S., Estermann, T., Stoffel, M., 2025. Hydrometeorological triggers of debris flows derived from historical archives and tree-ring data: Insights from the Swiss National Park. Science of The Total Environment, 968, 178880. https://doi.org/10.1016/j.scitotenv.2025.178880

Rashid, M. A., Leonelli, G., & Chelli, A., 2024. Quantitative characterization of geomorphological and topographical features of debris-flow channels at the Alpe di Succiso mountain, Northern Apennines (Italy). Journal of Maps, 20 (1), https://doi.org/10.1080/17445647.2024.2422549

Rashid, M. A., Chelli, A., Petrella, E., Pescio S., Melada J., Manara V., Arcuri B., Maugeri M., Brunetti, M., Trombino, L., Masseroli, A., Leonelli, G., 2026. Multi-disciplinary reconstruction of debris flow events and dynamics in the Northern Apennines, Italy: a multi-scale approach linking ground evidence with climatic triggers. CATENA, 263, 109708. https://doi.org/10.1016/j.catena.2025.109708

R Core Team (2024). *R: A Language and Environment for Statistical Computing.* R Foundation for Statistical Computing, Vienna, Austria. https://www.R-project.org/

Remitti, F., Bettelli G. & Vannucchi P., 2007. Internal structure and tectonic evolution of an underthrust tectonic mélange: the Sestola-Vidiciatico tectonic unit of the Northern Apennines, Italy. Geodinamica Acta, 20, 37-51.

Ricci Lucchi, F., 1986. The Oligocene to Recent foreland basins of the Northern Apennines. Foreland Basins. P.A. Allen & P. Homewood, 8, 105-139.

Rickenmann, D., & Zimmermann, M., 1993. The 1987 debris flows in Switzerland: Documentation and analysis. Geomorphology, 8(2-3), 175–189. https://doi.org/10.1016/0169-555X(93)90036-2

Rickenmann, D., Laigle, D., McArdell, B. W., & Hübl, J., 2006. Comparison of 2D debris-flow simulation models with field events. Computational Geosciences, 10(2), Article 2. https://doi.org/10.1007/s10596-005-9021-3

Riihimäki, H., Kemppinen, J., Kopecký, M., & Luoto, M., 2021. Topographic Wetness Index as a Proxy for Soil Moisture: The Importance of Flow-Routing Algorithm and Grid Resolution. Water Resources Research, 57(10), e2021WR029871. https://doi.org/10.1029/2021WR029871

Riley, S.J., De Gloria, S.D., & Elliot, R. (1999). A terrain ruggedness index that quantifies topographic heterogeneity. Intermountain Journal of Science 5, 1-4, 23–27

Rocchi, I., Gragnano, C.G., Govoni, L., Bittelli, M., Gottardi, G., 2020. Assessing the performance of a versatile and affordable geotechnical monitoring system for river embankments. Physics and Chemistry of the Earth, 117, 102872. https://doi.org/10.1016/j.pce.2020.102872

Roering, J., Mackey, B., Marshall, J., Sweeney, K., Deligne, N., Booth, A., Handwerger, A., & Cerovski-Darriau, C., 2013. 'You are HERE': Connecting the dots with airborne lidar for geomorphic fieldwork. Geomorphology, 200. https://doi.org/10.1016/j.geomorph.2013.04.009

Rosso, R., Ceppi, A., 2023. Land–Sea Distribution of Ground Precipitation in Mediterranean Storms. Water 15, 1894. https://doi.org/10.3390/w15101894

Różycka, M., Migoń, P., & Michniewicz, A., 2017. Topographic Wetness Index and Terrain Ruggedness Index in geomorphic characterisation of landslide terrains, on examples from the Sudetes, SW Poland. Zeitschrift Für Geomorphologie, Supplementary Issues, 61(2), 61–80. https://doi.org/10.1127/zfg_suppl/2016/0328

Sakai, Y., Hotta, N., Kaneko T., Iwata, T., 2019. Effects of grain-size composition on flow resistance of debris flows: behavior of fine sediment. J Hydraul Eng 145(5):06019004. https://doi.org/10.1061/(ASCE)HY.1943-7900.0001586

Saleem, N., Huq, M. E., Twumasi, N. Y. D., Javed, A., & Sajjad, A., 2019. Parameters derived from and/or used with digital elevation models (DEMs) for landslide susceptibility mapping and landslide risk assessment: A review. ISPRS International Journal of Geo-Information, 8(12), 545. https://doi.org/10.3390/ijgi8120545

Salm, B., Burkard, A., & Gubler, H. U., 1990. Berechnung von Fliesslawinen. Eine Anleitung fuer Praktiker mit Beispielen | DORA WSL. Retrieved March 8, 2025, from https://www.dora.lib4ri.ch/wsl/islandora/object/wsl%3A26106

Scheidl, C., Rickenmann, D., & McArdell, B., 2012. Runout Prediction of Debris Flows and Similar Mass Movements. In Landslide Science and Practice: Spatial Analysis and Modelling (Vol. 3). https://doi.org/10.1007/978-3-642-31310-3-30

Scherrer, S.C., Fischer, E.M., Posselt, R., Liniger, M.A., Croci-Maspoli, M., Knutti, R., 2016. Emerging trends in heavy precipitation and hot temperature extremes in Switzerland. Journal of Geophysical Research: Atmospheres 121, 2626–2637. https://doi.org/10.1002/2015JD024634

Schläppy, R., Jomelli, V., Eckert, N., Stoffel, M., Grancher, D., Brunstein, D., Corona, C., Deschatres, M., 2016. Can we infer avalanche–climate relations using tree-ring data? Case studies in the French Alps. Reg Environ Change 16, 629–642. https://doi.org/10.1007/s10113-015-0823-0

Schraml, K., Thomschitz, B., McArdell, B. W., Graf, C., & Kaitna, R., 2015. Modeling debris-flow runout patterns on two alpine fans with different dynamic simulation models. Natural Hazards and Earth System Sciences, 15(7), 1483–1492. https://doi.org/10.5194/nhess-15-1483-2015

Scognamiglio, S., Terribile, F., Iamarino, M., Orefice, N., Vingiani, S., 2016. Soil properties and debris flows in Italy: potential relationships. Rend. Online Soc. Geol. It., Vol. 41, 199-202.

Segoni, S., Ajin, R.S., Nocentini, N., Fanti, R., 2024. Insights Gained from the Review of Landslide Susceptibility Assessment Studies in Italy. Remote Sensing 16 (23), 4491. https://doi.org/10.3390/rs16234491

Seijmonsbergen, A., 2013. The Modern Geomorphological Map. In Treatise on Geomorphology, 14, 35–52. https://doi.org/10.1016/B978-0-12-374739-6.00371-7

Sørensen, R., Zinko, U., & Seibert, J. (2006). On the calculation of the topographic wetness index: Evaluation of different methods based on field observations. Hydrology and Earth System Sciences, 10(1), 101–112. https://doi.org/10.5194/hess-10-101-2006

Servizio Cartografico - Ufficio Pedologico, 1994. Carta dei suoli dell'Emilia-Romagna. Scala 1:250.000. Regione Emilia-Romagna.

Shroder, J.F., 1978. Dendrogeomorphological analysis of mass movement on Table Cliffs Plateau, Utah. Quaternary Research 9, 168–185. https://doi.org/10.1016/0033-5894(78)90065-0

Šilhán, K., Stoffel, M., 2015. Impacts of age-dependent tree sensitivity and dating approaches on dendrogeomorphic time series of landslides. Geomorphology 236, 34–43. https://doi.org/10.1016/j.geomorph.2015.02.003

Šilhán, K., & Tichavský, R., 2016. Recent increase in debris flow activity in the Tatras Mountains: Results of a regional dendrogeomorphic reconstruction. CATENA, 143, 221–231. https://doi.org/10.1016/j.catena.2016.04.015

Šilhán, K. 2020. Dendrogeomorphology of landslides: Principles, results and perspectives. Landslides, 17(10), 2421–2441. https://doi.org/10.1007/s10346-020-01397-4

Šilhán, K., Brázdil, R., Zahradníček, P., Pánek, T., 2023. The longest tree-ring based chronology of mass movements in Central Europe and their meteorological triggers. CATENA 227, 107123. https://doi.org/10.1016/j.catena.2023.107123

Šilhán, K., De la Peña Guillén, K.A., Carlón Allende, T., Tsou, C.-Y., Zhang, Y., 2024. Tree-ring eccentricity-based dating of landslide movements: Defining a new effective approach. CATENA 234, 107576. https://doi.org/10.1016/j.catena.2023.107576

Smith, T. C., Hart, E. W., (with a contribution by Baldwin, J. E., Rodrigues, R.J., 1982. Landslides and related storm damage, January 1982, San Francisco Bay Region. Calif Geol 35: 139-152

Sørensen, R., Zinko, U., & Seibert, J. (2006). On the calculation of the topographic wetness index: Evaluation of different methods based on field observations. Hydrology and Earth System Sciences, 10(1), 101–112. https://doi.org/10.5194/hess-10-101-2006

Stoffel, M., Butler, D. R., Corona, C., 2013. Mass movements and tree rings: A guide to dendrogeomorphic field sampling and dating. Geomorphology, 200, 106–120. https://doi.org/10.1016/j.geomorph.2012.12.017

Stoffel, M., Tiranti, D., Huggel, C., 2014. Climate change impacts on mass movements — Case studies from the European Alps. Science of The Total Environment 493, 1255–1266. https://doi.org/10.1016/j.scitotenv.2014.02.102

Stoffel, M., Allen, S.K., Ballesteros-Cánovas, J.A., Jakob, M., Oakley, N., 2024. Climate Change Effects on Debris Flows. In: Jakob, M., McDougall, S., Santi, P. (eds) Advances in Debris-flow Science and Practice. Geoenvironmental Disaster Reduction. Springer, Cham. https://doi.org/10.1007/978-3-031-48691-3_10

Stokes, M.A. and Smiley, T.L., 1968. An Introduction to Tree-Ring Dating. Univ. of Chicago Press, Chicago/London, 73.

Storti, F. and Balsamo, F., 2010. Particle size distributions by laser diffraction: sensitivity of granular matter strength to analytical operating procedures. Solid Earth, 1(1), 25-48.

Takahashi, T., 1981. Estimation of potential debris flows and their hazardous zones, soft countermeasures for a disaster. Journal of Natural Disaster Science, 3, 57–89.

Takahashi, T., 2007. Debris Flow: Mechanics, Prediction and Countermeasures. Pure appl. geophys. Taylor & Francis, 165 (2008) 995–996. https://doi.org/10.1201/9780203946282

Takahashi, T., 2014. Debris Flow: Mechanics, Prediction and Countermeasures, 2nd edition. CRC Press.

Tarolli, P., & Dalla Fontana, G., 2009. Hillslope-to-valley transition morphology: New opportunities from high resolution DTMs. Geomorphology, 113(1), 47–56. https://doi.org/10.1016/j.geomorph.2009.02.006

Tarquini S., Isola I., Favalli M., Battistini A., Dotta G., 2023. TINITALY, a digital elevation model of Italy with a 10 meters cell size (Version 1.1). Istituto Nazionale di Geofisica e Vulcanologia (INGV). https://doi.org/10.13127/tinitaly/1.1.

Tichavský, R., Fabiánová, A., Koutroulis, A., Spálovský, V., 2022. Occasional but severe: Past debris flows and snow avalanches in the Helmos Mts. (Greece) reconstructed from tree-ring records. Science of The Total Environment 848, 157759. https://doi.org/10.1016/j.scitotenv.2022.157759

Tichavský, R., 2023. Understanding hydrometeorological triggers of natural hazards through dendrogeomorphology: Methods, limitations, and challenges. Earth-Science Reviews 244, 104546. https://doi.org/10.1016/j.earscirev.2023.104546

Tiranti, D., Bonetto, S. and Mandrone, G., 2008. Quantitative basin characterisation to refine debris-flow triggering criteria and processes: an example from the Italian Western Alps. Landslides, 5(1), pp.45-57.

Tiranti, D., Crema, S., Cavalli, M., & Deangeli, C., 2018. An Integrated Study to Evaluate Debris Flow Hazard in Alpine Environment. Frontiers in Earth Science, 6, 60. https://doi.org/10.3389/feart.2018.00060

Tiranti, D., Cremonini, R., Sanmartino, D., 2021. Wildfires Effect on Debris Flow Occurrence in Italian Western Alps: Preliminary Considerations to Refine Debris Flow Early Warnings System Criteria. Geosciences 11, 422. https://doi.org/10.3390/geosciences11100422

Tognetti, R., Lasserre, B., Di Febbraro, M., Marchetti, M., 2019. Modeling regional drought-stress indices for beech forests in Mediterranean mountains based on tree-ring data. Agricultural and Forest Meteorology 265, 110–120. https://doi.org/10.1016/j.agrformet.2018.11.015

Treves B., 1984. Orogenic belts as accretionary prisms: the example of the Northern Apennines. Ofioliti, 9, 577-618.

Trigila, A., & Iadanza, C., 2008. Landslides in Italy: Special Report 2008. ISPRA - Italian National Institute for Environmental Protection and Research, Rapporti 83/2008, ISBN 978-88-448-0355-1.

Trimble, 2023. Trimble DA2 GNSS receiver – High-accuracy positioning. Retrieved from https://geospatial.trimble.com/da2

Uchida, T., Nishiguchi, Y., McArdell, B.W., Satofuka, Y., 2020. The role of the phase shift of fine particles on debris flow behavior: a numerical simulation for a debris flow in Illgraben Switzerland. Canadian Geotechnical Journal 58(1):23–34. https://doi.org/10.1139/cgj-2019-0452

Ulbrich, U., Lionello, P., Belušić, D., Jacobeit, J., Knippertz, P., Kuglitsch, F.G., Leckebusch, G.C., Luterbacher, J., Maugeri, M., Maheras, P. and Nissen, K.M., 2012. Climate of the Mediterranean: synoptic patterns, temperature, precipitation, winds, and their extremes. Elsevier, 301–346.

USGS., 2004. Landslide types and processes. Fact Sheet 2004–3072. Available at: https:// pubs. usgs. gov/ fs/ 2004/ 3072/ fs- 2004- 3072. Html

Vai, G.B., & Martini, I.P., 2001. Anatomy of an Orogen: The Apennines and Adjacents Mediterranean Basins. Dordrecht/Boston/ London, Kluwer Academic Publishers.

Vannucchi, P., Remitti, F., & Bettelli, G., 2012. Lateral variability of the erosive plate boundary in the Northern Apennines, Italy. Italian Journal of Geosciences, 131(2), 215-227.

Varnes, D.J., 1978. Slope movement types and processes. In: Schuster RL, Krizek RJ (eds) Landslides analysis and control. Transport Res Board Spec Rep 176. Nat! Acad Sci, Washington DC, pp 11~33

VAW, 1992. Murga¨nge 1987, Dokumentation und Analyse, Bericht Nr.: 97.6 der Versuchsanstalt fu¨r Wasserbau, Hydrologie und Glaziologie, ETH Zu¨rich

Vicari, H., 2018. Physical and numerical modelling of debris flows (Doctoral dissertation, Politecnico di Torino).

Wang, B., Li, Y., Liu, D., & Liu, J., 2018. Debris flow density determined by grain composition. Landslides, 15(6), 1205–1213. https://doi.org/10.1007/s10346-017-0912-x

Wang, ZY., Lee, J.H.W., Melching, C.S., 2015. Debris Flows and Landslides. In: River Dynamics and Integrated River Management. Springer, Berlin, Heidelberg. https://doi.org/10.1007/978-3-642-25652-3_5

Wang, S., Niu, X., Xiao, S., Sun, Y., Zong, L., Liu, J., & Zhang, M., 2025a. Landslide Susceptibility Assessment Based on a Quantitative Continuous Model: A Case Study of Wanzhou. GeoHazards, 6(3), 48. https://doi.org/10.3390/geohazards6030048

Wang, Y., Wu, J., Zhang, J., Guan, T., Wang, G., Jin, J., Wang, Z., 2025b. Depth distributions of soil temperature: Seasonal sensitivity and simulation across dryness/wetness conditions. Agricultural Water Management, 316, 109571. https://doi.org/10.1016/j.agwat.2025.109571

Whipple, K., & Dunne, T., 1992. The Influence of Debris-Flow Rheology on Fan Morphology, Owens Valley, California. Geological Society of America Bulletin, 104, 887–900. https://doi.org/10.1130/0016-7606(1992)104<0887:TIODFR>2.3.CO;2

Wilford, D. J., Sakals, M. E., Innes, J. L., Sidle, R. C., Bergerud, W. A., 2004. Recognition of debris flow, debris flood and flood hazard through watershed morphometrics. Landslides, 1(1), 61-66. https://doi.org/10.1007/s10346-003-0002-0

Wilson, J. P., & Bishop, M. P., 2013. 3.7 Geomorphometry. In Treatise on Geomorphology (pp. 162–186). Elsevier. https://doi.org/10.1016/B978-0-12-374739-6.00049-X

Winzeler, H. E., Owens, P. R., Read, Q. D., Libohova, Z., Ashworth, A., & Sauer, T. (2022). Topographic Wetness Index as a Proxy for Soil Moisture in a Hillslope Catena: Flow Algorithms and Map Generalization. Land, 11(11), Article 11. https://doi.org/10.3390/land11112018

Wistuba, M., Malik, I., Gärtner, H., Kojs, P., Owczarek, P., 2013. Application of eccentric growth of trees as a tool for landslide analyses: The example of Picea abies Karst. in the Carpathian and Sudeten Mountains (Central Europe). CATENA 111, 41–55. https://doi.org/10.1016/j.catena.2013.06.027

Yang, K., Xu, Z.-M., Tian, L., Wang, K., Ren, Z., Tang, Y.-J., Luo, J.-Y., & Gao, H.-Y., 2020. Significance of coarse clasts in viscous debris flows. Engineering Geology, 272, 105665. https://doi.org/10.1016/j.enggeo.2020.105665

Yilmaz, C., Topal, T., & Süzen, M. L., 2012. GIS-based landslide susceptibility mapping using bivariate statistical analysis in Devrek (Zonguldak-Turkey). Environmental Earth Sciences, 65(7), 2161–2178. https://doi.org/10.1007/s12665-011-1196-4

Zei, C., Ciucciarelli, C., Tarabusi, G., Guerra, C., Ghirotti, G., Valensise, G., 2024. Earthquakes in the Valmarecchia area (Northern Apennines, Italy). Italian Journal of Engineering Geology and Environment.

Zhang, L., Zhang, J., Ming, Z., Li, H., Chen, R., Jia, Y., 2024. Effects of changing spatial scale on debris-flow hazard assessment: A case study in the Dadu River basin, China. Science of The Total Environment 954, 176482. https://doi.org/10.1016/j.scitotenv.2024.176482

Zou, Q., Cui, P., Zeng, C., Tang, J., & Regmi, A. D., 2016. Dynamic process-based risk assessment of debris flow on a local scale. Taylor & Francis. https://www.tandfonline.com/doi/abs/10.1080/02723646.2016.1169477

Acknowledgements

I express my deepest gratitude to God Almighty, whose infinite wisdom and grace have granted me the knowledge and strength to complete this Ph.D. research journey.

First and foremost, I would like to express my heartfelt gratitude to my supervisors, Prof. Alessandro Chelli and Prof. Giovanni Leonelli, whose unwavering support, guidance, and profound knowledge have been invaluable throughout my Ph.D. journey. Their motivation, enthusiasm, and belief in my potential have not only shaped my research but have also inspired me to overcome challenges and reach new academic heights. I am deeply grateful for their trust and mentorship.

I am also sincerely grateful to Prof. Roberto Valentino, Prof. Emma Petrella, and Prof. Maurizio Maugeri for their valuable suggestions, constructive feedback, and the time they dedicated to my work. Their expertise was instrumental in refining my research and broadening my understanding of the subject.

Special thanks to Prof. Marco Roveri and Prof. Fabrizio Balsamo for their coordination and support, which greatly assisted me in navigating the complexities of my Ph.D. research. I also extend my gratitude to Dr. Mattia Pizzati for his invaluable assistance in the laboratory, and for the insightful discussions and knowledge shared throughout my work.

I would also like to express my heartfelt thanks to my friends, whose encouragement, camaraderie, and emotional support have been a constant source of strength throughout this journey. Their understanding and kindness have made this experience much more rewarding.

Finally, I would like to express my deepest gratitude to my parents, Mr. and Mrs. Rashid, whose unwavering support, love, and prayers have been my greatest source of strength. Their encouragement and sacrifices have been fundamental in helping me achieve my goals and complete this journey.

I am also extremely grateful to the University of Parma and the Department of Chemistry, Life Sciences and Environmental Sustainability for providing me with the opportunity to pursue this Ph.D. program. The intellectual environment, resources, and academic guidance provided by the department have been essential in enabling me to complete my research and contribute to the field of Earth Sciences.

Muhammad Ahsan Rashid